Chia, Yen Yee (2014) Integrating supercapacitors into a hybrid energy system to reduce overall costs using the genetic algorithm (GA) and support vector machine (SVM). PhD thesis, University of Nottingham.

The University of Nottingham, Malaysia Campus
Department of Electrical and Electronic Engineering

INTEGRATING SUPERCAPACITORS INTO A HYBRID ENERGY SYSTEM TO REDUCE OVERALL COSTS USING THE GENETIC ALGORITHM (GA) AND SUPPORT VECTOR MACHINE (SVM)

by YEN YEE CHIA

Thesis submitted in candidature for the degree of Doctor of Philosophy, August 2014

To my Family and Supervisor

ABSTRACT

This research deals with optimising a supercapacitor-battery hybrid energy storage system (SB-HESS) to reduce the implementation cost for solar energy applications using the Genetic Algorithm (GA) and the Support Vector Machine (SVM). The integration of a supercapacitor into a battery energy storage system for solar applications is proven to prolong the battery lifespan. Furthermore, the reliability of the system was optimised using a GA within the Taguchi technique in the supercapacitor fabrication process. This is important to reduce the spread in tolerance of supercapacitors values (i.e. capacitance and Equivalent Series Resistance (ESR)) which affect system performance.

One of the more important results obtained in this project is the net present cost (NPC) of the Supercapacitor-battery hybrid energy storage system is **7.51%** lower than the conventional battery only system over a 20-years project lifetime. This NPC takes into account of components initial capital cost, replacement cost, maintenance and operational cost. The number of batteries is reduced from 40 (conventional – battery only system) to 24 (SB-HESS) with the inclusion of supercapacitors in the system. This leads to reduction cost in the implemented hybrid energy storage system. A greener renewable energy system is achievable as the number of battery is reduced significantly. An optimised combination of the number of components for renewable energy system is also found. The number of batteries is sized, based on the average power output instead of catering to the peak power burst as in a conventional battery only system. This allows for the reduction in the number of batteries as the peak power is catered for by the presence of the supercapacitor. Subsequent efforts have been focused on the energy management system which is coupled

with a supervised learning machine – SVM, switches and sensors are used to forecast the load demand beforehand. This load predictive-energy management system is implemented on a lab-scaled hybrid energy storage system prototype. Results obtained also show that this load predictive system allows for accurate load classification and prediction. The supercapacitor in the hybrid energy storage system is able to switch on to cater for peak power without delay. This is crucial in maintaining an optimised battery depth-of-discharge (DOD) in order to reduce the rate of battery damage thru a degradation mechanism which is caused from particular stress factors (especially sulphation on the battery electrode and electrolyte stratification).

ACKNOLEDGEMENT

This thesis and research would not been possible without the support of many people, whose contribution should not be disregarded. If there is the person to whom I have owed the most during the course of PhD, he would be my principal supervisor, Professor Dino Isa. For my supervisor's guidance and supervision during my PhD course assisted me in further enhancement of my personal development and analytical skill as well as the freedom given to do research with optimal supervision, understanding, patience and support, words cannot express my sincere gratitude. My second supervisor – Dr. Niusha is thanked for the generous assistance in Genetic Programming and the effort in proofreading my thesis. All these have brought significant and positive impact on this thesis.

Encouragement and financial support from my loving parents, Mr. Chia Kang Seng and Chua Ah Moy mean a lot to me in completing this research. I would like to thank my siblings to be attentive to my research. Also, this process would have been unthinkable without the unlimited support and love from my best friend, Miss Lennie. Lastly, I dedicate this thesis to my late brother who watched me from a distance while I worked towards my PhD.

AFFIRMATION

The work presented in this thesis is, to the best of my knowledge, original, and has not been submitted for any other degree. This research was carried out in the Department of Electrical and Electronics Engineering, University of Nottingham, Malaysia Campus during the period of January 2010 – December 2013. This thesis does not exceed 90000 words. The following publications have been partially based on the research work reported in the thesis:

- **Chia Yen Yee**, Ridhuan Ahmad Samsuri, Dino Isa, Ahmida Ajina and Khiew Pooi Sim, 'Optimization of Process Factors in Supercapacitor Fabrication using the Genetic Algorithm to Optimize Taguchi Signal-to-*Noise Ratios'*, International Journal of Engineering Science and Innovative Technology (IJESIT) Volume 1, Issue 2, November 2012.

- Tijjani Adam and Uda. Hashim, Dino Isa and **Chia Yen Yee**, 'An Electric Double-Layer Capacitor (EDLC) Production for Optimum Energy Driven Communication System Using Taguchi Technique', 2012 Fourth International Conference on Computational Intelligence, Modelling and Simulation, September 2012.

- **Chia Yen Yee**, Niusha Shafiabady, Dino Isa, 'Optimal Sizing of a Hybrid Supercapacitor-battery Energy Storage System in Solar Application using the Genetic Algorithms', Volumne 1, Issue 1, International Journal of Robotics and Mechatronic, 2014.

- **Chia Yen Yee**, Lee Lam Hong, Niusha Shafiabady, Dino Isa, 'A Load Predictive Energy Management System for Supercapcitor-Battery Hybrid Energy Storage System in Solar Application using the Support Vector Machine', Applied Energy, 2014. (Submitted and under review, April 2014).

- **Chia Yen Yee**, Niusha Shafiabady, Dino Isa, 'System Configuration for Hybrid Supercapacitor-Battery Energy Storage System in Solar Application', International Journal of Energy Research 2014. (Submitted and under review, June 2014).

- **Chia Yen Yee**, Ridhuan Ahmad Samsuri, Dino Isa, 'Using Genetic Algorithm to Optimize Supercapacitor Fabrication', World Academy of Science, Engineering and Technology WASET August 2012 Kuala Lumpur International Conference.

TABLE OF CONTENTS

LIST OF FIGURES

LIST OF TABLES

NOMENCLATURE

GA	Genetic Algorithm
SVM	Support Vector Machine
RES	Renewable Energy System
SOC	State-of-Charge
DOD	Depth of Discharge
O&M	Operational and Maintenance
BMS	Battery Management System
SLA	Sealed-lead Acid Battery
SB-HESS	Supercapacitor-battery hybrid energy storage system
SVMR_EMS	Support Vector Machine/Regression Energy Management System
ESR	equivalent series resistance
NPV	Net Present Value
LCE	Levelised Cost of Energy
NPC	Net Present Cost
IC	Intermittent Charging
TSC	Three Stage Charging
ICC	Interrupted Charge Control
EDLC	Electric/Electrochemical Double Layer Capacitor
HESSS	Hybrid Electrical Energy Storage Systems
ECU	Electronic Control Unit
SRM	Structural Risk Minimization
HYBRID2	The Hybrid Power System Simulation Model
GAMS	The General Algebraic Modeling System
ORIENTE	Optimization of Renewable Intermittent Energies with Hydrogen

for Autonomous Electrification

HOMER   Micropower Optimization Model

PV   Photovoltaic

LOLP   Loss of Load Probability

LPSP   Loss of Power Supply Probability

UL   Unmet Load

ARES   Advanced Reciprocating Engine Systems

WECS   wind energy conversion system

HOGA   Hybrid Optimization by Genetic Algorithm

ACS   annualized cost of system

PSO   Particle Swam Optimization

SOH   State-of-Health

PbO_2   lead dioxide

$PbSO_4$ lead sulphate

Pb   Lead

H_2SO_4   sulphuric acid

Ah   battery capacity

U_O   Equilibrium voltage

g   Electrolyte coefficient

ρ   Internal resistance

M   Transfer overvoltage coefficient

C   Capacity coefficient

U_{cell} Voltage of the cell

I_{batt} Current of the battery

NREL   National Renewable Energy Laboratory

C.S.F	capacity shortage fraction
STC	standard test conditions
L_d	Critical Discharge Power
C_{PV}	Capital cost of PV
C_{WG}	Capital cost of wind
C_{BAT}	Capital cost of battery
C_h	Capital cost of wind generator per meter
C_{CH}	Capital cost of charge controller
y_{CH}	Estimated lifespan of charge controller
y_{INV}	Estimated lifespan of invertor
y_P	Lifespan of battery
C_{INV}	Capital cost of inverter
R	Battery expected lifetime
N_{BAT}	number of batteries
$C_{cycleDOD}$	the number of charge and discharge cycle
ECU	electronic control unit
AR	Autoregressive Technique
ARMA	Autoregressive Moving Average
MAPE	mean absolute percentage error
BPNN	Back-propagation neural network
SRM	Structural Risk Minimization
ACS	annualized cost of system

CHAPTER 1

INTRODUCTION

1.1 Overview

This thesis deals with using constraint optimization implemented using a Genetic Algorithm (GA) for guaranteeing robustness in the manufacturing process. A GA with a different objective function was also used to reduce the implementation cost of supercapacitors in solar energy systems. This was done by first fabricating supercapacitors of 22 Farad to be tested in a lab scale system in order to establish the hypothesis that including supercapacitors in a Support Vector Machine (SVM) hybrid battery energy management system increases the operating lifespan of the battery in question.

These supercapacitors were fabricated in the Supercapacitor Pilot Plant at the University of Nottingham Malaysia Campus using a Genetic Algorithm to optimise Taguchi Signal-to-Noise ratios in order to obtain a more robust supercapacitor better suited for solar application conforming to those standards - IEC 62391 [1], IEC 62391-2-1 [2]. In actual fact, supercapacitors of 165F, 48V are used for 2kW solar applications, however in the supercapacitor pilot-plant here, equipment to fabricate a supercapacitor of this size were not available.

(a)

(b)

Figure 1 (a) (b) Supercapacitor Pilot Plant

Developed by John Holland, Genetic Algorithms (GA) are general-purpose global search and optimization methods applicable to a wide variety of real life problems [3, 4]. GA are meta-heuristic search algorithms based on the evolutionary ideas of natural selection and genetics [3, 4, 5, 6]. This means that in meta-heuristic algorithms rules and randomness are combined to imitate

natural phenomena. Furthermore, the GA is one of the most popular meta-heuristic search algorithms that is used by many researchers to solve real-world engineering optimization problems [3]. GA's successfully overcome deficiencies of conventional numerical methods [4] by intelligent exploitation of the search landscape it passes thru [7]. It manipulates the population of potential solutions through genetic operators that mimic the biological evolution process, hence converging to an optimal solution [8, 9, 10]. Although randomized during initialization, GA's are by no means random; the algorithms employ some form of selection to bias the search towards good solutions which follows the principle of 'survival of the fittest' [11, 3]. It efficiently exploits historical information gained from previous generations to directly search the region where better (fitter) performing individuals lie within the search space [9].

The Taguchi technique is used when a more robust product is needed under volume manufacturing conditions [12, 13]. It is not used to obtain just one 'golden' unit, but it is used to optimise the whole process for certain parameters, which in our case is capacitance and equivalent series resistance (ESR). Here robust and optimise means reproducible and consistent rather than the biggest or smallest value.

Figure 2 Fabricated Supercapacitor - Enerstora

Furthermore cells of 22 Farad, 2.3V were fabricated in a cylindrical package in order to be used in the lab scale system for determining how much battery life can be prolonged due to the presence of the supercapacitor.

(a)

4
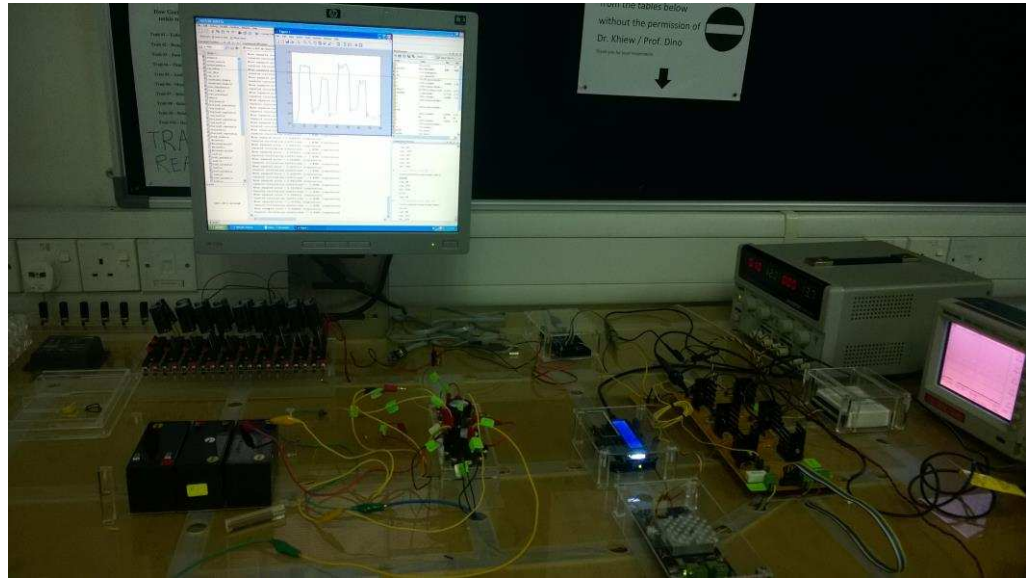
(b)
Figure 3 (a) (b) Lab Scale hybrid energy storage System

With this, it is hoped to prove that incorporating supercapacitors in an energy management system, which contains a battery, will allow the battery to have a longer lifespan due to it being able to stay at a higher state-of-charge SOC) for a longer period of time. This result is reflective of the situation when supercapacitors are included in energy management systems which operate at a much higher voltage such as the one available at the University of Nottingham Malaysia Campus (2kW solar cabin).

To further improve the performance of the implemented system on the lab scale level while reducing its overall implementation cost due to power electronics, the Support Vector Machine (SVM) was employed in the energy control strategy. Basically, this enables a supercapacitor to be integrated into a prototype hybrid energy storage system used for solar applications in an economically feasible way. For large systems, such as the 2kW solar cabin, based on the research carried out here, this saving is even greater. It is approximately 36%.
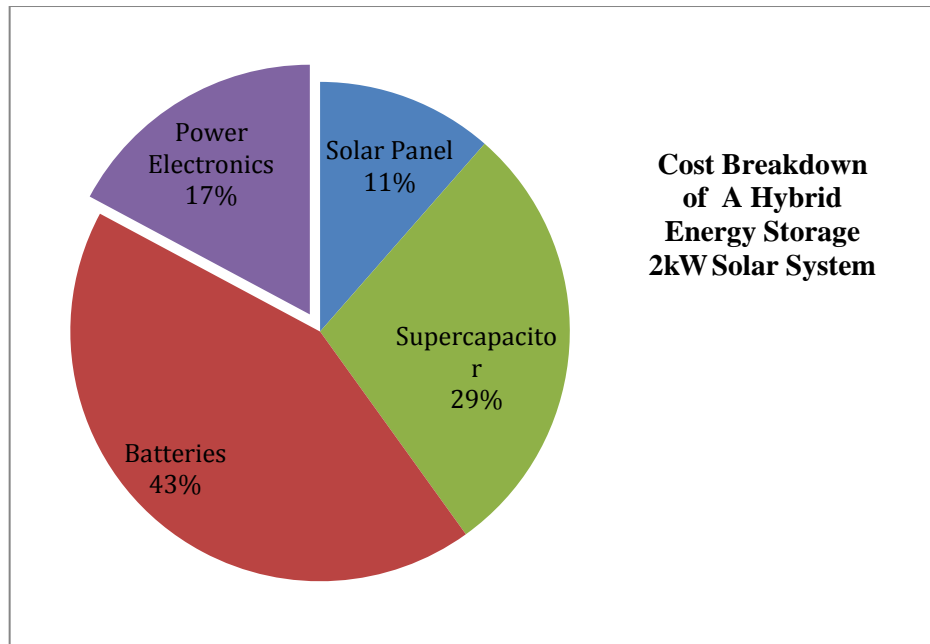
(a)
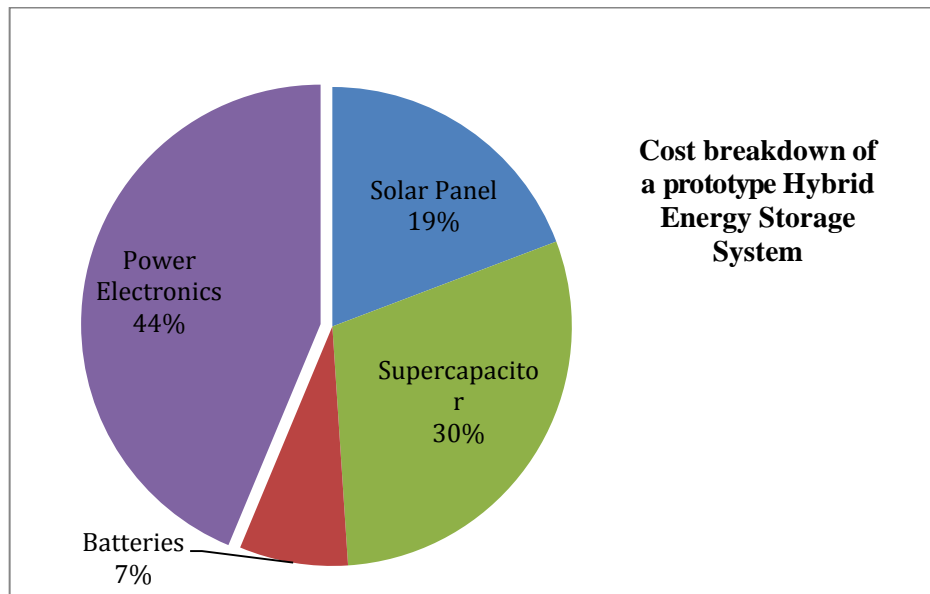
(b)

Figure 4 (a) (b) Comparison between cost breakdowns of A Hybrid Energy Storage 2kW solar system with lab-scale prototype Hybrid Energy Storage system
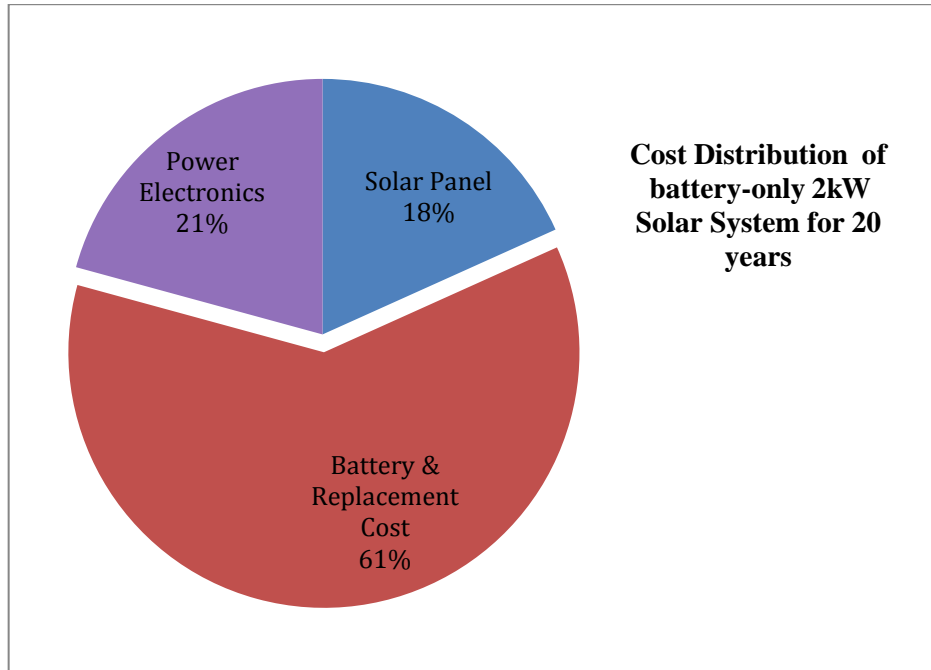
(a)
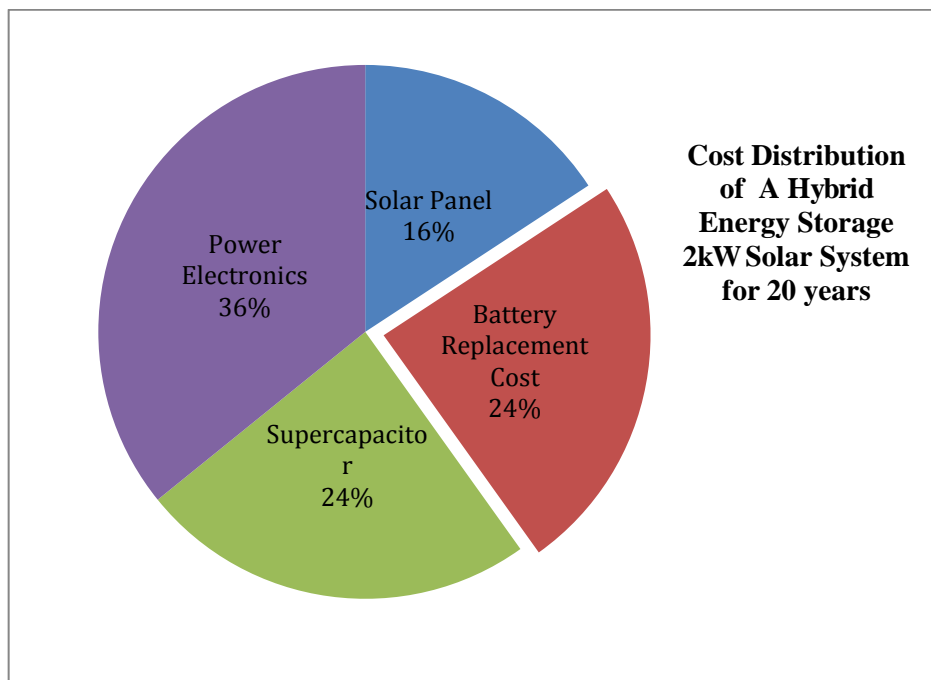
(b)

Figure 5 (a) (b) Comparison between cost breakdowns of 2kW system with and without supercapacitors for 20-years.

(a)

Cost Breakdown of a Battery-only Energy Storage Prototype Solar System

Solar Panel 12%

Power Electronics 17%

Battery & Replacement Cost 71%

(b)

Cost Breakdown of a Hybrid Energy Storage Prototype System

Solar Panel 6%

Supercapacitor 15%

Power Electronic 20%

Battery & Replacement Cost 59%
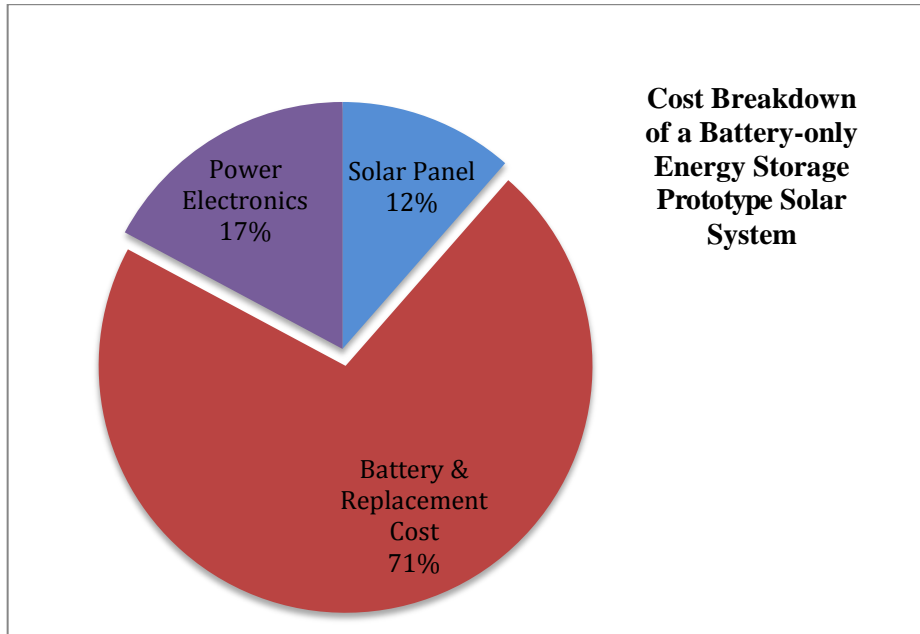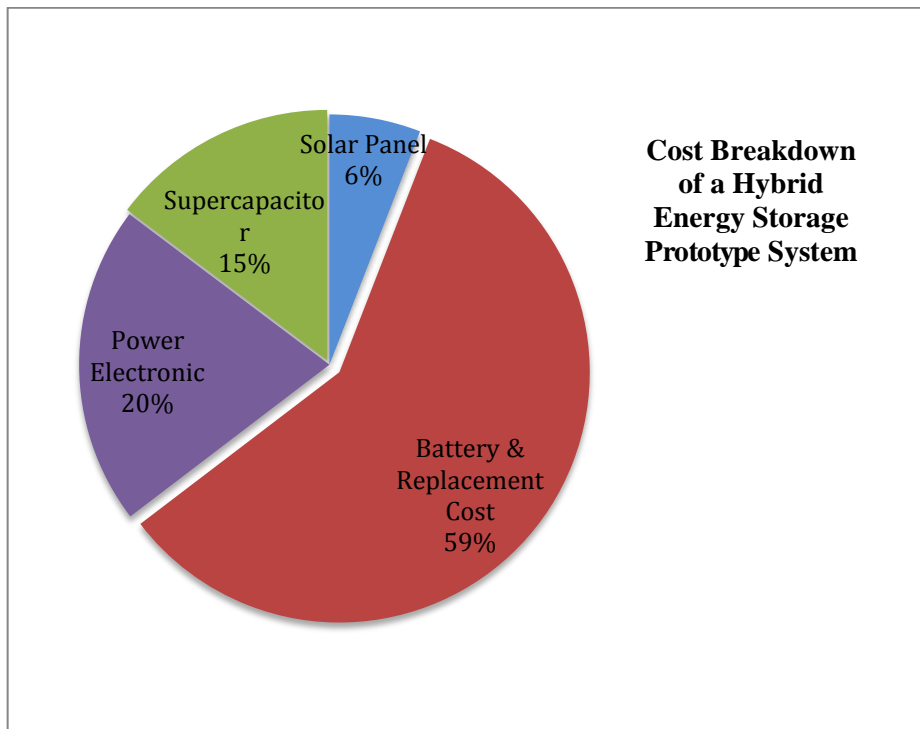
Figure 6 (a) (b) Comparison between cost breakdowns of prototype system with and without supercapacitors for 20-years.

The four previous pie charts in Figure 5 and 6 are the comparisons between 2kW and the lab scale model for 20 years period. From the pie charts shown above, conventional renewable energy system is not cost effective mostly is due to the replacement cost of the batteries for long run. Replacement cost of the battery often causes high impact on the total cost of the system. One of focus in this project is to reduce the cost of replacement battery by prolonging battery lifespan (about more than 5 years prolonged). Besides that, the expensive power electronics to build the bi-directional converter in hybrid energy storage system is eliminated by implementing an energy management system which predicts load demand using SVM.

In relation to real life applications such as those that can be represented by the 2kW solar cabin in this project, a GA with a new fitness function also known as (objective function) was used to minimise the number of cost components, which includes the initial cost of the components, operational and maintenance cost in the proposed supercapacitor-battery hybrid energy storage system. The proposed fitness function was proven to reduce the net present cost of the system and improve the loss of power supply probability for a 20-year round power system based on a comparison with a commercially available software called Hybrid Optimization Model for Electric Renewable (HOMER) [14].

In summary, the main motivation of this project is to incorporate a supercapacitor within a solar energy system to minimise the cost in terms of the number of batteries and the power electronics, subject to the constraint that the load demand is completely covered, resulting in zero load rejection. One further aim is to be able to propose a method of consistently manufacturing robust

supercapacitor cells which are able to conform to the standards previously mentioned. This aids in the cost reduction of the overall system by making the supercapacitor cheaper to produce than the battery it replaces.

This research consists of three main components.

1. The first component in this project chiefly deals with a practical methodology in tackling multiple-criterion optimization manufacturing process by considering the advantages of both the Taguchi technique and GA. The outcome of this part of the research is to achieve a robust supercapacitor by searching the weighted signal-to-noise ratio as the measure performance in relation to capacitance (C) and equivalent series resistance (ESR) of a supercapacitor. It shows the robustness of the fabricated supercapacitor is preferable than the commercial supercapacitor according to the British Standard. The standard deviation for the supercapacitor values (capacitance and ESR) is lower after the process fabrication supercapacitor is optimised. – (this is presented in Research Methodology Chapter 3, Section 3.3 and result shown in Section 4.3.2 of this thesis).

2. The next component of the thesis focuses on the optimal sizing of the proposed solar supercapacitor battery hybrid storage system using GA. This proposed stand-alone solar system incorporates photovoltaic panels, charge controller, a hybrid energy storage system and load. A solar energy source is a clean and noise free source of electricity, even so, a reliable energy storage system is required as an energy buffer to bridge the mismatch between available and required energy. The proposed energy storage technology employed in this project is the

integration of lead-acid batteries (that acts as a main energy storage device) and an auxiliary energy storage device which is the supercapacitor. The proposed hybrid energy storage system leads to system cost reduction. This is accomplished by reducing the number of batteries and also the battery replacement costs by prolonging battery lifespan. This is important, for example, in a common household load profile, where there is certain intermittent demand for high current such as when a motor starts up. This can be 6-10 times the normal operating current of the motor and thus affects battery life [15, 16]. In a conventional stand-alone solar system, lead-acid batteries are always used to satisfy peak current burst. Other than reducing battery life, the number of lead-acid batteries in this situation can be impracticable large in order to match the peak current requirement. Non-optimal sizing of the battery for this purpose is proven to be costly and not effective as the peak current demand might only need to be met for a few seconds at a particular time. Hence the need for an optimization strategy which minimises the quantity of batteries while still satisfying the load requirement. − (this is presented in Research Methodology Chapter 3, Section 3.2.2 of this thesis).

3. The batteries in a conventional stand-alone solar system are replaced typically every 3-5 years depending on the load demand curve [15, 16]. If not, an oversized battery system is suggested to cater for the peak power and also to save the battery lifespan. Generally, this is due to inconsistent battery charging by the solar energy source, as the output of the source is heavily dependent on weather condition. The output of the

solar energy source fluctuates according to the intensity of the light, resulting an inconsistent battery charging and discharging cycle. Also, heavy current discharging due to a heavy load requirement will equally affect battery life.

The stress factor on the battery such as irregular discharging rate and extensive time at the low state-of-charge (SOC) could increase the rate of damage to the battery. The notable damage mechanisms are related to battery electrolyte stratification and also irreversible sulphation, which greatly shortens battery lifetime.

Ideas have been put forward to extend battery lifespan and reduce battery quantity used in the system, where one solution is done by pairing batteries with super capacitors as mentioned previous part. When paired with supercapacitors, the former can act as a buffer, relieving the battery of pulsed or high power drain, as well as reducing the depth of charge discharge cycles by means of buffering. This idea emerges because the supercapacitor has a greater power density than the battery and this allows the supercapacitor to provide more energy over a short period of time. Conversely, the battery has a much higher energy density and this allows the battery to store more energy and supply to the load over a longer period of time. Hence, the role of supercapacitors is to supply sufficient energy for peak power requirements while the role of battery is to supply continuous power at a nominal rate. – (this is presented in Research Methodology Chapter 3, Section 3.2.3 and result is shown in Section 4.2.3 of this thesis).

Pairing supercapacitors and batteries however requires expensive and extensive power electronics, elevating the already high costs associated with these hybrid photovoltaic systems. Figure 7 [17] shows the power electronics associated with conventional hybrid energy system.

(a) Prototype bi-directional dc-dc converter unit module	(b) The bi-directional DC/DC converter(full-bridge type topology)

(c) Power stage design of converter unit module

item	symbol	device	note
MOSFET	Sc1-Sc4, Sa	IXFN180N20	180A, 200V Rds(on):10mΩ
IGBT	Sb1-Sb4	SGL50N60RUFD	50A, 600V Vce : 2.2V
transformer	T1	PQ5050	Nb : 9 turns Nc : 6 turns
inductor	Lf	PQ5050	N : 15 turns
clamp capacitor	Ch	35uF/250V	
filter capacitor	Cf	220uF/400V, #2	Parallel Connection
fuse	F1	100A/100V	Low Voltage Stage
fuse	F2	25A/500V	High voltage stage

Figure 7 (a) (b) (c) Bi-directional dc-dc Converter from [17]

There are however, other methods, which could be used in developing these systems. For example, in this project the wide availability and affordability of microcontrollers nowadays allows these hybrid systems to be controlled using purely software methods such as by employing the Support Vector Machine (SVM) pattern classifier to decide when to switch energy sources depending on the load requirement. The supervised learning system in SVM allows the

prediction of load demand before it occurs. These aid in reducing the delay in delivering power even when there are a few possible cases to be considered in connecting or disconnecting battery and supercapacitor to the load. This would not only lower the operational cost, but at the same time, allows the hybrid photovoltaic system to be flexible, which comes in handy in places with different seasons and unpredictable weather. The implementation using a microcontroller also allows the monitoring of multiple parameters, which may affect the efficiency of the hybrid photovoltaic systems, optimising the operation of these systems by taking appropriate actions when needed.

1.2 Problem Statement

The main effort in this research is to solve the problem of combining supercapacitors with batteries into a hybrid energy system which is made economically feasible thru process and operational optimization using genetic algorithms and the use of software in place of some of the power electronics.

Robustness of a product or process is important in increasing the yield and the consistency of the product to make it economically feasible in the application. The effort in robust design strategy for process fabrication of supercapacitors is to make the supercapacitor insensitive to the probable causes of performance variation. The goal of this component project is to determine the optimal configuration of the supercapacitor process parameters that reduces variation. In the proposed supercapacitor-battery hybrid energy storage system, a robust process fabrication strategy eliminate those undesired spread in capacitance values which can be attributed to several factors such as manufacturing equipment tolerance, the temperature gradient in the system, input material characteristics and cell aging. In most of power applications, considerably high voltages are always required. However, the supercapacitor has a low operational voltage, the maximum voltage that can be applied to a supercapacitor is about 2.3V. To reach the required application voltage the supercapacitors are connected in series or matrix to form a power system. However, series connection leads to unequal voltage distributions because the capacitance is not exactly the same for each device. In some cases this leads to the use of balancing circuits which reduce the efficacy of the supercapacitor bank. When balancing circuits are not used (sometimes to save operational costs), the systems runs the risk of depleting the battery even more because the

supercapacitor will act as an additional load when its voltage is lower than the batteries nominal voltage.

Capacitance also varies with different DC bias voltages [18, 19, 20]. The change in capacitance with applied DC voltage (a phenomenon also known as DC bias) further complicates the task of choosing the right capacitance. Therefore, a manufactured supercapacitor, which has high reproducibility and reliability, is crucial in maximizing the power reliability of the supercapacitor after it is integrated in the power system to meet peak power demand.

Optimization the fabrication process of supercapacitors is a multi-response problem, which involves optimising two output responses to improve the product robustness. In optimising the fabrication process with the proposed Taguchi-GA technique, inconsistent engineering judgment has been eliminated. The limitation of the Taguchi Technique in performing well for multi-response optimization problems has been overcome by formulating a way to include the Genetic Algorithm within the Taguchi method. In previous research [21], Vining and Myers presented a methodology within the framework of Taguchi's technique using Response Surface Method using a dual response approach. Del Castillo and Montgomery [22] discussed that non-linear programming solutions, i.e. Generalized Reduced Gradient algorithms can lead to better solutions than those obtained with the dual response approach. Therefore, a consistent optimization technique that eliminates engineering's judgment is important to obtain a set of optimised process parameters for fabrication supercapacitor. This is to ensure small standard deviation of the supercapacitor capacitance and voltage.

Optimal sizing the supercapacitor-battery energy storage system for solar application using GA is presented in Section 3.2.2. Again, consistent values of capacitance and voltage are important for an optimised system operation. This is because the optimal configuration of the system components such as the number of solar panel, number of batteries, number of supercapacitors and number of charge controller is determined based on the specification of the components and the required design of the system. Furthermore, the optimization algorithm is often constraint by the nominal state-of-charge (SOC) batteries, power output of components and lifespan of the components. A mismatch of the capacitance and voltage of supercapacitors could activate and speed-up the damage mechanism of batteries. This is not advantageous in the system as replacing batteries in the system is costly in the long run. However, the optimization strategy proposed here also minimises the number of batteries but it still able to bridge the mismatches between supply and load demand when renewable energy sources are low. The system is also able to deliver peak power without delay by coupling to an optimal number of supercapacitors.

Another challenge in coupling supercapacitors and batteries is implementing an energy management system to control the energy flow from the hybrid energy storage system economically and accurately. A block diagram depicts the system architecture for the implemented prototype is shown in Figure 8.
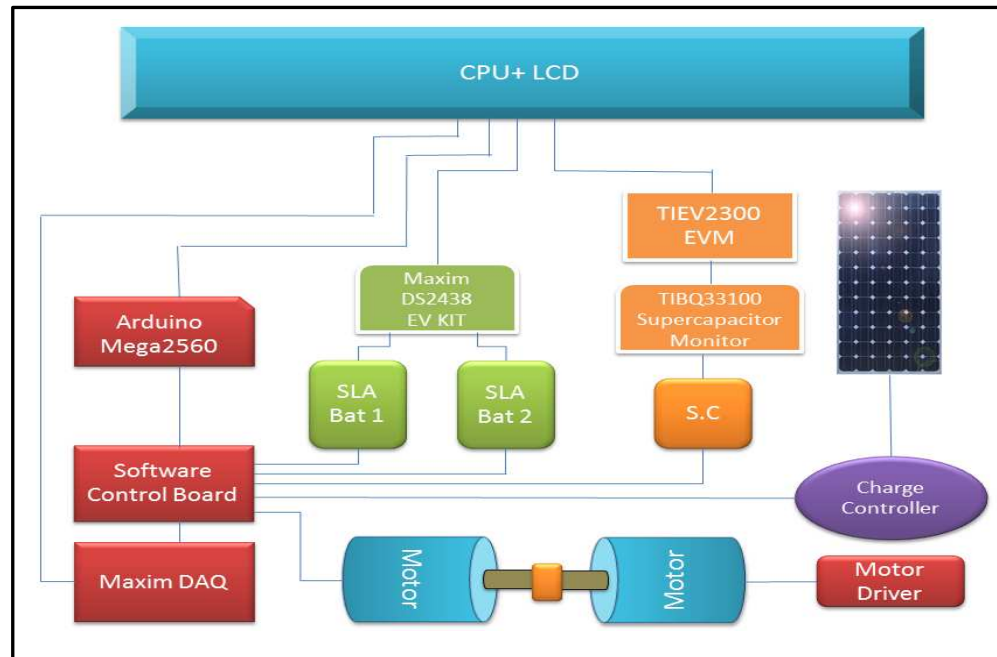
Figure 8 System Architecture for Prototype

To be able to compete with the efficiency and cost of other approaches in balancing the voltage level of both battery and supercapacitor in the system without delay, a load forecasting system using SVM and SVR is implemented in the energy management system. The lead acid battery will be recharged when its SOC reaches 80%. This is to improve the lifespan of the lead-acid battery as its recommended Depth of Discharge (DOD) is 50%. Battery supplies the continuous energy to meet the average load demand; while, the supercapacitor provides instantaneous power to cater for the peak load demand. The role of supercapacitor to meet peak load demand allows for the downsizing of battery capacity, reducing the depth of discharge (DOD), reducing the sulphation of battery, and most importantly, improving the battery's lifespan [23]. Hence, it's crucial for the two storage banks to be switched 'ON' and 'OFF' at the right timing in accordance to the occurrence of peak load current to achieve optimal performance. In this, the SVM-SVR will analyse the real

time data of the system, perform classification, followed by regression to predict the load currents, and perform the switching action efficiently.

1.3 Research Objectives

The main effort in this research is to solve the problem of combining supercapacitors with batteries into a hybrid energy system which is made economically feasible thru process and operational optimization using genetic algorithms and the use of software in place of some of the power electronics. In other words we aim to minimise operational cost of a solar system by integrating supercapacitors into a hybrid lead acid battery energy management system.

This can be accomplished by reducing the number of batteries used for storage and extending battery life by allowing the supercapacitor to cater to peak current demand. One further aim is to be able to propose a method of consistently manufacturing robust supercapacitor cells which are able to conform to the standards previously mentioned.

In supporting the main aims stated above, several research issues are to be investigated and solved:

1. To identify and optimise the significant parameters of the fabrication process simultaneously, by combining the Genetic Algorithm with Taguchi DOE methodology and improving the Taguchi Signal-to-noise Ratio which is a measure of product robustness.

2. To implement a fitness function which determines the optimal size (and therefore reduce the cost) of a stand-alone hybrid supercapacitor-lead acid battery solar energy system using a Genetic Algorithm.

3. To design a supercapacitor-lead acid battery hybrid energy storage system, which prolongs battery life and reduces the number of batteries used.

4. To employ Support Vector Machine in the hybrid energy storage control system in order to reduce the use expensive power electronic components.

1.4 Scope of Research

This project covers and focuses on increasing product robustness and the reduction of operational cost of a hybrid energy storage system consisting of a supercapacitor and battery. It is not within the scope of this project to discuss material improvements or the absolute improvement of capacitance and ESR thru the materials or the process.

1.5 Thesis Structure

In Chapter 1, an overview, the objectives, and the scope of the project are covered. The most important points are related to cost reduction issues for hybrid solar energy systems. In chapter 2, the appropriate literature review is presented. This chapter reviews the current state of the art for hybrid solar energy storage systems in terms of the system configuration, the alternative energy storage device, the optimization strategy, cost improvements and energy management systems.

Chapter 3 covers the research methodology which was followed to fulfil the objectives stated in this chapter which includes the improvements afforded by the hybrid system as opposed to "battery only" energy storage strategies.

Chapter 4 presents the result and discussion of the three main parts of the project; the integrated Taguchi- GA method in process optimization; the optimization of the system size for the complete hybrid renewable energy storage strategy and the use of the SVM to predict load requirements based on a certain LPSP (Loss of Power Supply Probability).

Finally Chapter 5, reviews the project objectives and discusses the results obtained using the methodology prescribed in chapter 3. Potential future work is also presented.

CHAPTER 2

LITERATURE REVIEW

This chapter reviews the current state of the art for hybrid solar energy storage systems in terms of the system configuration, the alternative energy storage device, the optimization strategy, cost improvements and energy management systems.

2.1 System Configuration of Conventional Battery Single Energy Storage System in Renewable Energy System (RES)

There have been a lot of researches being done to improve the practicability of renewable energy generation systems. It appears to be common for renewable energy generation systems to incorporate a storage element such as a battery to complement the system. Several papers regarding the improvement on renewable energy generation systems were reviewed and a brief description of each paper are included below.

Ravinder Singh Batia, S. P. Jain, Dinesh Kumar Jain and Bhim Singh conducted various simulations in their study titled "Battery Energy Storage System for Power Conditioning of Renewable Energy Sources" to demonstrate the role of an energy storage system. The aim of this study is to reduce the transient voltage variations, load leveling, reactive power control and harmonics elimination in renewable energy sources [24]. A controller has also been included to manage the charging and discharging of the battery. The modeled system however, does not include an element to buffer the rapid charging and discharging of the battery as well as load buffering to protect the

battery, hence the battery is subjected to stresses which greatly reduce its lifespan.

There are many types of battery technologies available. Niraj Garimella and Nirmal- Kumar C. Nair examined the use of different types of batteries as an energy storage system in small-scale renewable energy in the paper titled 'Assessment of Battery Energy Storage Systems for Small Scale Renewable Energy Integration' [25]. A comparison of various characteristics has been made between 4 types of batteries, which are lead acid, NiCd, NiMH and Li-Ion batteries. It is found that NiMH and Li-Ion batteries have a faster rate of increase in battery voltage and these batteries also reached their nominal voltage in a faster time compared to lead acid and NiCd batteries. The power output of the batteries were also compared and it is found that the NiMH battery produces more power than the other batteries, while the lead acid and NiCd type has similar power output whereas the Li-Ion have the lowest peak compared to the other batteries, mainly because of its lower voltage value.
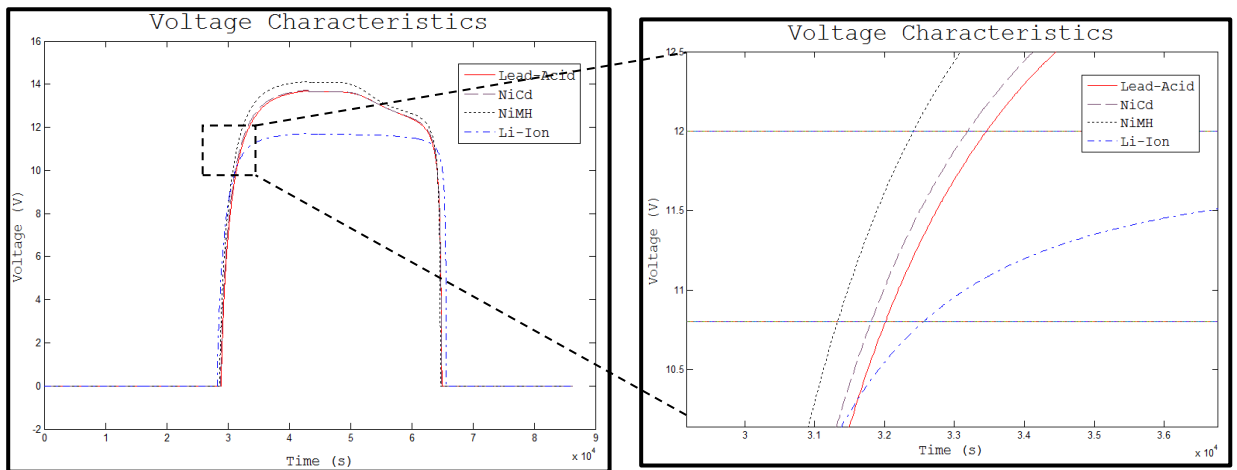
**Figure 9 Battery Voltage Characteristics
[25]**
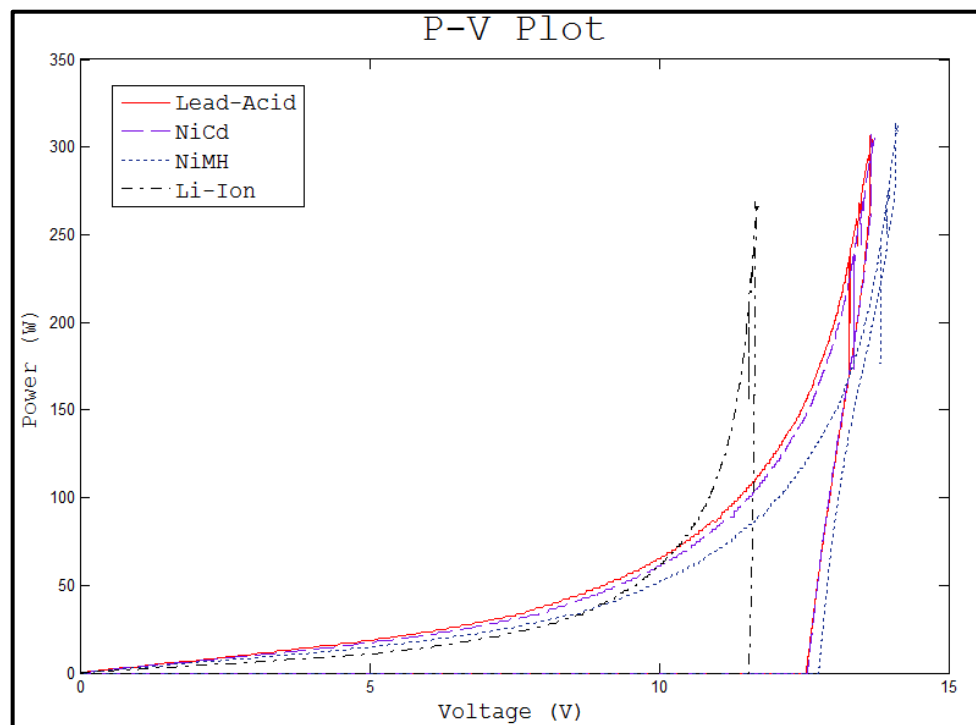
Figure 10 Power Voltage Plot Comparison [25]

Figures 9 and 10 (Retrieved 28th February 2011 [25]) show the comparison of characteristics of different batteries. The study concluded that

24

Nickel-Metal Hydride batteries shows the best potential in terms of power output, charge – discharge characteristics and voltage performance whereas lead acid batteries are the most common and affordable for a small scale setup among the other batteries [26, 25]. Hence, lead-acid batteries are chosen for the primary energy storage devices in this project.

2.1.1 Conventional System configuration for Maximizing Operating Lifespan of Batteries in Photovoltaic Systems

In the study titled 'Recommendations for Maximizing Battery Life in Photovoltaic Systems', James P. Dunlop and Brian N. Farhi observed the use of batteries in photovoltaic systems and made recommendations in issues related to battery type and characteristics, system sizing, installation, operation and maintenance as well as battery charge control in order to maximize the operating lifespan of batteries used in photovoltaic systems [27]. Recommendations were made based on different battery types and trade-offs between load availability and battery sizes as well as appropriate charge controlling of different types of batteries, however, the study does not take into account the use of buffering elements and the host of advantages it brings with it. The use of buffering elements in these systems on top of the design tweaks made based on the recommendations could further enhance the battery operating lifespan in photovoltaic systems.

S. Armstrong, M.E. Glavin, W.G. Hurley in another study titled 'Comparison of Battery Charging Algorithms for Stand-Alone Photovoltaic Systems' evaluates the effectiveness of different types of battery charging

algorithm namely, Intermittent Charging (IC), Three Stage Charging (TSC) and Interrupted Charge Control (ICC) and their ability to maintain a high State-of-Charge (SOC) [28]. The TSC was found to be the most suitable charging algorithm for a regularly cycled battery in a photovoltaic system as the TSC restored the battery's SOC to 100% in the quickest time although there were signs of overcharging. However, the TSC was found to cause the battery to have a higher average temperature compared to IC and ICC, nonetheless, the IC and ICC are only best utilized for standby applications [29].

SOC of the charging algorithms under the absence of a load [28]	SOC of the charging algorithms under varying load profiles [28]
Comparison of the charging efficiencies of the charging algorithm [28]	Battery temperature during the different charging algorithms [28]
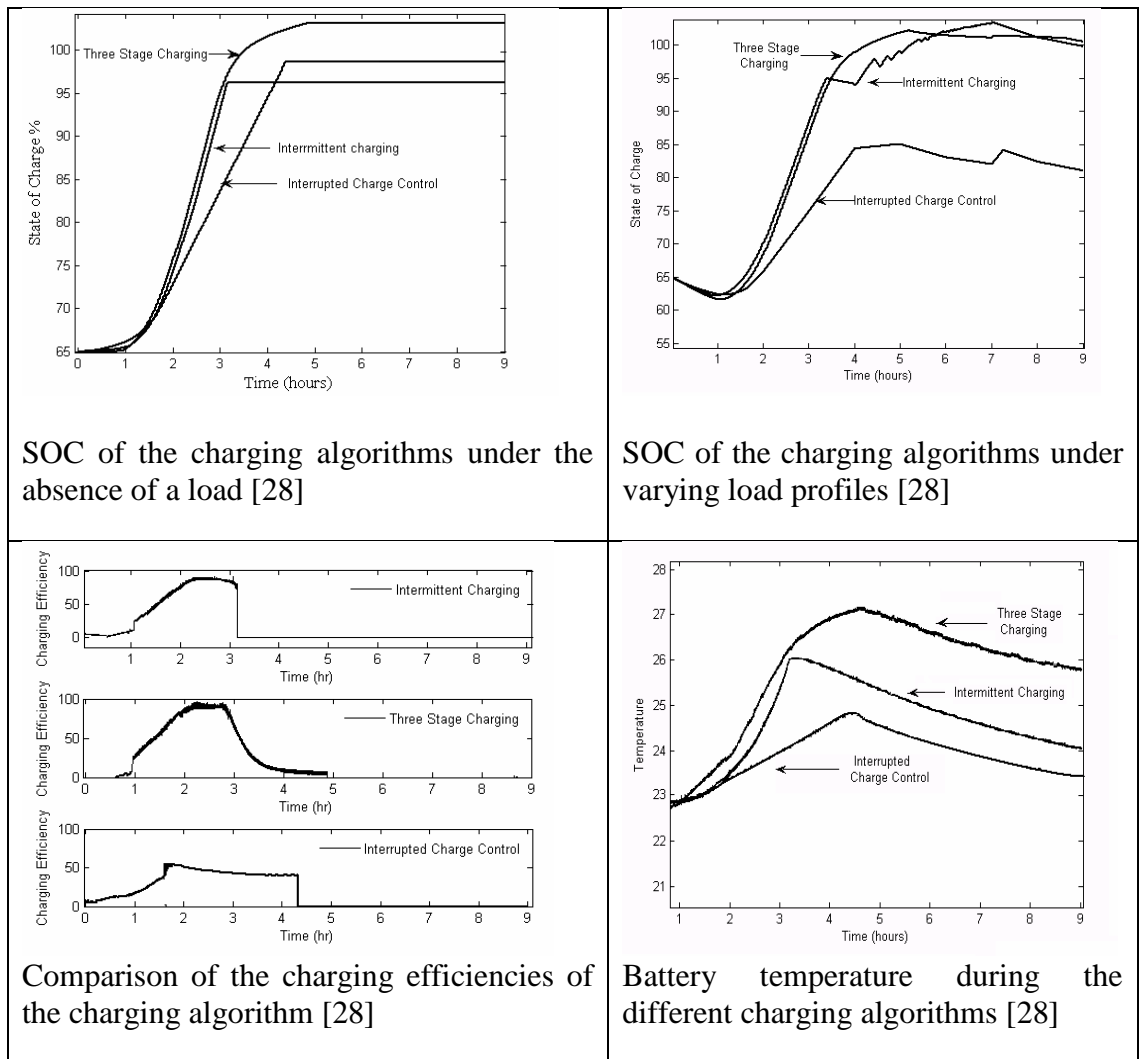
Figure 11 Characteristics of the different charging algorithm

However, the charging algorithms do not take into account the use of buffering elements during discharging phase, which further improves the

lifespan of batteries. In this project, only the discharging phase of the hybrid energy storage devices (battery and supercapacitor) is considered. This was done because the project addressed issues related to load rather than issues related to device resistance or other factors that affected energy storage. Battery individual energy storage system and Supercapacitor-Battery hybrid energy storage system are compared in this research. It prolongs battery lifespan and hence, improves system cost for the long run especially when the replacement cost of batteries and operational/maintenance (O&M) cost are taken into account.

In the paper titled 'A Battery Management System for Standalone Photovoltaic Systems', Shane Duryea, Syed Islam and William Lawrance outline the use of a Battery Management System (BMS), which consist of a series solar regulator and a discharge protection to allow intelligent control of charging and discharging of the battery in Photovoltaic Systems. The study also analyses the various techniques in measuring the SOC of batteries, which among others are methods based on Ampere-Hour Balancing with variable losses and terminal voltage measurements. The BMS measures the SOC of the battery to determine the available capacity, which enables intelligent control schemes to be implemented to prolong battery lifespan [30]. The study however does not take into account the use of buffering elements, which in turn limits the prolonging of the battery operating lifespan in a PV system as well as the host of advantages which comes with the use of a buffering element. Figure 12 [30] shows the model of the BMS integrated into a small standalone PV system. In this project, the energy control management system monitors the voltage drop of the batteries and microcontroller takes action switching on

supercapacitor for power bust) accordingly. SOC is measured to evaluate the remaining charges in the battery after every 20 cycles.
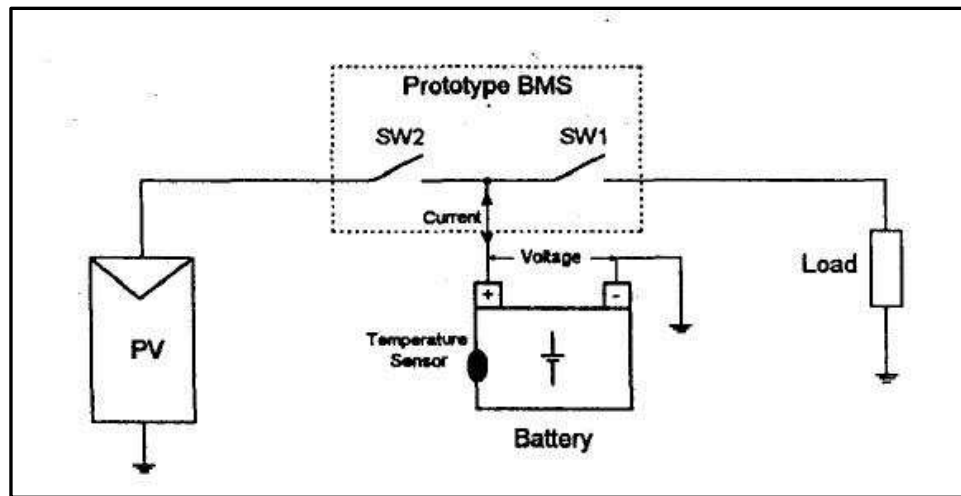
Figure 12 Modelled small standalone PV system with integrated BMS

Many researchers recognized the output of the renewable energy sources are not an ideal source for battery charging [16, 31]. The output of renewable energy sources is heavily dependent on the weather hence an unreliable supply curve is produced. An undeniable challenge of the renewable energy system is to show that the supply curve matches the demand curve. The conventional battery single system for solar application is remarkably costly and impractical. A huge number of batteries are required to meet the demand requirement [15]. Furthermore, an inconsistent of charging and discharging cycle is always the biggest damage mechanism for batteries. This is due to the unreliable power output from solar energy. The fluctuated power output does not guarantee an optimum charge and discharge cycle that resulting in a low battery state of charge for a long period. This is a very common stress factor that causes one of the damage mechanisms in battery, which is sulphation. Sulphation forms in sealed lead acid battery when it is constantly being cycled

at low state-of-charge (SOC). This is proven in [32, 33] that shorten the battery lifespan.

This project shows that the supercapacitor-battery hybrid energy storage system increases the practicability of the system which delivers power without delay and reduces the initial number of batteries and number of replacement batteries. It is also more environmental-friendly as most of the composition in supercapacitor can be more biodegradable as compared to battery.

2.1.2 System Configuration of Hybrid Energy Storage System

In this session, a buffer element is introduced – Supercapacitor (also known as ultracapacitor) to pair with battery. Fuel cells with hydrogen tank is not considered as an auxiliary energy storage device in this project as :

- It is costly due to the electro-catalyst used at the anode faradic reaction in fuel cells is expensive [34].

- Furthermore, output voltage drops approximately 50% of its rated voltage due to the second law of thermodynamics.

- Production storage of hydrogen tank can be tedious and less mobility as hydrogen has to be stored at pressure of 700atm in cylindrical-tanks. For rural area, fuel cells is not a good option as travelling to replace hydrogen tank in deep outskirt area is costly.

In the section below, some of the characteristics of the battery and supercapacitor are presented to explain what motivates supercapacitor act as an auxiliary energy storage device for our system. Furthermore, literature in this section also focus on the topology of the converter and energy control system

that have been researched to control the energy flow between the two energy storage devices. This section mainly covers the hardware approach and software approach used to control the energy flow within hybrid energy storage system which emerged repeatedly.

2.1.2.1 Battery

Based on the literature mentioned above, for solar charging application, the energy storage choice favors batteries with deep cycle . Deep cycle batteries are designed to have bigger plates and dissimilar chemistry to prevent the corrosive effect when full capacity is frequently utilized [35].

Lead acid batteries, which offer deep cycles, large capacity and wide availability is typically the choice for this application [15]. The comparison between flooded lead acid battery which has higher heritage and the Sealed Lead Acid (SLA) or VRLA battery are shown as below:

Table 1 Comparison between Flooded Lead Acid Battery and SLA battery

	Flooded Lead Acid battery	SLA battery
Cost	Significantly less expensive	Less expensive
Ventilation required	YES	NO
Maintenance	YES	NO
Potential liability	Tipping or spilling	NO

As shown in Table 1, the SLA battery is more costly as compared to flooded lead acid battery. However, SLA battery is chosen as the energy storage for its quality such as low capacity loss over time, maintenance-free, no poisonous gas and acid fumes emission, and installation freedom [36, 37]. Since SLA battery contains electrolyte that could last the life time of the battery, it

does not require watering as flooded lead acid battery do. The SLA also absorb the hydrogen gas within itself, hence it could be recharge without much ventilation. Lastly, SLA battery offers installation freedom as spilling will not occur even if it's overturned. On the other hand, SLA has shorter lifespan than flooded lead acid battery and it can only be discharged to 50% SOC for optimum performance unlike the flooded lead acid which could reach 80% [37]. Yet, the physical qualities has made SLA battery the better choice of energy storage for solar application.

The lead acid batteries have relatively high energy density; however, it does not have capability of instantaneous charging and discharging as those of a supercapacitor [38, 39]. It could store much energy but it takes a longer time to discharge and recharge. If it is driven at high C-rates especially in application which requires a sudden load current burst, the lifespan of the battery will be severely diminished. Besides that, high current drawing cause battery heat up and possibly causing a fire hazard due to thermal runaway [40, 41]. The deep discharge due to the large bust current drawn also cause the battery SOC to be lowered. The low battery SOC causes to stratification and sulphation of the battery, which reduces its lifespan [23, 27]. This is because the terminal voltage decreases when the battery discharges to a load. A cut-off voltage or the minimum allowable voltage is defined to designate the 'empty' state of the battery. The cut-off voltage varies according to the type of battery and the requirement of the application. In real life, a battery does not discharge in a constant voltage due to the internal cell resistance, IR losses and polarization effects of the electrodes [23, 42]
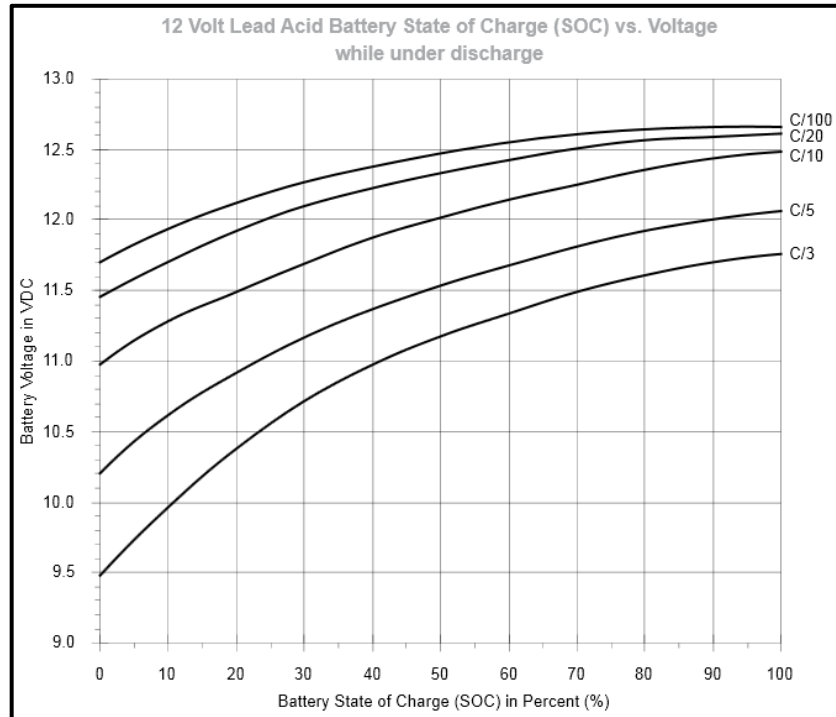
Figure 13 Battery discharge curves under different discharging rates
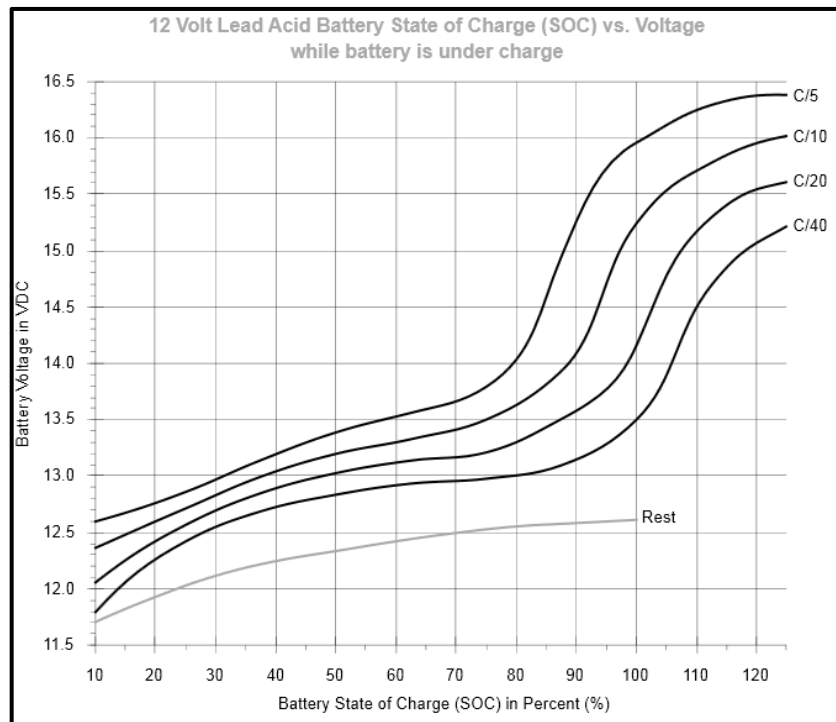
Figure 14 Battery charging curves under different charging rates

Figure 13 and Figure 14 (retrieved from [42] on December 2012) shows the effect of different charging and discharging rate or current on the voltage and the state-of-charge (SOC) of the battery. The C-rates shows the rate of charging and discharging in Amperes in order to normalize against battery capacity [42, 43]. For example, considering a battery of 100Ah, a C/5 rate means that the battery will discharge at a discharging current of 20 in an hour. As can be seen in Figure 14, 'Rest' means that where is no current flowing through the cells which leads to no charging or discharging cycle occurring.

As the current moves through the battery cells, the battery voltage reduces due to the internal cell resistance [42]. The cell's voltage will increase when there is current flow across the cell during the charging cycle. If the charging rate or current is high, the voltage increases faster. For discharging phase, the cell voltage drops due to the discharging current. As the discharging rate or current increases, the battery's voltage depression will be greater. This theory is valid for all battery regardless of its type, size or environment [42]. These stress factors that happened on the battery have increased the rate of damage mechanism of the battery. In the section below, damage mechanism and stress factor of lead acid battery are explained.

Damage mechanism and stress factor of lead acid batteries

Battery lifespan is shorter in battery alone system due to the higher rate of the damage mechanism within the battery [15, 32]. This is because the ageing mechanism of the lead-acid battery results from various stress factors which result from the performance characteristic of the energy storage systems. The most crucial stress factors listed are [44, 23, 45]:

1. Long hour in low SOC,

2. Inadequate discharging rate,

3. Elevated temperature,

4. Rare full charges,

5. Ah throughput

6. Partial cycling in low SOC,

7. Charging factor .

Lead-acid batteries lifespan are often affected in different ways depending on the conditions under which the batteries are operated. In report [23], a clear distinction has been made between the battery damage mechanism and battery ageing processes. Damage mechanism is irreversible damage on battery composition which cannot be restored as a new battery. Whereas, stress factor can be defined as the characteristic feature of the battery operating condition which ultimately changes the rate of damage mechanism. Stress factors and damage mechanism affect performance of a battery and the conclusively battery lifespan.

Pb +	**2H$_2$SO$_4$**	**+ PbO$_2$**	**Discharging**	**PbSO$_4$ +**	**2H$_2$O**	**+ PbSO$_4$**
Porous Lead	**Sulfiric Acid**	**Porous lead Dioxide**		**Lead Sulfate**	**Water**	**Lead Sulfate**
Active material of negative plate	Electrolyte	Active Material of positive plate	**Charging**	Active material of negative plate	Electrolyte	Active material of positive plate
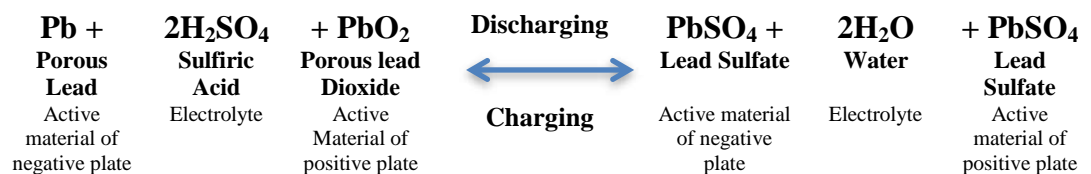
Electrochemical Reaction of Lead acid battery

The electrochemical reaction equation in a lead acid battery can be written as shown above and the chemical reaction is shown in Figure 15 [46]. During the discharge portion of the reaction, lead dioxide (PbO$_2$) is converted

into lead sulphate ($PbSO_4$) at the positive plate. At the negative plate sponge lead (Pb) is converted to lead sulphate ($PbSO_4$). This causes the sulphuric acid ($2H_2SO_4$) in the electrolyte to be consumed [45].
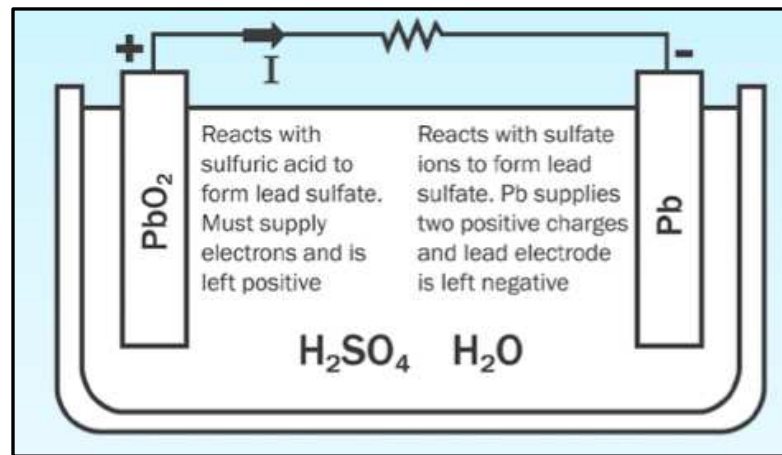
Figure 15 Chemical Reaction when a battery is being discharged

The idea of this supercapacitor-battery hybrid energy storage system (SB-HESS) has put forward to

'the less number of battery is discharged, the more frequently it is fully charged; the more favourable is the effect on the lifetime of a lead acid battery.'

Therefore, it is good to avoid deep discharge or over-discharge battery [47]. This is done to reduce the impact of certain stress factors, such as the forming of hard (or non-reversible) sulphation on the battery electrode [45], shedding, active material degradation, electrolyte stratification and a small impact on corrosion on the positive plate of the battery. In manufacturer technical manual, it is often mention to avoid or disconnect the battery from the load either electronically or manually when the end voltage (a function of the discharge rate) is reached [47]. It is the voltage point at which 100% of the usable capacity of the battery has been consumed or continuation of the discharge is useless because of the voltage dropping below useful levels.

Generally, the final discharge voltage per cell depends on the battery discharge rate and is given in battery data sheet. According to Power-Sonic [46], 'deep discharge' is defined as one that allows the battery voltage under load to go below the cut-off or ('final') voltage of a full discharge [46].

In most cases of typical RES, the batteries are stressed to supply power peak at times resulting large current drawn from the battery in a short period. However, in this approach, the battery discharge current is always fixed at a nominal value based on the desired state-of-charge. State-of-charge (SOC) or on the contrary depth of discharge (DOD) of battery indicates the remaining amount of energy available expressed as the percentage of the rated energy (SOC = 1 − DOD) [48]. In other words, SOC can also be defined as an expression as the available present battery capacity (Ah) as a percentage of the rated capacity (Ah) [49, 50], whereas, DOD can be explained as how deeply the battery is discharged.

This idea is aided by coupling the supercapacitor. The power peak deliveries are taken over mostly by supercapacitor and a small amount of energy from battery. This brings benefits in delivering power peak on time without delay and avoiding tremendous drain on the battery. With the exception of temperature, a SVM (Support Vector Machine) energy control system can favourably control all factors, so that the negative influence of temperature can be reduced.

2.1.2.2 EDLC Supercapacitor

Many literature have been presented to explain what motivates coupling supercapacitors with batteries to overcome the high depth of discharge of

battery in renewable energy system [51]. HEESS employs a supercapacitor, which has high power density, high rate of charging/discharging, no overcharging risk, and much higher life cycles as compared with lead-acid battery. This mainly benefits from how supercapacitor stores energy [52, 53].

EDLC supercapacitor fabrication is an emerging technology and has already been associated with many applications [53] due to its unique ability to fill the void between batteries and capacitors owing to its characteristics of higher energy density than conventional capacitors and higher power density than batteries [54, 55] as demonstrated in the Ragone plot below (retrieved from [54] on 6th November 2012) .
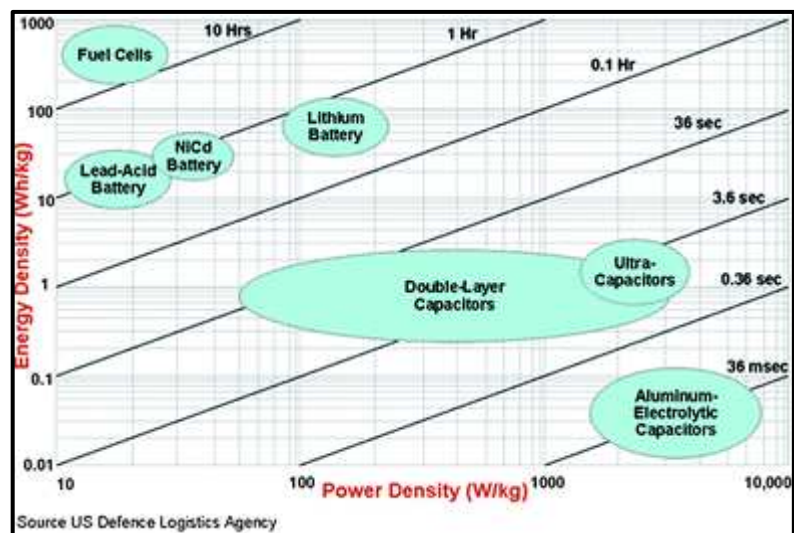
Figure 16 Ragone plot

A capacitor is an electric circuit element used to store an electrical charge temporarily [56]. Generally, it consists of two metallic plates separated and insulated from each other by a nonconductive material such as glass or porcelain [53]. Very high surface areas activated capacitors use a molecule-thin layer of electrolyte as the dielectric to separate charge [53, 39]. Supercapacitor resembles a regular capacitor except that it offers a very high capacitance in a

small package. Energy storage is by means of static charge rather than of an electro-chemical process inherent to the battery [34, 38, 39] The supercapacitor is categorized into two groups: the electric double layer capacitor (EDLC), and pseudo-capacitor, where both groups differs in the way they store the charges [57]. The electrochemical supercapacitor stores the charges through the reversible absorption of ions from an electrolyte on two porous electrodes [58]: This creates an electric double layer at the electrode. EDLC is used in this project due to its cycle life is higher than pseudocapacitor. It has about 5 times more cycle life than pseudocapacitor [53, 59]. Additionally, the capacitance of supercapacitor is dependent primarily on the characteristic (surface area and pore size of the distribution) of the electrode material (such as carbon and activated carbon) [53, 60]. These materials are cheap due to its wide availability. This reduces the commercial price of supercapacitor in the market as time goes [57]. However, the price of supercapacitor is still higher compare to the price of battery. In this project, the idea of fabricating supercapacitors with the desired capacitance and voltage is important to best-suits our optimised system. This is a crucial step to further optimise the cost of the system for a desired capacitance which might not be found in the commercial market.

EDLC does not involve chemical reaction, it merely absorb the ion in physical means [41, 53]. Energy is stored in the double-layer capacitor as charge separation in the double-layer formed at the interface between the solid electrode material surface and the liquid electrolyte in the micropores of the electrodes [53, 38, 39]. As shown in Figure 17 [55] , the EDLC can achieve up to millions of life cycles as the charging and discharging process does not affect the electrode physically [55] .
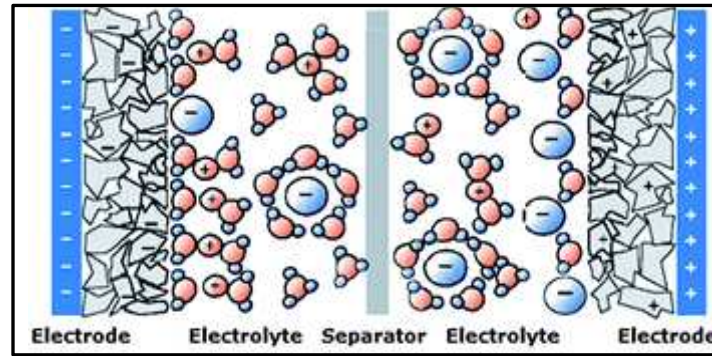
Figure 17 Electrochemical Double Layer Capacitor (EDLC)

The ions displaced in forming the double-layers in the pores are transferred between the electrodes by diffusion through electrolyte. The supercapacitor stores only a small amount of energy, yet it could deliver a rapid power discharge which made it suitable for high rate of charging and discharging operation.

$$C = \frac{\varepsilon_r \varepsilon_o}{d} A$$ **Equation 1**

where

ε_r is the electrolyte dielectric constant,
ε_0 is the permittivity of a vacuum,
A is the specific surface area of the electrode accessible to the electrolyte ions, and
d is the effective thickness of the EDL (the Debye length).

The energy stored can be calculated using the equation below:

$$E = \frac{1}{2} C V^2$$ **Equation 2**

Where

V is the cell voltage (in volts),

C_T is the total capacitance of the cell (in farads)

The EDLC has high capacitance as shown in the Equations 1 [61, 38, 39] and 2 [61, 38, 39] above. The reason behind its high power delivery capability lies in the fact that it has much lower internal resistance as compared to the battery [38, 39]. The Table 2 shows the internal resistance of lead acid battery and supercapacitor:

Table 2 Internal Resistance of Lead Acid Battery and Supercapacitor

Chemistry	Internal Resistances
Lead Acid Battery	2-30mΩ
Supercapacitor	0.02-0.2mΩ

As shown in Table 2 [40], since the internal resistance of supercapacitor is much lower than the battery the supercapacitor can supply a large burst of current to the load while the battery will supply the lower continuous power for a longer period of time. These properties complement the battery's limitation and allow the combination of SLA battery and supercapacitor in HEESS to possess both high energy and power density [51].

As mentioned early, a supercapacitor (also known as a ultracapacitor) is a double-layer electrochemical capacitor that can store thousands of times more energy than a common capacitor [62]. It shares characteristics with both batteries and conventional capacitors, and has an energy density [63] (the ratio of energy output to its weight) approaching 20% of a battery [64, 65]. In other words, a battery would have to be 80% heavier than the ultracapacitor in order to produce the equivalent energy output.

Moreover, the supercapacitor is very rugged and has a life expectancy of up to 50000 hours [15, 16]. This made it an ideal choice for remote solar application where maintenance is difficult. Hence, HEESS extends battery

runtime, reduces the battery size, minimises space requirements, reduces the pulse current noise and improve load balancing [56, 51]

In the HEESS formed by the supercapacitor and battery, their charging time, self- discharging time, power and energy densities and efficiency is listed in Table 3 [38, 15, 66]:

Table 3 Characteristics of Battery and Supercapacitor

	Battery	Supercapacitor
Charging Time	Several Hours	Fraction of seconds to minutes
Self-Discharging Time	Weeks to few Months	Hours to Days
Energy Density	10-100Wh/kg	<5 Wh/kg
Power Density	<500W/kg	>1000W/kg
Charging/Discharging efficiency	70%-85%	85%-98%

This means that a supercapacitor is suitable to couple with battery in situations where an instantaneous supply to power peak is required. It acts as a buffer element to bridge the supply to load demand when the battery is recharging [67, 16]. This hybrid system aims for zero load rejection. For example, consider an application in an environment where frequent outages last for less than two minutes. In such an environment, battery deterioration is excessive due to the high frequency of the outages. Moreover, the battery tends to require more time to recharge before it can supply to the next power peak. This would result in a highly reliable energy storage system that would require little or no maintenance. This is shown in Figure 18 [68].
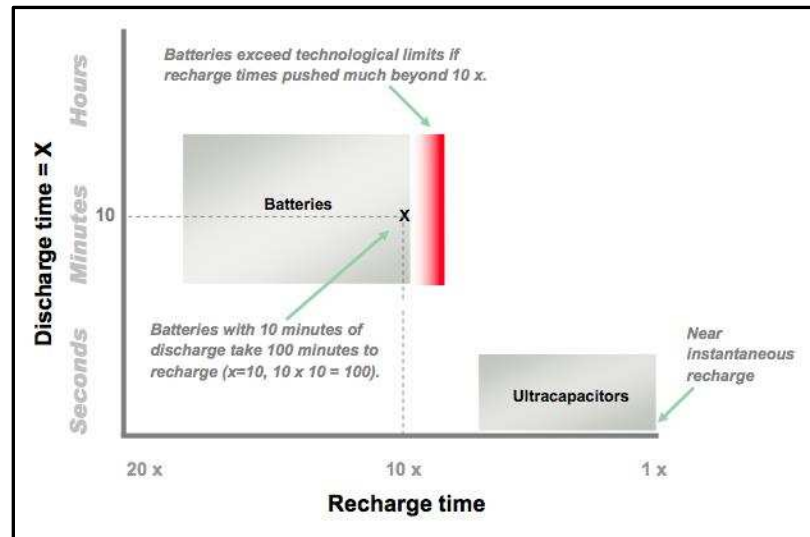
Figure 18 Comparison of energy storage technology discharge / recharge times

In short, supercapacitors are known as high power density storage devices that allow instantaneous delivery of power peak. The ability of supercapacitor to absorb and discharge large amount of energy in a short period of time, supercapacitors make a great secondary energy storage device especially in pulsed load applications, where a large amount of energy is drawn in short periods of time. Hence, supercapacitors are the suitable device to couple with battery in this project. Figure 19 [69] shows a comparison of the galvanostatic charge – discharge profiles of a supercapacitor and a battery under a similar duration where the supercapacitor discharges faster than battery hence, allowing it to fulfill peak load demand.
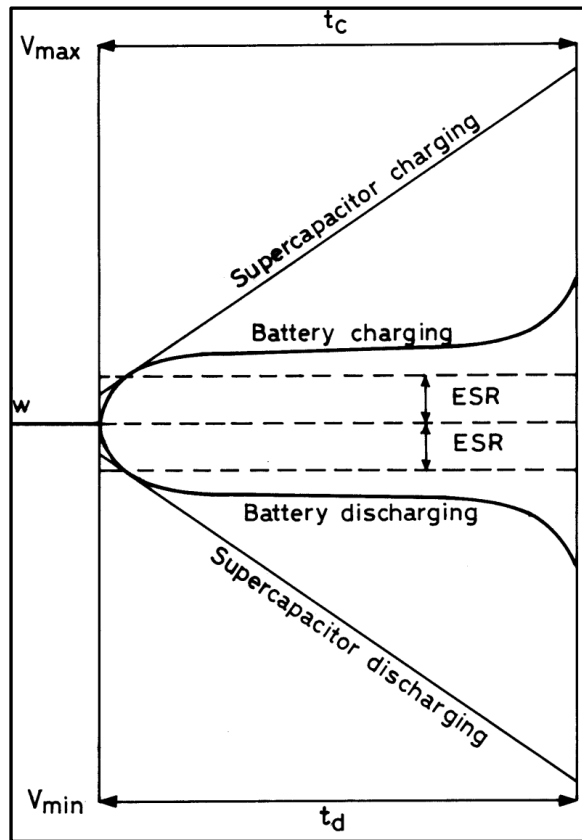
Figure 19 Charge – discharge profiles of a supercapacitor and a battery

2.1.2.3 System configuration of Hybrid Electrical Energy Storage Systems (HEESS)

In a HEESS, optimal design of the setup topologies between the supercapacitor and battery has been the subject of many researches. Most conventional approaches consider a direct parallel connection between the two storage banks [70], a bidirectional DC/DC converter interfacing the two storage banks [15] and dual input bidirectional DC/DC converter topology as shown in Figure 20 below [71, 72].
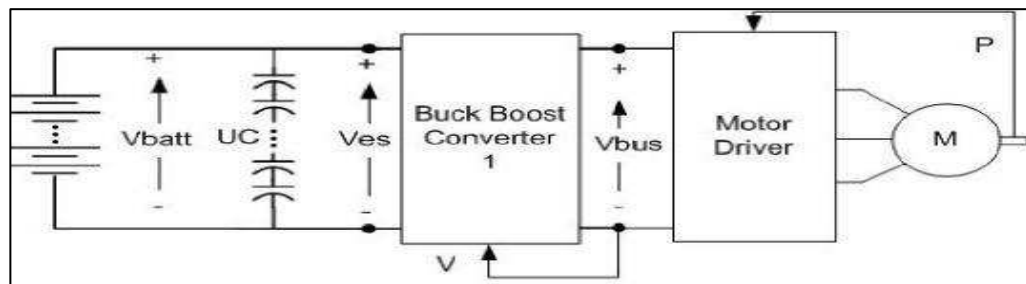
a) Topology of the passive parallel connection
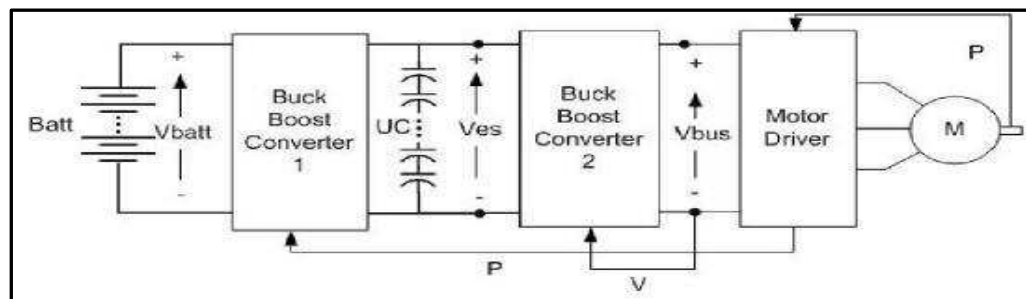
b) Topology of the Bi-Directional DC-DC Converter
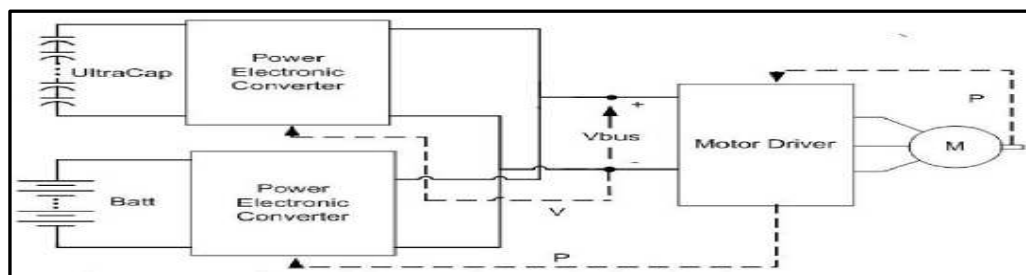
c) Topology of the Dual-input Bi-Directional DC-DC Converter

Figure 20 Topology of DC/DC converter

One of the challenge of coupling the supercapacitor and battery is the different voltage level between the two different energy storage devices. A conventional way of coupling supercapacitor and battery is connecting the two devices in parallel. However, it reduces the capacity of the supercapacitor [51]. This direct approach maintains the same voltage over both sources but limits the power delivered from the supercapacitor.

The single DC/DC converter controls the output current of the battery and allows the supercapacitor to supply the extra power requirement to the load. Lastly, the dual input bi-directional DC/DC converter give rise to highest efficiency, reliability and flexibility [71]. However, it involves the use of more costly DC/DC converters. Hence, the tradeoff between these topologies is the cost of power electronics and efficiency of the HEESS.

Tatsuto Kinjo, Tomonobu Senjyu, Katsumi Uezato and Hideki Fujita examined the use of Electrochemical Double Layer Capacitors (EDLCs) to stabilize the output of a wind power generation system in the paper titled "Output Leveling of Wind Power Generation System by EDLC Energy Storage System". The study uses an energy capacitor system which consists of an EDLC and power electronic devices to compensate for the fluctuating power of a photovoltaic system [73, 74]. The power electronic devices include a buck boost DC – DC converter and a bi-directional inverter to complete the current source of the photovoltaic system. Figure 21 [73] shows the current source of the photovoltaic system:
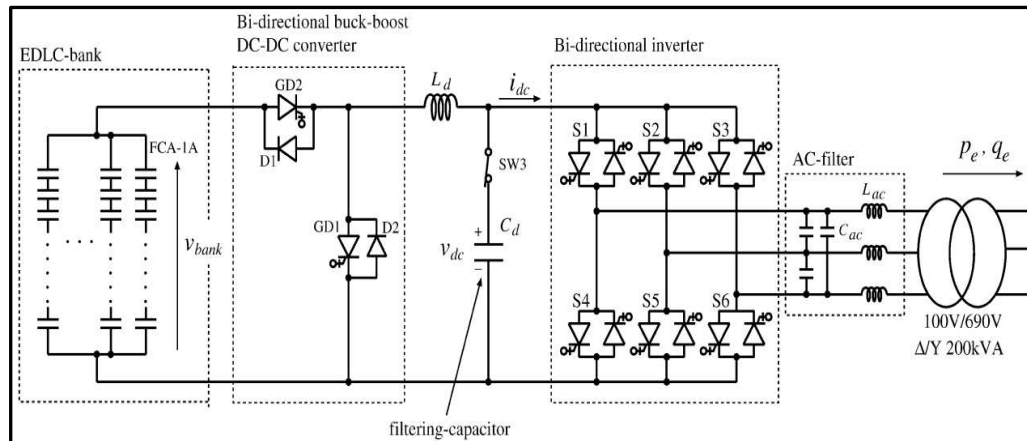
Figure 21 Current source of the photovoltaic system

GD1 and D1 acts as a boost converter to charge the EDLC bank where as GD2 and D2 acts as a buck converter to discharge the EDLC bank. The bi-directional inverter in the other hand inverts the output from DC to AC. The charging and discharging of the EDLC bank is controlled using a PI controller [73, 74]. The system demonstrated above uses power electronics, which are expensive electronic components especially in high-power applications.

In Harada, Sakau, Anan and Yamasaki's research, an investigation of the basic characteristic of the supercapacitors controlled by non-isolated DC-DC converter has been done [75]. In the research, the operating time, energy availability, input and output voltage and current were analysed.
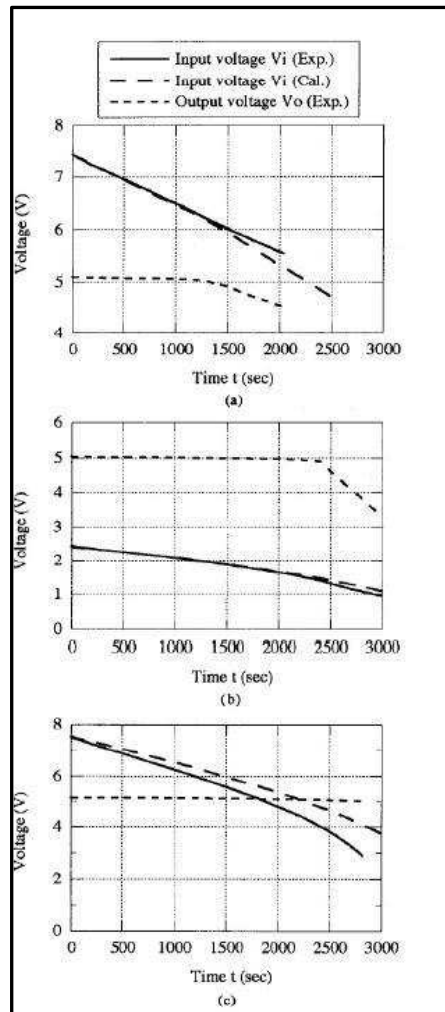
Figure 22 Input and output voltage versus operating time of (a) buck converters (b) boost converters (c) buck-boost converters with supercapacitors

From the result obtained as shown in Figure 22 [75], it can be seen that the maximum operating time of the buck-boost converter is the shortest whereas the buck boost converter has the longest operating time under similar conditions.
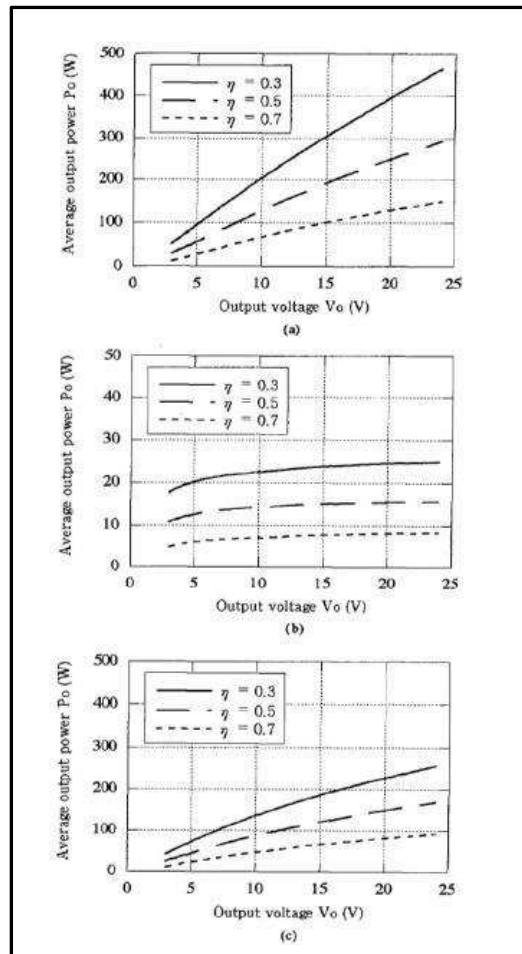
Figure 23 Average output power versus the output voltage of (a) buck converters (b) boost converters (c) buck-boost converters with supercapacitors

Figure 23 [75] shows the average output power versus the output voltage of the non-isolated DC-DC converters with supercapacitors for different energy availability. Energy availability is calculated from the output power divided by the input power of the converter. The buck and buck boost converter's output power increases as the output voltage increases whereas for boost converter, the output power is almost constant although the output voltage increases .

From Harada, Sakau, Anan and Yamasaki's research, it also can be seen that the energy availability, η of the buck converter depends on the output

48

voltage and the number of supercapacitors connected [75]. However, for buck-boost converter, the energy availability, η does not depend on the output voltage and the number of supercapacitors [75]. To obtain high output power from a buck converter, many units of supercapacitors are needed to be connected in series in order to have higher voltage from the supercapacitor bank compared to the output voltage of the DC-DC converter. This causes to a problem of uneven charging due to the dispersion of capacitances of the supercapacitors [75]. This causes to serious safety problem under British Standard of IEC To overcome this problem, an additional voltage monitoring and current bypass circuit is needed for each supercapacitor to keep the balanced voltage [75].

M.E. Glavin, Paul K.W. Chan, S. Armstrong, and W.G Hurley, in the study titled 'A Stand-alone Photovoltaic Supercapacitor Battery Hybrid Energy Storage System', examined the role of an electronic control unit (ECU) in a battery supercapacitor hybrid energy storage system under different load conditions. The ECU is responsible in determining the State-of-Charge (SOC) of the supercapacitor and battery and the supplying of energy to the load by either the supercapacitor or battery with the aid of various sensors [16, 15] . The proposed ECU had a behavior shown in Table 4 [15].

Table 4 Behaviour of ECU

No.	Condition	Action
1	PV Power = Load (Battery SOC High)	• PV supplies load • No battery charging
2	PV Power = Load (Battery SOC Low)	• PV supplies load • No battery charging
3	PV Power > Load (Battery SOC High)	• PV supplies load • No battery charging
4	PV Power > Load (Battery SOC Low)	• PV supplies load • PV charges battery
5	PV Power < Load (Battery SOC High)	• PV supplies load • Battery supplies load
6	PV Power < Load (Battery SOC Low)	• PV supplies load • Battery supplies load until minimum SOC is reached then shut down load
7	No PV Power (Battery SOC High)	• Battery supplies load
8	No PV Power (Battery SOC Low)	• Shut down load

The ECU mentioned was just a proposal and it was not stated that if the ECU was software or hardware controlled. However, simulations showed that the supercapacitor bank did increase the SOC of the battery under peak and pulse current loads. This shows that the battery lifespan is not prolonged with this strategy.

In the paper titled 'Power and Life Extension of Battery – Ultracapacitor Hybrids', R. A. Dougal, Shengyi Liu and Ralph E. White investigated the peak power enhancement and prolonged battery life of battery – ultracapacitor hybrids over conventional systems. A simplified model was created to analytically describe the performance of a battery – ultracapacitor hybrid power source. Complementing a battery power source with ultracapacitor banks was proven to greatly enhance peak power output, considerably reduces internal losses and also prolongs the discharge life of the battery. Figure 24 [76] shows

the plot of the normalised load current, battery current and supercapacitor current [76].
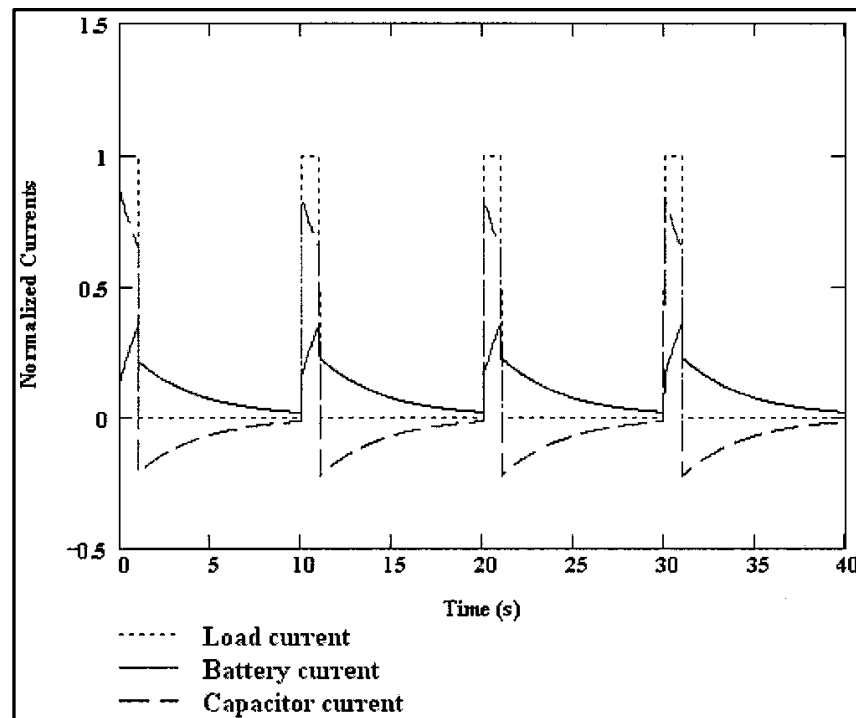
Figure 24 Normalised load current, battery current and supercapacitor current

Observations from the plot shows that the during the load on-state, both the battery and ultracapacitors (also known as supercapacitor) provides the current consumed by the load while the during the load off-state, the battery charges the ultracapacitor. The peak instantaneous current of the battery had been greatly reduced with the assistance of the ultracapacitors, which would otherwise have been the same as the output or load current. This greatly relieves the battery off the peak stresses, reducing battery deterioration and positively influencing the performance of the system [76].

2.1.3 Energy management of HEESS to Maximum Power Transfer (load prediction)

J. C. Lima, A. Medeiros, V. M. Canalli, F. Antunes and F. S. Dos Reis investigated the use of a neural network control system implemented on a PIC microcontroller to track the maximum power point transfer between the load and PV system in their study titled 'A PIC Controller for Grid Connected PV Systems using a FGPA based inverter'. A neural network is implemented on a PIC to control the maximum output voltage in a DC-DC converter connected to solar panels to obtain the maximum power transfer of the panels. The power control is done to obtain the maximum power transfer which extracts the best performance from the solar panel and is obtained through the control of the duty cycle of the DC/DC boost converter, which supplies an adapted voltage to a 3-phase inverter [77, 78].
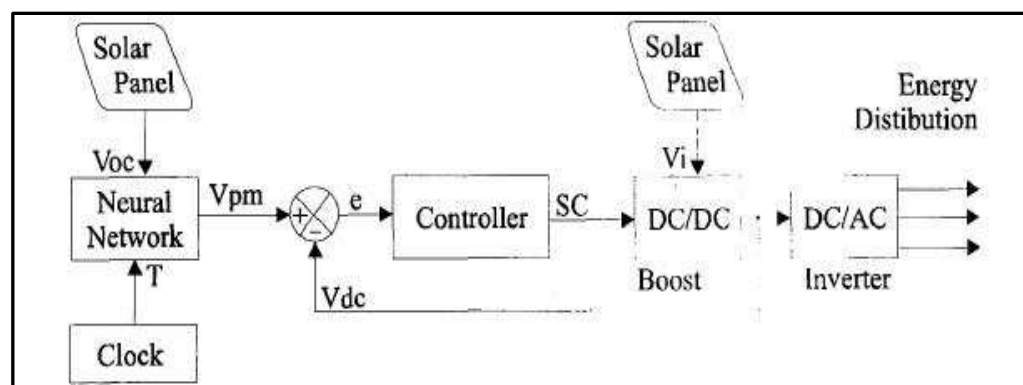
Figure 25 Block diagram of the power system suggested in [77]

This implemented system shown in Figure 25 does not have an energy storage system which can mitigate the problems associated with low-light conditions.

Furthermore, high power rating electronic and complexity of designing bi-directional converter cause impracticability of HEESS. In order to achieve an efficient HEESS with lower cost, software based Energy Management

System (EMS) has been researched into. L. Gao, R. Dougal and S. Liu presented the software approach which offers modularity, design simplicity and reduces the reliance on power electronics [79]. Previous research in [80], had shown a Sequential Programing based EMS which adopts the 'Monitor and Respond' strategy but has shown unsatisfying results. This is due to the time required in software approach to measure, process and respond accordingly. A 70ms delay was recorded in the respond of the supercapacitor after a peak load current is monitored. This does not meet the performance requirement in small DC machine, as the starting current is usually quite short in period. For example, it's measured that a 12 V, 1A DC motor load has a starting current of only 5ms in duration [79]. Hence, the motor load will draw the large current burst from the battery and causing the adverse effects on the battery as mentioned earlier. In order to respond to this downfall of the software approach, load prediction capability has to be integrated into the EMS in order to match the respond of the supercapacitor with the performance required.

To implement the load prediction, the Support Vector Machine (SVM) is researched into and it was applied in the prototype system. The SVM, a form of supervised machine learning founded by V. Vapnik which is a non- parametric statistical model based on Structural Risk Minimization (SRM) principle that offers excellent generalization and predictive capability for limited sample size [81]. Since the Load demand could be predicted by using recursive time series, Support Vector Machine for Regression (SVR) was chosen to implement the load prediction for its high generalization, single global minimum characteristic and this will yield a good non-linear system model [82, 83].

In [84] Chang et al. proposed a SVR approach for the EUNITE Network Competition which is the prediction of daily maximal electrical load of January 1999 based on temperature and electricity load demand (data used is from 1997 to 1998). It is interesting to mention that there is a periodic component within the data set due to the seasonal variation of consumer electricity demand (such as 'holiday' effects use of less electricity during major holidays) and the impact of weather on electricity demand. Their inputs were several attributes, including binary attributes for indicating which day of the week or holiday, etc. [85]. From these attributes, they formulated the predicted max load, which is a numerical value. They concluded that the use of the temperature data did not work as well because of the inherent difficulty in predicting temperature and they also concluded that this SVR approach was feasible for determining an accurate load prediction model. Chen et al. in [84] approach described in [85] was the winning approach for the EUNITE Network Competition. These papers [84] [85] described the SVM implementation. With respect to the design details, it is interesting to note that the use of temperature in their model actually decreases the accuracy of the predictions. This is due to the wide variance of the output and resulting an improper temperature estimation [86]. Change et al. also experimented with data inputs excluding the previous (in time series) load data. The result obtained shows unsatisfied performance. It is worth to mention that the inputs to the SVR are not only time series load data [86].

In [87], Zhang et al. discussed the use of SVM for short-term load forecasting. The author stated that most linear models such as Kalman filtering, AR (Autoregressive), and ARMA (Autoregressive Moving Average) models

are not typically sufficient to model the nonlinearities associated with short term load forecasting processes. The use of SVR, with both electrical load data and corresponding weather time series data, appears to outperform other neural network (NN) based techniques including a back- propagation neural network (BPNN). The authors also used cross validation to select the parameters for the RBF kernel function as well as the regularization constant. The result obtained shows that MAPE (mean absolute percentage error) of the SVM approach was lower than that of the BPNN [87].

It appears that the reviews and studies conducted above show the advantages of having an energy storage system in renewable energy systems. The battery storage system could however be further enhanced using a buffering element, in this research a supercapacitor, thus prolonging the battery lifespan and reducing maintenance and operational costs at the same time.

Moreover, a load forecasting-energy management system (using SVM) aided with the use of sensors could be used in the supercapacitor-battery hybrid energy storage system (SB-HESS) to achieve maximum optimization in terms of system cost and power delivery. From the literature search mentioned above, there is none of the energy management system that is implemented with SVM load-predictive software to control the energy flow between the hybrid energy storage devices and load.

2.1.4 Background theory of Support Vector Machine and Support Vector Regression

2.1.4.1 Support Vector Machine for classification

The foundation of the Support Vector Machine (SVM) have been developed by Vladmir Vapnik in year 1995. SVM has been gaining popularity over the 20 years due to many potential features and good empirical performance. The Support Vector Machine is a form of supervised machine learning. SVM formulation employs the Structural Risk Minimization (SRM) principle which minimises an upper bound on the expected risk [88]; whereas the traditional neural network or the ARIMA models which implement the Empirical Risk Minimization (ERM) solely minimises the error on the training data [89]. SRM principle that focuses on minimizing the upper bound of the generalization error instead of minimizing the training error [90]. Implementing SVM classifier with greater ability to generalize is often the ultimate foal in any classification or pattern recognition task [91, 92]. The SVM optimises the network structure through seeking the right balance between the Vapnik-Chervonenkis (VC) confidence interval and the empirical error [89]. It is by bounding the generalization error between the optimal balance of summation of training error and the confidence interval term that a good generalization performance could be achieved. Good generalization ability is an important characteristic of SVM which is proven to perform better than neural networks under certain circumstances [91]. The SVM also prevents overfitting as it perform well with small training set. Besides that, SVM is equivalent to solving a linear constrained quadratic programming problem which ensures a unique and global optimal solution [93].

SVM functions by creating a hyperplane that separates a set of data containing two classes [94]. According to the SRM principle [90], there will be one optimal hyperplane (which has the maximum distance called maximum margin) to the closest data points of each class as shown in Figure 26 [94]. These points, closest to the optimal hyperplane, are called Support Vectors.

Assuming there are k training samples {xi, yi} where i =1..., k, and each sample has l inputs ($x_i \in \mathbb{R}^l$) with an output class label of ($y_i \in$ -1, 1). The vector, w which is the vector perpendicular to the hyperplane, parameterize the hyperplanes in $\mathbb{R}^l$ and with a constant, b as shown in the following [95]:

$$w \cdot x + b = 0 \qquad \qquad \textbf{Equation 3}$$

Hence the function which classifies the training data is [96]:

$$f(x) = sign(\boldsymbol{w} \cdot \boldsymbol{x} + b) \qquad \qquad \textbf{Equation 4}$$

However, the hyperplane can also be expressed by all pairs of {λw, λb} for λ $\in$ $\mathbb{R}^+$. Hence, the canonical hyperplane was defined to separate the data from the hyperplane by a minimum distance of 1 unit [94]. Hence,

$$y_i(\boldsymbol{x_i} \cdot \boldsymbol{w} + b) \geq 1 \qquad \forall_i \qquad \qquad \textbf{Equation 5}$$

In a hyperplane, all pairs of {λw, λb} describe the same hyperplane, but all are different from each other in terms of the functional distance to the data point. By normalizing the magnitude of w, the geometric distance [96] was given by

$$\frac{y_i(x_i \cdot \boldsymbol{w} + b)}{\| \boldsymbol{w} \|} \geq \frac{1}{\| \boldsymbol{w} \|} \qquad \qquad \textbf{Equation 6}$$

For good generalization, maximum geometric distance of the data point from the hyperplane is sought after. To achieve this, the ‖w‖ is minimised by using Lagrange multiplier [96]. Hence the minimization is given by:

Minimise:

$$W(\alpha) = -\sum_{i=1}^{l} \alpha_i + \frac{1}{2}\sum_{i=1}^{l}\sum_{j=1}^{l} y_i y_j \alpha_i \alpha_j (x_i \cdot x_j)$$

Equation 7

Subject to

$$\sum_{i=1}^{l} y_i \alpha_i = 0$$

Equation 8

$$0 \le \alpha_i \le C \quad \forall_i$$

Where α is the vector of l non-negative Lagrange multipliers, and by defining the matrix of $(H)ij = y_i y_j (x_i \cdot x_j)$, this term is translated to Quadratic Programming Problem (QP) which can be solved the method of Lagrange multipliers [95]:

Minimise:

$$W(\alpha) = -\alpha^T \mathbf{1} + \frac{1}{2}\alpha^T H \alpha$$

Equation 9

Subject to

$$\alpha^T y = 0$$

Equation 10

$$0 \le \alpha_i \le C, \ i = 1, \dots, n,$$

Besides, from the dual formulation, the optimal hyperplane is :

$$w = \sum_i \alpha_i y_i x_i$$

Equation 11

when the functional distance of an data point is >1, then α_i =0. Hence, only the data point that lies on the margin has α_i>0 which are required to define the optimal hyperplane. These data points are called the support vectors. The α_i is also a measure of the data point weight in contribution to the hyperplane. To find b, the positive and negative support vectors were used [90]:

Hence,

$$b = -\frac{1}{2}(w \cdot x^+ + w \cdot x^-)$$

Equation 12

Constructing a separating hyperplane in this feature space leads to a non-linear decision boundary in the input space as shown in Figure 27 [94]. Expensive calculation of dot products in a high-dimensional space can be avoided by introducing a kernel function, K below [92].
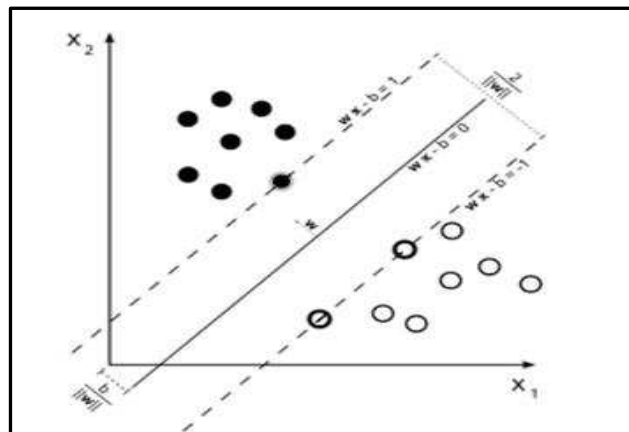
Figure 26 2D Hyperplane

When the soft margin constant, C= ∞ in Equation 10, the optimal hyperplane will be able to separate all the data theoretically. Yet, with a finite C

the classifier is now a soft-margin which allows tradeoff between classifying all data correctly with the complexity of the hyperplane model [96].

If the dataset is not linearly separable, it is like to be linearly separable in the higher dimensional feature space [97]. This is done through the introduction of kernel trick, where the input data was mapped into a higher dimensional space. It is shown in Figure 27 below [98]:
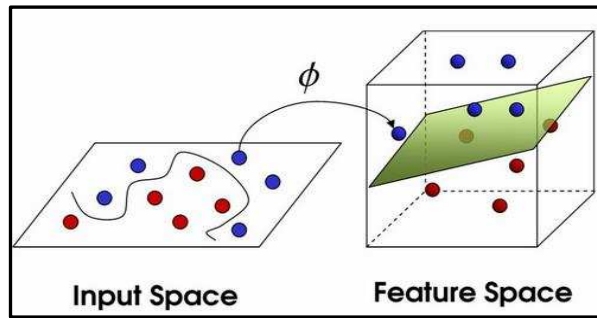
Figure 27 Mapping of data in Input Space to Feature Space

The kernel which define the dot product in the higher dimensional feature space as shown below [94, 96]:

$$K\left(x_i, x_j\right) = \;(x_i) \times \;(x_j) \qquad \textbf{Equation 13}$$

Kernel function, $K(x_i, x_j)$, plays an important role. In practice, various kernel functions can be used [94] , such as

- Linear: $K(\mathbf{x}_i, \mathbf{x}_j) = \mathbf{x}_i^T \mathbf{x}_j.$

- Polynomial : $K(\mathbf{x}_i, \mathbf{x}_j) = (\gamma \mathbf{x}_i^T \mathbf{x}_j + r)^d, \gamma > 0.$

- Radial Basis Function (RBF) : $K(\mathbf{x}_i, \mathbf{x}_j) = \exp(-\gamma \|\mathbf{x}_i - \mathbf{x}_j\|^2), \gamma > 0.$

- Sigmoid: $K(\mathbf{x}_i, \mathbf{x}_j) = \tanh(\gamma \mathbf{x}_i^T \mathbf{x}_j + r).$

The kernel function reflects the geometric relationship between the input vector and the support vector, or the similarities of the features of the faults.

For example [94], the polynomial kernel function in Figure 28 (a) describes the similarity of the two vectors, since the dot product depicts the canonical correlation. Choosing different order, p, would result in different similarity measures and hence different results. The RBF kernel function, as shown in Figure 28 (b), approximates the relationship between the two vectors using a bell shape function. Tuning the parameter s would be similar to tuning the covariance. The sigmoid kernel function in Figure 28 (c) is similar to the polynomial kernel function. The parameters v and c can be used to adjust the shape of the sigmoid function [99].
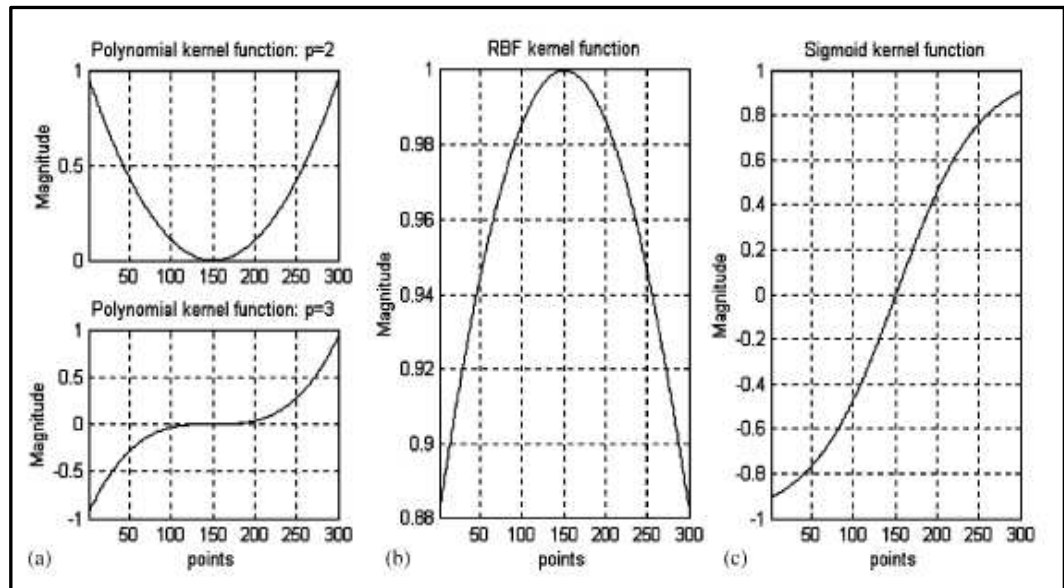
Figure 28 The Kernel Functions: (a) Polynnomial Function with p = 2 and 3; (b) RBF Function; and (c) Sigmoid Function.

Hence the classifying model is now

$$f(x) = sign(\sum_i \alpha_i y_i \big(K(\pmb{x_i}, \pmb{x}) \big) + b)$$

Equation 14

As such, using the support vector machine (SVM) good generalization is guaranteed and this will enable an efficient and accurate classification of the sensor input data. This is appropriate to be used in this project to identify the load pattern. Table 5 [100, 101, 102, 103] tabulates the advantages and disadvantages of SVM for load identification.

Table 5 Advantages and Disadvantages of SVM for Load Identification

Advantages	Disadvantage
• It has high generalization and good nonlinear modelling capability which is suitable for time series load prediction.	• Poor performance is inevitable when the number of sample is very much smaller than the number of features in the input vector.
• The adjustable penalty parameter in SVM avoids the overfitting problem. It also ensures a global minimum output.	• Cross-validation is used as performance measure instead of probability estimation, which can hamper the performance.
• The use of soft margin classifier gives better immunity to noise.	
• It has high efficiency in high dimensional spaces; hence the number of features of input vector is not limited by the curse of dimensionality.	
• It is effective in case when the training samples size is smaller than the number of features/dimensions.	
• The computation requirement depends on the support vectors instead on the whole training data, which yield a good processing and memory efficiency.	
• The SVM decision function depends on the kernel function, which offers modularity. The choice of kernel functions range from the widely used common kernel to specific custom made kernel.	

2.1.5.2 Support Vector Regression (SVR)

The SVM was originally developed for pattern recognition task, however; with the predictive capability of Vapnik's ε-insensitive loss function it has been extended into the nonlinear regression estimation domain [104, 105]. It has been proven to exhibit excellent performance for time series forecasting [86]. The regression and classification task are similar.

For a training sample [106] :

$$K = \{(x_1, y_1), (x_2, y_2) \dots (x_n, y_n)\}$$

Equation 15

And the linear function f x):

$$f(x) = (\boldsymbol{w} \cdot x) + b$$

Equation 16

Hence, solve the optimization problem:

$$\min_{\alpha^{i*j} \subset R^{i*}} \frac{1}{2} \sum_{i,j=1}^{n} (\alpha_i^* - \alpha_i)(\alpha_j^* - \alpha_j)(x_i \cdot x_j) + \varepsilon \sum_{i=1}^{n} (\alpha_i^* + \alpha_i) - \sum_{i=1}^{n} y_i(\alpha_i^* + \alpha_i)$$

Equation 17

Subject to

$$\sum_{i=1}^{n} (\alpha_i^* - \alpha_i) = 0$$

$$0 \le \alpha_i^*, \alpha_i \le C, i = 1,2, \dots, n$$

Equation 18

By attaining the optimum value to get $\boldsymbol{\omega}$ and the constant $\mathbf{b}$

$$\boldsymbol{\omega} = \sum_{i=1}^{n} (\alpha_i^* - \alpha_i)\, x_i$$

Equation 19

$$b = y_i - \sum_{j=1}^{n} (\alpha_j^* - \alpha_j)\,(x_i \cdot x_j) + \varepsilon$$

Equation 20

Where

C is the regularization parameter, α is the Gaussian kernal function's variance and ε is the insensitive loss function.

From this, the linear regression function can be constructed. To extend this linear condition to non-linear domain, the use of kernel trick to transform the input data into higher dimensional space, which solved the problem of curse of dimensionality [106, 104].

LIBSVM

There are many tools available for implementation of the Support Vector Machine. For example, Online SVR, Smooth Support Vector Regression (SSVR), MATLAB in-built SVM toolbox, LIBSVM and such.

In this project, LIBSVM has been chosen for its well-established library, update availability and its cross platform interfaces. It's an integrated program for SVM (C-SVC, nu-SVC), distribution estimation (one class SVM) and regression (epsilon-SVR, nu-SVR) [102]. It also provides an efficient multiclass SVM which is based on one-against-one approach which offer shorter training time as compared with one-against-the-rest approach [103]. The MATLAB extension of LIBSVM also allows the integration of the SVM, SVR, Arduino Mega 2560, and MAXIM USB 6009 DAQ to run the SVMR-EMS, all

in one single MATLAB environment. The kernel choices offered in LIBSVM

[94]:

Table 6 Kernels choices in LIBSVM

Kernels name	Kernels Equation
Linear	$K(\mathbf{x}_i, \mathbf{x}_j) = \mathbf{x}_i^T \mathbf{x}_j.$
Polynomial	$K(\mathbf{x}_i, \mathbf{x}_j) = (\gamma \mathbf{x}_i^T \mathbf{x}_j + r)^d, \gamma > 0.$
Radial Basis Function RBF)	$K(\mathbf{x}_i, \mathbf{x}_j) = \exp(-\gamma \|\mathbf{x}_i - \mathbf{x}_j\|^2), \gamma > 0.$
Sigmoid	$K(\mathbf{x}_i, \mathbf{x}_j) = \tanh(\gamma \mathbf{x}_i^T \mathbf{x}_j + r).$

Load prediction

Electricity Load forecasting plays a great role in modern energy management

system. An accurate load forecast helps eliminate the short transitional time

exists between the switching of power from the battery to the supercapacitor

bank. The predictive strategy in the energy management system predicts the

incoming load demand. This means the supercapacitor turns on before the real

power peak happens.

The Load Forecasting can be divided into four classes depending on the

utilized time frame and presented in Table 7 [107, 108]:

Table 7 Type of Load Forecasting

Forecasting Type [109]
1. Long Term Load Forecast (LTLF)   **The time frame for this class used is typically 1 to 10 years; it focuses to predict the load requirement for future power generation planning, line building etc. Since the investment, designing and construction of power plan takes up to decade long, this class of forecast is important for meeting the demand in future.**

2. Medium Term Load Forecast (MTLF)

The time frame for this class is typically within months to a year. The load prediction focuses on meeting the medium term supply and capacity constraint. Example, the load prediction is to match the supply with the peak load demand in various seasons.

3. Short Term Load Forecast (STLF)

This class focuses on the load forecast of one day ahead. It is used to aid the real time generation control and energy transaction planning.

4 Very Short Term Load Forecast (VSTLF)

This class focuses on the load forecast of hours and minutes ahead. It is used to help the merchandizing and dispatch.

Most of the load forecast research paper focuses on the prediction of maximum load demand. The research paper authored by Anthony Setiawan [110] shows five minutes ahead VSTLF to set the production schedule of the generators in Australia. The result for the prototype is shown in Section 4.2.2.3. From the forecasted load, the generator and network operator will share their maximum supply capacity with NEMMCO [111], and this enable the rest of market player to react to meet the regional demand forecast. However, maximum load demand prediction is not the main focus of this energy control strategy. This energy control strategy success relies on its peak load prediction capability within a short period of time in order for the supercapacitor to be turned on before power peak. Hence, the load forecast for this project falls under the VSTLF class with the objective for early detection of approaching peak load to yield a good energy management response without any lag time.

Most research focuses on the STLF and a few of the research papers have been focused on the VSTLF scope. Table 8 [110] below shows the summary of

load forecast techniques used for these two classes:

Table 8 Summary of Load forecasting techniques for STLF and VSTLF

Method	STLF	VSTLF
Statistical methods		
Autoregressive integrated moving average	✔	✔
Autoregressive moving average	✔	✔
General exponential smoothing	✔	
Kalman filter	✔	
Multiple linear regression	✔	✔
State space	✔	
Stochastic time series	✔	
Support vector regression	✔	
Artificial intelligence - based methods		
Artificial neural networks	✔	✔
Expert system	✔	✔
Fuzzy inference	✔	✔
Fuzzy neural system	✔	✔

Hence VSTLF is used in this load prediction system. To implement a VSTLF, the factors that affect the electricity demand have to be understood. They are listed as follows [112]:

Table 9 Factors which affect the load demand

Factors
1. Time
The time is an important factor that influences the load demand as it relates to the routine and activities of a population. The electricity demand differs from day to night, weekday, to weekends etc. However, a cyclic nature is observable where the demand at different date but same time and day is likely to be similar. This is important point as the previous demand data could be used to predict the future demand.

2. Random Effects:

In power system, the load demand is constantly subjected to random disturbances of different scale. Sudden load variation could occur due to operation of big motor machines, strike events and bad weather could lead to oversupply as factories were shut down etc. All these add to the difficulties of predicting the load demand.

3. Irregular Days:

In special day such as holiday or day with national event, the electricity demand will see a fluctuation from the ordinary days.

A typical daily electrical load profile is shown in Figure 29. This figure shows the peak in daily profile the opportunity for load prediction.
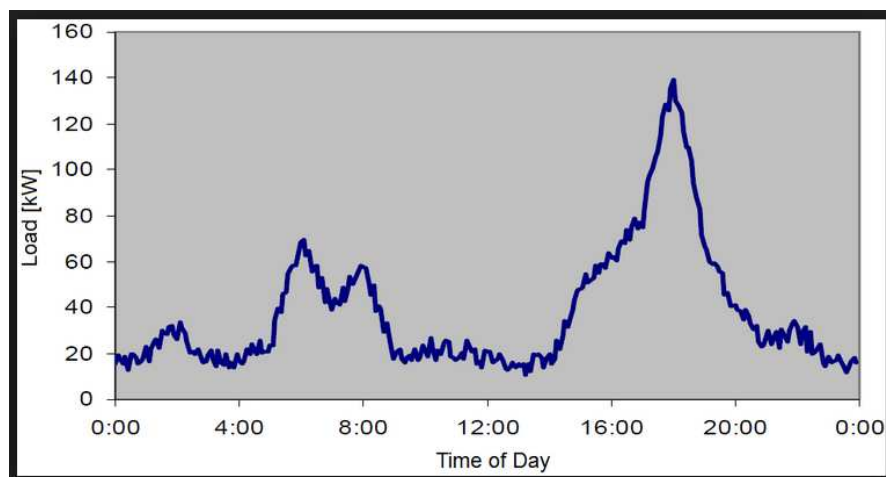
Figure 29 Daily Electrical Load Profile

As can be seen in Figure 29 [111], the load demand varies from time to time within a day. Hence, it is greatly dependent upon the time variable as the daily social and operating activities which consume electricity power are mostly repetitive in nature. Others factor such as weather and random effect will affect the load profile add more exogenous variable to the modeling function. In this off grid PV system, the simulated load is used where it does not have underlying factor such as random effect or weather effect. Hence, time

and the previous load current values are the only variables that hold the relation to the load demand output. It can also be observed that the relationship between the time and the load demand is nonlinear in nature; hence the prediction technique used will require good modeling of the nonlinear relationships.

In order to implement a VSLTF with good accuracy and speed, it is crucial to select the suitable feature variables. The correlation factor between the variable and the predicted output should be used as a measure of the relevance of the variable. The conventional prediction technique using neural networks has high number of parameters which require tuning and this causes performance degradation. The load prediction using neural network is also highly prone to overfitting problem. Overfitting describes the situation where the training data yields good results but with fresh data the modal output is erroneous. Hence, SVR which has only a few tuning parameters and does not overfit can be used in place of neural network to achieve good result in load prediction [109, 86].

Autoregressive modal of Time Series

The forecast technique consists of three main branches: The judgmental model, Causal Method and Time Series Method. The first is a form of opinionated prediction, which is not suitable for modeling the electricity demand. The second is a prediction through constructing model which describes the relationship between the dependent output variable to be forecasted and the independent input variables. However, the implemented SVMR-EMS is an off grid PV system, with the absence of any historical load data and the use of programmable load to simulate the load, the variable that could relate to the

load current output are time and load current itself. Hence, the third forecasting technique, the time series, specifically the autoregressive (AR) modal is chosen for this task.

The autoregressive (AR) modal is a subset of the time series method [86]. It's a more specific type of the Autoregressive–moving average model (ARMA) which represents a random process. However, the AR output (dependent variable) is solely dependent linearly on its own previous values only [113]. Hence, it is not capable of dealing with nonlinear model representation in load forecast. Since SVR can perform well in the nonlinear domain, the concept of AR was applied to SVR to approach the trend of load demand.

Time series is a representation in time of a certain phenomenon. It is an important physical phenomenon as most data holds time-dependent information [86]. Time Series analysis is a problem of investigating the implicit system to create a model for the time series data. On the other hand, Time Series Prediction is the use of such model built with past historical data that could forecast the future trend. It's widely used for forecast in electricity load, stock prices, weather etc. However, the main problems in modeling the time series are non-stationary and noise. Noise Aspect refers the inadequacy of the past data to reflect the dependency between the future and past in any time series. The non-stationary refers to the relationship between input and output is varying over time bit by bit [114]. Hence, the dynamics of recent data contains more weight of information than the previous one [115].

The modeling of time series could be considered as regression problem in a high dimensional input space more than one input feature (variable).

70

However, many time series problems regard the prediction of a sequence of future data from the previous data only. This method is called multistep ahead time series prediction. A single model is first constructed from past data of the time series, and then it will be used stepwise for future values prediction. As the predicted values will be used to predict the next value, this multi-stage prediction/Recursive prediction is prone to error accumulation problem as has been proven experimentally in the result section [116] . This prediction method is normally used for long term load prediction and the model can be predicted by iteratively using one-step-ahead prediction model [116]:

$$X(t+1) = F(X(t), X(t-1)...X(t-m+1))$$ **Equation 21**

where F is the prediction model and m is the size of regressor.

By using the predicted value obtained in Equation 21, the next value can be predicted using the same model [117],

$$X(t+2) = F(X(t), X(t-1)...X(t-m+2))$$ **Equation 22**

For n iteration, the nth prediction :

$$X(t+n) = F(X(t+n-1), X(t+n-2)...X(t-m+n))$$ **Equation 23**

An alternative to the Multi-stage Prediction method for long term prediction, called the independent value prediction which preserve the use autoregressive modal, where previous variable value is used for predicting its future value, yet it construct separate model for each prediction step. This

71

method is complicated in the sense that it requires many models to be constructed to achieve the task [116].

Development of the K-step-ahead prediction:

For the SVMR-EMS, the load prediction is VSTLF; hence, being a short term load forecast, it involves the use of one-step-ahead prediction as mentioned earlier:

$$Y(t+1) = F(Y(t), Y(t-1)...Y(t-m+1)) \qquad \textbf{Equation 24}$$

Yet, empirically, it was tested that SVMR-EMS failed to perform well with just one step ahead prediction. The supercapacitor still turned ON after the peak has passed, this implementation and experiment is proven in MEng dissertation [118]. This is due to the processing time of SVMR-EMS for classification and regression that require longer than the one-step-ahead buffer time. Hence, to improve the load prediction capability of SVMR-EMS, **K-step-ahead** autoregressive strategy, an improvised version of one-step-ahead strategy was implemented.

$$Y(t+K) = F(Y(t), Y(t-1)...Y(t-m+1)) \qquad \textbf{Equation 25}$$

This **K-step-ahead** autoregressive strategy will yield a predicted output value which leads the actual load current (K* sampling time –processing time) in advanced. This will ensure the SVMR-EMS to have good management response. However, it creates certain shadow time in between the pattern recognition to the output of the predicted value. During this short period of time the SVMR-EMS will not be responsive to the load value. Hence, it is crucial for

suitable value of K to be chosen for the successful implementation of SVMR-EMS.

Comparison of techniques for load prediction

The conventional techniques used for time series load prediction focuses on statistical method and neural network. The former required the time series to be steady, having normality and independence characteristic. Hence, it is not suited for complex, nonlinear time series system [119]. The latter performs well on nonlinearity, yet it suffers from overfitting, under fitting, and local minima issues. In these, Autoregression and Moving Average (ARMA), Auto-regressive Integrated Moving Average (ARIMA), Regression Models, Gaussian Process (GP), Simplified Fuzzy Inference, Radial Basis Function Network (RBFN), Multilayer Perceptron (MLP), Kalman filtering, Back Propagation Neural Network (BPNN) was the techniques developed [120]. The ARIMA model has been extensively implemented for seasonal time series predicting models. Table 10 [86] below lists the models and their drawbacks in load prediction:

Table 10 Drawbacks of various techniques in electricity load forecast

Forecasting Techniques	Drawbacks in electricity load forecast
ARIMA	It lacks of flexibility for short term load forecasting as the output state is dependent on the weighted sum of previous states. Besides, the autoregressive model cannot capture a nonlinear relationship in the output variable and the previous values of the underlying variables whereas, in load forecast, the time series are mostly nonlinear.

Regression Models	Load forecasting is too complicated for Regression Models which is widely used to predict the weather.
Gaussian Process [121]	It is not sparse and required whole sample to perform prediction. Besides, It has poor performance in high dimensional space which limits the number of feature to less than a dozen.
Artificial Neural Network ANN) such as MLP , BPPN and RBFN	It yields good nonlinear modeling for load forecasting however, this techniques requires many parameters for tuning, and need a large training sample and it will be easily relapsed into local minima.
Kalman Filtering [122]	Its error covariance matrix will not converge to adjacent if the load demand sudden changes even though with repetitive estimation.

The level of uncertainties in load forecasting has been upscale due to the growth in intermittence generation such as Solar and Wind power generation in smart grid system. This is due to the fact that intermittence generation suffers from larger fluctuation of voltage magnitude and frequency as compare to the traditional centralized electricity generation [119]. For this reason, more sophisticated forecasting technique has to be used in place of the conventional ones. Hence, the SVM which implements the structural Risk Minimization Concept and has good generalization capability, good nonlinear modeling feature of ANN and yields only a global minima output, has been selected for performing the load forecasting task in this study [86].

2.2 Optimal Sizing of Renewable Energy System

The previous part of this chapter presents the system configuration for conventional battery-individual system and system configuration of pairing supercapacitor with battery in an energy storage system for solar application. Various approaches to control energy flow in a hybrid electrical energy storage system (HEESS) have been reviewed. In this section, review on different optimization techniques and methodology optimal sizing for renewable energy system are presented.

Conventionally speaking, lead-acid batteries are the main energy storage device technology used in renewable energy systems (RESs) and autonomous power-supply systems due to their maturity and low cost as mentioned in Section 2.1, this factor will remain valid for the next few years. It is often stated, however, that batteries in RES applications exhibit shorter lifetimes than those expected by manufacturers' data or those experienced in real applications. Battery lifetime often alters with different load profile as this is closely related to the ageing processes within a battery which lead to a loss of performance and the stress factors which induce ageing and influence the rate of ageing [44]. Overall, in relation to all other components in RESs, the battery lifetime is short. Adding the supercapacitor increases battery lifetime hence reduce costs.
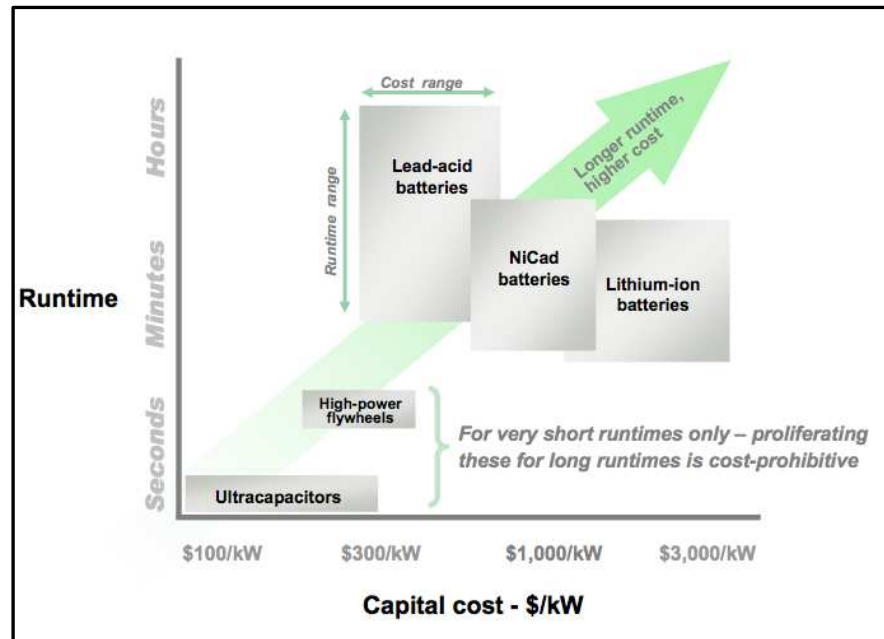
Figure 30 Capital cost vs. runtime for different energy storage devices

The figure 30 [68] above shows the initial cost of the energy storage devices. The capital cost is an important financial parameter, it should be recognized that the total cost of ownership (which includes operational and maintenance costs) is a much more meaningful index for analysis. For example, the capital cost of lead-acid batteries is relatively low, however, they may not necessarily be the least expensive option for environments experiencing frequent outages of short duration. Under such circumstances, lead-acid batteries will likely experience a shortened life span. Figure 31 is intended to provide an overview cost comparison of different energy storage devices, it is taken in [68].

On the other hand, lifespan for PV panels and wind generator are said to be approximately 20 years however, lead acid battery has the shorter lifespan. That being said, the efficiency of PV panel and wind generator degraded after 12 years, from 90% to 85% or 80% according to [123, 124, 125]. Furthermore,

battery lifespan has a distinct impact on the costs of the total system in the long run. The cost of replacing batteries contributes a big portion in the overall cost of the system for 20 years. In this project, supercapacitor-battery hybrid energy storage system is implemented with the designed operation management system (operation condition, set point SOC of battery) to prolong the battery lifespan. Evidently, the cost for replacing the batteries is decreased throughout the 20 years.

In order to efficiently and economically utilize the renewable energy resources and energy storage devices, an appropriate optimization technique is required to accommodate all the number of parameters in this domain (supercapacitor-battery hybrid energy storage system (SB-HESS) for solar application). This area has been gaining interest from researchers and various approaches were recommended by the researchers [48]. Generally, the aim of this sizing is to determine the optimal configuration of the power system and optimal location, type and sizing of generation units installed which subject to constraint of the system meeting load requirements at minimum cost [126]. The design of the hybrid renewable energy systems can be evaluated through its lifetime cost and emission. The lifetime cost which subjects to the system typically consists of two or more components. This means that the lifetime cost of these components includes the capital, maintenance and operational cost. Among all possible hybrid system configurations that are optimally dispatched, the configuration with the lowest Net Present Value (NPV) is chosen as the optimal configuration or it is called the optimal design [127, 128].

The common current optimal sizing tools are divided into two main sessions. Firstly, software tools are commercially available that can be helpful

for real time system integration [129]. Secondly, there are number of optimization techniques have also been applied by researchers for the sizing of hybrid renewable energy systems [129] .

2.2.1 Commercially Available Software Tools

Commercial simulation programs are common tools to evaluate the performance of the renewable energy systems. There are many energy tools that can be downloaded from the websites of several research laboratories or universities as mentioned in [129]. In [130], 68 energy tools and only 37 of the energy tools were reviewed and used in energy analysis. These energy tools are used for designing hybrid energy system such as the Hybrid Power System Simulation Model (HYBRID2) [131] , the General Algebraic Modeling System (GAMS) [132] , Optimization of Renewable Intermittent Energies with Hydrogen for Autonomous Electrification (ORIENTE) [133], OptQuest [134, 135], LINDO [136] , WDILOG2 [137] , Dividing Rectangles (DIRECT) [138, 139], Determining Optimum Integration of RES (DOIRES) [140], Simulation of Photovoltaic Energy Systems (SimPhoSys) [141], Geo-Spatial Planner for Energy Investment Strategies (GSPEIS) [142, 143], Grid-connected Renewable Hybrid Systems Optimization (GRHYSO) [144] and H_2RES [145]. The authors in [144] have developed the HOGA program (Hybrid Optimisation by Genetic Algorithms), a program that uses a Genetic Algorithm (GA) to design a PV-Diesel system (sizing and operation control of a PV-Diesel system). The program has been developed in C++. A more detailed literature survey specifically on commercially available software tools for the performance evaluation of hybrid renewable energy systems in [130, 129].

By using the software program mentioned above, an optimum configuration can be obtained by comparing the performance and energy production cost of different system configurations. HYBRID2 simulates hybrid systems with very high precision calculations, but it does not optimise the system configuration [129]. TRNSYS (Transient Energy System Simulation Program) was initially developed to simulate thermal systems. Besides that, PV systems is also incorporated in this program to simulate hybrid systems, however, this tool cannot be used to optimise the energy system configuration [146]. Seeling-Hochmuth [144, 147] covers the optimization of PV-hybrid energy systems. The hybrid control algorithm is simple, where the state-of-charge (SOC) set point is the only parameter considered. Since there is no detailed description of the GA, with the results being compared with those of a simulation program (such as HYBRID2), this work can be considered to be in the area of simulations and not in optimization of hybrid systems.

One of the most famous sizing simulation programs for renewable energy system is HOMER, which developed by National Renewable Energy Laboratory, United State [148, 129].

2.2.1.1 HOMER

HOMER is a user-friendly micro-power design tool developed in 1992 by the National Renewable Energy Laboratory in the USA [14]. NREL released 42 versions of the program. It can be freely downloaded from [149]. According to [130], there are more than 32,000 user have downloaded HOMER. HOMER is a very user-friendly optimization program, a typical design and simulation can be run after one day of training [130].

HOMER simulates and optimises stand-alone and grid-connected power systems with any combination of wind turbines, PV arrays, hydro power, biomass power, internal combustion engine generators, micro-turbines, fuel cells, batteries, and hydrogen storage, serving both electric and thermal loads (by individual or district-heating systems). All costs with any pollution penalties (except fuel handling costs) and taxes are included in HOMER.

HOMER includes several energy component models, such as photovoltaic, wind turbines, hydro, batteries, diesel and other fuel generators, electrolysis units, and fuel cells, and evaluates suitable options considering cost and availability of energy resources [150]. Grid connection is also considered in HOMER design procedure. The software requires initial information before the user run the simulation. Initial information such as energy resources, economical and technical constraints, energy storage requirements and system control strategies. Moreover, information on the components such as component type, capital, replacement, operation and maintenance costs, efficiency, operational life, etc. are also required [151]. The architecture of the software is presented in Figure 24 [152, 153, 154, 130]. Sensitivity analysis in HOMER could be done with variables having a range of values instead of a specific number computed by the user [130].
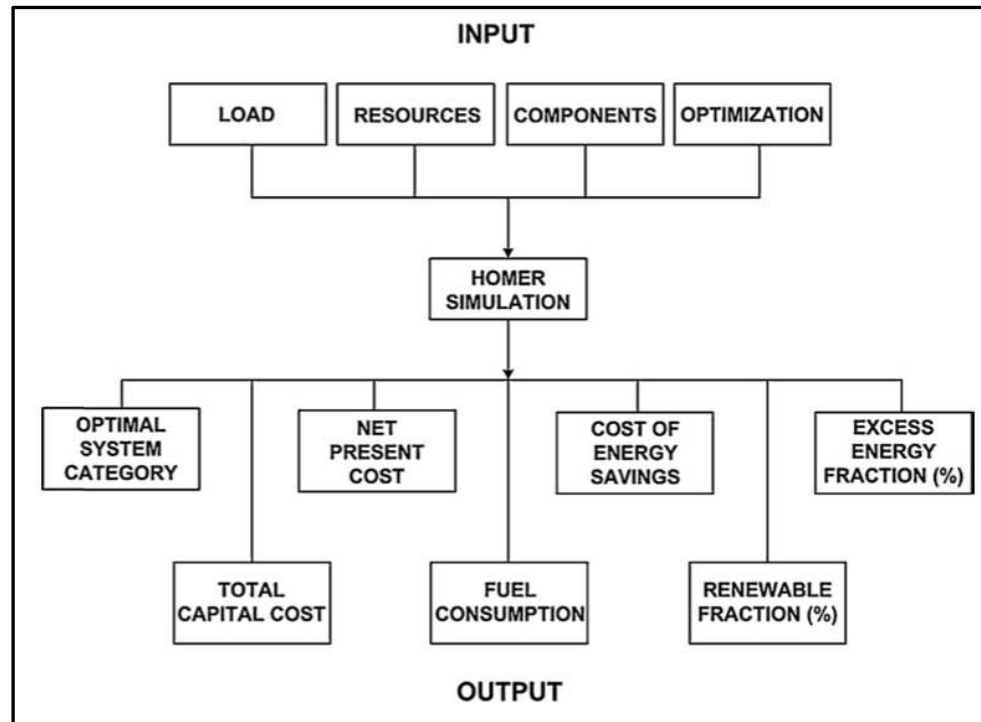
Figure 31 Architecture of HOMER software

HOMER has widely been used in previous renewable energy system case studies as presented for example in the literature [150, 155, 156, 157]. Both grid-parallel and stand-alone systems have been investigated using HOMER. On the other hand, the parallel combination of renewable energy sources and conventional systems such as diesel generators has also been considered in many studies. These case studies are mentioned in papers [151, 128, 152, 153, 158]

In the literature mentioned above, researchers have shown optimum sizing of hybrid systems using HOMER. A list of publications that involved HOMER is available from its homepage [149]. HOMER has previously been used to assess the wind energy potential at individual locations in Ethiopia [158], to assess the feasibility of a stand-alone wind-diesel hybrid in Saudi Arabia [151], to assess the feasibility of zero-energy homes [159] and simulate a stand-alone system with hydrogen in Newfoundland, Canada [155]. Diaf et al.

81

[160] presented an application of hybrid PV–Wind– Battery systems (in Corsica France) which minimises the Levelised Cost of Energy (LCE). Dalton et al. [161] carried out the optimization minimization of NPC using HOMER for a PV–Wind–Diesel–Battery system in Australia. In HOMER, total net present cost (NPC) is used to represent the life-cycle cost of a system. The total NPC condenses all the costs and revenues that occur within the project lifetime into one lump sum in today's dollars, with future cash flows discounted back to the present using the discount rate. Himri et al. [162] optimised a wind–diesel system using HOMER, with no batteries, to supply a remote village in Algeria. In addition, simulations of the optimum system are carried out, using HOMER and HYBRIDS for this purpose, comparing the simulations obtained with each of the two programs [146].

HOMER considers 2 different types of control strategies .

1. **Load-following Strategy** [163, 150]: the diesel generator supplies power to meet load demand at that moment only. Lower priority activities such as, renewable sources are used to charge up the battery banks.

2. **Charge-following Strategy** [14]: The definition of the cycle charging strategy is that whenever the generators run. The generators run at full blast and charge the battery with any excess power. It works regardless of the presence of, or value of, the set point SOC. But in the absence of a SOC set point, HOMER will stop charging the battery. That might be after only one time step. So without a set point SOC, the system sometimes remains the battery at low SOC for a long time without charging it up. That does not affect the simulation in HOMER at all, but

it could drain lead-acid batteries in real life. The battery set point state of charge has no effect on whether HOMER charges the battery. The set point SOC only affects how long HOMER continues to charge the battery. The set point says that when the system starts charging the battery, it will drain well continue doing so until the battery reaches the set point SOC.

In HOMER simulation, control strategy on the system is also important. It affectes the simulation result by changing the different type of control strategy. The authors in [164], applied neural networks to the control strategies of power PV–Diesel systems. Knowing the energy demand and the solar irradiation, dynamic programming is used in order to optimise the operation of the diesel generator and minimises the fuel costs. For this system, an adaptive intelligence strategy is used. The authors also compared the results obtained by applying two types of neural networks. In [165, 166] the authors proposed various strategies for the operation of hybrid PV–Diesel–Battery systems. One hour intervals are considered and the system parameters remain constant. They also considered ideal batteries, without taking into account losses or the influence of the cycles in the lifespan of the same. The three basic control strategies proposed are the following [146]:

- Zero-charge strategy (Load Following Diesel): the batteries are never charged using the diesel generator. Therefore, the set point of the State of Charge (SOC_Setpoint) is 0%.

- Full cycle-charge strategy: the batteries are charged to 100% of their capacity every time the diesel generator is on (SOC_Setpoint = 100%).

- Predictive control strategy: the charging of the batteries depends on the prediction of the demand and the energy expected to be generated by means of renewable sources, so there will be a certain degree of uncertainty. With this strategy, the energy loss from the renewable energies tends to decrease.

The authors propose having an optimum point for the SOC_Setpoint between 0% and 100% in such a way that the total operation cost of the system is minimal. That is to say, the strategy will be between zero charge and full cycle-charge.

In [165], the authors improved the control strategies model of [166] by introducing new parameters that have become of great importance in the control strategies of the software tools HYBRID2, HOMER, and HOGA [42]. The Critical Discharge Power (L_d) is the value as from which the net energy (that demanded by the charges minus that supplied by the renewable sources) is more profitable when supplied by means of the diesel generator than when supplied by means of the batteries (having previously been charged by the diesel generator). The authors propose four control strategies frugal dispatch strategy, load following strategy, SOC_Setpoint strategy and operation strategy of diesel at maximum power (for a minimum time charging the batteries) [146].

In this research, HOMER is used to design and optimise battery-alone system for solar and wind application. Result obtained from the established Micropower Optimization Model (HOMER) is compared with the result obtained from our implemented fitness function in the Genetic Algorithm (GA). This is done to validate the implemented GA fitness function and the GA program are working appropriate. Limitation in HOMER does not allow

optimal sizing of supercapacitor-battery hybrid energy storage system as the software does not provide library for supercapacitor.

2.2.2 Other Optimisation Techniques

There are various optimization techniques such as the probabilistic approach, graphical construction method and iterative technique have been proposed by researchers [48]. Numerous papers have been written about the optimum designs of PV and/or Wind and/or diesel systems with single energy storage in batteries.

Generally, the optimum design in those papers reviewed were carried out minimizing the Net Present Cost (NPC: investment costs plus the discounted present values of all future costs during the lifetime of the system) or by minimizing the Levelised Cost of Energy (LCE: total cost of the entire hybrid system divided by the energy supplied by the hybrid system) [14]. Additionally, restrictions are usually included that are applied to reliability, evaluating the same by means of one of the following parameters [146]:

- Loss of Load Probability (LOLP): power failure time period divided by a given period of time generally one (year).

- Loss of Power Supply Probability (LPSP): probability that an insufficient power supply will result when the hybrid system is unable to satisfy the load demand.

- Unmet Load (UL): non-served load divided by the total load of a period of time normally one year).

Borowy and Salameh [167] presented a graphical construction method to

optimise the size of the PV generator and the capacity of the batteries in PV–wind– battery systems. As initial data, the desired unmet load (UL) value is considered. The required type of wind turbine, PV panel and battery are chosen and fixed. By changing the number of photovoltaic panels and the number of battery, systems that comply with the maximum UL value are achieved. In this study [167], the systems are economically assessed, and the system with the lowest cost is selected. This means that the system operation is simulated for various combinations of PV array, battery sizes and based on the desired loss of power supply probability (LPSP). For the desired LPSP, the PV array versus battery size is plotted. The optimal solution with the minimal system cost is chosen.

Another graphical technique has been given by [168] to optimise the size of a hybrid solar–wind energy system by considering the monthly average solar and wind energy values. However, in both graphical methods, only two parameters for energy sources or energy storage device (either PV and battery, or PV and wind turbine) were included in the optimization process [48].

Chedid and Saliba [169] proposed a method for the optimum design of autonomous hybrid PV–Wind–Diesel–Battery systems by means of the economic optimization of the system by applying lineal programming. Based on literature review in [144, 146], Kaiser et al. presented a method to simultaneously optimise the control strategies and the characteristics of the elements of PV–Diesel–Battery systems, as well as online optimization of the control strategy. Online optimization of the control strategy allows the parameters to be redefined during the system operation based on decision-taking theory.

Morgan et al. [170] described the Advanced Reciprocating Engine Systems (ARES) program on simulation and optimization of hybrid PV–Diesel–Battery systems, where the batteries are modeled with great precision. Seeling-Hochmuth [147] carried out the optimization (minimization of the NPC) of a hybrid PV–Wind–Diesel–Battery system by means of the Genetic Algorithm technique. El-Hefnawi [171] presented an optimization method of PV–Diesel–Battery systems. This method is based on the definition of a model of a diesel generator, and from this, the optimum dimensioning of the PV generator and of the batteries are obtained. On the other hand, Protogeropoulos et al. [172] run the optimization of PV-Wind–Battery systems, modifying the size of the batteries until a configuration that ensures sufficient autonomy is achieved. Kellogg et al. [124] presented an iterative optimization method for PV–Wind–Battery systems.

Elhadidy and Shaahid [173] have studied the effect of the size of the batteries on the operation hours and on the energy provided by the diesel generator in Wind–Diesel–Battery systems. The diesel back-up system is operated at times when the power generated from wind energy conversion system (WECS) fails to meet the load or when the battery storage is depleted . The researchers in [173] showed that for economic considerations, for optimum use of battery storage and for optimum operation of diesel system, storage capacity equivalent to one to three days of maximum monthly average daily demand needs to be used. It has been found that the diesel energy to be generated without any storage is considerably high; however, the use of one day of battery storage reduces diesel energy generation by about 35%; also the number of hours of operation of the diesel system is reduced by about 52%.

Dufo-López and Bernal-Agustín [174] carried out the optimization of hybrid PV–Diesel–Battery systems by using Genetic Algorithms (GA). In a prior paper [175], they determined the correct performance of GA as a technique for the design of hybrid systems. Thus, with the use of GA in , the optimum or a very similar system to the optimum can be obtained with low simulation and calculation time. The results obtained are compared in the optimization of a hybrid system applying GA with the results obtained with an enumerative method by assessing all the possible designs [175].

Koutroulis et al. [176] presented a paper for economic optimization by means of Genetic Algorithms on PV–Wind–Battery systems. Shaahid and Elhadidy [177] used the HOMER software for the economic optimization. The authors in [177] minimised the NPC of a PV–Diesel–Battery system to supply a shopping center located in Dhahran Saudi Arabia. Ashok [178] presented an optimization method for PV–Wind–Diesel–Battery systems that includes microhydro. The LCE of all of the possible component combinations is assessed in [178]. It is applied to an example located in India. Diaf et al. [160] presented an application of hybrid PV–Wind– Battery systems in Corsica France), which minimises the LCE. Table 11 [146] shows a summary on the optimization of renewable energy system

Table 11 Publications on Optimization of PV and/or Diesel Hybrid Systems with battery energy system.

	PV–Diesel–Batteries	PV–Wind–Batteries	PV–Wind–Diesel–Batteries	Wind–Diesel–Batteries	Optimization of components	Optimization of control strategy
Borowy and Salameh, 1996		×			×	
Chedid and Saliba, 1996			×		×	
Kaiser et al., 1997	×				×	×
Morgan et al., 1997	×				×	
Seeling-Hochmuth, 1997			×		×	×
El-Hefnawi, 1998	×				×	
Protogeropoulos et al., 1998		×			×	
Kellogg et al., 1998		×			×	
Elhadidy and Shaahid, 1999				×	×	
Dufo-López and Bernal-Agustín, 2005	×				×	×
Koutroulis et al., 2006		×			×	
Shaahid and Elhadidy, 2006	×				HOMER	
Ashok, 2007			×		×	
Yang et al, 2007, 2008		×			×	
Diaf et al, 2008		×			×	
Dalton et al., 2008			×		HOMER	
Himri et al., 2008				× No batteries	HOMER	
Shaahid and El-Amin, 2008	×				HOMER	

2.2.2.1 Optimal sizing RES using GA

GA has been widely used in renewable energy system sizing studies due to certain advantages. As mentioned earlier, Koutroulis et al. [174, 156, 176], Yang et al. [48, 179] and Bilal et al. [180] utilized GA for sizing of a stand-alone hybrid PV-Wind system. Lagorse et al. [181] applied a hybrid GA and simplex-based methodology to economically design a multi-source hybrid unit composed of PV, wind generator, fuel cell. In [129], a more comprehensive system consisting of PV, wind, fuel cell, microturbine, and battery was optimally sized using a GA. Lopez et al. developed a simulation program named HOGA (Hybrid Optimization by Genetic Algorithm) based on utilization of a GA in order to design different optimal combinations of autonomous hybrid energy systems including a diesel generator as backup in [174, 182]. GA was also utilized in other different cases of energy system sizing studies based on [183, 184, 185, 186, 187, 188, 189, 190].

Tina et al. [191] presented a probabilistic approach based on the convolution technique to incorporate the fluctuating nature of the resources and the load, thus eliminating the need for time-series data, to assess the long-term performance of a hybrid solar–wind system for both stand-alone and grid-connected applications.

A graphical construction technique for determining the optimum combination of battery and PV array in a hybrid solar–wind system has been presented by Borowy and Salameh in [167]. The system operation is simulated for various combinations of PV array and battery sizes and the loss of power supply probability (LPSP). Then, for the desired LPSP, the PV array versus battery size is plotted and the optimal solution, which minimises the total system cost, can be chosen. Another graphical technique has been given by Markvart [168] to optimise the size of a hybrid solar–wind energy system by considering the monthly average solar and wind energy values (input and output). However, in both graphical methods, only two parameters (either PV and battery, or PV and wind turbine) were included in the optimization process.

Yang et al. in [192] have proposed an iterative optimization technique following the loss of power supply probability (LPSP) model for a hybrid solar–wind system. The number selection of the PV module, wind turbine and battery ensures the load demand based on the power reliability requirement (desired LPSP) and the system cost is minimised. Similarly, in [124] an iterative optimization method was presented by Kellogg et al. to select the wind turbine size and PV module number needed to make the difference of generated and demanded power as close to zero as possible over a period of time. From this iterative procedure, several possible combinations of solar–wind generation

capacities were obtained. The total annual cost for each configuration is then calculated and the combination with the lowest cost is selected. This represents the optimal configuration for the system.

Eftichios Koutroulis et al. [176] proposed a methodology for optimal sizing of stand-alone PV/WG systems. This proposed methodology suggests (among a list of commercially available system devices) the optimal number and type of units ensuring that the 20-year round total system cost is minimised subject to the constraint that the load energy requirements are completely covered, resulting in zero load rejection. It means the authors finds the global optimum system configuration with relative computational simplicity. However, the configurations are not always cost effective. This is due to the small amount of load rejections are actually tolerable in order to gain an acceptable system cost. Since this is a zero load rejection system, this optimization algorithm has the potential of searching the oversized system.

A common disadvantage of the optimization methods described above is that the proposed methodology do not mention the best compromise point between system power reliability and system cost. The minimization of system cost function is normally implemented by employing probability programming techniques or by linearly changing the values of corresponding decision variables, resulting in suboptimal solutions and increased computational effort requirements [48]. Also, these sizing methodologies normally do not take into account some system design characteristics, such as PV modules slope angle and wind turbine installation height, which also affect the resulting energy production and system installation costs.

In this paper [48], one optimal sizing model for a stand-alone hybrid solar–wind system employing battery banks is developed based on the loss of power supply probability (LPSP) and the annualized cost of system (ACS) concepts. The optimisation procedure aims to find the configuration that yields the best compromise between the two considered objectives: LPSP and ACS. The decision variables included in the optimisation process are the PV module number, wind turbine number, battery number, and also the PV module slope angle as well as the wind turbine installation height. The configurations of a hybrid system that meets the system power reliability requirements with minimum cost can be obtained by applying an optimization technique such as the genetic algorithm (GA). It is said to be an advanced search and optimization technique in [179]; it is robust in finding global optimal solutions, particularly in multi-modal and multi-objective optimisation problems, where the location of the global optimum is a difficult task [129].

2.2.3 GA acts as an Optimal Sizing Algorithm

This part of review focuses on benefits of using the Genetic Algorithm (GA) in sizing renewable energy system instead of the theory of GA.

GA is an optimisation method based on the genetic process of biological organisms [193, 194].By mimicking this process, GA provides solutions to complex real world problems. The concept of GA was firstly proposed by Holland [5] and then widely utilized in many types of applications.

In the review paper [129], the input data of GA-based methodology is listed as follows:

1. The meteorological conditions.

2. The unit prices of the projected hybrid system components including installation and maintenance costs.

3. Some constraints can also be added to the algorithm. Example constraints can be given as limiting the maximum number of PV panels on a building roof that is constrained by roof area, limiting the number wind turbines installed on specific land constrained by land area, or limiting the power change slope of a fuel cell, etc. Many different constraints can be defined due to the type and preferences of application.

4. A fitness function must be defined as an input to the GA approach. This is the crucial highlight for this method.

5. The parameters for GA operators such as the percentage of selection and rate of mutation should be provided before the GA-based sizing process starts.
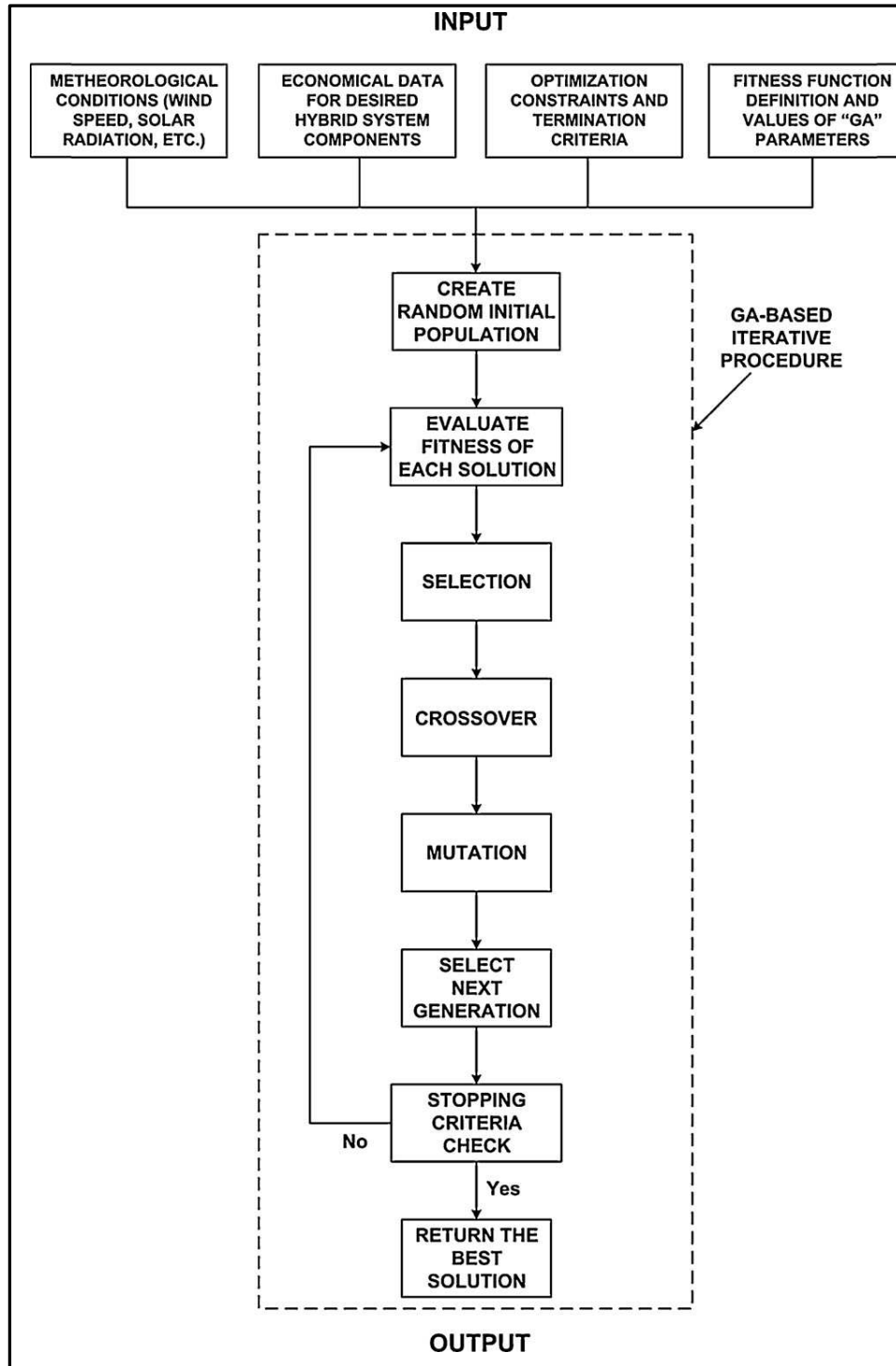
Figure 32 GA Flow Chart

With the given input data, GA sizing methodology provides an iterative procedure utilizing the GA operators until a predefined termination criteria or maximum iteration number are reached.

Briefly, a basic GA consists of five components. These components represents a random initial population generator, a 'fitness' evaluation unit and genetic operators for 'selection', 'crossover' and 'mutation' operations [193, 194, 195]. With the random population generation at the beginning, GA hence initiates random population for the hybrid system components that satisfies the load demand and power generation balance at each step. Each of the random solutions is evaluated according to he defined fitness function. The Selection operator selects the predefined percentage of the initial population base on their fitness value [196, 197]. Utilizing these selected solutions, the Crossover operator provides new possible solutions with the aim of achieving higher fitness values. This can be explained using the example shown below: For a PV–wind–fuel cell hybrid system, the selection operator may choose two different solutions of

1. 10/20/15 (10 kW wind turbine, 20 kW PV system, 15 kW fuel cell)

2. 5/25/12 (5 kW wind turbine, 25 kW PV system, 12 kW fuel cell).

When these two solutions undergo Crossover operation, two new possible solutions that can either have a lower or greater fitness value than current solutions can be written as following:

1. 5/25/15 (5 kW wind turbine, 25 kW PV system, 15 kW fuel cell) and

2. 10/20/12 (10 kW wind turbine, 20 kW PV system, 12 kW fuel cell).

The new population is created with the solutions selected by the Selection operator which this new solutions are previously undergone the

Crossover operation. Then, the selection of the solutions with greater fitness values and creation of a new population continues at each iteration during the iterative procedure. During the iterative process, the Mutation operator is applied to prevent getting trapped at a local minimum. For example, by changing the fuel cell size from 15 kW to 5 kW in a 10/20/15 solution (10 kW wind turbine, 20 kW PV system, 15 kW fuel cell) can be done by applying the mutation operator. This means that the fitness value of a part of the particular solution is changed or mutated. This procedure which consists of the selection, crossover and mutation operators is continued until the termination criteria of the iterative process [6, 198] is applied. This termination criterion is often defined by the designer.

The efficient performance of the GA iterative searching methods for finding the global optimum enables the utilization of an objective function in sizing renewable energy methodology [48]. GA avoids local minimum traps because GA operators avoid premature convergence and permutation problem. Mutation is one of the GA operators, which introduces random walk in search space. This explains how GA has higher probability of getting global optimal [176]. Moreover, GA operators also prevent the population chromosomes from becoming too similar to each other thus slowing or even stopping evolution during each iterative steps. The GA is relatively harder to code due to its complex structure; however, the advantage of being able to code large number of parameters on a chromosome makes GA suitable for sizing renewable energy system [129]. This advantage is not available in some other mostly applied approaches like simulated annealing, Particle Swam Optimisation (PSO) [129, 7]. It is more practical in which consists of more than three main components

such as PV module, wind turbine, battery and supercapacitor. The idea in combining more than one energy source with hybrid energy storage in the proposed renewable energy system provides a more economic, environment friendly and reliable supply of electricity in all load demand conditions compared to single-use of such systems [146].

In this study, optimal sizing of renewable energy system using the GA is carried out to design and search the optimal cost of the SB-HESS with the optimal configuration set of the components used. From the literature review done, there is none of the previous work on optimisation system cost was done for a hybrid energy storage energy system. However, authors in [176] shows the optimal sizing of a conventional PV-wind-battery system in terms of the number of components and the total system cost.

GA optimal sizing of renewable energy system is also best suited to this optimization domain where the system consists of larger number of components (such as PV panels, wind turbines, batteries and supercapacitor). This is because GA is a stochastic algorithm; randomness as an essential role in GA. Both operators in GA (selection and reproduction) require random procedures. Moreover, it also reduces the risk of trapping at the local optimal due to its nature and characteristic of GA. GAs always operate on a whole population of points (strings) i.e., GA uses population of solutions rather than a single solution for searching. This plays a major role to the robustness of GAs. It improves the chance of reaching the global optimum and also helps in avoiding local stationary point. Another operator in GA, mutation also aids in the randomness of algorithm and avoid algorithm to get trapped at the local optimal point. This increase the efficiency and accuracy of searching optimal

number of components used in our SB-HESS and the weight of the output responses in process supercapacitor fabrication.

2.2.3.1 Background of Genetic Algorithm

Genetic algorithms (GAs) were invented by John Holland in the 1960s and were developed by Holland and his students and colleagues at the University of Michigan in the 1960s and the 1970s [199, 200]. Holland's 1975 book Adaptation in Natural and Artificial Systems presented the genetic algorithm as an abstraction of biological evolution and gave a theoretical framework for adaptation under the GA [8]. Holland's GA is a method for moving from one population of chromosomes (which is also known as bit strings that made up of ones and zeroes) to a new population using a kind of 'natural selection' that controlled by the genetics (which is inspired by operators of crossover, mutation, and selection). Each chromosome consists of genes (which is also called bits) and each gene being an instance of a particular allele (it is either 0 or 1). The selection operator selects chromosomes in the population that is allowed to reproduce for the next population and on average the fitter chromosomes produce more offspring than the less fit ones. Crossover exchanges subparts of two chromosomes, roughly mimicking biological recombination between two single chromosome organisms [9]. Whereas, mutation randomly changes the allele values of some locations in the chromosome. While, selection reverses the order of a contiguous section of the chromosome, thus rearranging the order in which genes are arrayed. In most of the GA concept, 'crossover' and 'recombination' could mean the same thing.

Holland's introduction of a population - based algorithm with crossover, selection, and mutation was a major innovation. Moreover, Holland was the first to attempt to put computational evolution on a firm theoretical footing [199]. Until recently this theoretical foundation, based on the notion of schemas was the basis of almost all subsequent theoretical work on GAs [7, 201, 202]. This said, evolution is a method of searching among an enormous number of possibilities for desired solutions [6]. In biology the enormous set of possibilities is the set of possible genetic sequences, and the desired solutions are highly fitted organisms. This means the organisms are well able to survive and reproduce in those particular environments. Evolution can also be seen as a method for designing innovative solutions to complex and real-life problems [2, 203].

For example ,

> 'The mammalian immune system is a marvelous evolved solution to the problem of germs occupying the body.'

The mechanisms of evolution inspired the computational search methods.

The fitness of a biological organism depends on many factors. For example, its physical characteristics and how well it can compete with or cooperate with the other organisms around it. The fitness criteria continually change as creatures evolve. Evolution is searching through a constantly changing set of possibilities [9]. Moreover, evolution is a massively parallel search method [204, 200] . This means, evolution tests and changes millions of species in parallel rather than works on one species at a stage. This would also mean the high level rules of evolution are straightforward. Species evolve by means of random variation. This could be done by applying mutation, recombination, and other operators, followed by natural selection in which the

fittest tend to survive and reproduce, thus propagating their genetic material to next generations. In the section below, a brief explanation for the biology terminology, element of GA, inspiration of GA, and optimization and search space in GA are presented for a better understanding on the GA:

1. **Biology Terminology**

In the context of GAs, these biological terms are used in the analogy with real biology.

All living organisms consist of cells, and each cell contains the same set of one or more chromosomes - strings of DNA—that serve as a blueprint for the organism. A chromosome can be conceptually divided into genes - each of which encodes a particular protein [8]. Very roughly, one can think of a gene as encoding a trait, such as eye colour. The different possible settings for a trait (for example, blue, brown, hazel) are called alleles. Each gene is located at a particular locus (position) on the chromosome [205].

Many organisms have multiple chromosomes in each cell. The complete collection of genetic material (all chromosomes taken together) is called the organism's genome [8]. The term genotype refers to the particular set of genes contained in a genome. Two individuals that have identical genomes are said to have the same genotype. The genotype (information) [205] gives rise and later development, to the organism's phenotype - its physical and mental characteristics, such as eye colour, height, brain size, and intelligence .

Organisms whose chromosomes are arrayed in pairs are called diploid; organisms whose chromosomes are unpaired are called haploid.

In nature, most biologically reproducing species are diploid, including human beings, who each have 23 pairs of chromosomes (in each somatic non−germ) cell in the body. During biologically reproduction, (recombination or crossover) occurs: in each parent, genes are exchanged between each pair of chromosomes to form a gamete (a single chromosome), and then gametes from the two parents pair up to create a full set of diploid chromosomes. In haploid reproduction, genes are exchanged between the two parents' single−strand chromosomes [204]. Offspring are subject to mutation (in which single nucleotides elementary bits of DNA) are changed from parent to offspring, the changes often resulting from copying errors. The fitness of an organism is typically defined as the probability that the organism will live to reproduce viable or as a function of the number of offspring the organism is fertile enough to produce [6].

In GAs, the term chromosome typically refers to a candidate solution to a problem, often encoded as a bit string. The genes are either single bits or short blocks of adjacent bits that encode a particular element of the candidate solution [206]. for example, in the context of more-than-one parameter function optimization, the bits encoding a particular parameter might be considered to be a gene. An allele in a bit string is either 0 or 1; for larger alphabets more alleles are possible at each locus. Crossover typically consists of exchanging genetic material between two single chromosome haploid parents. Mutation consists of flipping the bit at a randomly chosen locus (or for larger alphabets,

replacing a the symbol at a randomly chosen locus with a randomly chosen new symbol) [205, 204].

Most applications of genetic algorithms employ haploid individuals, particularly, single−chromosome individuals [203]. The genotype of an individual in a GA using bit strings is simply the configuration of bits in that individual's chromosome. Often there is no notion of 'phenotype' in the context of GAs.

2. Elements of Genetic Algorithm

The chromosomes in a GA population typically take the form of bit strings. Each locus in the chromosome has two possible alleles: 0 and 1 [8]. Each chromosome can be thought of as a point in the search space of candidate solutions [207]. The GA processes populations of chromosomes, successively replacing one such population with another. The GA most often requires a fitness function (that assigns a score fitness) to each chromosome in the current population [6]. The fitness of a chromosome depends on how well that chromosome solves the problem at hand [203].

Table 12 Comparison of natural evolution and genetic algorithm terminology

Natural Evolution	Genetic Algorithm	Explanation
Chromosome	String (individual)	Solution (Coding)
Gene	Feature or character bit)	Part of solution
Allele	Feature value	Values of gene
Locus	String position	Position of gene
Genotype	Structure or coded string	Encoded solution
Phenotype	Parameter set a decoded structure	Decoded solution

3. Inspiration of Genetic Algorithm

Genetic Algorithm (GAs) is inspired by the way living organisms are adapted to the harsh realities of life in a hostile world, i.e., by evolution and inheritance. The algorithm imitates the process of evolution of population by selecting only fit individuals for reproduction. Therefore, a GA is an optimum search technique based on the concepts of natural selection and *survival of the fittest*. It works with a fixed-size population of possible solutions of a problem, called individuals, which are evolving in time. A GA utilizes three principal genetic operators: selection, crossover, and mutation [208].

Recombination or biological reproduction is a key operator for natural evolution [8]. Technically, it takes two genotypes and it produces a new genotype by mixing the gene found in the originals. In biology, the most common form of recombination is crossover. Crossover happens when two chromosomes are cut at one point and the halves are spliced to create new chromosomes. The effect of recombination is very important because it allows characteristics from two different parents to be assorted [209]. If the father and the mother possess different good qualities, it is expected that all the good qualities will be passed to the child. Thus the offspring, just by combining all the good features from its parents, may surpass its ancestors. Many people believe that this mixing of genetic material via reproduction is one of the most powerful features of GAs especially it was mentioned in [210]. As a quick parenthesis about reproduction, Genetic Algorithms representation usually does not differentiate male and female

103

individuals without any perversity. As in many livings species (e.g., snails) any individual can be either a male or a female. In fact, for almost all recombination operators, mother and father are interchangeable.

Mutation is the other way to get new genomes. Mutation consists in changing the value of genes [211]. In natural evolution, mutation mostly engenders non-viable genomes. Actually mutation is not a very frequent operator in natural evolution. Nevertheless, is optimization, a few random changes can be a good way of exploring the search space quickly. It is basic but it is more than enough to understand the operation and theory GAs.

The fitness of an individual in a genetic algorithm is the value of an objective function for its phenotype [6]. For calculating fitness, the chromosome has to be first decoded and the objective function has to be evaluated. The fitness not only indicates how good the solution is, but also corresponds to how close the chromosome is to the optimal one [211].

As mentioned earlier, GAs were envisaged by Holland [15] in the 1970s as an algorithmic concept based on a Darwinian-type survival-of-the-fittest strategy with reproduction. This means that the stronger individuals in the population have a higher chance of creating an offspring.

A genetic algorithm is implemented as a computerized search and optimization procedure that uses principles of natural genetics and natural selection. The basic approach is to model the possible solutions

to the search problem as strings of ones and zeros. Various portions of these bit-strings represent parameters in the search problem. If a problem-solving mechanism can be represented in a reasonably compact form, then GA techniques can be applied using procedures to maintain a population of knowledge structure that represent candidate solutions, and then let that population evolve over time through competition (survival of the fittest and controlled variation) [7, 212].

A GA generally includes the three fundamental genetic operations of selection, crossover and mutation [213]. These operations are used to modify the chosen solutions and select the most appropriate offspring to pass on to succeeding generations. GAs consider many points in the search space simultaneously and have been found to provide a rapid convergence to a near optimum solution in many types of problems; in other words, they usually exhibit a reduced chance of converging to local minima [10] .

Genetic algorithm applications are appearing as alternatives to conventional approaches and in some cases are useful where other techniques have been completely unsuccessful. Genetic algorithms are also used with other intelligent technologies such as neural networks, expert systems, and case-based reasoning. As mentioned in Section 2.2, methodology optimal sizing renewable energy system using are shown.

4. Optimization and search space

An optimization algorithm searches for an optimum solution by iteratively transforming a current candidate solution into a new, hopefully better, solution. Optimization methods can be divided into

two main classes, based on the type of solution that is located. Local search algorithms use only local information of the search space surrounding the current solution to produce a new solution. Since only local information is used, local search algorithms locate local optima (which may be a global minimum) [6]. A global search algorithm uses more information about the search space to locate a global optimum. It is said that global search algorithms explore the entire search space, while local search algorithms exploit neighbourhoods [9]. Optimization algorithms are further classified into deterministic and stochastic methods. Stochastic methods use random elements to transform one candidate solution into a new solution. The new point can therefore not be predicted. Deterministic methods, on the other hand, do not make use of random elements [214].

Based on the problem characteristics, optimization methods are grouped in the following classes (within each of these classes further subdivision occurs based on whether local or global optima are located and based on whether random elements are used to investigate new points in the search space) [9]:

- unconstrained methods, used to optimise unconstrained problems;

- constrained methods, used to find solutions in constrained search spaces;

- multi-objective optimization methods for problems with more than one objective to optimise;

- multi-solution (niching) methods with the ability to locate more than one solution [215]; and

- dynamic methods with the ability to locate and track changing optima. Subsequent sections discuss each of these optimization method classes.

Most often one is looking for the best solution in a specific set of solutions. The space of all feasible solutions (the set of solutions among which the desired solution resides) is called search space [6]. Each and every point in the search space represents one possible solution. Therefore each possible solution can be marked by its fitness value, depending on the problem definition. With Genetic Algorithm one looks for the best solution among a number of possible solutions- represented by one point in the search space i.e. GAs are used to search the search space for the best solution (minimum or maximum) [6]. The difficulties in this ease are the local minima and the starting point of the search.

In this project, constraint optimization is applied to Genetic algorithm. Many real world optimization problems are solved subject to sets of constraints. Constraints place restrictions on the search space, specifying regions of the space that are infeasible [9, 216]. Genetic algorithms have to find solutions that do not lie in infeasible regions. That is, solutions have to satisfy all specified constraints. There are three types of constraint, it can be linear or nonlinear. These type of constraints are used in this methodology step 3.2 and it is described as below [9]:

- Boundary constraints, which basically define the borders of the search space. Upper and lower bounds on each dimension of the search space define the hypercube in which solutions must be

found. While boundaries are usually defined by specifying upper and lower bounds on variables, such box constraints are not the only way in which boundaries are specified. The boundary of a search space can, for example, be on the circumference of a hypersphere. It is also the case that a problem can be unbounded.

- Equality constraints specify that a function of the variables of the problem must be equal to a constant.

- Inequality constraints specify that a function of the variables must be less than or equal to or, greater than (or equal to) a constant.

  There are numerous way of constraint handling [9, 217, 218]:

  - Reject infeasible solutions, where solutions are not constrained to the feasible space. Solutions that find themselves in infeasible space are simply rejected or ignored.

  - Penalty function methods, which add a penalty to the objective function to discourage search in infeasible areas of the search space.

  - Convert the constrained problem to an unconstrained problem, then solve the unconstrained problem.

  - Preserving feasibility methods, which assumes that solutions are initialized in feasible space, and applies specialized operators to transform feasible solutions to new, feasible solutions. These methods constrict solutions to move only in feasible space, where all constraints are satisfied at all times.

- Pareto ranking methods, which use concepts from multi-objective optimization, such as non-dominance, to rank solutions based on degree of violation.

- Repair methods, which apply special operators or actions to infeasible solutions to facilitate changing infeasible solutions to feasible solutions.

Both reject infeasible solutions and penalty function methods are used in this methodology step (optimal sizing RES using the GA).

2.3 Optimization of the fabrication process for element buffer in HESS

Optimization of process manufacturing supercapacitor is crucial in this project as it gives further reduction in the cost of the system. The concept of fabricating supercapacitors with the desired capacitance and voltage is to best-suits this project requirement after the system size is optimised. This is a crucial step to further optimise the cost of the system for a desired capacitance which might not be found in the commercial market.

The market price of supercapacitor is costly compare to lithium battery in terms of energy (Wh). The cost of both energy storage devices are shown in Table 13 [219] below:

Table 13 Performance of supercapacitor and lithium-ion battery

Function	Supercapacitor	Lithium-ion (general)
Charge time	1–10 seconds	10–60 minutes
Cycle life	1 million or 30,000h	500 and higher
Cell voltage	2.3 to 2.75V	3.6 to 3.7V
Specific energy (Wh/kg)	5 (typical)	100–200
Specific power (W/kg)	Up to 10,000	1,000 to 3,000
Cost per Wh	$20 (typical)	$0.50-$1.00 (large system)
Service life (in vehicle)	10 to 15 years	5 to 10 years
Charge temperature	–40 to 65°C (–40 to 149°F)	0 to 45°C (32°to 113°F)
Discharge temperature	–40 to 65°C (–40 to 149°F)	–20 to 60°C (–4 to 140°F)

The significant difference of the cost of the supercapacitor motivates a robust supercapacitor fabrication process. Besides that, the optimal sizing RES also prompted an idea of giving a big degree of freedom to fabricate the desired capacitance of supercapacitor for the system. The optimised size and specification of supercapacitor might hard to be found in the market. To avoid oversized supercapacitor to be used in the optimised system (and this definitely increases the cost of the system), a robust manufacturing supercapacitor process

using genetic algorithm within Taguchi Signal-to-noise ratio is implemented in this project. This is described in detail in Section 3.3 of this thesis. A brief literature review and theory of the Taguchi technique is also described below.

2.3.1 Taguchi Method

The Taguchi method, proposed by Genichi Taguchi, contains system design, parameter design, and tolerance design procedures to achieve a robust process and result for the best product quality. The purpose of system design procedure is to determine the suitable optimal levels of the process factors. The parameter design procedure determines the factor levels that can generate the best performance of the product or process. The tolerance design procedure is used to fine-tune the results of parameter design by tightening the tolerance levels of factors that have significant effects on the product or process. The Taguchi method can efficiently improve the effectiveness of the product or process by using a loss function and achieve the robust product quality in terms of the parameter design. Generally, the parameter design of the Taguchi method utilizes orthogonal arrays (OAs) to minimise the time and cost of experiments in analyzing all the factors and uses the signal-to-noise (S/N) ratio to analyse the experimental data and find the optimal parameter combination. Moreover, an analysis of variance (ANOVA) is employed to estimate the error variance and determine the significant parameters.

Optimization of multi-response problems in Taguchi Method

The conventional optimization method involves the study of one variable at a time, which requires a number of combinations of experiments that are time, cost and also labour intensive. The Taguchi method of design of experiments is a statistical tool involving a system of tabulated design (arrays) that allows a maximum number of main effects to be estimated in an unbiased (orthogonal) fashion with a minimum number of experimental runs. It has been applied to predict the significant contribution of the design variable(s) and the optimum combination of each variable by conducting experiments on a real-time basis. These set of data essentially relates to signal-to-noise ratio (SNR) to the control variables in a 'main effect only' approach. This approach enables both multiple response and dynamic problems to be studied by handling noise factors using Overall Evaluation Criteria (OEC). However, there is limitation of using OEC in optimization multi-response problems. The significant contributions of the Taguchi concepts is bringing focused awareness to robustness, noise and quality. Taguchi method has been widely applied in many industrial sectors; however, its application in fabrication of supercapacitor has been limited.

Conventional Method in conducting experiments

The conventional method of performing experiment to optimise process or product using an experimental design by identifying various independent factors and levels, and later conducting the experiments by altering one variable at a time (OVAT), while keeping all others at a predetermined level is very inefficient and unorganized. This is because the conventional method involves

carrying out many experiments, which is time consuming and not cost effective. Another problem arises is, these OVAT designs often neglect some of the interactions among the variables. Statistically designed experiments consist of several well-planned individual experiments conducted at a time. Generally, in designing of a statistically based experiment, it involves several steps such as [13] :

(i)   Selection of responses (performance characteristics of interest) that will be observed;

(ii)   Identification of the factors (the independent or influencing factors) to be studied;

(iii)   The different treatments (or levels) at which these factors will be set in different individual experiments; and

(iv)   Consideration of blocks (the observable noise factors that may influence the experiments as a source of error of variability).

The Taguchi Methodology

Taguchi's methodology has been widely applied in industrial process design. This technique is to generate enough process information to establish the screening for optimal conditions of parameters for a particular process using a minimum number of experiments [13]. The main difference of Taguchi's method compared to ordinary factorial optimization lies in the accounting for performance variations due to noise factors beyond the control of the design. Taguchi has emphasized the idea of robustness within the engineering community, and this is a major contribution to robust design methodology.

Taguchi states that 'quality engineering is not intended to reduce the sources of variation in products directly. Instead, one needs to make the systems of products or production processes less sensitive to sources of uncontrollable noise, or outside influences, through parameter design (off-line quality control) method'.

To account for design uncertainties in the framework of quality engineering were closely connected with the methodology of Taguchi. Taguchi proposed a three stage design methodology [13]:

1. System Design - to help determine the basic performance parameters of the product and its general structure;
2. Parameter Design - to enable optimisation of the design parameters to meet the quality requirements; and
3. Tolerance Design - to allow the fine-tuning of the design parameters obtained in the second stage.

Methodology steps is presented in Section 3.3 for optimisation of multi-response problems in process fabrication of supercapacitor by integrating the GA within Taguchi technique.

CHAPTER 3

RESEARCH METHODOLOGY

This project combines the fields of manufacturing and artificial intelligence in order to reduce the cost of implementation for hybrid supercapacitor battery systems in solar energy applications. In order to do this the following methodology was followed:

Table 14 Methodology, justification and implementation steps

	Methodology Steps	Justification	Implementation steps
1	**Identify the advantages of combining the supercapacitor and battery in one energy storage system.**	Enable the quantitative analysis of supercapacitor battery hybrid energy storage systems relative advantages.	• Battery SOC is calculated theoretically in a battery system with and without supercapacitor. This theoretical estimate value is used to set a guideline for the design of the energy management system. • A load profile is simulated by using a programmable load. • This is previously described in objective 3 of chapter 1.

2	**Breakdown the current cost structure of supercapacitor battery systems for solar application.**	Enable the quantitative analysis of cost improvements afforded by combining the supercapacitor and battery to form a hybrid energy storage system.	• Utilize the SVM to reduce the cost of the power electronics. • Use a GA to find the optimal number of supercapacitors and batteries for solar application in order to meet the **peak demand** at the lowest possible cost. • This is previously described in objectives 2 and 4 of Chapter 1.
3	• **Identify the PV Standards, which governs the characterization of supercapacitors used in PV systems.** • **Justify the Taguchi-GA because the standard deviation for the conventional process is big.**	Manufacture of supercapacitors which are fit to use and are economically feasible for solar applications.	• Implement a GA within the Taguchi Method to optimise the process factors of supercapacitor fabrication. This method improves the standard deviation of manufactured capacitance and ESR. • This standard deviation was identified as very important for this project because inconsistencies in the manufactured values will cause failures in matching **peak demand** as our systems are optimised using the GA and hence we do not have any excess capacitance which may otherwise be the case the GA was not used to optimised the SNR. • This is previously described in objective 1 of Chapter 1.

| 4 | **Construct lab scale prototype design and fabrication** | A low cost testing of ideas and methods previously mentioned above. | • Run system with predictive SVM and compare result by running system with power electronics.

 • Run both systems with and without supercapacitor in the circuit.

 • SOC profile (100 cycles life battery) for both battery system, with and without supercapacitor are monitored and compared. |

Table 15 summarizes how the methodology steps optimise the cost of the Supercapacitor-Battery Hybrid Energy Storage system (SB-HESS).

Table 15 Methodology steps that contributes to Cost Reduction

No.	Methodology Steps	Cost Reduction	Outcome
1	Identify the advantages of combining the supercapacitor and battery in an energy storage system.	• Decelerate the rate of damage mechanism of battery by coupling the supercapacitor. • This reduces the number of replacement battery throughout the lifespan of the system.	• Operational and maintenance cost for renewable energy system (RES) is reduced for long run.
2	Identify the current cost structure of supercapacitor battery systems for solar application and formulating an appropriate objective function.	• Optimal sizing supercapacitor-battery hybrid energy storage system (SB-HESS) using Genetic Algorithm (GA).	• An optimal system configuration of the system is obtained according to user requirement. • Therefore, sizing excess in initial number of components for the system to cater the power burst is avoidable, allowing a more feasible RES.
3	Use of the Taguchi with a GA method to optimise the standard deviation of the fabrication process.	• A robust supercapacitor is fabricated for the SB-HESS which reduced spread in tolerance of values which improve system performance.	• Consistent supercapacitor value is produced for an optimised SB-HESS.
4	Construct lab scale prototype design which allows low cost method of testing out idea before large scale implementation.	• The energy control system is controlled by switches and the SVM-load prediction system (Support Vector Machine).	• This energy management system reduces the cost of power electronics between the energy source/storage and the load.

3.1 Methodology Step 1
Identify the advantages of combining the supercapacitor and battery in an energy storage system

This step was done to show how the supercapacitor-battery hybrid energy storage (SB-HESS) maintains the high end of discharge voltage of the battery. This helps prolong batteries lifetime as mentioned in the literature review chapter. Hence, initial number of battery used is less and number of replacement battery thourhgout the project lifetime is decreased as well.

Lead-acid batteries are often used in energy storage system for solar application due to its low cost and wide availability [15]. System cost of a renewable energy system (RES) often incorporates with initial cost, replacement cost and operational/maintenance of the components. Lead-acid batteries have a high impact on lifetime cost of stand-alone solar energy systems [32, 15]. A higher lifetime cost means the batteries has shorter lifetime as compared with other components in the system. Lifetime of battery is dependent on battery C-rate (charge and discharge rate) which also subjects to different power peak value. Economically, oversized batteries and extensive fuel consumption (from diesel generator) should be avoided to cater the highest peak for a short period of time. This increases the overall cost of the system. Furthermore, RES is said to be greener if the number of batteries is minimised as lead acid battery is heavy and filled with toxic and corrosive chemical [220, 221].

To highlight the advantages of this hybrid energy storage system (prolong battery lifespan), an operation management for supercapacitor-battery hybrid energy storage system (SB-HESS) in stand-alone solar application with

optimised discharge strategies and knowledge on State-of-charge (SOC) and State-of-Health (SOH) are unavoidable.

In this research, SOC of a battery is important to estimate the cycle life before it fails to store electrical energy. In conventional system, batteries are always operated at low SOC and are recharged with low currents to cater the unpredictable sudden power peak. These stress factors are proven that it affects lead-acid battery lifetime [44, 32, 23]. An operation management is implemented based on the parameter which is said to be advantageous to save the battery lifespan. This operation management controls the energy flow from battery and supercapacitor to load by monitoring the voltage and current across the battery running on a simulated load profile.

In this section, the cell voltage values for both battery alone system and SB-HESS are shown theoretically. The cell voltage values are calculated to design and implement this operation management.

3.1.1 System Description

Two systems are evaluated and compared in terms of state-of-charge (SOC):

1. The **conventional single battery system** which consists of battery alone system. The system is often said to be infeasible due to the oversized of the batteries. The system is designed such a way that the batteries accommodate one power peak in the load profile when there is zero power output from the renewable energy resources. This is not cost effective as the energy storage system is oversized.

2. The **supercapacitor-battery hybrid energy storage system (SB-HESS)** which consists of battery (behaves as a primary energy storage device) and

supercapacitor (acts as an auxiliary energy storage device). The supercapacitor caters for the entire power peaks, while battery supply an optimal level of energy (average power demand) to avoid end deep discharge voltage of the battery, keeping the optimal C-rate (in our strategy: discharge rate) at a low discharge current.

In Section 4.2.3.2, SOC of the battery is monitored and plotted for both systems mentioned above. Cycle life for a battery is the number of charge / discharge cycles that can be accomplished during the lifetime of the device. It is an estimation and depends upon an assumption of an average depth-of-discharge. The load profile of battery cycle life provides a way of comparing energy storage systems and also to prove that SB-HESS is optimal for the power characteristics of the RES installation.

3.1.1.1 Battery individual energy storage system in RES

For this project, focus has been brought to the energy storage system in RES. In stand-alone power supplies that utilize solar energy, the energy input fluctuates substantially depending on climatic and meteorological conditions. As a result, the batteries are frequently operated at low state-of-charges (SOC), are frequently partial cycled and are recharged with low currents. This adversely affects the lifetime of lead-acid batteries.

An impractical solution to this problem could be an oversized battery with an early load shedding, to prevent deep SOC. Nevertheless, battery remains a lack of full charges with this method. Stand-alone power-supply system is incorporated with an additional controllable power supply, such as a

diesel generator Figure 33 [167, 222]. With such a generator, a full charge can be reached anytime even when the battery still has sufficient energy stored to supply the stand-alone system. However, this causes additional fuel consumption adding to the operational cost of the system. Utilization of diesel generator in RES is an increase in battery lifetime. However, it reduces the solar fraction. Solar fraction is the ratio of the amount of input energy contributed by a solar energy system to the total input energy required for a specific load profile. For a greener system, RES with generator is not favourable and considered in this project. Over-increased number of batteries which evidently spikes up the investments costs should be omitted.
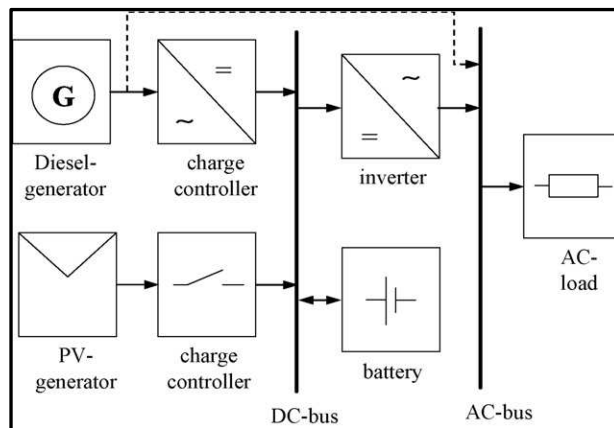
Figure 33 Conventional Stand-alone renewable energy system with PV-generator and diesel generator

3.1.1.2 Supercapacitor-battery hybrid energy storage system (SB-HESS) in RES

Two important enhancements are done to improve the conventional PV system mentioned above by coupling supercapacitors with the batteries as follows:

1. The number of batteries is reduced, while the system still able to deliver power peak.
2. Extend the battery life by avoiding deep discharge through high currents at a short instant.

Certain load applications require high current for a period of time e.g. motor starting applications; the starting current requirement can be 6-10 times the normal operating current of the motor [15]. Normally the peak current requirements are satisfied by the seal lead acid battery alone. The number of sealed lead acid batteries in this situation is large in order to deal with the high current. The peak current demand might only need to be met for a few seconds at a particular time. Sizing the battery based on the power peak can be costly.

By utilizing supercapacitor-battery hybrid energy storage system as shown in Figure 34 [15] , the number of battery is proven to be reduced and a higher SOC is maintained. This is greatly due to the characteristic of the supercapacitor and battery. Supercapacitor has a greater power density than the battery, which allows the supercapacitor to provide more power over a short period of time [38, 52, 53]. Conversely, the battery has a much higher energy density compared to a supercapacitor allowing the battery to store more energy and release it over a long period of time. In the hybrid system the peak power requirements of the load are supplied by the supercapacitor and the seal lead

acid battery supplies the lower continuous power requirements [223, 79, 76, 224].
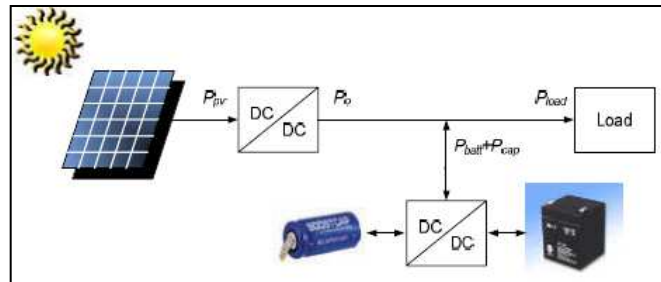
Figure 34 Supercapacitor-Battery Hybrid Energy Storage System (SB-HESS)

This supercapacitor-battery hybrid energy storage system solution would be effective for applications that reside in remote sites where regular battery maintenance is impractical or even impossible.

The supercapacitor is also a solution where ambient temperatures make it difficult to keep batteries inside the recommended operating range without compromising battery capacity and lifetime. SB-HESS aids in maintaining the battery to operate at an optimal range without draining it.

Supercapacitors are safer for the environment since they contain fewer hazardous materials compared to batteries [38]. Therefore, the lesser number of battery is used, the greener is the system.

3.1.2 Operation of SB-HESS (prototype) Management

The strategy focuses on optimising battery discharging. A quantitative assessment of the efficiency of operation management of the proposed hybrid energy storage system is shown below. Equation 26 shown below is used to design an operation management system for the proposed hybrid energy storage system. It is proven in [23, 32] that partial SOC of battery leads to strong and partially irreversible sulphation of the battery and thus reduces the battery lifetime. A threshold voltage of battery for the system is determined by considering the parameters shown below. This threshold voltage value is important to ensure the battery is individually switchable according to a threshold voltage level that is calculated based on the desired current state-of-charge (SOC), depth-of-discharge (DOD) and other parameters data set of the lead acid battery. This operation management system reduces time for battery to remain at low SOC, a decrease in the battery current rate, and hence full chargers during normal operating condition (steady-state).

This model describes the current-voltage characteristic of the lead-acid battery. It is reported in [32], it has an average accuracy for currents typically applied in stand-alone system for better than 2%. The required parameters used in the equations were already determined on the basis of experimental data in [32]. It is regardless of the physical significance of each parameter, which results from derivation, a theoretical calculation of the parameters is not possible. A second set of parameters reported in [3] has extended in the charging process. The terminal voltage of a battery has an additive composition consisting of open-circuit value, which approximately is in proportion to the

acid density and thus to the SOC, as well as the reaction, diffusion, crystallization and resistance over-voltages. These over-voltages are taken in the individual terms in Shepherd Model as a basis [23].

The concentration of the electrolyte changes as part of the chemical processes that take place when the battery is charged and discharged. During repeated cycles a concentration gradient can build up (from top to bottom) and the battery then behaves as several batteries of different concentrations working in parallel. Consequently, the charge acceptance is reduced and the capacity deteriorates. Eventually, the concentration gradients are levelled through diffusion. However, this takes a long time. They can be quickly removed by periods of gassing, where the rising bubbles effectively mix the electrolyte resulting in a more homogeneous electrolyte [23]. Hence, diffusion processes based on concentration gradients are not taken into consideration. Another term of the Shepherd Model [23, 32], which describes the crystallization overvoltage, is disregarded as well.

The formulation used in the model (Equation 26 [23]) consists of four terms:

$$U_{cell}(t) = U_{Od} - g_d SOC(t) + \rho_d(t)\frac{I_{batt}(t)}{C_N} + \rho_d(t)M_d\frac{I_{batt}(t)}{C_N}\frac{SOC(t)}{C_d - SOC(t)}$$

Equation 26

Table 16 Terms and Explanation for Equation 26

Terms	Explanation [32]
Open-circuit voltage, $\mathbf{U_o} = U_{0d}$	Full discharge equilibrium voltage i.e. the voltage of the cell when it is fully discharged and rested long enough for the electrolyte to reach constant density.
$g_d SOC(t)$	This term is associated with the state of charge (SOC) of the battery. It is assumed that this term is linear with respect to the depth of discharge (DOD).
$\rho_d(t)\dfrac{I_{batt}(t)}{C_N}$	Ohmic losses in the battery through the use of the internal resistance, which is an aggregate value of the various loss mechanisms which are proportional to the current. The major factors are the grid resistance and the resistance of the electrolyte.
$\rho_d(t)M_d\dfrac{I_{batt}(t)}{C_N}\dfrac{SOC(t)}{C_d - SOC(t)}$	The last term in the equation shows the reaction over-voltages. M represents the transfer overvoltage coefficient. It models the charge factor over voltage and is significant when the battery is very close to being empty or full.

However, several terms are neglected including dynamic terms to model the electrolyte diffusion and the dependence of the resistive elements to the SOC. This is unproblematic. The dynamic behavior of batteries is not relevant

in this context and the dependence of the resistive elements on SOC is both small and, as far as a parameter fit for determining the constants is concerned, is taken into account by the fourth term.

Table 17 shows the parameter data set [23] for batteries which was used for the Equations 3 above.

Table 17 Parameter data set for batteries

Terms (Units)	Charge, c	Discharge, d	Description index
U_{0i} (V)	2.26	2.1	Equilibrium voltage
g_i (VAh-1)	0.13071	0.09654	Electrolyte coefficient
ρ_i (ohm-cm)	0.43609	0.37885	Internal resistance
M_i	0.36488	0.28957	Transfer overvoltage coefficient
C_i	1.001	1.642	Capacity coefficient

where i = c or d.

Two energy storage systems are examined and compared, which are battery-individual energy storage system and supercapacitor-battery hybrid energy storage system theoretically. In conjunction with that, the I_{batt} and the DOD varies in different cases. At peak demand, battery individual energy storage system and battery supercapacitor hybrid energy storage system show different values for battery voltage and current ($U_{cell}(t)$ and $I_{batt}(t)$). According to the equation shown below, two different cell voltages are compared in two different operating conditions. It is assumed that:

1. A same type of sealed-lead-acid battery is used.

2. Both systems are applied on the same load profile generated by a 3A programmable load for a lab scale prototype system.
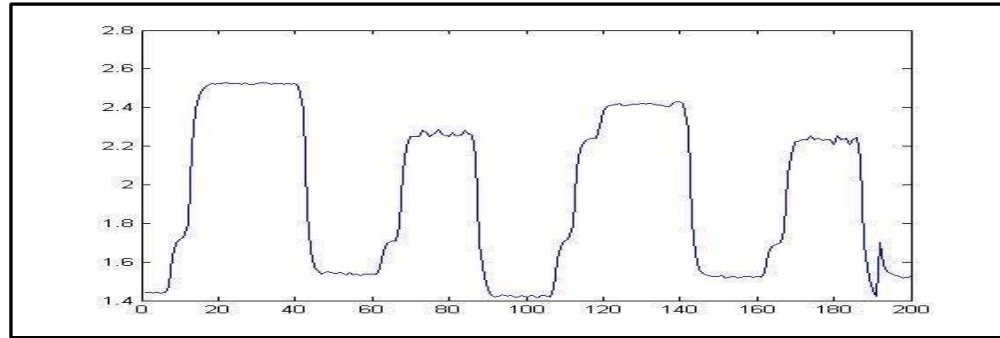
Figure 35 Simulated Load Profile

3. The critical situation is to be considered (night or rainy day) where only energy storage system is supplying to the peak load demand.

4. When the cell is discharging, for all $(I_{batt}t) \leq 0$

Table 18 Theoretical U_{cell} (V) and U_{batt}(V) Battery

Systems	I_{batt} (A)	DOD (%)	U_{cell} (V)	U_{batt}(V)
Battery Individual System	2.5	80	1.99	11.99
Supercapacitor/Battery hybrid system	1.5	20	2.06	12.41

Theoretically speaking, the I_{batt} value is taken from the load_profile 1 which is presented in Figure 35 above. Battery individual system suffers high current peak (2.5A) as the batteries cater for the entire power peak. However, batteries are not stressed up for the power peak in the hybrid energy storage system with the presence of supercapacitor.

The battery stand-alone system suffers a longer period of low SOC cycle. It means that the battery individual system remains for an extended period in a partial SOC, which leads to sulphation within battery and thus reduces the battery lifetime [76, 45]. Partial state of charge means the cycling has an inherent advantage in that, within a fairly broad SOC window of

approximately 20% - 80%, the battery is neither deep discharged nor put into overcharge under normal conditions of charge and discharge. This is not a good approach as only a fraction of the available energy is delivered on each cycle. Hence, the DOD is always higher for the conventional system to cater the power peak.

3.1.3 Summary

- Theoretically proven that the operating cell voltage is lower for the battery individual energy storage system. This shows that the battery is drained to supply the high current peak and the battery is approaching lower end-discharge-voltage. This shortens battery life as the battery is deep discharging high rates for short periods.

- By coupling supercapacitor and battery in an energy storage system, it maintains high SOC of the battery and avoids low DOD. It certainly reduces the rate of damage mechanism of batteries.

- I_{batt} is lower in hybrid energy storage system as the battery is not required to supply power peak in the load profile. Hence, the number of battery (overall capacity of battery) is reduced.

- Values of desired DOD, desired SOC and U_{batt} (V) set as a guideline to design an energy control strategy which is presented in Methodology Steps 2.

- The role of supercapacitor in a hybrid energy storage system is to meet peak load demand and also allows for the downsizing number of battery, reducing the depth-of-discharge (DOD), reducing the sulphation of battery, and most importantly, prolongs the battery's lifespan.

3.2 Methodology Step 2
Identify the current cost structure of supercapacitor battery systems for solar application

In the previous section, it explains how the presented advantages of pairing supercapacitor to the battery system extends battery lifespan. In this section, design, simulation and optimisation on the hybrid energy storage system are carried out using HOMER and GA. The rationale shown below motivates the design, simulation and cost optimisation on the hybrid energy storage system:

1. Maintain an optimal level of SOC battery during discharge.

2. Avoid low sudden DOD.

3. Avoid end-of-discharge voltage suggested in the data sheet before the battery has to be recharged.

Optimal sizing PV-Wind-Battery system using a GA and HOMER are carried out in this section. HOMER covers energy storage devices other than lead acid batteries such as flywheels, hydrogen and flow batteries. However, supercapacitor is not incorporated in HOMER library. Designing and optimising system with supercapacitor is merely impossible in HOMER. The idea has been presented using the GA to optimal size the autonomous SB-HESS due to the flexibility of the GA in coding a large number of components. The implemented GA fitness functions embeds with the essential information which is related to initial, maintenance and operational cost of the components used in the systems based on the market price. The conventional battery alone system and SB-HESS are designed and optimised for 20 years. 20 years is selected based on the longest lifespan components in the system for this simulation and optimization, which is PV panel [123]. According to [123], PV panel can last

approximately 20 – 25 years of lifespan, but the efficiency drops after 12 years

installation and it is estimated from 90% to 85%-80%. It applies in HOMER

component input and GA fitness function.

In the sub-sections below, methodology steps on:

1. optimal sizing PV-wind-battery system using HOMER

2. optimal sizing PV-wind-battery system using GA, and

3. optimal sizing PV-battery-supercapacitor system using GA are shown

3.2.1 Design, Simulation and optimization of PV-wind-battery system using HOMER

HOMER, Micropower Optimization Model is a computer model developed by

the U.S National Renewable Energy Laboratory (NREL) to assist in the design

of micropower systems and to facilitate the comparison of power generation

technologies across a wide range of applications [14]. Generally, HOMER

models a power system's physical behaviour and its life-cycle cost, which is the

total cost of installing and operating the system over life span. This also means,

in the simulation process, it models a particular system configuration; the

optimization process determines the best possible optimal system configuration

which satisfies the user-specified constraints at the lowest total net present cost

(NPC) [225] .

In this project, HOMER was used to validate the efficacy of the GA and

its objective function where this is proven approximately the same GA was

used for the prototype system.

3.2.1.1 Design and Simulation of RES

i. System Description

A PV-Wind-battery system is designed and simulated using HOMER. The specification of the components used is described in the section below. This design of renewable energy system consists of hybrid energy sources that is coupled with batteries only system. Diesel generator is not considered in the system. This is to ensure a zero CO_2 emission system. The simulation result obtained in paper [146, 226] shows that the power system with PV-Diesel generator-Battery has a lower installation cost, but higher operation and maintenance costs; additionally, it was less efficient and released contaminating emissions (such as CO_2, NO_x and particles). Diesel generator is not taken into consideration for this project. The reason being is to guarantee zero emission of hazard gas and a greener system. Hence, PV-Wind-Battery is designed and simulated using HOMER.

1. **Location**

   In this study, hypothetical model a household in a residential area in the geographical coordinate of the location Semenyih is

   - Latitude: 2.9° N,
   - Longitude: 101°53 E,
   - Altitude: 39 m (approximately) above sea levels

Coordinate: 2°9N longitude, 101°53E latitude

Figure 36 Location for the hypothecial model

Figure above is extracted from Google Earth **[227]**.

2. Electrical Load Profile

Deciding the load profile is important to design PV-Wind-Battery system because an optimised design of RES is always catered for a specific load profile. Oversized of energy sources are infeasible and cost ineffective. Load profile is simulated based on the electrical appliances power rating shown in Table 19.
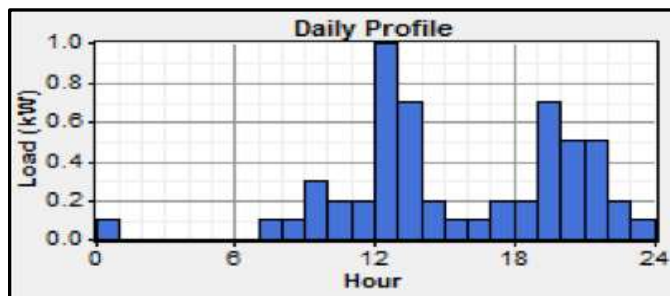
Figure 37 Load Profile from HOMER

134

HOMER simulates the operation of a system by making energy balance calculations for each of the 8760h in a year. Measured hourly load profiles are not available, so load data were synthesized by specifying typical daily load profiles and then adding some randomness of daily 10% and hourly 15% noise. These have scaled up the annual peak load to 1.5 kW and primary load to 5.4 kWh per day.
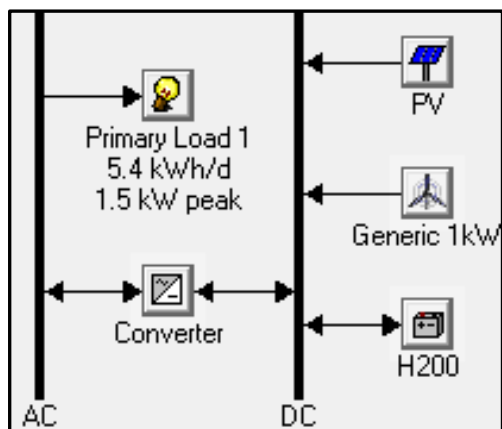
Figure 38 HOMER implementation of PV-Wind-Battery Energy System

Table 19 Energy demands of the electrical appliances

Electrical Appliances	Power (W)
Compact Fluorescent Bulb	15
Refrigerator	700
Personal Computers	600
Control System/Electrical Power Point	500
Fans	150
Washing Machine	300

3. Renewable Energy Sources

- **Solar Energy**

HOMER synthesizes solar radiation values for each of the 8760h of the year by using Graham algorithm [228, 229]. This algorithm produces realistic hourly data, and it is easy to use because it requires only the geographical coordinates and the monthly average solar data values. The synthetic data displays realistic day-to-day and hour-to-hour pattern. The synthetic data are created with certain statistical properties that reflect global average values. Result obtained in [228] show that synthetic solar data produced virtually the same simulation results as real data as the result obtained in [229].

Solar radiation data for the selected region was obtained from the NASA Surface Meteorology and Solar Energy website (NREL) [156, 230]. The solar radiation data and the clearness index for the selected site mentioned above is shown below in Table 20 and Figure 39. The solar irradiance data shown is the monthly average data for year 2012 at the longtitude and latitude mentioned above.

Table 20 Baseline Data for PV

Month	Clearness Index	Daily Radiation (kWh/m²/day)
January	0.458	4.505
February	0.481	4.918
March	0.489	5.126
April	0.488	5.023
May	0.474	4.669
June	0.496	4.733
July	0.485	4.671
August	0.497	4.994
September	0.475	4.912
October	0.483	4.944
November	0.477	4.709
December	0.481	4.488
Average:	0.481	4.806

Scaled Annual Average(kWh/m²/day): 4.12
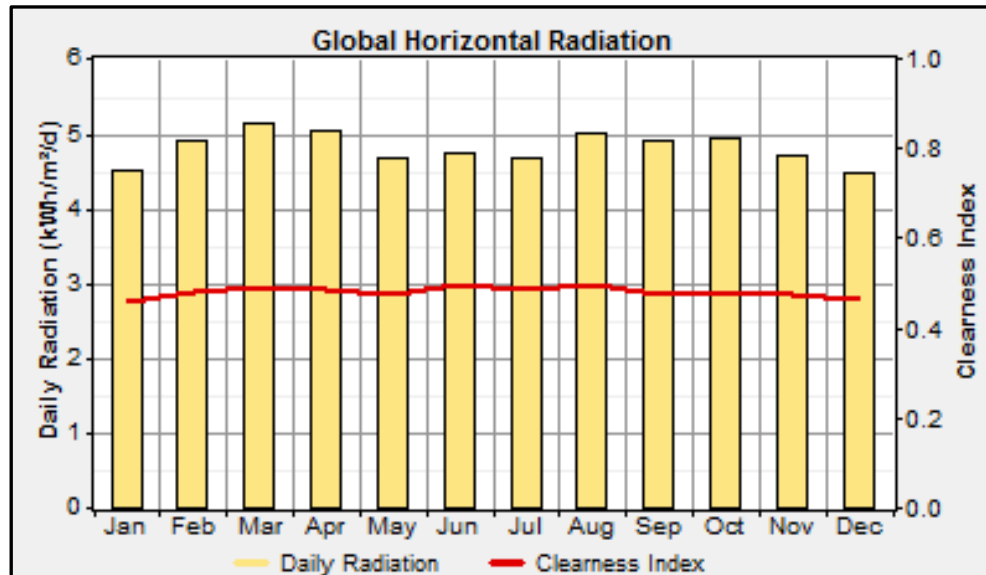
Figure 39 Average monthly solar radiation kWh/m²/day and clearness index

The clearness index has a simple definition. It is equal to the global solar radiation on the surface of the earth divided by the extra-terrestrial radiation at the top of the atmosphere. In other words, it is the proportion of the extra-terrestrial solar radiation that makes it through to the surface [231, 232]. It varies from around 0.8 in the clearest conditions to near zero in overcast conditions. The monthly average clearness index may vary from near 0.8 down to maybe 0.2 surface [231].

One can calculate precisely the amount of solar radiation that strikes the top of the atmosphere anywhere on earth with just the latitude. Therefore, if the amount of radiation striking the surface is specified, HOMER immediately divides that value by the amount of radiation striking the top of the atmosphere to calculate the clearness index [233]. If the clearness index is specified instead, HOMER multiplies that value by the extra-terrestrial radiation to calculate the amount of radiation striking the surface.

In this case, the average of the clearness index and daily radiation are 0.481 and 4.806 respectively. The value of clearness index and daily radiation do not fluctuate much. From Table 20, it tells us that the guaranteed annual power is 4.12 kWh/m^2/day which is good for solar energy system.

- **Wind Energy**

Since the energy from the PV array is not sufficient to supply the average daily energy demand, wind turbine is one of the supporting combined

alternative to provide the remaining power needed to charge up the battery and load demand. Scaled annual average shown in the Table 21 is used to determine the sensitivity analysis in HOMER simulation. This also implies that the annual guaranteed wind speed is 2.89m/s. HOMER determines a scaling factor by dividing the scaled annual average by the baseline annual average and multiplies each baseline value by this factor. By default, HOMER sets the scaled average equal to the baseline average, which results in a scaling factor of 0.95. This scaled annual average examines the effect of higher or lower wind speeds on the feasibility of system designs.

Table 21 Baseline Data for wind speed

Month	Wind Speed (m/s)
January	1.800
February	1.800
March	3.000
April	3.000
May	3.000
June	3.000
July	4.000
August	5.000
September	5.000
October	3.000
November	2.000
December	1.800
Average:	3.041

Scaled Annual Average (m/s): 2.89

In [161, 228] say that as the wind turbine tower is higher, it increases the initial, operational and maintenance cost, however the wind speed is tends to be higher at higher position. An anemometer height is one of the parameter in HOMER simulations.

When hourly wind speed data is not available, hourly data can be generated synthetically from the monthly averages. HOMER's synthetic wind speed data generator is different to use than the solar data because it requires four parameters [157, 229].

i.   The Weibull (k) value: k value is a measure of distribution of wind speed over the year. The default value is 2 because this has been shown to represent most wind regimes fairly accurately. The default value is used in this study.

ii.   The autocorrelation factor: this factor measures the randomness of the wind. Higher values indicate that the wind speed in 1h tends to depend strongly on the wind speed in the previous hour. Lower values mean that the wind speed tends to fluctuate in a more random fashion from hour-to-hour. The autocorrelation factors tend to be lower (0.70−0.80) in areas of complex topography and higher (0.90−0.97) in areas of more uniform topography. In this study, 0.85 is used. 0.85 is the default value and is the mid-value of the higher and lower value.

iii. The diurnal pattern strength: it is a measure of how strongly the wind speed depends on the time of day. In most locations, the afternoon trends to be windier than the morning. A high value of the diurnal pattern strength shows that there is a relatively strong dependence on the time of day and vice versa [234, 235]. In this study, 0.25 is used.

iv.   The hour of peak wind speed: it is the time of day that tends to be windiest on average throughout the year. In this study, 15:00 is used

as the hour of peak wind speed according to the simulated wind speed in HOMER. Table 22 shows advanced parameters for HOMER wind resource input.

Table 22 Advanced parameters for HOMER wind resource input

Parameter	Unit
Weibull (k) value	2
autocorrelation factor	0.85
diurnal pattern strength	0.25
hour of peak wind speed	15:00

The parameters shown in Table 22 are taken from [234, 235] . Based on the studies carried out in [234, 235], these values are said to be optimal values in order to obtain high wind energy.

4. Economics

Considering the project lifetime to be 20-years, the annual real interest was taken as 0%. Generally speaking, the real interest rate is equal to the nominal interest rate minus the inflation rate. The appropriate value for this variable depends on current macroeconomic condition, the financial strength of the implementing entity, and concessional financing or other policy incentives [236, 156]. However, in this case, annual real interest is not our concern as Malaysia government subsidises the renewable energy system. The capacity shortage fraction (C.S.F) is the fraction of the total load plus operating reserve that system fails to supply. For this HOMER's simulation part, C.S.F of 0%, 0.01% and 0.02% are simulated.

5. Photovoltaic panels

HOMER deals with PV array in terms of rated kW, not in m^2. HOMER assumes that the output of the PV array is linearly proportional to the incident solar radiation. The PV modules composed of several solar cells are clustered in series–parallel arrangement to form solar arrays with the necessary capacity. In the proposed systems, PV array sizes taken into account were 0 (no PV array), 2, 4, 6, 8, 10, 12, 14, 16, 18 and 20 kW.

The parameters considered for the simulation of solar PV panels are tabulated in Table 23. Efficiency of solar panels drops as the temperature of the solar panels increase. It is worth mentioning that HOMER's PV input GUI has a derating factor. Ought to be the slightly hotter climate according to [233] a derating factor of 80% was applied to the electric production from each panels instead of the default value of 90%. The purpose of 'derating factor' is to compensate the reduction in efficiency of the PV panels as in the actual conditions are less favourable than standard test conditions STC, (cell temperature = 25°C and solar irradiance = 1 kW/m^2, provided by the manufacturer, as well as the ambient temperature and irradiation conditions) [176]. This derating factor reduces the PV power production by 20% to approximate the varying effects of temperature, dust and wiring losses on the panels. The PV panels were modelled as fixed and tilted south at an angle equal to latitude of the location.

Table 23 PV Panel Technical Parameters and Cost

Parameter	Unit	Value
Rated Power	kW	0.100
Capital Cost	$	443
Replacement Cost	$	443
Operational and Maintenance Cost O&M)	$	12
Lifetime	Years	20
Derating Factor	Percentage %	80
Tracking System	No tracking System	

The capital cost for PV panels are slightly higher than the cost shown in Genetic Algorithm fitness function in the next section. The commercial price for that particular PV panel is $335, however, HOMER does not model the battery charge controller as a separate component [237]. Therefore, its cost and efficiency in the values you specify for other components and the best place to include the charge controller costs and efficiency is the PV array inputs. In the cost of the PV array, the cost of the charge controller is included. Moreover, the PV derating factor is also reduced to account for the efficiency of the charge controller. In this case, initially the derating factor of 90% is to account for losses in the PV array, and the efficiency of the charge controller is 90%. Therefore, the final derating factor is 81%.

6. Wind Turbine

The wind turbine was simulated in the model based on the technical data and economic parameters of the wind turbines Generic 1kW. Every wind turbine has a power curve specifying power output versus wind speed. HOMER just refers to the power curve when calculating wind turbine power output.

143

Technical and economic parameters for selected wind turbine are tabulated in Table 24.

Table 24 Wind Turbine-Technical Parameters and Cost

Parameter	Unit	Value
Rated Power	kW	1
Capital Cost	$	2240
Replacement Cost	$	2240
Operational and Maintenance Cost (O&M)	$	118
Lifetime	Years	20
Hub Height	m	15

7. Converters (Inverter)

A power converter is used to maintain the flow of energy between the AC and DC components. Table 25 shows the technical and economic parameters of the converter. The inverter and rectifier efficiencies were assumed to be 85% and 90% for the sizes of 2, 4, 5, 6, 7, 8, 9, 10, 12, 14, 16 kW considered. The sizes are defined for the purpose of providing a search space in HOMER simulation. HOMER also simulates each system with power switched between the inverter and the generator. These devices were not allowed to operate in parallel.

Table 25 Converter-Technical Parameters and Cost

Parameter	Unit	Value
Rated Power	kW	1.5
Capital Cost	$	1942
Replacement Cost	$	1942
Operational and Maintenance Cost (O&M)	$	19
Lifetime	Years	20

8. Batteries

HOMER allows user to add new component with the new specification and cost of the battery. A Hoppecke 12V, 120Ah batteries are used in this PV-Wind-Battery system. The specifications are shown in Table 26. According Hoppecke data sheet [238], the minimum battery life is 10 years if the battery is not drained more than DOD 80-90% for ~600 cycles at an optimal temperature. Battery lifetime greatly depends on the pattern of the load profile.

HOMER uses the Kinetic Battery Model and represents batteries as a 'two tank' system [239]. One tank provides immediately available capacity while the second can only be discharged at a limited rate.

HOMER set the DC bus voltage by defining a number of batteries per string. This defines the number of battery connects in series. On the battery input page, the number of batteries per string is specified. HOMER displays the bus voltage, which it calculates by multiplying the battery's nominal voltage by the number of batteries per string.

Table 26 Specification of Hoppcake Battery

Parameter	Unit	Value
Nominal Voltage	Volt	12
Nominal Capacity	Ah (kwh)	118 (1.42)
Maximum Charge Current	A	60
Round-trip efficiency	Percentage (%)	82.46
Maximum State-of-Charge	Percentage (%)	80
Capital Cost	$	316
Operational and Maintenance Cost O&M)	$	6.32
Replacement Cost	$	316

ii. Control Strategy

Control strategy used in HOMER simulation is charge-following. The set point of battery SOC is set to 0.8. After modelling is done, the model will be implement based on the parameters, constraint and the output obtained from HOMER.

In hybrid source systems with batteries and without diesel generators, the dispatch strategy is simple where the battery charges if the renewable energy is in excess after meeting the demand, and the battery discharges if the load exceeds the renewable energy.

3.2.1.2 Summary

- HOMER uses constraint to optimise the cost of the system. Stating the different constraints in HOMER leads to different optimization result. For example, the capacity shortage of the system is a constraint in HOMER.

- Cost and technical specification of components are defined in HOMER before the simulation and optimization result is obtained. This is important to ensure a feasible simulation.

- Simulation is the first step of implementing a prototype. This is important to save unnecessary cost in implementing a system.

- The result obtained in HOMER for the PV-Wind-Battery is compared with the result obtained from the implemented GA fitness functions shown in the next section.

3.2.2 Methodology Optimal Sizing of RES using the GA

Supercapacitor is the auxiliary energy storage in the implemented renewable energy system (RES). Design and simulation for the implemented RES cannot be done in HOMER as the HOMER library does not include supercapacitor. However, if model a large supercapacitor that functions as an energy storage device, this means that the system can use it to store energy from one time step to the next or from one day to another, it can be done that using HOMER's battery module. A flat capacity curve, a really high lifetime throughput, and a high round-trip efficiency for a supercapacitor are expected. On the other hand, if the supercapacitor does not store much energy and it is sufficient to serve the load for a few seconds, this primarily affects power quality or system stability. HOMER does not allow to model that because it does not model those effects as this is using the battery module theory. Therefore, it is not feasible to optimise the implemented system using HOMER.

GA is chosen for the optimal sizing the implemented RES as GA is not easy to trap in local optimal point and a higher freedom in coding more parameters as compared to other optimization techniques mentioned in Section 2.2.2. The proposed stand-alone system includes hybrid energy storage which consists of batteries and supercapacitors. This system is compared with the battery only RES. By considering the 20-year round total system cost, the objective function is made up of the sum of the respective components initial capital, maintenance and operational costs. Concept on constructing fitness functions which subjects to constraints is shown to optimise PV-wind-battery system, PV-wind-battery-supercapacitor system and a prototype PV-battery-supercapacitor are presented in Section 3.2.2-1, Section 3.2.2-2 and Section

3.2.2-3 accordingly. These GA fitness functions are computed to the GA code written using MATLAB R2011b. The code is documented in Appendix A2.

3.2.2.1 Optimal Sizing of Battery Single Energy Storage System (SB-HESS) using the GA

The objective function is the total net present cost (NPC) of the system which also represents the life-cycle cost. Net present cost includes the initial cost of the components, and all the future cost which consists of the maintenance and operational cost of the components throughout the total life of installation. The maintenance and operation cost of each unit of the components per year has been set to 2% of the corresponding capital cost. Normally, the life span of the system follows the life span of the solar panels [123, 240] . This is because the life span of solar panel in the system has the longest life span among the other components [123, 240, 169]. A same location mentioned in the previous part is used for GA optimal sizing RES, which is Semenyih. The objective function optimises the following costs:

- Cost of purchasing solar panels, wind turbines, the batteries, the inverter, the PV battery chargers.

- Cost of maintenance and operational of the solar panels, wind turbines, the batteries, the PV battery chargers and the inverters.

- Cost of replacing the batteries, the PV battery chargers, and the inverters.

Based on the different type of cost listed above, fitness function and constraints are constructed to design and optimise the renewable energy system.

1. Fitness Function

i. PV-wind-battery system

$$Z_{(N_{\text{PV}},N_{WG},N_{\text{BAT}},N_{\text{CH}})} = N_{\text{PV}} \cdot (C_{\text{PV}} + y_{\text{P}} \cdot M_{\text{PV}}) + N_{WG} \cdot (C_{WG} + y_p \cdot M_{WG} + h \cdot$$

$$C_h + y_p \cdot h \cdot C_{hm}) + N_{\text{BAT}} \cdot (C_{\text{BAT}} + R \cdot C_{\text{BAT}} + (y_{\text{P}} - R - 1) \cdot M_{\text{BAT}}) + N_{\text{CH}} \cdot$$

$$C_{\text{CH}} \cdot (y_{\text{CH}} + 1) + N_{\text{CH}} \cdot M_{\text{CH}} \cdot y_{\text{P}} - (y_{\text{CH}} - 1) + C_{\text{INV}} \cdot (y_{\text{INV}} + 1) + M_{\text{INV}} \cdot$$

$$(y_{\text{P}} - y_{\text{INV}} - 1) \qquad\qquad \textbf{Equation 27}$$

where h is the height of the WG tower in meter, C_{PV}, C_{WG}, and C_{BAT} are the capital cost (\$) of one module, WG and battery respectively, C_h is the capital cost (\$) for the WG tower per meter (\$/m), C_{hm} is the maintenance cost per meter and year (\$/meter/year), C_{CH} is the capital cost of one PV battery charger (\$), y_{CH} and y_{INV} are the expected numbers of PV battery charger and DC/AC inverter replacements during the 20-year system lifetime (and it is equal to the lifetime 20 years) divided by the Mean Time Between Failures (MTBF) of power electronic converters [176, 241], C_{INV} is the capital cost of the DC/AC inverter, (\$). Project lifetime, y_{p} is 20 years. R is the expected number of battery replacement which depends on y_{batt}. y_{batt} is the expected battery lifespan during the 20-years system operation. It depends on the battery energy each hour of the simulation by dividing the total year-to-date of charging the battery bank by the total year-to-date amount of energy put into the battery bank. It is computed using Equation 28 shown below:

$$Battery\ lifetime, y_{batt} = N_{BAT} \cdot \frac{Q_{lifetime}}{Q_{annual}} \qquad \textbf{Equation 28}$$

Where lifetime throughput for a single battery, $Q_{lifetime}$ and annual throughput of the a single battery, Q_{annual} are shown in Equation 29 and Equation 30.

$$Q_{lifetime} = C_{cycleDOD} \cdot DOD \cdot V_N \cdot C_N$$

Equation 29

$$Q_{annual} = \eta_{RT} \cdot P_{annual}$$

Equation 30

N_{BAT}, the number of batteries,

DOD, Depth-of-discharge of the battery (where the state-of-charge minimum SOC of the battery is set). Simulation is carried out for, DOD = 1.0, 0.9, 0.8, 0.7, 0.6 and 0.5.

$C_{cycleDOD}$, the number of charge and discharge cycle of the battery (based on data sheet of the battery),

V_N, the nominal voltage of the battery, $V_N = 12V$

C_N, the nominal capacity of the battery, $C_N = 118Ah$

η_{RT}, the round-trip energy efficiency, $\eta_{RT} = 87.46\%$,

M_{CH} and M_{INV} are the maintenance costs per year ($/year) of one PV battery charger and DC/AC inverter respectively. In addition, the number of PV battery chargers, N_{CH} is equal to the total number of PV power generation blocks which depends on the number of PV modules, N_{PV}. It is calculated using the equation below:

$$N_{ch}^{PV} = \frac{N_{PV} \times P_{PV}^m}{P_{ch}^m}$$

Equation 31

where P_{ch}^m is the power rating of the selected battery charger (W) and P_{PV}^m is the maximum power of one solar panel under standard test condition (W), under the manufacturers' specification. In this case, the power rating for solar panel, P_{PV}^m is 100 W and the power rating for PV battery charger, P_{ch}^m is 300 W.

ii. PV-battery system

Equation 32 shows the fitness function for PV-Battery system. Wind generator terms in Equation 27 is removed and Equation 32 is formulated as follows:

$$Z_{(N_{PV}, N_{BAT}, N_{CH,})} = N_{PV} \cdot (C_{PV} + y_P \cdot M_{PV}) + N_{BAT}$$
$$\cdot (C_{BAT} + R \cdot C_{BAT} + (y_P - R - 1) \cdot M_{BAT})$$
$$+ N_{CH} \cdot C_{CH} \cdot (y_{CH} + 1) + N_{CH} \cdot M_{CH} \cdot y_P$$
$$- (y_{CH} - 1) + C_{INV} \cdot (y_{INV} + 1) + M_{INV}$$
$$\cdot (y_P - y_{INV} - 1)$$

Equation 32

where

C_{PV} and C_{BAT} are the capital cost ($) of one module and battery respectively,

C_{CH} is the capital cost of one PV battery charger ($),

y_{CH} and y_{INV} are the expected numbers of PV battery charger and DC/AC inverter replacements during the 20-year system lifetime and it is equal to the lifetime 20 years) divided by the Mean Time Between Failures (MTBF) of power electronic converters Holtz et al., 1994),

C_{INV} is the capital cost of the DC/AC inverter, (\$), R is the battery lifetime.

Project lifetime, y_p is 20 years.

R is the expected number of battery replacement which depends on y_{batt}. y_{batt} is the expected battery lifespan during the 20-years system operation. It is computed using the Equation 28.

M_{CH} and M_{INV} are the maintenance costs per year (\$/year) of one PV battery charger and DC/AC inverter respectively.

2. Boundary

The fitness function for the battery alone RES is subject to the initial boundary

as shown below:

$$15 < N_{PV} < 30$$

$$1 < N_{WG} < 3$$

$$4 < N_{BAT} < 36$$

$$N_{CH} < 0$$

$$N_{INV} < 0$$

The total power of PV, P_{pv} and wind generator, P_{wind} is not more than

2.0 kW. This is defined based on the random variability (percentage) set for the

simulated load profile which is explained in the section below. For the

operaitng reserve (in this case battery) the maximum throughput for one battery

is 1.416 kWh based on the data specification of the battery. This throughput of

the battery is constrained based on the DOD defined in the system. The battery

is sized based on the highest peak in the load profile for the battery-only

system. It also depends on the loss of power supply probability (LPSP) set by the user. It is a trade-off between the system cost and the power failure time. The concept of the LPSP is explained in the section below.

3. Constraints

Constraints in a GA are important because it places the objective function in the proper search space which is related to real life conditions in which we wish to optimise the system. With proper constraints we are able to solve the objective function accurately and implement that solution in the practical situation under consideration. GA searches thoroughly over the search space. With improper constraints the GA will still find the optimal solution, however, it may not be practical to implement.

In order to optimise the cost of a renewable energy system, a compromise must be achieved between the size of the energy storage system and the power requirement. There are three constraints used for the implemented fitness functions.

i. Loss of Power Supple Probability (LPSP)

LPSP is defined as the probability that an insufficient power supply results (when the hybrid system PV array, wind turbine and battery storage) is unable to satisfy the load demand [48]. It is a feasible measure of the system performance for an assumed or known load distribution. A LPSP of 0 means the load will always be satisfied; and an LPSP of 1 means that the load will never be satisfied [48]. LPSP is a statistical parameter [242, 243]; its calculation is not only focused on the abundant or bad resource period.

153

Therefore, if renewable energy output is low, the system suffers from a higher probability of losing power. This is because of the intermittent solar radiation and wind speed characteristics, which highly influence the resulting energy production, power reliability analysis has been considered as an important step in any system design process. A reliable electrical power system means a system has sufficient power to supply the load demand during a certain period or it also means that it has a small LPSP [244].

Considering the energy accumulation effect of the battery, to present the system working conditions more precisely, the chronological method is employed in this research. The LPSP from time 0 to T can be expressed as follows,

$$LPSP = \sum_{t=0}^{T} \frac{Power\ failure\ time}{T}$$

$$LPSP = \sum_{t=0}^{T} \frac{(P_{available}(t) < P_{needed}t)}{T} \qquad \textbf{Equation 33}$$

where T is the number of hours in this study with hourly weather data input. From the load profile shown in Figure 40, T = 24. The power failure time is defined as the time that the load is not satisfied when the power generated by both the wind turbine and the PV array is insufficient and the storage is depleted battery SOC falls below the allowed value $SOC_{min} = 1 - DOD$ (and still has not recovered to the reconnection point).

As mentioned previously, there is trade-off between system cost and the power reliability. If the user willing to pay for a 0 LPSP system, the system cost

is higher and hence, the available power, $P_{available}$ is always more than

P_{needed}.

For example, if $LPSP = \frac{0}{24} = 0$. This tells us that there is no downtime

for this system every single peak of the load profile is covered even the highest

peak (1000W as shown in Figure 40). Simulation is done for 0, 0.01, 0.02 LPSP

systems and result obtained is presented in Section 4.2.2.

Figure 40 Load profile
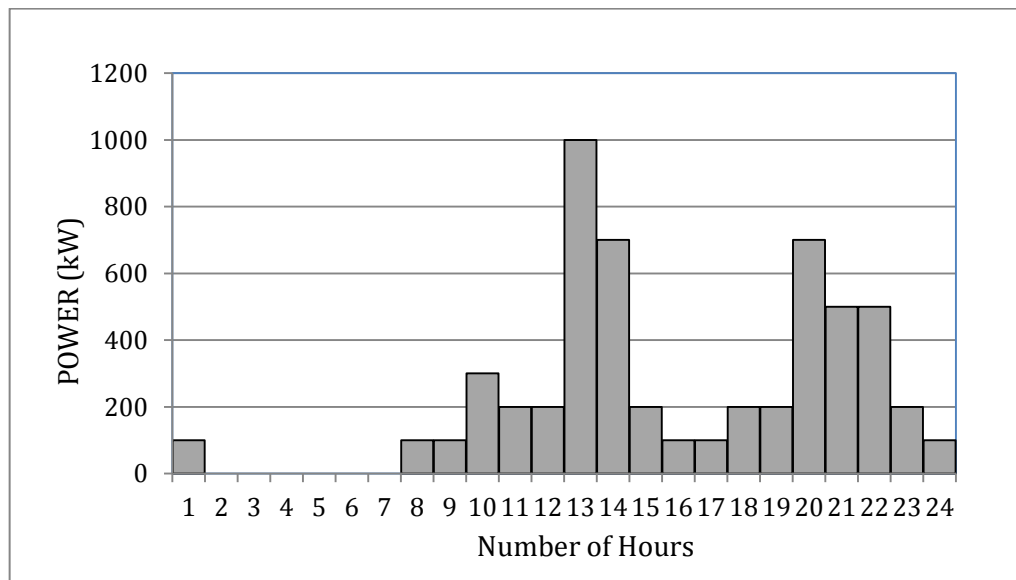
The same load profile in HOMER was used for GA optimal sizing RES shown

in Figure 40. From the figure above, the highest load peak is 1000W.

ii. Constraint for power from Renewable Energy Sources

Constraint for renewable energy sources is clear. The total power

generated from PV panel and wind generator are not more than 2.0kW for a 0

(zero) LPSP. As mentioned earlier, a random variability of 10% of day-to-day

and 20% time-step-to-time-step are added to the total power needed from the

renewable energy sources. The efficiency of the PV panel and wind generator

are 90% according to the data sheet from the manufacturer as shown in Table 27. However, in real life, the solar irradiance and wind speed are fluctuated. Based on the weather forecast from NASA Surface Meteorology solar irradiance in Semenyih is higher. The rated power of the PV panel and wind generator is 0.100kW and 1kW respectively. Equation 34 below shows constraints of the output power from renewable energy source.

$$G = (\%_{PPV} \cdot N_{PV} \cdot P_{ratedPV}) + (\%_{PWG} \cdot N_{WG} \cdot P_{ratedWG}) \qquad \textbf{Equation 34}$$

where,

N_{PV} is the number of PV panel,

N_{WG} is the number of wind generator,

$\%_{PPV}$ is the percentage of how much the PV panel could generate based on the solar irradiance at that specific site, the value of this 0.96 based on the weather forecast,

$\%_{PWG}$ is the percentage of how much the wind generator could produce based on the forecast velocity of the wind at that specific site, the value of this is 0.04,

$P_{ratedPV} = 0.100$kW,

$P_{ratedWG} = 1$kW.

From Figure 40, The load profile might fluctuate in actual case. A 50% of discrepancy is added to the highest power peak. The calculation for constraint shown below is based on 1.5kW as the peak power. A big portion of total generated power is contributed from solar energy due to the fact that the solar irradiance in Semenyih is higher than the wind velocity.

Hence, $G \geq 2.0kW$ as this is a 2kW RES for the initial boundaries of $15 < N_{PV} < 30 \; and \; 1 < N_{WG} < 3.$

iii. Constraint for battery connection

DC bus voltage is 48V. This is important to decide the number of battery in one string. This also means that how many batteries are connected in series based on the battery specification. Hopecake battery 12V, capacity of 118Ah and throughput of 1.416kW is used in this study. The minimum N_{Batt} is 4 ($N_{Batt} \geq$ 4, 8, 12, 16, 20, 24, 28, 32, 36) due to the DC bus voltage of the system.

iv. Constraint for Autonomy

A, autonomy of the system constraints the number of batteries used with different LPSP value. This is an autonomous system, operating reserve (battery in this case) plays an important role in the system and it has a big impact on the net present cost of the system to maintain a zero load rejection (0% LPSP). Different value of depth-of-discharge (DOD) are applied to the simulation. Total usable battery capacity is optimised to cater power, P_A. From Figure 40, the highest peak is 1kW, P_A is 1kW as battery is sized based on the highest peak for the battery-only system.

A is an inequality constraint where A, is the autonomy for the batteries in hours. The constant value of A is set by the user depends on the LPSP. If 0 LPSP, A is always more than 24 hours to avoid zero downtime. Equation 35 shown below is used to construct autonomy. For night, when wind speed is very low and no solar irradiance (the renewable energy source is nearly absent), operating reserve (battery in this case) plays an important role to ensure zero load rejection output. A of the system is assigned as follows:

$$A \leq 24$$

$$A = \frac{C_U, battery\ usable\ capacity}{P_A}$$

Equation 35

where

$$C_U = N_{BAT} \cdot DOD \cdot rated\ throughput$$

$$C_U = N_{BAT} \cdot C_{min}$$

Equation 36

$$C_U = N_{BAT} \cdot DOD \cdot V_N \cdot C_N$$

N_{BAT} is the number of batteries,

V_N is the nominal voltage of the battery, 12V
C_N is the nominal capacity of the battery, 118Ah

DOD is Depth-of-discharge of the battery (where the minimum SOC of the battery is set).

P_A is the power that battery is required to cater when there is zero output renewable power. It is also based on the load profile. For a battery alone system, P_A is 1kW. The highest peak in the load profile is supplied by the battery only.

3.2.2.2 Optimal Sizing of Supercapacitor-Battery Hybrid energy storage system (SB-HESS) using the GA

This methodology aims to minimise the 20-year round total system cost function (Z_x) by taking the total capital of the devices (C_c), the costs of the 20 years round maintenance (C_m). The set of variables (x) that consists of umber of PV modules (N_{PV}), WG (N_{WG}), batteries (N_{BAT}), supercapacitor (N_{SCAP}) battery chargers (N_{CH}), PV charges, and the height (**h**) of the installation of the wind generator is optimised. The focus of the objective function is the number of replacement batteries which is based on the battery lifespan, R and the number of batteries N_{BAT} that benefits from the inclusion supercapacitor N_{SCAP} in the energy storage system. The total system cost function is equal to the sum of the C_c in \$ and $C_{m\&o}$ in \$, the function is shown below:

$$\text{Min } Z(x) = \min \{C_c\,(x) + C_{m\&o}\,(x)\} \qquad \textbf{Equation 37}$$

where x is the vector of the decision variables mentioned above.

The decision variables are the unknowns that are to be determined by the proposed GA objective function. A specific decision is made when decision variables take on specific values. The decision variables in the objective function deal with component numbers and installation settings.

The objective function is a cost function in this part. It changes value as a result of changes in the values of the decision variables. This cost function measure the desirability of outcome of a decision. This cost function describes the initial cost and the maintenance plus operational cost of the components.

The initial cost are related to the technical specification of the components, capital cost of the components and the number of the components of PV module, wind generator, operation settings on the wind generator, battery and supercapacitor. These capital costs also include the installation cost of the devices. The maintenance and operation cost of each unit of the components per year has been set to 2% of the corresponding capital cost. In this approach, constraints play an important role. The constraints are used to link the objective function, which is non-physical to knowledge of the physical world through experiment. The constraints also restrict the range of decision variables as a result of socio-economic, technological and physical constraints on the power system. These constraints are implemented by considering the technical characteristic of components in the system such as solar panel, wind generator, batteries, supercapacitors, charge controller and inverter. Moreover, constraints are made by matching the supply to load demand. Section below presents construction of fitness function for supercapacitor-battery hybrid energy storage system which subjects to constraints. GA coding is written in MATLAB R2011b and documented in Appendix A2.

1. Fitness function

i. PV-wind-battery-supercapacitor system

$$
\begin{aligned}
Z_{(N_{PV}, N_{WG}, N_{BAT}, N_{CH}, N_{SCAP})} \\
= N_{PV} \cdot (C_{PV} + y_P \cdot M_{PV}) \\
+ N_{WG} \cdot (C_{WG} + y_p \cdot M_{WG} + h \cdot C_h + y_p \cdot h \cdot C_{hm}) + N_{BAT} \\
\cdot (C_{BAT} + R \cdot C_{BAT} + (y_P - R - 1) \cdot M_{BAT}) + N_{CH} \cdot C_{CH} \\
\cdot (y_{CH} + 1) + N_{CH} \cdot M_{CH} \cdot y_P - (y_{CH} - 1) + C_{INV} \cdot (y_{INV} + 1) \\
+ M_{INV} \cdot (y_P - y_{INV} - 1) + N_{SCAP} \cdot C_{SCAP}
\end{aligned}
$$

<div align="right">**Equation 38**</div>

ii. PV-battery-supercapacitor system

$$Z_{(N_{PV}, N_{BAT}, N_{CH}, N_{SCAP})}$$
$$= N_{PV} \cdot (C_{PV} + y_P \cdot M_{PV}) + N_{BAT}$$
$$\cdot (C_{BAT} + R \cdot C_{BAT} + (y_P - R - 1) \cdot M_{BAT}) + N_{CH} \cdot C_{CH}$$
$$\cdot (y_{CH} + 1) + N_{CH} \cdot M_{CH} \cdot y_P - (y_{CH} - 1) + C_{INV} \cdot (y_{INV} + 1)$$
$$+ M_{INV} \cdot (y_P - y_{INV} - 1) + N_{SCAP} \cdot C_{SCAP}$$

<div align="right">**Equation 39**</div>

With the initial boundary:

$$15 < N_{PV} < 30$$

$$1 < N_{WG} < 3$$

$$4 < N_{BAT} < 36$$

$$N_{CH} < 0$$

$$N_{INV} < 0$$

$$2 < N_{SCAP} < 8$$

Where h is the height of the WG tower in meter, C_{PV} , C_{WG} , C_{BAT} , C_{SCAP} are the capital cost (\$) of one PV module, WG, battery and supercapacitor respectively, C_h is the capital cost (\$) for the WG tower per meter (\$/m), C_{hm} is the maintenance cost per meter and year (\$/meter/year), C_{CH} is the capital cost of one PV battery charger (\$), y_{CH} and y_{INV} are the expected numbers of PV battery charger and DC/AC inverter replacements during the 20-year system lifetime and it is equal to the lifetime (20 years) divided by the Mean Time Between Failures (MTBF) of power electronic converters Holtz et al., 1994). MTBF is used in the manufacturing world and even in the military as a way to

measure a system's reliability. The assumption behind measuring MTBF is that a system will periodically fail and will correct itself according to its design [176, 241]. The higher the mean time between failures, the more reliable a system is. C_{INV} is the capital cost of the DC/AC inverter, ($). R is the expected number of battery replacement which depends on y_{batt}. y_{batt} is the expected battery lifespan during the 20-years system operation. It is computed using Equation 28. M_{CH} and M_{INV} are the maintenance costs per year ($/year) of one PV battery charger and DC/AC inverter respectively. In addition, the number of PV battery chargers, N_{CH} equal with the total number of PV power generation blocks which depends on the number of PV modules, N_{PV}. The equation of calculating number of charge controller is shown in Section 3.2.2-1 (Equation 31).

2. Constraint

From section 3.2.2-1, the same equations to construct the constraint of power from renewable energy sources, G (Equation 34) and constraint for number of battery, Autonomy *A* (Equation 35) are used since the LPSP, DC bus voltage, same specification of the components and hypothetical location are same. Constraint for the number of supercapacitor is presented below.

i. Loss of Power Supple Probability (LPSP)

Hybrid energy storage of RES with 3 different LPSP are simulated. 0, 0.01, and 0.02 LPSP systems as the capacity shortage of these three systems are almost negligible.

ii. Constraint for power from Renewable Energy Sources

$G \geq 2.0kW$ is obtained using Equation 35. The calculation is shown in previous section.

iii. Constraint for battery connection

DC bus voltage is 48V. The minimum N_{Batt} is 4 ($N_{Batt} \geq 4, 8, 12, 16, 20, 24, 28, 32, 36$) due to the DC bus voltage of the system.

iv. Constraint for Autonomy

$A \leq 24$ is obtained using Equation 35. The calculation is shown in previous section.

v. Constraint for Supercapacitor

48V, 83F of supercapacitor is chosen for this simulation. Data specification is shown in Table 27.

$$N_S = \frac{Load\ Voltage}{Cell\ Voltage}$$ **Equation 40**

$$N_S = \frac{48}{48} = 1$$

$$\therefore N_s \leq 1$$

where N_s is the cells in series

From the data sheet [245], ESR is the internal resistance of the supercapacitor, 10mΩ, C is the capacitance, 83F. Supercapacitor is constraint based on the load profile shown in Figure 40, , $P_{max} = 1000W$.

$$N_P = \frac{IN_S}{\Delta V}\left(\frac{\Delta t}{C} + ESR\right)$$ **Equation 41**

$$N_{PUpper} = \frac{I_{max}N_S}{\Delta V}\left(\frac{\Delta t}{C} + ESR\right)$$
$$N_{PUpper} = 8.333$$

$$N_{PLower} = \frac{I_{min}N_S}{\Delta V}\left(\frac{\Delta t}{C} + ESR\right)$$
$$N_{PLower} = 2.80$$

$$\therefore N_p \leq 2$$

$$\Delta t = 180s$$
$$\Delta V = V_{max} - V_{min}$$
$$I_{max} = \frac{P_{max}}{V_{min}} = 30.67A$$
$$I_{min} = \frac{P_{max}}{V_{max}} = 20.57A$$
$$I_{avg} = \frac{I_{max} + I_{min}}{2}$$
$$I_{avg} = 25.62A$$

where N_p is cells in parallel,

N_{PUpper} is number of supercapacitor in parallel for upper boundary,

N_{PLower} is number of supercapacitor in parallel for lower boundary,

Δt is the discharge period of the supercapacitor, ESR equivalent series resistance of the supercapacitor,

ΔV is the voltage drop, 16V
V_{max} is operating voltage, 48.6V
V_{min} is the minimum voltage, 32.6V

I_{max} , I_{min} , I_{avg} are the maximum current, minimum current and the average current which can be delivered by the cell,

For the SB-HESS, the focus has been put forward to the battery lifetime. As mentioned earlier, the battery lifetime is limited and it depends on the design and the control energy flow strategy of the system. In this proposed system, the main aim of the hybrid supercapacitor battery system is to prolong the battery lifetime and also reduce the battery size. The motivation of designing this system is to reduce the stress factor of the batteries, which is

greatly depending on the batteries operating condition by integrating the system with supercapacitor.

In the fitness function for this domain, there is no maintenance and operational cost for supercapacitor as supercapacitor is a maintenance-free energy storage device. In other words, supercapacitor has much longer shelf and cycle life than batteries. By 'much' is meant at least one order of magnitude higher. It also can be said that the cycle life of a supercapacitor is similar to the lifetime of a PV system for 20 years (in this case). This is due to the fact that supercapacitor often referred to as an electrochemical capacitor, which stores the energy by charge separation. Charge is stored in the micropores at or near the interface between the electrode material and electrolyte.

Stress factor of the batteries is the characteristic features of the operating condition of the battery and it alters the rate of action of the damage mechanism of the battery. The proposed system aims to stabilize the time series of voltage, current, temperature and SOC which markedly reflecting the operating conditions generally used and accepted as the criteria of indicating the lifetime of batteries. Battery cycle life, y_{batt} is the length of time that the battery will last under normal cycles before it requires replacement; it depends on the depth of discharge of individual cycles. During the battery lifetime, a great number of individual cycles may occur, including the charging and discharging process and every discharging process will result in some depletion of the battery. This expected battery lifetime is calculated using the Equation 28 shown earlier. The number of the batteries is reduced owing to the fact that the proposed combination of hybrid electrical energy storage system. The supercapacitor which is known as a much higher power density electrical

energy storage device is coupled with the battery which has high energy density. This allows the hybrid energy storage system deliver peak power by the supercapacitor over a short period while still maintaining high battery SOC and low depth of discharge (DOD). However, the battery stores energy and releases it over a longer period. It also aids in avoiding downtime in the electrification.

Table 27 is the list of the capital cost, operational/maintenance cost and data specification of the components used for this solar application.

Table 27 Cost and Specification list of the components

Components/ Specifications	Capital Cost ($)	Manufacturer brand	Operational/ Maintenance cost ($)
PV module $V_{OC} = 21V$ $I_{OC} = 7.22A$ $V_{max} = 17V$ $I_{max} = 6.47A$ $P_{max} = 100W$	335	Grape Solar Monocrystalline Solar	7
Wind Generator Power Rating = 1000W H_{high} = 14 -15m	2240	Maglev	45
Tower capital cost per meter $75/m	Tower maintenance cost per year per meter $0.75/year/m		
Battery Nominal capacity = 118 Ah Voltage = 12V Throughput =1.42kW DOD = 80%	361	Hopecake	

Supercapacitor Capacitance = 83F Rated Voltage = 48V Working voltage = 48.6V Absolute maximum voltage = 51V	1498.52	Maxwell	n/a
DC/AC Inverter Efficiency = 80% Power Rating = 1500W	2068	Akku Solar	41
Charge Controller N_1 = 95% N_2 = 100% Power Rating = 300W	266	MISOL ELECTRIC	2.66

3.2.2.3 Optimal Sizing of prototype supercapacitor-battery hybrid energy storage system using the GA

The similar implemented fitness functions using Equation 39 are used in a smaller scale renewable energy system (RES). However, the cost of the system is different as the component is cheaper for a lower power rating. For this prototype case, the power rating of PV panels is 34.52W and the power rating for charge controller is 102W. The DC bus voltage is scaled down from 48V to 12V. Therefore, the battery and supercapacitor chosen have the same rated voltage which is 12V. The minimum number of battery in a string is 1 ($N_{Batt} \geq 1$).
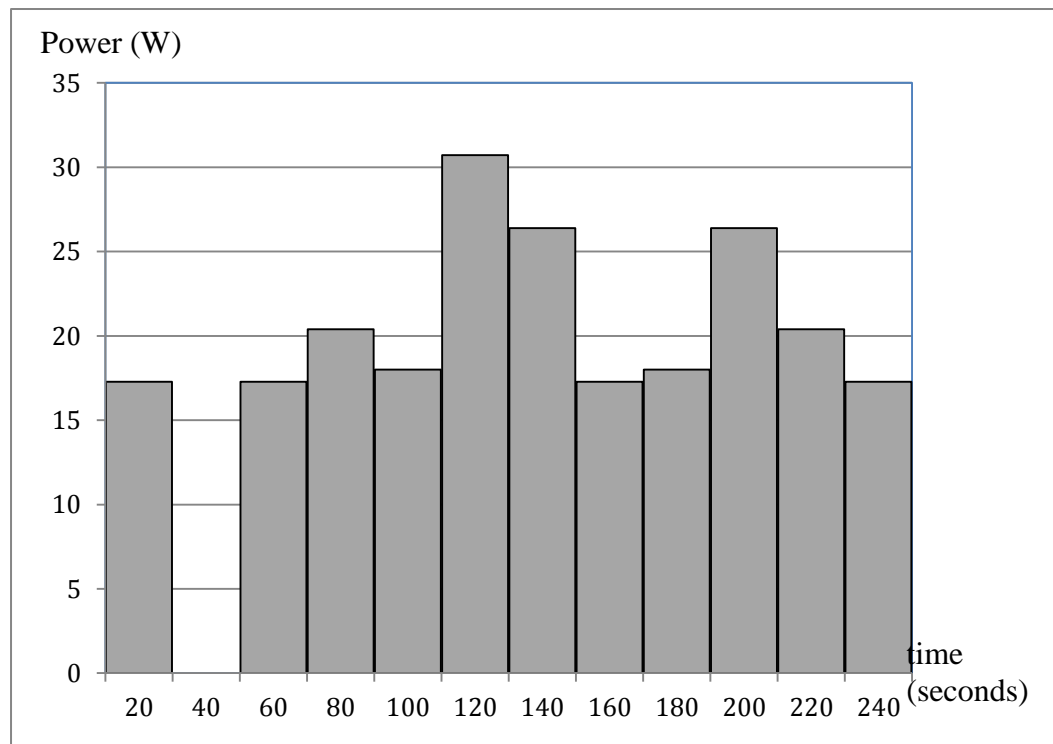
Figure 41 Load profile for a prototype system

Figure 41 above shows the scaled down version of RES. The simulated load profile used is taken from the load profile 1 as shown in Figure 35. The highest load peak of the prototype system is 30.72W. The pattern of the load profile for the prototype follows the pattern of the simulated load profile used in

2kW RES. A 50% of discrepancy is added to the highest power peak. The calculation for constraint shown below is based on the specification of the system 72W.The total power required, $P_{needed} = 266.04W$.

Firstly, constraint for renewable energy sources is straightforward as wind generator is not considered in our prototype due to the geographical issue. The total power generated from PV panel is not more than 72W for a 0 (zero) loss of power supply probability (LPSP). The efficiency of the PV panel is 90% according to the data sheet as shown in Table 28. However, in real life, the solar irradiance is fluctuated. Constraint, G is shown in the calculation below:

The rated power of the PV panel is 34.25W based on the manufacturer specification.

$$G \geq (N_{PV} \cdot 34.25)$$

where the initial boundary is $1 < N_{PV} < 5$ Only single renewable energy sorces is considered due to the fact that the solar irradiance in Semenyih is higher. Moreover, the scaled down system specification stated earlier is 72W, therefore,

$$\therefore G \geq 72W$$

DC bus voltage is 12V. This is one of the criteria of deciding the number of battery in one string. This also means that how many batteries are connected in series based on the battery specification. GP battery 12V, capacity of 1.2Ah and throughput of 14.4W is used. Constraint for usable capacity from the battery, Autonomy A is assigned using Equation 35.

$$\therefore \textbf{Autonomy, } A \leq 1,$$

where DOD = 0.5,

$V_N \cdot C_N = 14.16Wh$,

P_A= 11.085W, battery turns off when the load current is above 0.95A. which

means P_A= 11.085W.

From data sheet of this battery [246], the recommended DOD is 80%,

for this battery alone system, battery is drained to the recommended DOD. This

80% of its capacity is used to cater the sudden power peak. The minimum N_{Batt}

is 1 and the initial boundary is $N_{Batt} \geq 1$ due to the DC bus voltage of the

system. A decides the number of batteries used in system with different capacity

shortage.

A smaller scaled of supercapacitor with the rating of 2.3V, 30F from

Panasonic [247] is chosen. However, in this lab-scaled prototype system, the

total voltage of the supercapacitor has been added and subjected to the fitness

function (Equation 39) due to the availability of supercapacitor can be found in

the market.

The first criteria to set the constraint for the number of supercapacitor

are the total voltage of the supercapacitor which depends on the DC bus of the

system .

The total voltage of the supercapacitor connected in series [38]:

$$V_{series} = V_1 + V_2 + \cdots + V_n$$
$$V_{series} = 2.3V * 6$$
$$V_{series} = 13.8$$

The total effective voltage of the other sets supercapacitors connected in

parallel [38]:

$$V_{eff} = V_{series1} = V_{series2} = \cdots = V_{seriesn}$$
$$V_{eff} = 13.8V$$

Table 28 Components and Data Specification for Prototype system

Components/ Specifications	Capital Cost (RM)	Manufacturer brand	Operational/ Maintenance cost (RM)
PV module $V_{max} = 13.7V$ $I_{max} = 2.5A$ $P_{max} = 34.25W$	161	IB Solar	3.22
Battery Nominal capacity = 1.2 Ah Voltage = 12V Throughput =14.4W DOD = 80%	45	GP	0.9
Supercapacitor **Capacitance = 30F** **Rated Voltage = 2.3V**	25	Panasonic	n/a
Charge Controller $N_1 = 95\%$ $N_2 = 100\%$ Power Rating = 102W	130.90	ProStar	2.618
Inverter Inversion Efficiency <87% Output Power = 100W Voltage = 12V	106.61	Must Solar H1-A (100W)	2.13

*All operational and maintenance costs are 2% of the component capital cost.

3.2.3 Energy Flow Control Strategy

A software-based approach is presented to control the energy flow between the supercapacitor-battery hybrid energy storage systems (SB-HESS) and load demand. As shown in the pie chart in chapter 1, power electronics in a hybrid energy storage devices system scope a huge initial cost in RES. To further reduce the overall cost of RES, power electronics for constructing DC-DC converter between supercapacitor and battery is eliminated and in place with a supervised learning machine – Support Vector Machine (SVM). There are two onerous challenges in coupling supercapacitor and battery in a hybrid energy storage system:

1. Balancing different voltage level for each of the energy storage devices by implementing MOSFET switches and microcontroller to completely switch off battery during power peak time.

   - Voltage level of supercapacitor drops faster than lead acid battery by the ratio of seconds and hours. In this case, balancing circuit is avoided to save the operational cost. If voltage of supercapacitor is lower than nominal voltage of battery, supercapacitor acts as an additional load to battery. Eventually, battery discharges to charge up supercapacitor. This is impractical as this scenario shortens battery life greatly. Furthermore, it delays the power supply to fulfill load requirement.

2. Eliminate delay in time response for supercapacitor to supply power peak.

   - It is proven in undergraduate student final year projects [80, 248, 249] that a hardware-based approach by implementing buck-boost

converter for hybrid energy system is more efficient than a software-based approach which uses if-else conditional algorithm. Measure metric of efficiency is based on the time response for supercapacitors to supply power peak demand. A short transitional time also exists between the switching of power from the battery to the supercapacitor bank, disrupting the delivery of power to the load. Whereas, the hardware approach does not exhibit any form of delay or lag from the moment a pulsed load occurs and the moment the supercapacitor bank starts supplying power to the load. This is because the hardware approach draws power from the supercapacitor bank directly all the time, without taking into account any circumstances. Enhancement is done in this methodology step to eliminate the time delay for supercapacitor to match power peak. SVM is implemented to classify different types of load profile and Support vector regression (SVR) is used to predict the load (autoregressive model of time series).

Real world time series prediction applications normally do not fall into the category of linear prediction. However, these real world applications (in our case, load forecasting) are typically characterized by non-linear models. Steps constructing lab-scale prototype energy management system, which consists of software control board and how SVM and SVR are trained for load forecasting.

3.2.3.1 Steps of Implementing the SVM and SVR on the Lab-scale Prototype

Step 1: Design of Hybrid Energy Storage System

The standalone storage system consists of sealed-lead acid (SLA) battery bank only while the hybrid storage system consists of supercapacitor bank paralleled with the SLA battery bank. As mentioned in the literature review section, the integration of supercapacitor and battery as a HESS will yield the energy storage with high power and energy density, where the battery will supply for the average power demand while the supercapacitor will supply for the peak power demand. The motor load in this project is rated at 12V. Hence, 2.3V, 30F supercapacitor (which is manufactured by Panasonic, data specification is shown in Table 28) in the storage bank has to be configured to give a voltage close to the rated voltage of the motor load. For this configuration, each string of supercapacitor is designed to have 6 supercapacitor connected in series to yield a voltage of 13.8V.

The total voltage of the supercapacitor connected in series:

$$V_{series} = V_1 + V_2 + V_3 + \cdots + V_n$$
$$V_{series} = 2.3V \times 6$$
$$V_{series} = 13.8V$$

The total effective voltage of the 3 sets of 6 serially connected supercapacitors connected in parallel:

$$V_{eff} = V_{series1} = V_{series2} = V_{series3} = \cdots = V_{seriesn}$$
$$V_{eff} = 13.8V$$

There are 3 sets of the supercapacitor string connected in parallel to yield a total of 15F.

The capacitance of six supercapacitors connected in series:

$$\frac{1}{C_{series}} = \frac{1}{C_1} + \frac{1}{C_2} + \frac{1}{C_3} + \cdots + \frac{1}{C_4}$$
$$\frac{1}{C_{series}} = \frac{1}{30} \times 6$$
$$C_{series} = 5F$$

The effective capacitance of 3 sets of 6 serially connected supercapacitors connected in parallel:

$$C_{eff} = C_{series1} + C_{series2} + C_{series3} + \cdots + C_{seriesn}$$
$$C_{eff} = 5F \times 3$$
$$C_{eff} = 15F$$

This configuration reduces the total capacity available in the supercapacitor bank but it is necessary to give a 13.8V bank voltage as shown in Figure 42 and 43. The specification of the batteries and supercapacitors used are shown in Table 28.
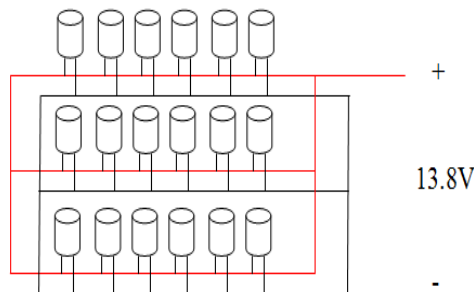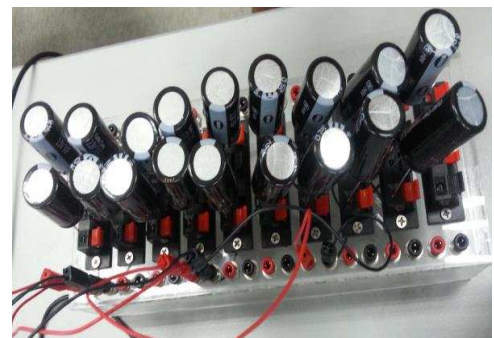
(a)   **(b)**

Figure 42 (a) Supercapacitor Configuration, (b) Supercapacitor Bank on prototype

On the other hand, three 12V, 1.2Ah SLA batteries manufactured by GP is connected in parallel as a single battery string. This gives rise to a 12V, 3.6Ah battery bank prior to Genetic Algorithm (GA) optimization as shown in the following:

(a)

(b)
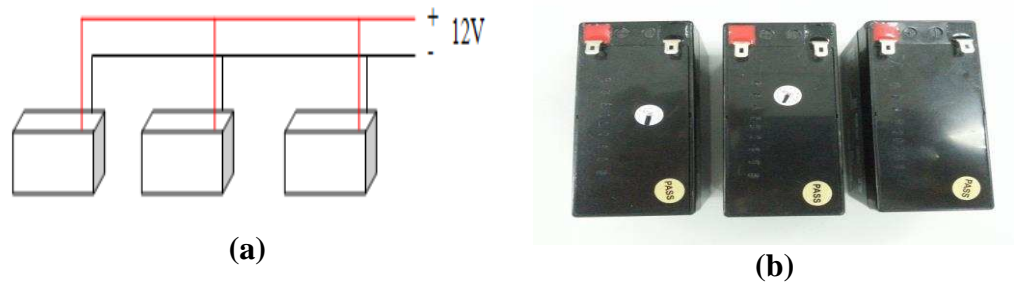
Figure 43 (a) Battery Configuration, (b) SLA Battery Bank

With the integration of supercapacitor with the battery, it is expected that the battery remaining capacity in the hybrid will be maintained over a long period than that of the standalone system. The aiding effect of supercapacitor was justified through the SOC comparison between the standalone and hybrid system as shown in Section 4.3.

Cost optimization is done using the GA for the prototype system (as mentioned in section 3.2.2-3), the battery bank is downsized but the 12V DC bus voltage is maintained. This software approach will still be able to operate with the optimised system due to similar bus voltage. Hence, the software approach offers modularity to the energy management system.

System Architecture Integration

To implement the dual stages software approach EMS known as SVMR_EMS, the MATLAB R2011b has been selected as the platform to link the various devices involved. The devices and their role in the SVMR_EMS were listed as follows:

Table 29 Roles of devices used in Prototype

Devices and Tools	Role
MAXIM USB 6009 DAQ	Perform load current data acquisition
Arduino Mega2560	Perform voltage monitoring task and switching control with the Software Control Board
LIBSVM	Perform Load Identification and Load Prediction

The MATLAB R2011b allows the control of the MAXIM USB 6009 DAQ Session interface through its DAQ toolbox, the Arduino Mega2560 through the Arduino IO package and the LIBSVM through the LIBSVM MATLAB extension. Hence, all these devices control was brought under one single software environment which simplifies the data communication between the devices and tool. Besides, since the MATLAB R2011b runs on a dual core Intel Pentium CPU which has higher processing speed and memory capability than the Arduino Mega2560 chip, the SVMR_EMS management decision can be carried out more efficiently in the MATLAB environment.

Software Control Board

The software approach Energy Management System (EMS) requires a control circuit to implement its management decision. With the integration of the Solar Photovoltaic Panel and the HESS system, the software control circuit was designed to allow charging operation, discharging operation of the supercapacitor and battery banks. Besides that, multiple cell battery management is also required to implement a zero downtime system in day time. This allows the alternate battery to discharge to the motor load while the other is recharging when sunlight is available. The specification of the software control board is as follows:

1. One supercapacitor bank charging/discharging control

2. Two battery banks charging/discharging control

3. Load Current Sensing with filtered output

4. Batteries and Supercapacitor bank voltage monitoring

5. Over current protection of 3A due to current handling limitation of veroboard.

6. Backflow power protection for battery and supercapacitor banks

7. Backflow power protection for Solar PV Panel.

Software Control Board Prototype

The following control circuit prototype was built to ensure that the discharging process using the new architecture could be implemented before the full scale control circuit was built.
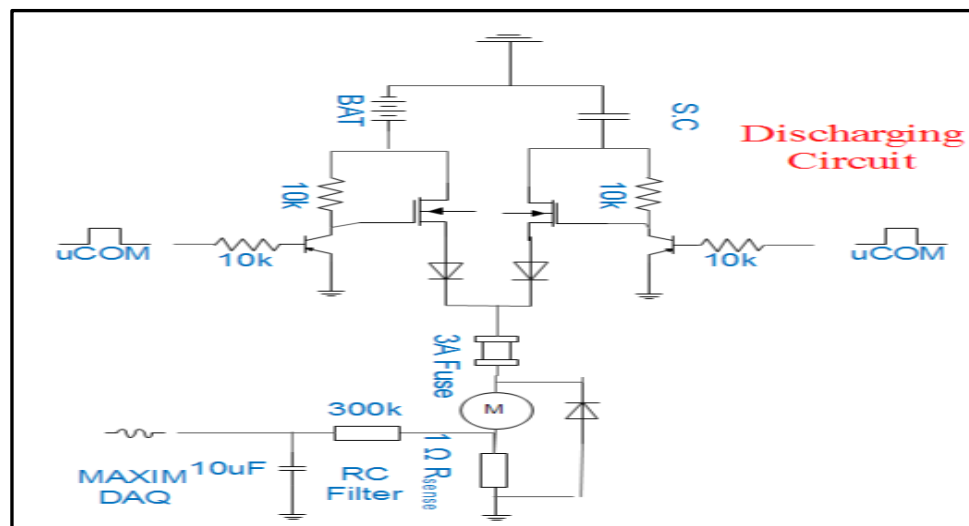
Figure 44 Schematic of control circuit prototype

As shown in Figure 44, the prototype consists of two MOSFET switches which control the turning ON/OFF of battery and supercapacitor through the Arduino MEGA 2560 microcontroller. This software control approach adopts the EITHER ON strategy where only one storage bank will be turned ON at any

time. Hence, the voltage mismatch between supercapacitor and battery storage

will not pose an issue unlike the hardware approach which requires a DC/DC

Diode

1Ω Resistor   converter to interface the battery with the supercapacitor.

P-channel MOSFET is chosen for switching as it is suitable for application

where load is directly connected to ground. However, the P channel MOSFET

requires a gate driver circuit which was formed of NPN BJT transistor and a

resistor tied to the source. Besides, a current sense resistor is also used as

voltage transducer for load current measuring. Lastly, protective measure was

also built into the system: the components such as diodes, freewheeling circuit

and fuse were used to prevent backflow power from load to storage supply. The

prototype built was based on the schematic shown in Figure 44. The prototype

which was built on the veroboard is shown in Figure 45 below:

3A Fuse   **P-channel**   **Current**
              MOSFET   **Sense**
                            Resistor
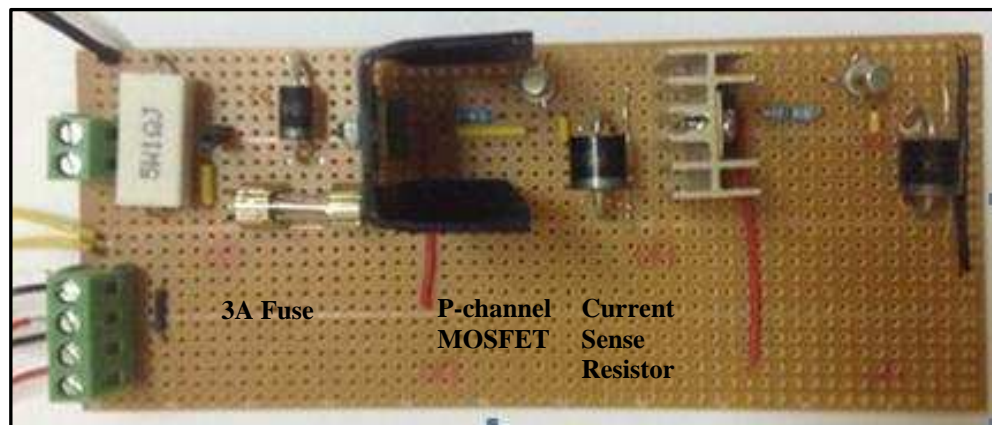
Figure 45 Control Circuit Prototype

Full scale Software Control Board

The prototype control circuit only allows discharging control between the

supercapacitor banks and the battery bank. To ensure the integration of the solar

photovoltaic and HESS, complete software control circuit architecture which

enables the control of charging and discharging operation of the batteries and supercapacitor bank. Besides, the software control board also allows alternate battery to be charged by the solar charger while the other is supplying to the Motor. By applying this multiple cell battery concept, downtime of the HESS system during charging operation can be eliminated. Lastly, through the use of SVR, the load current could be predicted multiple steps in advanced to allow for intelligent turning ON of supercapacitor. This will improve the software approach EMS time response. Figure 46 shows the schematic of the software control board:
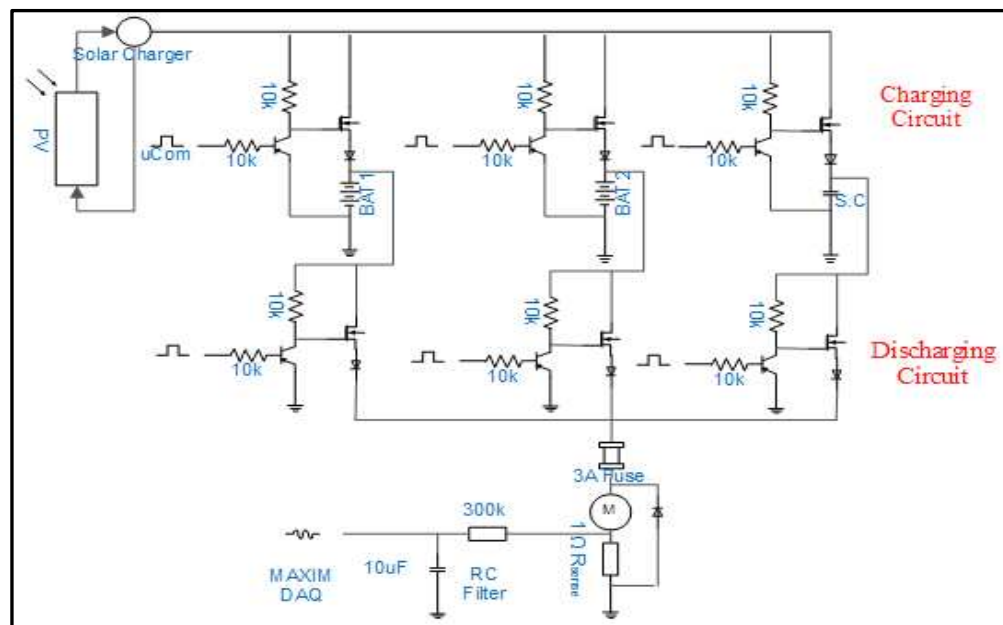
Figure 46 Schematic of software control board

As shown in Figure 46, the upper row of switches is designed for charging control and the lower row of switches is for discharging control. In the charging circuit, diodes are used to protect the Solar Panel from backflow power from the battery and supercapacitor, while; in the discharging circuit, diodes are used to protect the P-channel MOSFET from reversed high surging voltage when the Motor is turned OFF. The presence of freewheeling diodes

also ensures that the stored energy of inductive load is dissipating by the motor itself rather than damaging the other components. A 3A fuse was used to protect the software control board in case the Motor is drawing excessive current. The battery and supercapacitor voltage sensors are excluded from the circuit diagram for simplification purpose. The Software Control Board circuit is shown in Figure 47:
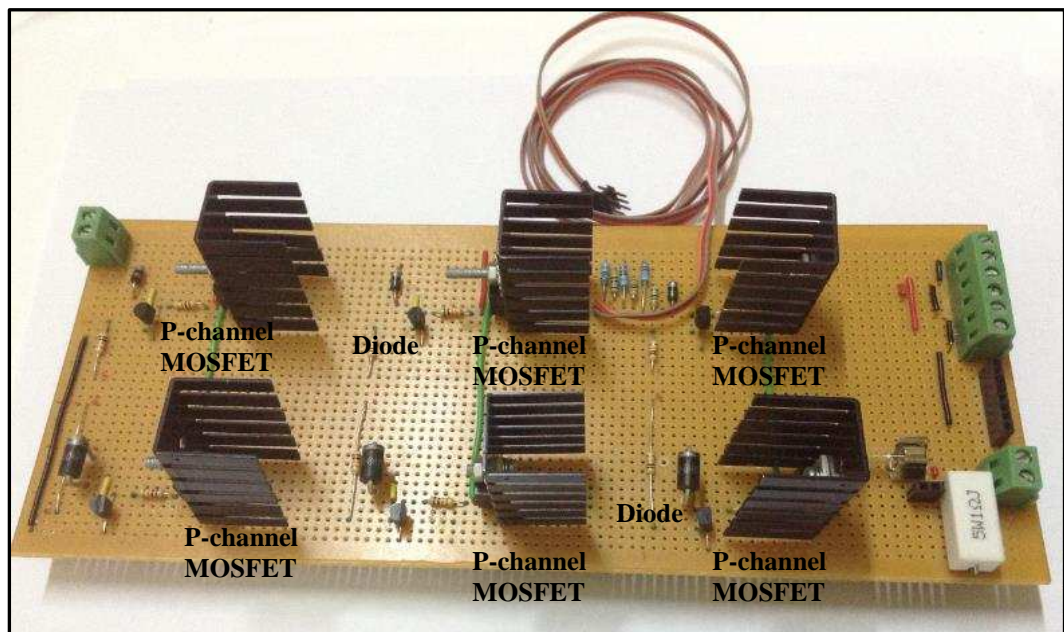
Figure 47 Software Control Board

To measure the load current, a 1Ω current sensing resistor is used in such that the voltage read out from the MAXIM USB 6009 DAQ will be equivalent to the Motor current. As the DC Motor load is generally noisy, the voltage across the current sensing resistor has to be filtered prior to the Analog-Digital Converter (ADC). In such, low pass RC filter with cut off frequency of $f_c \sim 1.5$ Hz and 122 Hz are used to test their performance which is shown in the Figure 48:

<table>
<tr><td>(a)</td><td>(b)</td></tr>
</table>
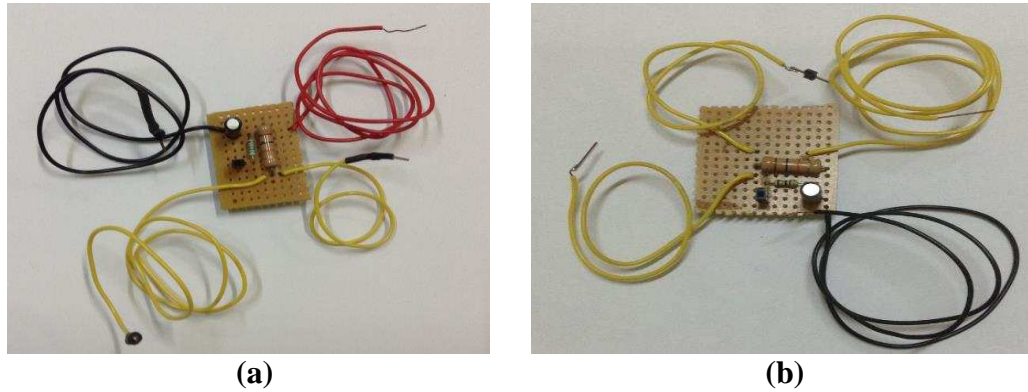
Figure 48 (a) RC filter with 122 Hz cut off, (b) RC filter with 1.5Hz cut off

(a) F_c =122 Hz load profile readout	(b) F_c =1.5Hz load profile readout
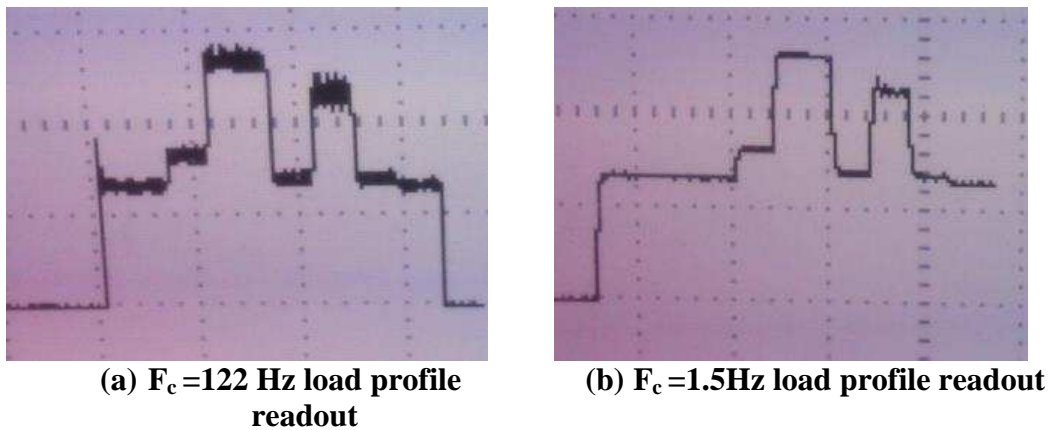
Figure 49 RC filter performance comparisons

The same load profile was generated twice using the programmable load. The first load profile and the second load profile is readout (retrieved) by the Maxim USB 6009 DAQ with the RC filter with Fc=122Hz and 1.5Hz respectively. As seen in Figure 49 (b), the load current profile using RC filter of F_c = 1.5Hz is cleaner and has less harmonics noise. Another RC filter with F_c= 0.05 Hz was tested, it yield a clean DC value output but the response time is much slower as the time constant of the RC filter has increased by 30 times. Hence, for a good filtering performance and response time, the RC filter with 1.5 Hz was chosen to filter off the unwanted noises to ensure an approximately DC output value**.**

182

Programmable Load for prototype

In order to train and test the classification and load prediction accuracy of the SVM, the load profile has to be replicated by using a programmable load. To achieve this, 2 identical motors were clamped together along with a motor driver to form a programmable load as follows:
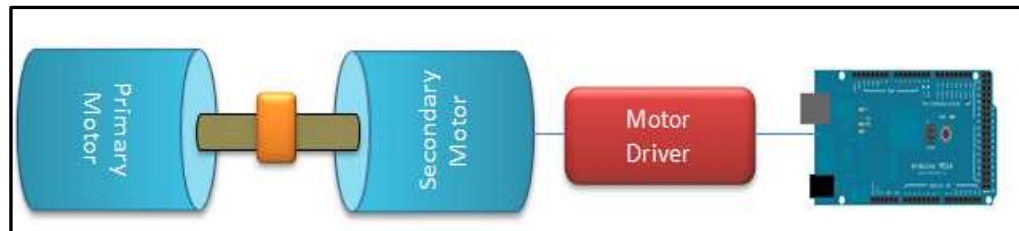
Figure 50 Programmable load block diagram

The primary motor will be driven from the Software Control Board, while the secondary generator will be driven by a motor driver that is configured by the Arduino UNO. The motor driver was suplied by an external power supply that is fixed to 13V and rated 1.6A to achieve a replicable load whom torque generated will be consistent. The secondary motor will attempt to rotate in the opposite direction of the primary motor according the PWM output from the motor driver. However, the secondary motor PWM putput voltage level was kept lower than the supply voltage from the primary motor. Hence, the Secondary motor will act as a generator, and back e.m.f is fed into the motor driver. However, by controlling the PWM output of the motor driver, the back e.m.f level can be controlled and hence manipulating the load torque of the primary motor. This will cause the current drawn by the primary motor to be programmable. The actual programmable load was shown as follows:
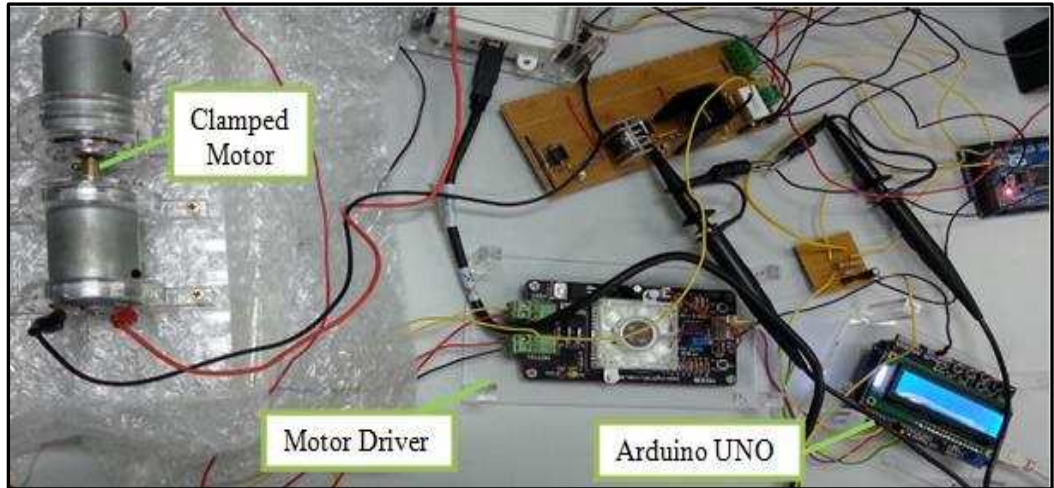
Figure 51 Programmable load

The programmable load was used to generate 5 different load profiles. In order to synchronize the time when the programmable load and the MAXIM DAQ sensing started, which is required for accurate classification, a signal will be send from the arduino UNO to the arduino MEGA to contemporize the operation between the two devices. The programmable load was coded in the arduino environment to yield the load profile as in Figure 52:

Name	Simulated load profile
Load 1	
Load 2	

Load 3

Load 4

Load 5
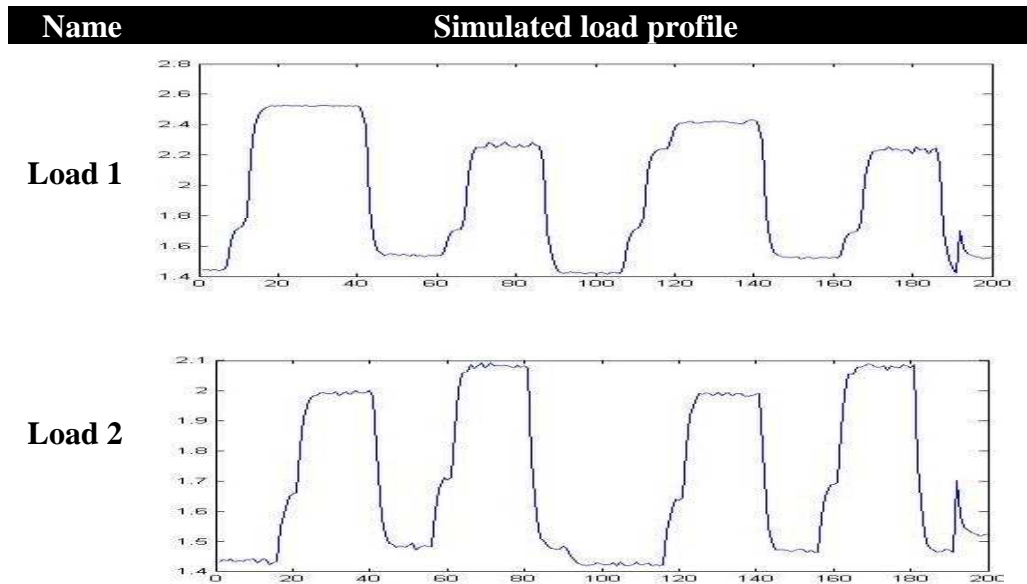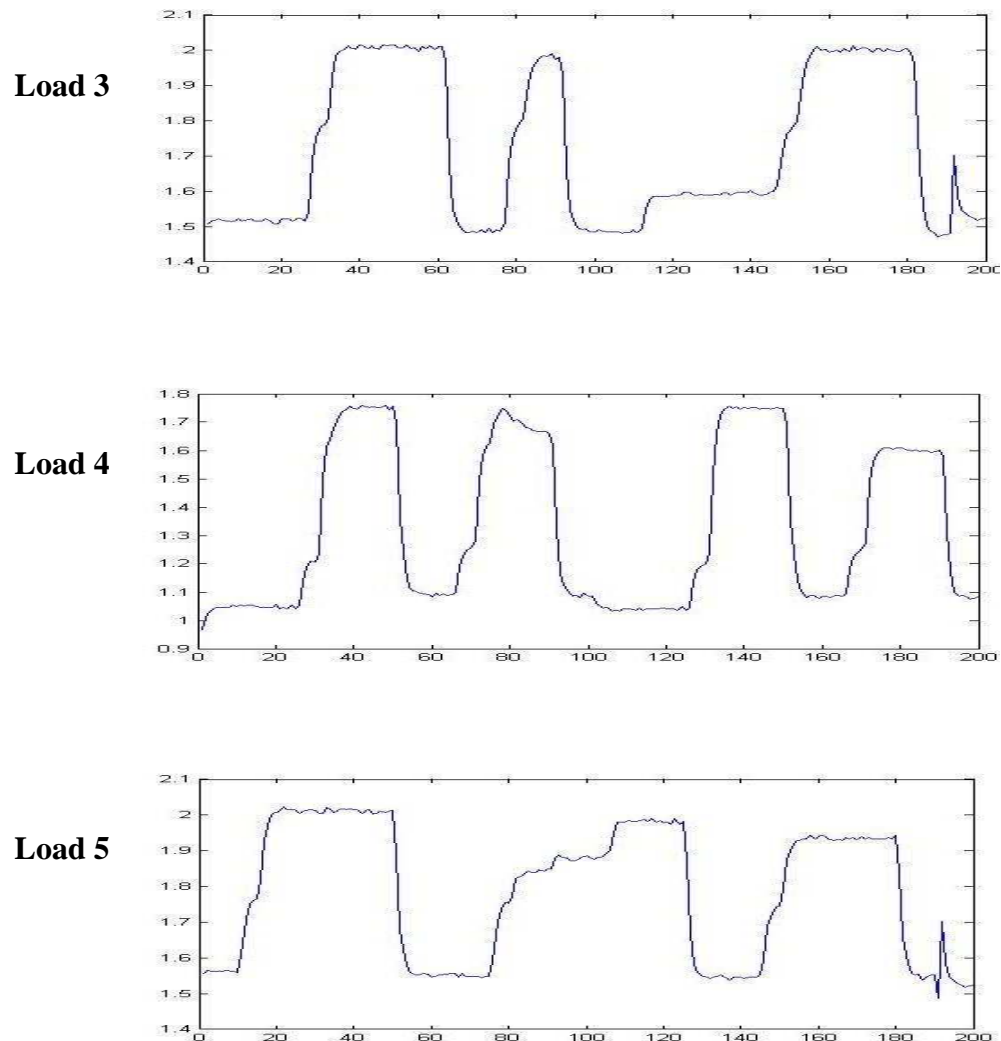
Figure 52 Simulated load profiles

As shown in Figure 52, different load profiles that vary in time and magnitude of the load current were simulated from the programmable load. The load profiles could represent the different energy demand during weekday, weekend, holiday and special events. For this project, only 5 load profiles were simulated and trained with the SVMR-EMS for simplification and time constraint reason. In real application, more profiles could be included into the training to yield a more reliable load prediction. Load profile 1 represents weekends as the power peak is highest among all other load profiles, load

profile 2 represents days public holiday as the power peak is second highest where the possibility of some people leave the house and go back hometown or vacation; load profile 3 represents a long weekends or special months for special festival such as Christmas, wedding and so; load profile 4 represents the normal weekdays for working and school days as the power peak is the lowest; load profile 5 represents the school holiday starts but no a public holidays as the peaks also happen during daytime.

Since the programmable load generates the load current pattern through PWM variation on the secondary motor, a certain issues has surfaced which cause the replication of load profile to be rather difficult. Firstly, the power supply for the motor driver has to be fixed to ensure the opposing torque produced by the secondary motor remains consistent. Hence, an external power supply with fixed voltage and maximum current limit is required for this task. Secondly, the SLA battery voltage level drops as its discharging continuously and this has cause the load current drawn by the primary motor to drop accordingly. Hence, the load profile is not fully replicable for the training and testing purpose. This adds to some difficulties in training and testing of the load prediction. However, with the use of SVM which has excellent generalization capability, the load prediction could still work well with the same load profile which differs slightly due to the voltage drop as shown in the results section.

Determination of Time Respond Improvement Required

In the literature section, it was mentioned that a sequential programming that adopts '*monitor and respond'* strategy was implemented and the results shows a 70ms delay in the time response of the supercapacitor corresponding to the

peak load current. However, in this project the software control board topology and the constraint of charging and discharging for the battery and supercapacitor bank was redesigned. Hence, it's required that the time response improvement needed to be known to estimate the K value required in the K steps-ahead technique used in the SVR. By running the sequential programming with the charging, discharging constraint, it is found that the time delay of the supercapacitor corresponding to the peak load is around 200ms as shown in the following:
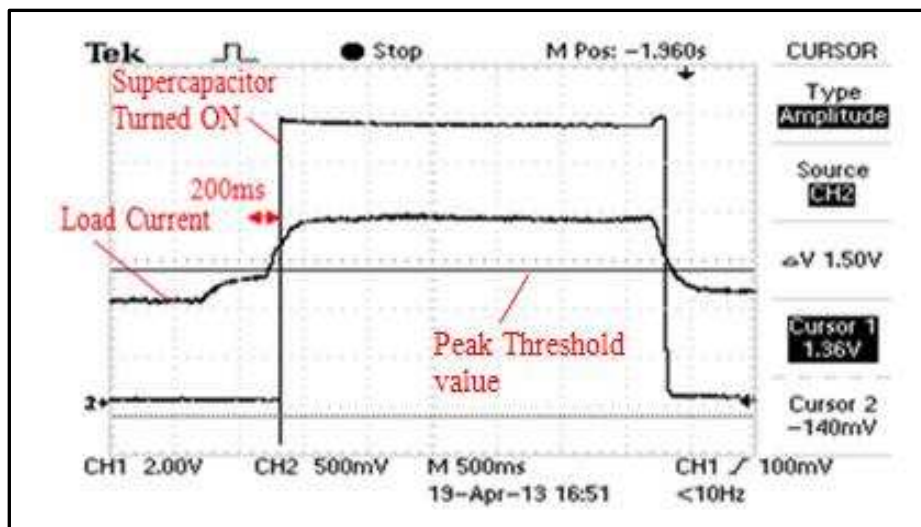
Figure 53 Time Response of Supercapacitor with Sequential Programming

As shown in Figure 53, the Supercapacitor was turned ON 200ms after the load current had met the peak load threshold value of 1.5 A (since 1 Ω current sense resistor is used, the voltage is equivalent to the current value). Hence, it is estimated that the K-value required is estimated to be 2-7 points ahead (also means 200ms-700ms ahead) for the peak load prediction after taking into account the classification and prediction processing time.

187

Step 2: Load current prediction

The measure and respond strategy is deemed to have time delay and this shows the need for SVMR_EMS to predict the peak load current in advanced to improve the time response performance. As mentioned in the introduction section, the load current in this project is simulated with programmable load which has no external variable correlation with it except time and its own previous values. Thus, it is proposed to use the K-step ahead autoregressive model where the output variable is dependent only on its previous own values. However, autoregressive model gives poor performance in nonlinear time series modeling. Hence, the load forecast technique used in this project is the autoregressive model of time series by using SVR to compensate the poor performance of ARIMA in nonlinear domain as SVR has a good modeling of nonlinear time series. Besides, due to the good generalization capability of the SVR, the SVMR_EMS could still yield a good load prediction results albeit there are inconsistency in the load profile generated.

The relationship between the SVR independent input variables and dependent output variable by using the K-step ahead approach is shown in literature section :

$$Y(t+K) = F(Y(t), Y(t-1)...Y(t-m+1)) \qquad \textbf{Equation 25}$$

where K is the points in advanced of time to be predicted and m is the number of previous points to be used for the next step prediction. Based on the time response improvement requirement determined empirically, the K value was chosen to be 7 and the m value to be 3. The implementation steps are explained in Figure 54:
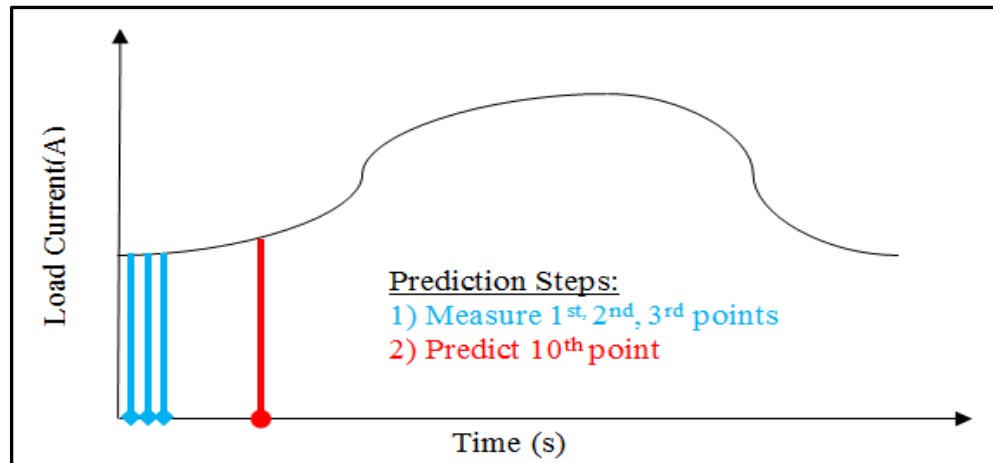
Figure 54 The 7-steps ahead load prediction

As shown in Figure 54, the Maxim DAQ USB 6009 will scan for three load current data points, and feed the data as the features of the input vector. By mean of pattern recognition on the input features, it can be used to predict the 10th point load current. This process will be repeated throughout the whole load profile to give the SVMR_EMS the ability to predict the peak load current in advanced. By implementing the 7-steps-ahead load prediction with 3 previous variable values in the SVR, it has yielded a good supercapacitor time performance as shown in the results Section 4.2.3.

Step 3: Support Vector Regression (SVR) Training & Testing

To implement the K-step ahead prediction for each load profiles, the SVR model that describe the relationship between the previous 3 load current values to the 7 points ahead load current value has to be trained and optimise to ensure the model has good descriptive accuracy. There are 3 steps to the modeling process: data preprocessing, model selection, and cross-validation and grid search.

1. **Data Preprocessing**

This step involves data acquisition, data adjustment for implementation of 7-steps ahead forecast technique, and data format conversion to the required format in LIBSVM. First, the Maxim USB 6009 DAQ was used to collect the load current data from load profile 1 with a sampling rate of 10Hz by using the Data_Collect.m written in MATLAB. Hence, there are in all 200 points of data for each load profiles. Second, the Data_Adjustment.m written was used to prepare the input vector by making every 3 previous load current value as the input feature variables. The output label linking each of the input vectors will be the 7th points in advanced load current value as shown in the following:

Table 30 Data adjusted for 7 point ahead forecast

	Input Vector		
Output Label	**Feature variable 1**	**Feature variable 2**	**Feature variable 3**
1.250736	1.215048	1.2074	1.220146
1.243088	1.2074	1.220146	1.217597
1.230343	1.220146	1.217597	1.225244
1.220146	1.217597	1.225244	1.220146
1.215048	1.225244	1.220146	1.222695

7th point in advanced load current value

3 previous load current values

Finally, the dataset was converted into sparse format which is required by the LIBSVM. By using the libsvmwrite ('txt filename', label vector, instance vector) function provided, the dataset was converted into the following format which could be readily read by the LIBSVM

```
1.25074     1:1.21505 2:1.2074 3:1.22015
1.24309     1:1.2074 2:1.22015 3:1.2176
1.23034     1:1.22015 2:1.2176 3:1.22524
1.22015     1:1.2176 2:1.22524 3:1.22015
1.21505     1:1.22524 2:1.22015 3:1.2227
```

Figure 55 Sparse Format in LIBSVM

Scaling of the data is usually recommended prior to SVM training. This is to prevent input attributes/features which have greater numeric value to dominate the smaller ones. Besides, it could also improve the processing performance, as big numerical value will cause the calculation of inner product in the kernel to be difficult. Hence, it is recommended to scale the data to the range (0-1) [101, 102]. However, in this project, only one single variable is involved which will not cause any domination issue and the value of the load current is only in the range of 1-3A which is considerably small. Besides, the scaling also requires the real time downscaling of the input current value which will add to processing requirement. The scaling process was not applied in this project.

2. **Model Selection**

This step involves the selection of the suitable kernel model which is available in the LIBSVM: linear, polynomial, radial basis function (RBF) and sigmoid as mentioned in the literature review section. The RBF could perform nonlinear mapping of the samples into a higher dimensional feature space unlike the linear kernel. This gives the RBF a good nonlinear modeling capability which suit the nonlinear time series forecast requirement. Besides, the RBF has fewer tuning parameter than the polynomial kernel which makes the selection of parameter process easier.

Moreover, the sigmoid kernel faced some validity issues under certain parameter condition [102]. Thus, the RBF kernel has been selected as the primary choice. Yet, all kernels were tested for every single load profile regression by selecting the kernel which yields the highest squared correlation coefficient and lowest mean squared error. The squared correlation coefficient (r^2) shows the proportion of variance of output that could be predicted by having the input. While, the mean squared error (MSE) is a risk function that measure difference between the predicted output and the true output [117].

3. Cross-validation and Grid-search

This step involves the search for best hyper/tuning parameter for the model to predict the real time load current data accurately in every cases of load profile. The hyperparameter serve to optimise the loss function on the training dataset [250] . In the cross validation method, the dataset was split into v portion: where (v-1) portions are for training and one portion is for testing and validation. The accuracy of prediction obtained from the testing set reflects the model's ability to predict the unknown dataset, which prevents the overfitting problem. For the load profile regression, the cross-validation was done differently unlike the v-fold cross validation method used in classification problem [251]. This is because only one load profile dataset has to be included into the training set for autoregressive time series prediction. Hence, the validation was done by another similar set of load profile where there are slight differences due to the voltage drop. For the parameters tuning, grid search was used along with the cross validation

method. Pairs of the hyper-parameter/tuning values in exponentially growing sequence were tested and the pairs which yield lowest mean squared error was selected [96].

The five load profiles models was trained with the steps above and the optimised parameter values for each load profiles were tabulated in result Section 4.2.3.

Step 4: Load Profile Identification

After the 5 models for each load profile has been trained and optimise, the load prediction could be performed excellently, provided that the correct load profile model was chosen for the regression task. However, the load profile was chosen manually and with the foreknowledge of the load profile generated by the programmable load. This has a drawback of lacked of automation and the choosing of load profiles could be difficult as there could be hundreds of load profile in real application. In order to implement the SVMR_EMS with complete automation, it has to be equipped with load profile identification capability to ensure the load current prediction is based on the correct model. Without the load profile identification, wrong models of trained load profile could be used to predict the peak load current when real time data is polling into the system. This will yield erroneous results as shown in the result Section 4.2.3.

The load profile identification by using SVM classification was done through pattern recognition. Since every load profile exhibit different load demand pattern, it is proposed that through classification of the pattern the load profiles can be separated and identified. This can be implemented with the use

193

of multiclass, multidimensional SVM. SVM was chosen for this classification task as it has excellent generalization capability. Since this project deals with real time peak load prediction, where the forecasting task will occur right after the identification of SVR load profile model was made, its assumed that beginning part of the load profiles holds a distinguish pattern which is recognizable. For this, the load profiles simulated was designed to have distinctive load pattern from each other at the beginning part for simplifying the classification. Figures show the initial patterns suggested for the load profiles:
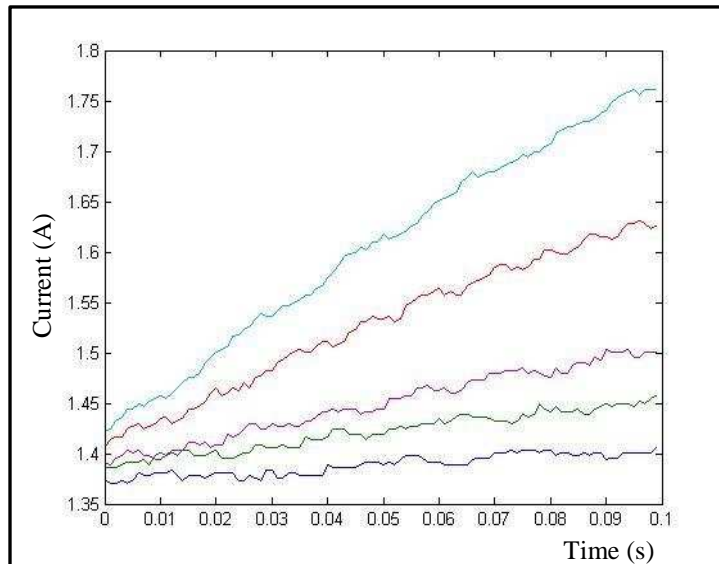
Figure 56 Initial pattern 1
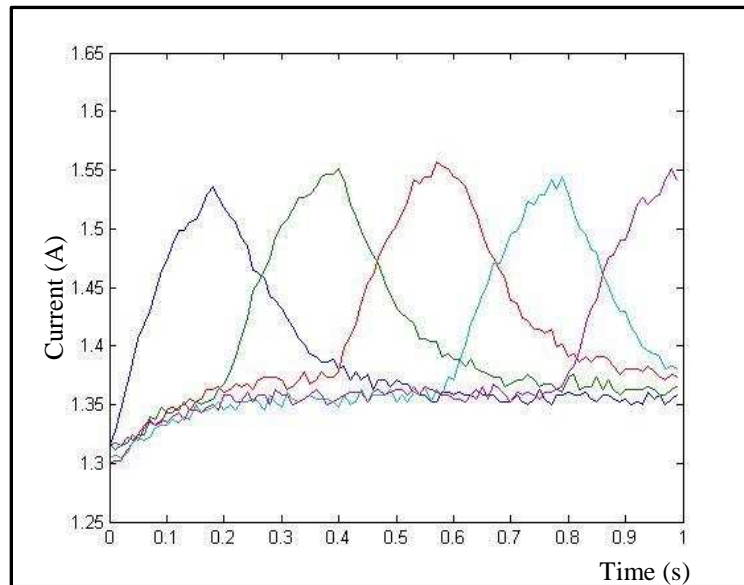
Figure 57 Initial Pattern 2

In the initial pattern 1 (Figure 56), five of the load profiles start with different load current rising gradient level as controlled by the programmable load PWM; hence by recognizing the pattern of the first 100 data points, the unknown load profile could be identified. However, since the load profile replicability was influenced by the battery voltage level, it will yield erroneous classification results when the battery voltage level dropped too much.

For this reason, the initial pattern 2 (Figure 57) was chosen as the starting pattern of the five simulated load profiles. The load profiles have a peak that differs from each other in terms of time. This pattern yields more consistency for the classification as the battery voltage level drop will only affect the peak load current magnitude but not the time of peak load occurrence. Hence by recognizing the pattern of the first 100 points, the load profile could be identified. In real application, the load profiles initial patterns are much more complicated and require sophisticated data mining to generate a model that could perform the load identification.

Step 5: Support Vector Machine (SVM) for Classification Training & Testing

To implement the load profile identification, a SVM model which correctly classifies the actual load profile from the five SVR load profile models will have to be trained and validated. This again, involves the 3 steps as mentioned in the load current prediction section.

1. Data Preprocessing

This step involves the data acquisition, data adjustment and format conversion for use with the LIBSVM. The MAXIM USB6009 DAQ was used to acquire the first 100 points of data from each of the load profiles by using the classification.m written. These data are sampled at 100Hz to speed up the load identification process. The 100 points of data was then made into the feature variables of the input vector as shown below:

Table 31 Data adjusted for Load Profile Classification

Class Label	Input Vector								
	F1	F2	F3	F4	F5	F6	F7	…	F100
1	1.31	1.32	1.34	1.36	1.38	1.40	1.41	…	
2	1.31	1.31	1.31	1.31	1.32	1.31	1.32	…	
3	1.29	1.30	1.30	1.31	1.31	1.32	1.33	…	
4	1.30	1.30	1.30	1.30	1.31	1.32	1.31	…	
5	1.31	1.31	1.31	1.32	1.31	1.32	1.32	…	

There are in all 8 sets of data were obtained from each load profiles where 5 sets of each was selected as the training data sets and the other was used a testing data for validation.

2. **Model Selection**

This step deals with the selection of suitable kernel which is used in the model for classification of the load profile. The various kernels were tested and the kernel with optimised parameter which yields the highest accuracy with lowest number of support vector was chosen.

3. **Cross Validation and Grid Search**

For the SVM, the 8 fold cross validation was chosen, but instead of one, three sets of data was used as the testing data while the other 5 sets was used as training data. This allows the classification accuracy to better reflect the model's ability in classifying new data. Besides that, the best_parameter.m in Matlab was used to perform the grid search which yields the optimise value of C and g. The optimise SVM model was shown in the results section.

3.2.3.2 Flow Chart of SVMR_EMS algorithm

With the establishment of the classification model and the load profile regression models, the algorithm which includes the charging and discharging constraint of the batteries and supercapacitor was written in MATLAB environment, code name SVMR_EMS.m was shown as follows:
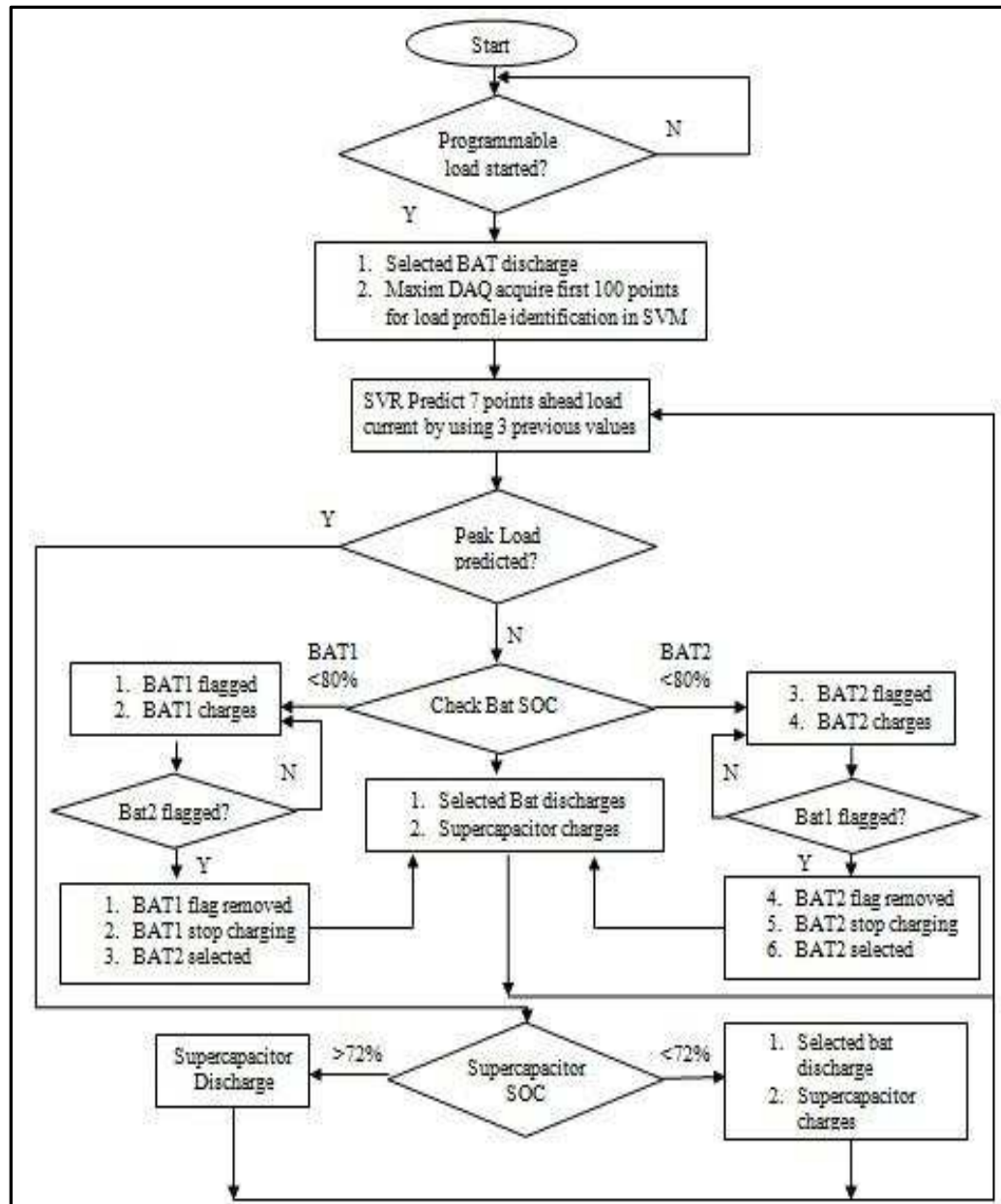
Figure 58 Algorithm of SVMR_EMS

Algorithm Explanation

After the SVMR_EMS.m program in MATLAB was run, it will loop continuously until a signal was send from the programmable load when the load profile is started. Then Either the Battery A or Battery B will start to supply to the motor load depending on the previous selection. The Maxim DAQ will also pole the first 100 load current data points for the classification.

After the load profile is identified, The Maxim DAQ will continue to pole 3 load current data points into the SVR model to predict the load current which is 7 points ahead of time. If the predicted value is greater than the threshold value set for the particular load profile, the supercapacitor terminal voltage will be measured by the Arduino Mega 2560 to determine its SOC. If the SOC level of supercapacitor is greater than 72% (equivalent to approximately 10V), the supercapacitor will supply the load. If the SOC is lower than 72%, the selected battery will continue to supply to the load while the supercapacitor will be charged by the solar charger.

On the other hand, if the predicted value is lower than the threshold set for the particular load profile, the Battery terminal voltage will be measured to check its SOC. If the SOC level of battery 1 is < 80%, the battery 1 will be flagged and charged up by the solar charger while battery 2 will supply to the load. This will go on until the battery 2's SOC is lower than 80%, then the battery 2 will be flagged and start to be charged up by the solar charger. This will simultaneously stop the charging of battery 1 and battery 1 will be selected for the discharging operation. Meanwhile, the supercapacitor will be charged whenever the battery is supplying to the load to ensure a more reliable supply

from the supercapacitor when peak load is detected. This process will be repeated until the program is shut off. The code is shown in Appendix A4.

3.2.3.3 Summary

- The SVM is used for load identification and SVR is used for load prediction.

- This load prediction software was implemented using LIBSVM in the MATLAB environment.

- Five important steps on implementing the software control box, data acquisition device, microcontroller for the SB-HESS.

- The energy control system allows the cost reduction in SB-HESS by eliminating the power electronics to build bi-directional converter and also avoid the direct coupling of a supercapacitor and battery energy source in parallel.

- SB-HESS with SVM_SRM allows load prediction which is used to avoid the shortfall between the switching supercapacitor for peak power and battery for the average power.

3.3 Methodology Step 3
Identify the PV Standards, which governs the characterization of supercapacitors used in PV systems

Reduction system cost by integrating the supercapacitor to the conventional RES with the implemented SVM energy control system is shown in the previous methodology steps. This part of the chapter emphasizes on the manufacturing of fabrication supercapacitor. The aim of this step is to manufacture supercapacitors, which have robust capacitance and voltage, and which are economically feasible for solar applications. Supercapacitors are manufactured based on the previous GA simulation in designing and optimally sizing for the required specification of RES. Robustness in supercapacitor fabrication is important. Since the energy stored in supercapacitors (shown in Equation 2) is proportional to its capacitance and voltage squared, reducing the maximum voltage of the unit will have a significant effect on its useable energy density.

The fabricated supercapacitors conform to the British Standards IEC 62391-1, fixed electric double-layer capacitors for use in electronic equipment – Part 1: Generic Specification and IEC 62391-2-1, Fixed electric double-layer capacitor for use in electronic equipment – Part 2-1: Electric double – layer capacitor for power application – Assessment level EZ.

Part 2.2 Preferred Values of Ratings of IEC 62391-1 is the standards, which the fabricated supercapacitor is conformed to. It governs the preferred rating and characteristic of supercapacitor which is used in solar system.

From IEC 62391-1, Part 2.2 [1],

2.2.1 Rated capacitance (*CR*)

The rated capacitance shall be expressed in farads F) and as agreed between the sending and receiving parties. *Preferred values of rated capacitance are the values from the E24 series of IEC 60063 and their decimal multiples.*

2.2.2 Tolerance on rated capacitance

The preferred values of tolerance on rated capacitance are: ±20 % and −20 %/+80 %.

2.2.3 Rated voltage (*UR*)

The rated voltage shall be as agreed between the sending and receiving parties. The preferred values of the rated direct voltages are taken from the R20 series of ISO 3 and their decimal multiples.

2.2.4 Rated temperature

The value of the rated temperature is 60 °C or 70 °C.

2.2.5 Internal resistance

The internal resistance shall be as agreed between the sending and receiving parties. The internal resistance shall be measured with the d.c. resistance method. However, if a coefficient can be obtained from both d.c. and a.c. resistance methods, the a.c. resistance method may be used for measurement.

Figure 59 British Standard IEC

An integrated optimization approach is proposed in the supercapacitor fabrication process. Genetic Algorithm is implemented within the Taguchi method to optimise the process factor of supercapacitor fabrication. Orthogonal array in Taguchi method is highlighted to reduce the number of experiments for Design of Experiment (DOE) and GA is utilized to optimise the Signal-to-Noise Ratio (SNR) in Taguchi method. SNR is an ideal metric for deciding the best values, levels for the control process factors.

3.3.1 Process Fabrication Supercapacitor

This section reflects brief procedures of fabricating an electrochemical double layer capacitor (EDLC). This supercapacitor fabrication process Table 32 (data specification is retrieved from the bottle of the raw material) below shows the material used in the process fabrication supercapacitor and the corresponding supplier's information.

Table 32 Raw Material used in Supercapacitor Fabrication

Material	Supplier	Details
Activated Carbon (AC) for EDLC	RHE Resources (Manufacturer's Origin: China)	• Surface Area: 2000~2500 it was tested in BET. bulk density: 0.4g/ml, Ash content: <0.5%, moisture content: <10%. • In a mixture of 10g active material, 75% of AC is used.
Carbon Black (CB)	Cobalt - Vulcan XC72R GP-3921	• In a mixture of 10g active material, 75% of CB is used.
N-methyl-2pyrrolidone (NMP)	Sigma-Aldrich	• 40ml of NMP (solvent) is used for a mixture 10g active material.
Polyvinylidene Difluoride (PvDF)	Semyung Ever Energy Co. LTD. KF Polymer (Binder) L#9130	• Polymer content in 1g of PvDF is 13%. • In a mixture of 10g active material, 15% of PvDF is used.
Filter Paper as Separator	Whatman®	• Grade 1: 11μm. • Dimension of the separator used is 50cm x 3cm.

Aluminium Foil as current corrector	n/a	Dimension of the current collector coated is 40μm.
Electrolyte 1M Tetraethylammonium tetrafluoroborate (TEABF4) in PC	Semyung Ever Energy Co. LTD.	n/a
Acetone	Sigma-Aldrich	Assay ≥99.5, puriss p.a

*1. Bulk density is a property of powders, granules and other divided solids, especially used in reference to mineral components, chemical substances, ingredients, foodstuff or any other masses of corpuscular or particular matter. It is defined as the mass of many particles of the material divided by the total volume they occupy. The total volume includes particles volume, inter-particle void volume and internal pore volume.

2. p.a. pro analysis

The procedure of fabrication supercapacitor is presented as below:

1) The first step is mixing process where the activated carbon and carbon black are assembled and weighted. The weighted activated carbon and carbon black are dry-mixed for 10 minutes with the speed of 100 rpm (revolution per minute). An overhead stirrer is used for this mixing process.

2) Next step is diffusion mixing by adding 40ml of NMP, which acts as a solvent. It forms a homogeneous mixture. The mixing duration is 20 minutes and the speed used is 300rpm.

3) The binder PvDF is then added to the active material (the mixture). A binder mixing process is required and it takes about 90 minutes at the speed of 400rpm for this process.

4) The active material, which is in the form of slurry, is coated on the surface of aluminium foil (current collector) using doctor blade (micrometer adjustable film applicator) on a coater machine. The thickness of the slurry coated on the current collector is 40μm. This desired thickness is set on the micrometer adjustable film applicator, which has the adjustable thickness

from 0.01mm - 5mm. This film applicator is pushed by the transverse pusher to ensure constant speed coating.

5) The electrode (the coated aluminium foil with active material) is sent to the vacuum oven for drying process. The temperature is set at 43°C for 5.5 hours.

6) The procedures of 1 to 5 are repeated for the backside of the aluminium current collector.

7) The current collector is coated both front and back sides. This coated film is called electrode. The electrode and the separator are cut.

Table 33 Length and Width of the Electrode and Separator

	Length (cm)	Width (cm)
Electrode	24	2.5
Separator	50	3

Figure 60 Supercapacitor Electrode
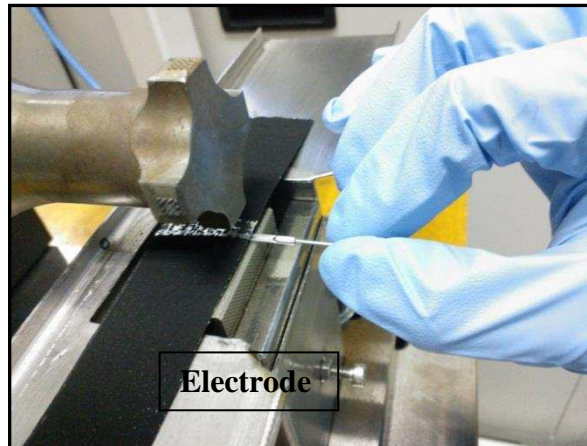
Figure 61 Process of Lead Attachment using Ultrasonic Welder Machine

8) Next is the lead attachment process. A lead is attached onto each of the electrode using ultrasonic welder machine as shown in Figure 61. This process is repeated for the second strip of the electrode as two electrodes are required to fabricate a full cell.

Figure 62 Seperator
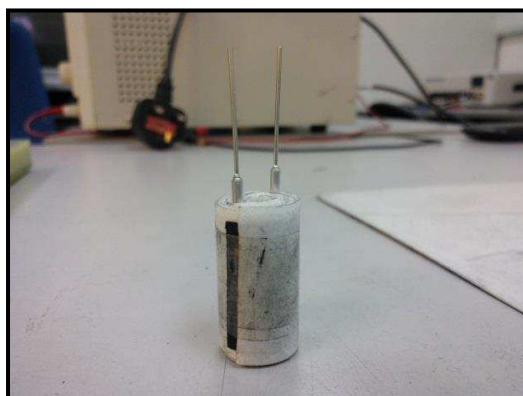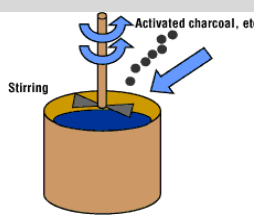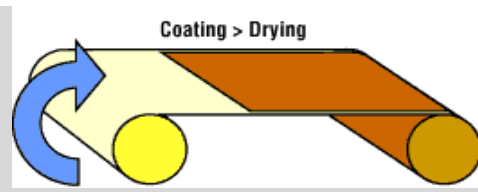
(a)   (b)

Figure 63 Cells and package

9) The separator as shown in Figure 63(a) is placed between the electrodes for the coiling process is carried out. A clean tweezers is used to handle the separators to prevent contamination. The end product for this process is shown in the Figure 63.

10) The obtained EDLC coil is immersed in the electrolyte (1M TEABF4 in PC). A rubber seal is placed on the leads and the cell is inserted into the case. This is done to prevent the leakage of electrolyte.

11) Finally the cell is crimped and curled. An ID number is assigned to the full cell for future tracking.

12) Test the performance of the cell using the potentionstat/galvaostat Autolab PGSTAT302N in order to evaluate the capacitance and ESR of the cell. A summary of the process shown in the table below:

Process	Details	Diagram
Weighing materials	AC:75%, CB:10%,PVDF:15%	
Dry - Mixing AC and CB	10 minutes at 100rpm Add 40ml NMP. Mix for 20 minutes at 300rpm. Add PVDF and mix for 90 minutes at 400rpm.	
Mechanical mixing		
Coating the aluminum foil with the active material	Thickness of the active material: 40μm.	
Dry the coating	43°C for 5.5 hours	

active material under vacuum oven.	
Cut into stripes with the dimension of 24cm X 2.5cm	Source roll Slit
Two leads are attached onto the electrode foil.	Welding machine Lead attachment Crimping Electrode foil Lead
A thin separator paper layers interposed between the cathode and anode foil layers.	Winding machine Anode layer Coiling Fastening Tape Electrolytic paper Cathode layer

Figure 64 Steps of supercapacitor Fabrication

Supercapacitor Testing Procedure

Testing is particularly crucial for supercapacitor because it affects the supercapacitor's leakage current and life characteristics [53]. One of the significant characteristics of supercapacitor is used to couple with battery is the long cycle and shelf life. Devices with very low leakage current have a long life as a low leakage current indicates the absence of low level Faradaic reactions

between the electrode material and the electrolyte which over long periods of time result in degradation of the devices. This means a reduction in capacitance and an increase in resistance. This is very important in a hybrid energy storage system as this SB-HESS is an optimised system. It affects the power delivery time to cater for peak power. Supercapacitor is known as high power density devices, it switches on instantaneously to cater for the peak power.

1. Brunauer-Emmett-Teller (BET) Analysis

The objective of carrying out this test is to evaluate the surface area of the activated carbon used in the fabrication supercapacitor process. The surface area analyser used is Micromeritics ASAP 2020 Accelerated Surface Area and Porosimetry System V3.01 [252]. The commercial activated carbon is purchased from Cobalt - Vulcan XC72R GP-3921. The BET model is one of the commonly used equations for the calculation of the surface area of the material [252]. The BET theory relates to the capacity of the monolayer formed on a particular surface (the amount of the adsorbed molecules in the monolayer) [252]. The equation is not covered in this thesis. The crucial value for this research is the BET surface area 2010.6896 m^2/g. The BET analysis is still the existing standard method of examining the surface area of materials as other methods might not provide better advantages over BET analysis. For this test, the setting is shown as follows:

Sample Mass: 0.0926 g
Cold Free Space: 90.5136 cm3
Low Pressure Dose: None
Analysis Adsorptive: N2
Analysis Bath Temp.: -195.842 °C
Thermal Correction: No

Warm Free Space: 28.8193 cm3 Measured
Equilibration Interval: 10 s
Automatic Degas: Yes

2. Cyclic Voltammetry

Generally, capacitance and Equivalent Series Resistance (ESR) are the main output response in this process fabrication supercapacitor. The cyclic voltammetry technique is one of the methods used in this project to obtain output responses of the supercapacitor. In this technique, potential applied to the electrode immersed in the organic or aqueous electrolyte is varied with the time and the relevant current-potential curves recorded. The linear sweep voltammetric technique is used in all testing the capacitance of the supercapacitor fabricated. The electrode potential is set from an initial value E_i to an ending value E_f at a constant scan rate, s. The equation is shown below:

$$s = \pm \frac{dV}{dt}$$
Equation 42

When the potential value E_f is met, the direction of the scan is inverted [253]; while still keeping the same scan rate, s, and the potential is returned to the beginning value (cyclic voltammetry).

With the relation to the equation of $I = C \times \frac{dV}{dt}$ and Equation 43, we can derive the two following Equations 43 and 44.

$$I = C \times \frac{dE}{dt} \equiv C.s$$
Equation 43

$$C = \frac{I}{s}$$
Equation 44

If C is constant with potential, then a rectangular current response against the potential would be generated, where the shape would be symmetrical around the zero-current line [253], given that the scan rate remains the same for both anodic and cathodic scans [254]. However, in most cases, C would not be constant with reference to the potential in the scan and the sweep rate, due to the kinetic or diffusion limitations of the current [254]. The electric current, I can be defined as the electric charge, q in coulombs transferred in t seconds, i.e.

$$I = \frac{dq}{dt}$$ **Equation 45**

Replacing Equation 44 and Equation 45 into Equation 46 and cancelling the dt term, the following term can be obtained:

$$C = \frac{dq}{dE}$$ **Equation 46**

It follows that to obtain an average value of capacitance from the cyclic voltammogram which includes a positive and negative scan, the following equation can be utilized, i.e.

$$C = \frac{q^+ + |q^-|}{2\Delta V}$$ **Equation 47**

where q^+ and q^- are the anodic and cathodic voltammetric charges on the anodic and cathodic scans respectively.

The cyclic voltammetry was performed in this project using scan rates between 2mV/s, 5mV/s, 10mV/s and 20mV/s.

(a)
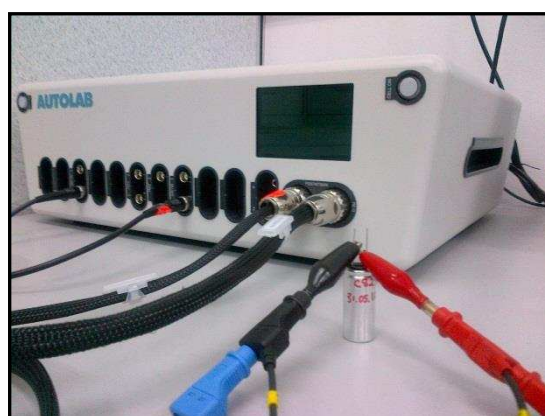
(b)
Figure 65 Autolab PGSTAT302N

3. Galvanostatic Charge-Discharge Test

According to the dissertation [254], the galvanostatic charge-discharge technique often applies in the application of a constant current source across the electrochemical cell and the recording of the potential response. When a constant current, i, is applied in an interfacial charging process, accumulation of charges Δq takes place across the interface to an extent that it is dependent on the potential of the electrode related to the potential difference built up across such an interface (ΔV) [255]. This implies the equation below:

$$C = \frac{\Delta q}{\Delta V}$$

Equation 48

And $\quad \Delta q = \int i.dt$

Equation 49

Therefore, $C = \frac{\int i.dt}{\Delta V} = i.\frac{\Delta t}{\Delta V}$

Equation 50

where Δt is the time interval taken to reach the particular

potential

As in the case of cyclic voltammetry an ideal rectangular
(voltammogram) [253] , Equation 50 implies for capacitance which is constant
with potential. However, from the test profile shown in section later, this is not
the case, so ΔV diverges from a linear dependence on time at a constant current.

3.3.2 Optimising Process factor using The Taguchi-GA method

Previous applications [256, 257, 258, 259] indicate that the Taguchi method emphasizes the solution of single-response problems with the aid of knowledge gained from past experience. Thus, it is not capable of handling multi response problems without requiring some modifications in the application.

The Taguchi method provides practitioners and designers with a systematic approach for conducting experiments to obtain near optimal settings of design factors for performance and cost [260, 261, 262] . The design (controllable) factors and noise (uncontrollable) factors, which influence the quality of the product, are considered together instead of individually [259, 263].

The objective of implementing the Taguchi method is to obtain the best combination of factors and levels in order to achieve the most robust product. This means, the selected levels of the various design factors from the Taguchi method allows the performance of the product/process to be less sensitive to the noise factors.

However, in today's manufacturing environment, many processes or products involve solving multi response problem to improve their product quality. One crucial fact is that the Taguchi method is incapable of performing well for multi-response optimization problem [260, 261]. In order to overcome this limitation, we have formulated a way to include a GA within the Taguchi method.

A common method of solving the multi response problems is to assign each response with a weight, as mentioned in [260, 261, 264]. A normal

question which arises is how to determine and define the weight for each response in a real case. The goal of this proposed strategy is to ensure that the performance characteristics (or the quality) have minimal variation while having its mean close to the desired target value.

The idea underlying this integrated strategy is to convert the problem of optimising a complicated multi process response into one that optimises a single weight of the SNR. This means, the weighted signal-to-noise ratio, WSNR is used in the overall evaluation of experimental data in the multi response optimization problem. In this case, the GA strategy utilizes the normalised SNR (Z) from the Taguchi method to form its fitness function. The optimal level for each individual process factor is the level with the highest WSNR.

Design of experiments (DOE) is a method that can be used to identify the critical areas that cause yield loss in a process. With proper application of DOE, design engineers or researchers are able to pinpoint the source of the yield problem and fix them to produce solid and robust designs with much higher yield [265]. In DOE, the three terms that need to be clearly defined are Factors, Levels and Replication. Factors or parameters are important variables that would affect the outcomes or output responses. However, all factors may not have equal importance as some factors may have a more prominent effect over other factors. 'Levels' in the simplest terms are possible values for each factor identified thru gathered data (for this case the levels are 'low' and 'high'). For example, if two levels are assigned to each factor, one of the lower levels is a lower level and the other is a higher level. The values of these levels are assigned in reference to literature, consultation with experts or one can

identify level values thru experimentation before the Taguchi method is carried out [256, 266]. A two-level factor assumes linear behavior while three-level factor best fits non-linear behavior but requires a larger number of trials while running experiments. Replication is necessary to address the concern on repeatability and also the spread of the variation in the experimental outcome. This is done in order to obtain adequately accurate statistical information of the process under study. This is done by producing several samples for each trial or by repeating the same trial several times.

The Taguchi method is famous for implementing robust (parameter and tolerance) design. Robust design is a result of determining the optimal factor combination/setting to reduce the response variation and brings the mean close to the target value consequently [267]. To implement the robust design, Taguchi employs an orthogonal array (OA) in order to reduce the number of experiments as compared to the full factorial DOE version. SNRs are used to evaluate the outcome of the experimental trials. It is common to include an ANOVA alongside SNR to study the percentage contribution made by each factor. Even though the Taguchi method has been successfully applied to processes in design and manufacturing, it has been criticized for its lack of efficiency because the method works well for single-objective optimization problems but not for multi-objective problems [12, 268]. Some modification on the existing method has to be made [261, 269, 270, 271] to make it work for some cases of multi objective problems.

Similarly, the Taguchi method for multi-objective problems, as discussed by Phadke as mentioned in [270], is purely based on judgmental and subjective process knowledge [272]. When dealing with a multi-objective

problem, one can use several techniques. The simplest way is by adopting the OEC (overall evaluation criteria) approach. This is done by assigning certain weighting to each of the output response criteria so as to normalize the two (or more) different response units. The weightings are arbitrarily chosen based on experience in order to make a response either dominate or have the same weight when compared to the other responses [265, 273, 274]. Such judgments are not very accurate [272]. A way of overcoming this problem is by using the GA approach. In section below, the GA method will be further discussed specifically on how it was used with the Taguchi method to make solving the multi-objective problem possible. The GA will search for the optimal weights that maximize the SNR for each output response to improve its immunity to noise and thus make the product more robust. The hypothesis here is that the GA approach will result in a better SNR as compared to the OEC (initial method) as stated in Table 80 (Chapter 4) method because the GA searches the entire solution space for the optimal point whereas the weights determined by experience does not. To proof this hypothesis, the percentage improvement of the SNR (if any) will be determined and then the process parameters will be implemented to confirm the increase in robustness of the product.

In this case, the integrated approach is divided into several repeatable steps that could also be applied in other process/product multi-objective optimization problem accordingly. There are four steps outlined (Step 1-4 mentioned below) for the initial experimental factors and levels design, including the computation of SNRs from the experimental data. Next, the integration of GA approach for determining the optimal weights based on the normalised SNRs (Z) in the range between zero and one are conducted (Step 5-

6). The WSNR is then computed by multiplying the weight with Z relates to each response. The final two steps (Step 7-8) will be the data analysis focusing on the main effect of each factor towards the WSNR values, which is essential for predicting the desired optimal setting. It continues with the confirmation experiments. Consequently, further statistical data analysis includes the measure of variability between OEC and the proposed strategy is conducted using standard deviation and ANOVA, in order to determine the percentage improvement acquired (if any) and subsequently identify the dominant factors that influencing the capacitive performance of the device.

The implemented Taguchi-GA method is applied in supercapacitor fabrication and the steps fall within the initial experimental design stage, are listed below.

3.3.2.1 Steps Implementing the Taguchi-GA Method

Step 1: Assigning factors and levels for each of the main processes

Table 34 provides the lists of control factors for mixing, calendaring, drying and electrolyte treatment process. All of the three factors (A, B and C) are assigned with two levels of factor each for the experiment. The rationale of choosing the Level 1 and Level 2 is based on the senior's experience in this fabrication process. For this study, the value of Level 1 and Level 2 were selected based on the parameters shown in [275]. For future work, if time and cost are allowed, more levels for the process factors could improve the output response.

Table 34 Process factors and their levels for the supercapacitors fabricated

Process	Factors	Level 1	Level 2	Output Response
1 Mixing	A Mixing Speed (rpm) B Mixing Time (min) C Amount of AC (%)	200 15 85	350 30 90	1. Capacitance (F) 2. ESR (Ω)
2 Calendaring	A Calendaring time (min) B Thickness (mm) C Machine temperature (^{o}C)	15 0.65 23	30 0.85 30	
3 Drying	A Heating time min) B Heating temperature (^{o}C) C Vacuum	20 50 Yes	45 80 No	
4 Electrolyte Treatment	A Electrolyte name B Electrolyte molarity (M) C Electrolyte amount (ml)	KCl 2 0.5	Na_2SO_4 3 0.8	

Step 2: Determining the minimum number of experiments required and the selection of Taguchi orthogonal array.

Here, the Taguchi multi-objective optimization begins with the selection of orthogonal array (OA) with specific number of levels (L) for factors A, B and C. The minimum number of experiments in the array is obtained by using the equation below [12]:

$$N = (L - 1) \cdot F + 1 \qquad \textbf{Equation 51}$$

where F = number of factors, in our case, F = 3

Thus, L_4 orthogonal array (OA) is selected due to four numbers of trials required and outlined as in Table 35. The selection of OA depends on the number of factors to be studied as shown in the Equation 51, the number of

interaction to be studied, time and cost constraints.

Table 35 4 x L$_4$ Orthogonal arrays for the process factors

Process	Experiment, i	A	B	C
1 **Mixing**	1	1	1	1
	2	1	2	2
	3	2	1	2
	4	2	2	1
2 **Calendaring**	1	1	1	1
	2	1	2	2
	3	2	1	2
	4	2	2	1
3 **Drying**	1	1	1	1
	2	1	2	2
	3	2	1	2
	4	2	2	1
4 **Electrolyte** **Treatment**	1	1	1	1
	2	1	2	2
	3	2	1	2
	4	2	2	1

Step 3: Conducting all experiments outlined with three replications (samples) each according to the Level which is assigned to the Factors shown in Table 34. Value of level 1, level 2 and factors for each of the process are defined in Step 1.

Step 4: Computing SNR for every output responses.

The SNR values for the respective responses (SN_{iC} and SN_{iE}) are calculated from the raw data from the experiment accordingly. The equations are shown below:

SNR for the capacitance response (larger-the-better)

$$SN_{iC} = -10 \log_{10}(1/n) \sum_{i=1}^{n} \frac{1}{y_i^2} \qquad \textbf{Equation 52}$$

SNR for the ESR response (smaller-the-better)

$$SN_{iE} = -10 \log_{10} (1/n) \sum_{i=1}^{n} y_i^2 \qquad \textbf{Equation 53}$$

where y_i is the experimental data at the ith sample and n is the

number of samples.

The Integrated Taguchi method with GA

The main aim of integrating the GA into the Taguchi technique is to search for definite and optimal weights for each response or performance characteristic and quality) in a multi-response system. As previously stated [12, 259, 263, 264], the Taguchi method has been mostly utilized in optimising single-response problems. One of the noted methods in tackling multi response systems is the problem of optimising weights for signal to noise ratio as mentioned in the literature [256]. In real multi-response cases as described in [12, 276], the weights are based on experience. For instance, in the OEC approach the relative weighting method is used to tackle problems with more than one objective [263]. The method of combining multi criteria of evaluation is truly based on the expertise and the experience gained in many experiments. However, in most real cases this does not result in a robust process or product. This might be due to a level of uncertainties in the decision-making stage especially when picking levels for the parameters. Furthermore, it is difficult for human experts to estimate the effect of the criteria used to evaluate a process as not all criteria have equal importance. As such, the key of obtaining a robust and practical process using this weighting method may be to eliminate the engineering judgment in deciding the weights (or the importance) of the criteria.

The GA is a powerful heuristic global search and optimization technique. It is an optimization technique which is built based on mimicking the evolutionary principles and chromosomal processing in natural selection and natural genetics [6]. It is a widely accepted approach to stochastic optimization, especially in dealing with a global optimization problems that consists of multi-modal search spaces. In a wider usage of the term, GA is any population-based model that uses selection and recombination operators to generate new sample points in a specific search space [277]. In his book [6], Goldberg demonstrated the possible domains where GA's can be applied. Moreover, many GA models have been introduced by researchers and are found to be effective from the experiment perspective [277]. In addition, many of them are application oriented and have adopted GA's as optimization tools [261, 11, 278]. The searching and selection of optimal weights for the process of fabrication of supercapacitors using the Taguchi method often involves problems related to constrained optimization which is similar to what is needed in manufacturing process optimization. Hence, it is appropriate that GA's are integrated with the Taguchi method to optimise the fabrication of coin-type supercapacitors. The capacitance and equivalent series resistance (ESR) of the device are adopted as the quantitative performance characteristic (quality) for evaluation in the current study.

GA's basically evolved from an idea of survival of the fittest and reproduction of new offspring to form a new population to create a novel and innovative search strategy [261, 279, 278]. It implies that the genetic pool in GA of a given population potentially contains the solution, or a better solution, to a given adaptive problem [277, 279]. This makes the GA different as

compared to other traditional point-to-point descending and ascending search techniques [280]. The GA initiates from a random set of solutions, known as the initial 'population'. Each individual solution in the population is known as a 'chromosome' or string). At each generation, the GA works with genetic operators namely crossover and mutation, on the selected individuals which act as parents to recombine part of the strings genes) and produce offspring child) to create a new and hopefully fitter generation [6, 281]

During each generation, these chromosomes evolve to have better fitness. This is done by executing an operation known as selection. Eventually, the chromosomes in the population will converge from generation to generation. The aim is to select the best fit chromosome [266, 6, 281]. By fulfilling the aim mentioned, GA utilizes the fitness function (or objective function) which will be used to create a new and conceivably better population of strings. The fitness function takes a chromosome and assigns a relative fitness value to the chromosome [6]. The fitness function evidently ranks the chromosome in some way by producing fitness values [10].

Step 5: Normalizing the SNRs so that all are in the range between 0-1.

Normalised y_{ij} as Z_{ij} [0, 1] by the corresponding formula to set the right effect of adopting different units, where i is the number of experiment (i.e. number of sample) and j is output response of the process. In this case, output response is capacitance and equivalent series resistance. Notation used in the equations below is C and E. The selection for Equation 54 is based on the fact that the output response of capacitance is expected to be as higher as possible for supercapacitor fabrication because this study is to maximize the capacitance by

optimising the setting configuration of the experiment [275]. However, the quality characteristic selected for the SNR is smaller the better, hence, Equation 55 is selected. This is because the output response ESR is expected to be as smaller as possible, therefore it is able to enhance pulse current handling by parallel connection with an electro-chemical battery [275].

Normalised SNR for the capacitance response (the-larger-the-better) [13]; **Equation 54**

$$Z_{iC} = (Y_{avg.} - Y_{min})/(Y_{max} - Y_{min})$$

Normalised SNR for the ESR response (the-smaller-the-better) [13]; **Equation 55**

$$Z_{iE} = (Y_{max} - Y_{avg})/(Y_{max} - Y_{min})$$

where Y_{avg} is the average out of the n number of samples produced, Y_{min} and Y_{max} are the least and highest data value out of the n number of samples produced respectively.

Step 6: Searching for the exact/optimal weighting value w associated with each Z that would give the maximum WSNR by using GA approach. The WSNR value is determined by using the weights (w_c and w_E) obtained from GA.

$$WSNR_i = w_C Z_{iC} + w_E Z_{iE}$$ **Equation 56**

where i is the number of runs/experiments

In the section below, GA is used to maximize $WSNR_i$ with the optimal w_C and w_E.

Initialization

The algorithm is carried out randomly to create the solution space which is used for searching the optimal weights so as to maximize Z. In this coin supercapacitor fabrication process, we have two output responses; hence there are only two weights which are considered as the gene. The initial population composes of 30 chromosomes. The 30 chromosomes in the initial population are generated subject to the feasibility condition, i.e. the sum of weights should always equal to one.

The Fitness Function

The total WSNR is used as the fitness function in GA strategy to calculate the fitness value. A fitness value in an objective function evaluates the performance level of an individual chromosome; therefore in this case, GA strategy utilizes Z from Taguchi method to form this fitness function. The particular fittest chromosome will be ranked against all other individual chromosomes. The fitness function is given as:

$$F(x) = \sum_{j=1}^{k} \sum_{i=1}^{n} (W_j Z_{ij}) \hspace{3cm} \textbf{Equation 57}$$

The Equation 57 above is written such that f(x) is the total WSNR to be maximised, w_{ij} is the weight to each response, Z_{ij} is normalised SNR values, n is numbers of observation (experiments/runs) and k is the number of response.

Selection

Selection is also known as reproduction in the family of computational model inspired by evolution [281]. It allows individual (string/chromosome) to be copied for possible inclusion in the next generation. The chance that a string will be copied is based on the string's fitness value which is calculated from the fitness function. For each generation, Selection chooses strings that are placed into the mating pool, which is used as the fundamental to create the next generation. Parent chromosomes are selected with a probability related to their fitness value. Therefore, highly fit strings possess the higher probability of being selected for mating [281]. In this supercapacitor fabrication process, the roulette wheel method is applied to the chromosome selection.

Crossover

Once the mating pool is created using Selection operator, the next operator is the crossover. The term 'Crossover' used in GA is analogous to reproduction and biological crossover. 'Crossover' is used to create a pair of offspring chromosome from the parent chromosome [281]. Crossover takes place by depending on the parameter known as the crossover probability, P_c [12]. If the crossover does not take place, two selected chromosomes are simply copied to the new population. The concept of this operator is the new chromosome may be better than both of the parent chromosomes as the offspring takes the goodness from each of the parents.

Mutation

One-gene mutation operation with a preset mutation probability P_m which indicates the frequency at which mutation occurs is applied to generate a new chromosome [12]. P_m should be preset at a very low value. In this case, mutation is performed during the crossover. Mutation occurs when a new gene's value is added to the new population pool. This is to avoid the population stagnating at any local optima [277].

Check for feasibility (constraint of the algorithm)

This is a step to obtain reliable and feasible weights for the fitness function. In this case, this step is crucial to ensure that the sum of the weights is always equal to one. This step is to encounters 3 possible cases mentioned below.

- Case 1 - the sum of the gene values of offspring is less than one.

  If the sum of the gene values of offspring is 0.9; there is a shortage quantity of 0.1 (since 1 -0.9 = 0.1). The shortage quantity will be equally divided, and added equally to the gene values.

- Case 2 - The sum of the gene values of offspring is more than one.

  If the sum of the gene values of offspring is 1.2, there is an excess quantity of 0.2 (since 1.2 − 1.0 = 0.2). The excess quantity will be equally divided, and added equally to the gene values.

- Case 3 - The sum of the gene values of offspring equal to one, the gene values will remain the same.

Stopping Condition

The most usual and popular method − setting the maximum number of generation is used for the stopping condition. This can guarantee the convergence of a GA. In this case, the stopping condition is the total number of generations fixed at 10,000 [6].

Step 7: Study the main effects on WSNR for each factor and level by plotting the Factor Effects on WSNR graphs. This will lead to our predicted optimal conditions.

WSNR is similar to the overall evaluation of experiment (OEC) data for a multi-response process but the weightings used are the main difference. The level for each factors with the highest WSNR is the optimal level (optimal setting for the particular process) of process factors. The computation of the main effect on WSNR is carried out by considering the average effect of each level with respect to each factor. Details and result are discussed in Section 4.3.2. For example, for Process 1 (Mixing), A_1 means the average value of $WSNR_1$ and $WSNR_2$ for Level 1 of the process factors where Level 1 is remained unchanged in that experiment, however the value of other process factor is changed. This is to evaluate the interactions of the process factor. This concept is applied to other average WSNR (A_1, A_2, B_1, B_2, C_1, C_2). These values also known as corresponding factor effects. The larger the WSNR implies the better quality. This is a step leads to select the optimal condition of the process.

$$A_1 = (WSNR_1 + WSNR_2) / 2 \qquad \textbf{Equation 58}$$

$$A_2 = (WSNR_3 + WSNR_4) / 2 \qquad \textbf{Equation 59}$$

$$B_1 = (WSNR_1 + WSNR_3) / 2 \qquad \textbf{Equation 60}$$

$$B_2 = (WSNR_2 + WSNR_4) / 2 \qquad \textbf{Equation 61}$$

$$C_1 = (WSNR_1 + WSNR_4) / 2 \qquad \textbf{Equation 62}$$

$$C_2 = (WSNR_2 + WSNR_3) / 2 \qquad \textbf{Equation 63}$$

Step 8: Running the confirmation experiment and compare the results

(Standard Deviation and SNR) with the earlier trials and initial condition.

Figure below tabulates the summary of the steps mentioned above.
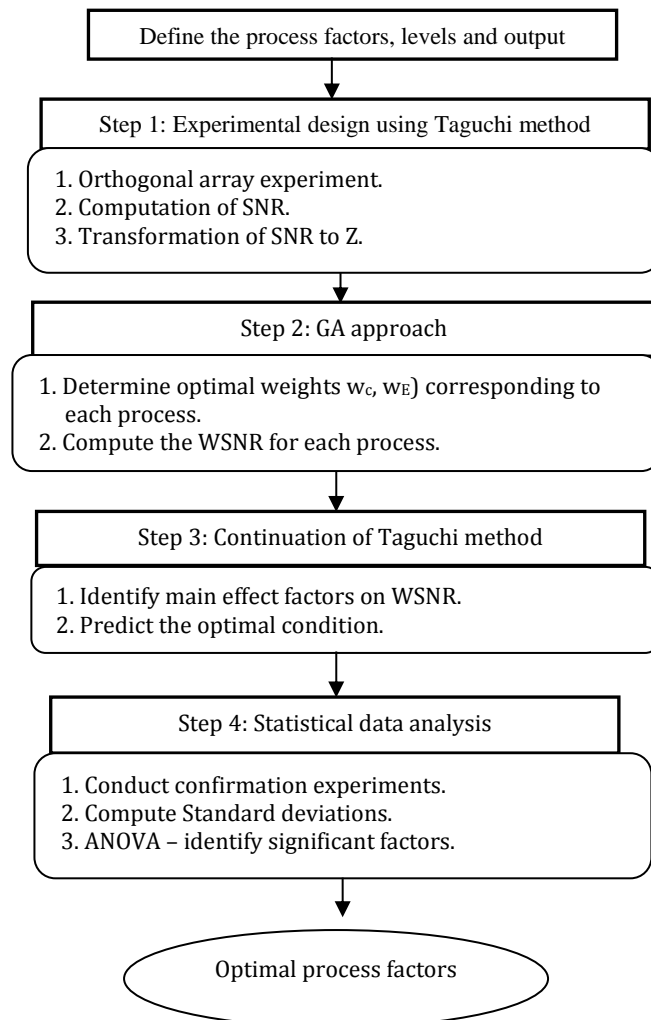
Figure 66 Figure: Flow Chart of the Integrated Taguchi-GA method

229

3.3.3 Summary

- The integrated Taguchi and GA method is used to optimise the process factors of supercapacitor fabrication process.

- The Taguchi-GA integrated strategy provides a robust design in the sense of reproducibility and reliability. This could not be achieved by the OEC approach alone as this approach is dependent on engineering judgment (that has higher variation), a mean value that is far from the desired target value if those judgments were inaccurately made.

- This methodology step is important because noise factor in the manufactured values will cause failures in matching **peak demand** as the hybrid energy storage system is optimised using the GA. Hence a slight drop in capacitance and ESR will cause the reliability of the system.

- The methodology step is important to reduce spread in tolerance of supercapacitor value (capacitance and ESR) which will affect the optimization in sizing RES and power reliability of the system.

3.4 Methodology Steps 4

Construct lab scale prototype design and fabrication

The optimised supercapacitor-battery hybrid energy storage system (SB-HESS) is tested on a lab scale trolley. The configuration of the system was explained in the Chapter 1-Introduction. The optimal sized of lab-scale SB-HESS is design and integrated with the unsupervised learning machine - Support Vector Machine of energy management system (SVM_EMS). Details on the energy management system are elaborated in Section 3.2.3. The integrated architecture was designed as shown in the following:
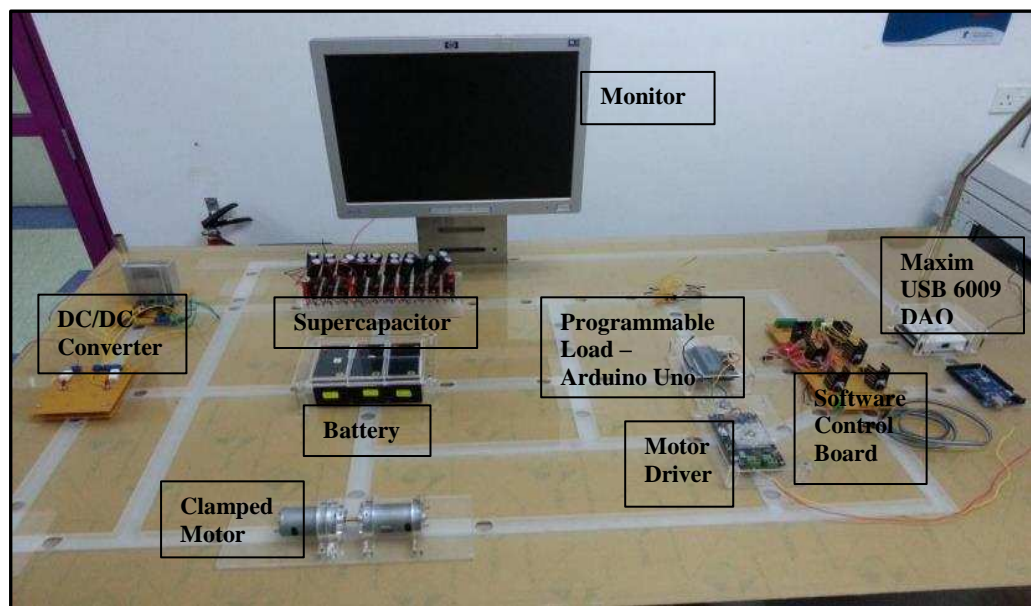
Figure 67 Integrated System on Trolley

3.4.1 Final Testing

The prototype system is tested with the performance metric shown below. There are three main testing for this prototype.

- The performance metric used in system is categorized into 3 groups: One for the performance definition of the SVM and SVR.

- Performance comparison between the standalone battery storage and hybrid energy storage in terms of cost and battery lifetime.

- The reliability and efficiency of HESS using SVMR_EMS and a HESS using hardware-based (DC/DC converter) approach.

	Comparison		Performance Metric
1	**Energy management system**		
	Support Vector Machine		• Classification Accuracy • Number of Support Vector • Training Time
	Support Vector Regression		• Mean Average Percentage Error MAPE)
2	Standalone battery storage system and hybrid storage system		• State of Charge SOC) • System Cost
3	Software Approach and Hardware Approach for energy management system EMS)		• Supercapacitor Time Response • Power Efficiency • System Cost

1. Mean Absolute Percentage Error (MAPE)

MAPE error is the accuracy measure for technique used in modeling time series. It is expressed as the average of the total difference in percentage as shown in the following:

$$MAPE = 100 * \frac{\sum_{i=1}^{n} \frac{L_{R_i} - L_{P_i}}{L_{R_i}}}{n}$$

Equation 64

where L_R is the actual value of load current and L_P is the value
of predicted load current

Besides that, n is the number of points to be compared. Hence, by this formula, the accuracy of the predicted load current can be measured.

2. State of Charge (SOC) stress test

The SOC of the standalone battery storage system and hybrid supercapacitor- battery storage system using hardware and software approaches were recorded for performance comparison. To implement this, a stress test of 1 minute pulse current cycle which is catered for high discharge rate and high depth of discharge (DOD) of the battery. The high discharge rate will reduce the stratification effect but will lead to high sulphation of the battery which give a greater negative impact on the battery. Besides, the high DOD will also lead to sulphation of the battery [282]. The stress test load profile was simulated using the programmable load as shown in Figure 68.
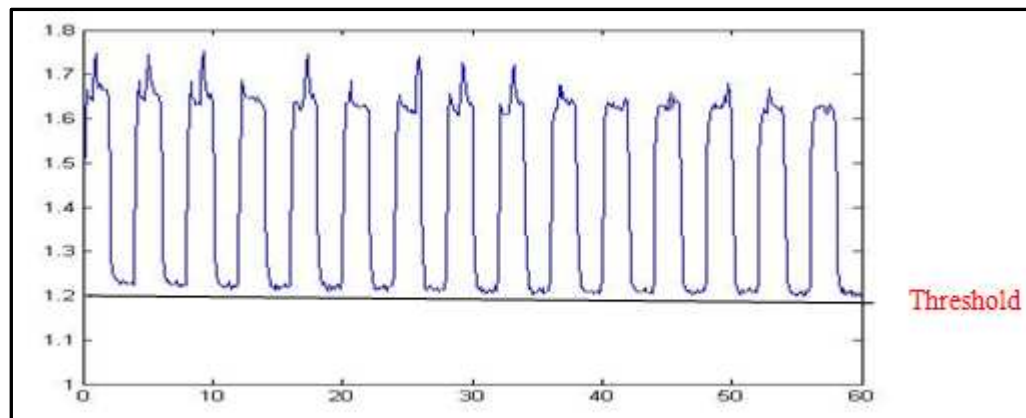
Figure 68 Stress Test Load Profile

The standalone battery system will supply for the whole load cycle, while; in the hybrid system, the battery will supply only when load demand is below the threshold value and supercapacitor will supersede the battery role in supplying for load demand above the threshold value. The battery will first be charged with a fixed charging characteristic of 14V, 1A to ensure the

233

consistency of fully charged battery voltage level as the battery final open circuit voltage varies with the charging rate. Besides, the battery is allowed to stabilize before attaining the SOC value. The battery will then undergo the stress test for 20 cycles. This process was repeated 4 times for the standalone battery system and the hybrid system.

By implementing the combination of Open Circuit Voltage method and Current Integration Method, a more accurate SOC monitoring system can be achieved. The SOC is measured using Open Voltage Method during unloaded operation and Current Integration method during loaded operation. In this project, the Maxim DS2438 Smart Battery Monitoring Evaluation Kit is used. This Chip can measure the battery voltage and current, the accumulated current flowing in or out of the battery with the integrated current accumulator, and the battery temperature with the on board direct to digital temperature sensor. The data acquired will be stored on the chip's onboard memory and will be transmitted through one wire interface which provides versatile operation with any microprocessor/microcontroller [283]. Since the EV kit comes with a window GUI and DS91230 serial to USB converter, it allows direct configuration and monitoring of the Battery SOC on the GUI as shown below: (The evaluation kit used is MAXIM DS2438EVKIT+. The evaluation kit is interfaced to a PC through a DS91230 USB adapter and RJ-11 cable connection).
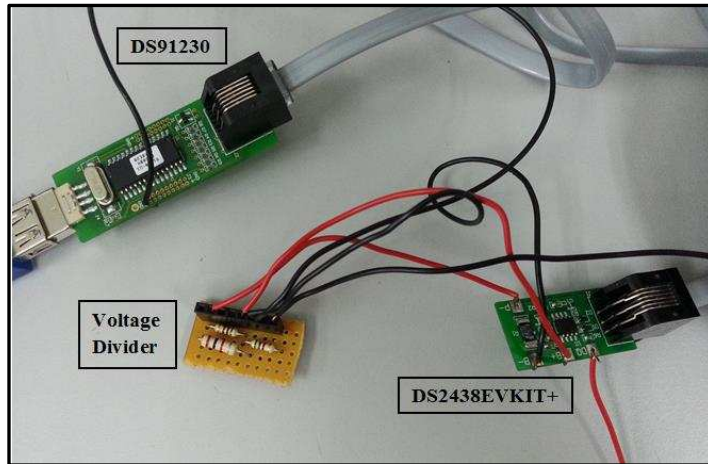
Figure 69 Circuit connection for MAXIM DS2438EVKIT+

This smart battery monitoring system is able to measure the temperature, voltage, current of the lead acid battery. Apart from that, it is also able to set the elapsed-time in order to be able to synchronize with the real time and able to log all data in a text file. Figure 70 shows the meters screen which displays the real time measurements of the battery voltage, temperature, current and remaining capacity of the lead acid battery.
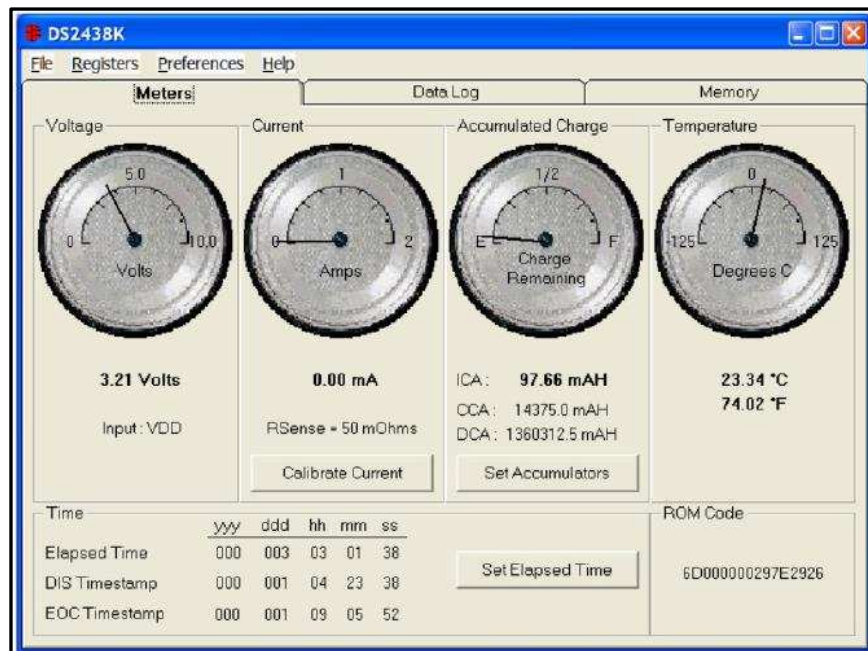
Figure 70 Meters screen of DS2438EVKIT+

A certain configuration is needed to measure the lead acid battery during charging and discharging phase as shown in Figure 71.
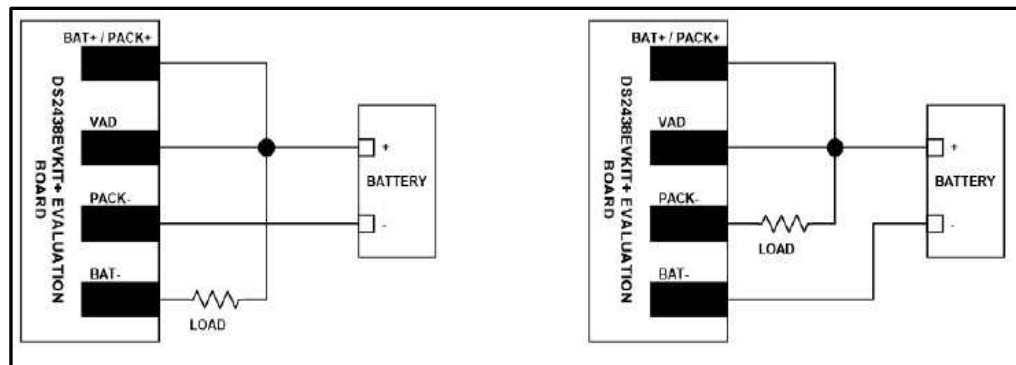
(a) **Charging**   (b) **discharging**

Figure 71 Connections to simulate the charging and discharging phase of the battery

However, the maximum voltage that can be measured by this evaluation kit is 10V and the lead acid battery is rated at 12V. Therefore, a voltage divider circuit is made to reduce the lead acid battery voltage by half. Two 500 Ω resistor is used for the voltage divider.

3. Supercapacitor Time Response

The Supercapacitor Response Time is the most important performance measure in this project. As mentioned earlier, the replaceability of the hardware DC/DC converter with the software approach lies in the successfulness of supercapacitor to response corresponding to the peak load demand. In the hardware approach, the switching action of the DC/DC converter is in a matter of milliseconds. Hence it has good time response but with the tradeoff of having more expensive power electronics which added to the cost of the overall system. In the software approach, the time required for the control includes the load current data acquisition time, storage banks voltage monitoring time,

processing time and control switches responding time which are reflected in the supercapacitor response towards the peak load demand. The previous sequential based programming shows a delay of 70ms which will not meet the requirement in rapid burst load application. Hence, the adoption of SVR to predict the load current will give a buffer time for the SVMR-EMS to compensate the control time required; allowing the supercapacitor to be switched ON before the peak load demand occurs. Since the battery will be turned OFF when supercapacitor is ON, the load current will be supplied only from the supercapacitor. Hence, to measure the response, the voltage supplied by supercapacitor and the load current will be probed on the oscilloscope to measure the difference between the supercapacitor turn ON time and the Peak Load demand occurrence time. In Figure 72, the supercapacitor response time is shown.
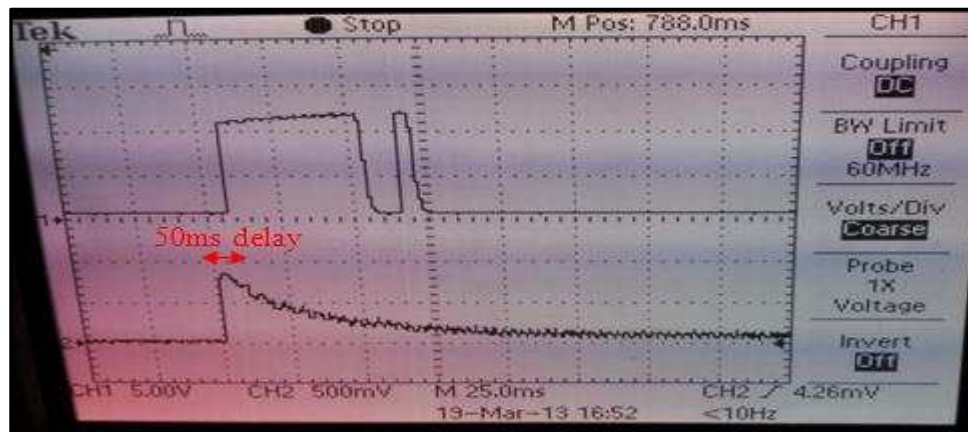
Figure 72 Supercapacitor Respond Time

4. Power Efficiency

Besides comparing the supercapacitor time response of the SVMR-EMS, the power efficiency between the hardware DC/DC converter approach and the

software approach are also compared. The power efficiency is defined as the ratio of the power delivered to the load over the input power as follows [284]:

$$\eta = 100\% \cdot P_{out} / P_{in}$$
Equation 65

where P_{out} is the output power and P_{in} is the input power.

As mentioned in the literature review section, the hardware approach's switch mode DC/DC converter has efficiency range of 75-98%. while; the software approach has voltage drop across the diode, current sensing resistor and the power losses associated with stray resistance in the circuit, hence the power supplied that actually reaches the load has to be measured in both cases to form a comparison. On the other hand, the software approach's Software Control Board has MOSFET switches and backflow protection diode and a 1ohm current sensing resistor. The MOSFET has resistive element and conduction losses is proportional to its on resistance $R_{DS\ (ON)}$, the current sensing resistor causes a voltage divide drop, and the diode has a 0.6V forward voltage drop. Besides, both approaches exhibit power losses which associates with the non-idealities such as stray resistances which has also contributed to the overall efficiency drop. As the load current is either supplied by the supercapacitor or battery, the load terminal voltage alone will determine the efficiency of the system.

5. System Cost

The system cost is one of the performance metrics for comparison between hardware and software appraoch energy management system (EMS).

As this project seeks the feasibility of software approach to replace the costly power electronics in the hardware approach, the cost of both system will have to be compared to justify the use of software approach in the EMS. The unit to measure the system cost of two different aprroaches used for the prototype system is in Malaysia Ringgit (RM).

Last but not least, cost of supercapaitor-battery hybrid energy storage system and battery individual system are compared. The system cost reduction resulting from minimizing the number of replacement battery for 20-years are shown in Chapter 4.

3.4.2 Summary

- This methodology step is a final integration and testing step. This step shows the feasibility and reliability of the implemented SB-HESS.

- In this section, five performance measures are used to measure the accuracy of load prediction system, the system cost, the state-of-charge (SOC) battery for of SB-HESS and battery-alone system, time response of the supercapacitor to react peak power and power efficiency of the systems.

CHAPTER 4

RESULT AND DISCUSSION

This chapter tabulates results that address the problem statements and principal aim stated in Chapter 1. The purpose of this chapter is to discuss the result obtained from the implementation steps shown in Chapter 3. The section is organized as follows:

- Section 1: presents the optimal operation parameters for the supercapacitor-battery hybrid energy storage system (SB-HESS) and how this SB-HESS benefits the battery lifespan.

- Section 2: The design and simulation for RES is presented using HOMER. HOMER is used to that our GA is working properly by comparing results between HOMER and the GA for battery-only system. The optimal cost of SB-HESS is presented and compared with the conventional renewable energy system (RES) using a genetic algorithm (GA). GA is used to design the prototype before it is implemented. There is trade-off between the system cost and the Loss of Power Supply Probability (LPSP). Simulation results show that if the LPSP is 100%, the system cost is higher than the system with 98% LPSP. GA acts as a searching algorithm is capable to search the optimised number of components used in the system at the lowest cost whish subject to constraints and the desired LPSP. GA optimises battery lifespan and evidently, the system cost.

- Section 3: discusses the energy control system for SB-HESS using the Support Vector Machine (SVM) and how this implemented system benefit the system cost (prolongs battery life and reduces number of power electronics) and system reliability (predict time to turn on supercapacitor before power peak delivery is needed). The system cost is said to be optimised where the system cost for the SB-HESS prototype is compared with the conventional system which energy flow is controlled by DC/DC converter. The results shows that the system cost is lower than the conventional system. This is because the implemented energy management system using SVM and relay switches successfully control the energy flow between the energy storage system and load while further optimises (reduces) the number of costly power electronics used. This section also shows the comparison of state-of-charge (SOC) of battery in both battery individual system and SB-HESS.

- Section 4: Shows the result on the performance of the supercapacitor fabricated in the supercapacitor pilot plant in terms of capacitance and equivalent series resistance (ESR). The implemented optimization technique combining Genetic Algorithm within Taguchi Signal-to-Noise ratio is proven in designing a robust process.

4.1 Determination of Optimal Parameter for Energy Management System

This section presents the result of optimal parameter for designing the energy management system (EMS) for this project. These parameters also identify the benefits of coupling supercapacitor with battery in a energy storage system. One of the crucial parameters in this energy management system is voltage level of battery. This value is always kept at a nominal value according to the depth-of-discharge (DOD) that it favors. This is done to ensure the implemented hybrid energy storage system (HESS) aids in prolonging the battery lifespan by limiting the voltage of batteries and hence, the system is setting an optimal set point for the SOC batteries. In a battery-alone system, the batteries are stored and drained to release energy to match the load demand at a short period. The conventional battery-alone system can be costly as compared with the SB-HESS. The main focus in SB-HESS is the delivery power peak by supercapacitors while the battery releases energy in a desired time and in a controlled manner. This implemented system is practical because the supercapacitor delivers power 99% accurately as this energy management system also predicts load beforehand as mentioned in Section 3.2.3. The price of battery is much higher than supercapacitor terms of kW/$ as supercapacitor has higher power density.

Therefore, an optimal voltage value is important for the implemented EMS to evaluate the depth to which a battery can safely be depleted. To further protect the battery from over-discharging, this implemented EMS prevents operation beyond the specified end-of-discharge voltage, which is obtained from the manufacturer data sheet. The end-of-discharge for a 1.2Ah battery is

1.75V/cell. This approach has been proven in Section 4.4 that it reduces the rate of damage mechanism of battery as mentioned in Section 3.1.

A high load current lowers the battery voltage, and the end-of-discharge voltage threshold should be set lower accordingly to cater that particular power peak in a conventional battery-alone system. However, in SB-HESS, a desired battery voltage which has been calculated is always above the final discharge value given in manufacturer data sheet. The battery in SB-HESS discharges at a nominal value of current for a prolonged time, it evidently causes less impact on the rate of damage mechanism of the battery. The strategy applied also ensures the battery always discharge at a constant optimal C-rate (according to technical manual of GP battery) to supply load and the battery final discharge voltage is not bounded by zero volts at any time. C-rates means charge and discharge rate of the battery. In this project, discharging phase is focused.

In SB-HESS, a higher and desired end-of-discharge voltage of batteries is maintained. This tells us that the voltage of the so-called healthier battery gradually recovers and rises towards the nominal voltage repeatedly. However, in long run, battery in a conventional battery alone system becomes aging more rapid and this aging battery with elevated self-discharge cannot recover the voltage. Battery used in our lab-scale prototype system is shown below:

Table 36 Data Specification of Battery

Manufacturer	GP Lead
Capacity	1.2Ah
Nominal Voltage	12
Final discharge Voltage	1.75

The result shows in Table 36 is calculated using the semi-empirical Equation 4 shown in Section 3.1, it shows that battery current (I_{batt}), voltage of

the cell (V_{cell}) and voltage of the battery (V_{batt}) is always below 1.6Amps, 2.07V and 12.41V respectively for the implemented EMS. This provides a clear view for designing the optimised prototype system where how much battery capacity can be used for delivering to the load and how many supercapacitors are required for delivering the power peak. Moreover, it also provides the important parameter to implement energy control management system for the load predictive software to predicts when the supercapacitor is switched on and cater for the peak power. Table 37 below shows the calculated and optimal parameters for supercapacitor-battery hybrid energy storage system.

Table 37 Theoretical values for parameter I_{batt}, V_{cell}, V_{bat}

Parameters	Battery individual energy storage system	Supercapacitor-Battery hybrid energy storage system
I_{batt} (A)	2.5	1.6
V_{cell} (V)	1.99	2.07
V_{batt} (V)	11.99	12.41

From the result above, it can be represented in the diagram shown below. Different level of current for battery-only system and SB-HESS are used to implement the prototype.

Battery-individual system	Implemented HESS
▢ = **supplied by the Batteries.**	▢ = **supplied by batteries,** ▢ = **supplied by supercapacitors**.
'C' for a 1.2 Ah battery, for example, is 1 – 1.2 amps. Full discharge is reached after about 30 minutes when the battery voltage drops to 1.5V/cell. At this point, only 50% of rated capacity has been discharged (1 C amps x 0.5 hrs = 0.5C Amp. Hrs). Continuing the discharge to zero volts will bring to the total amount of discharged ampere-hours (capacity) to approximately 75% because the rapidly declining voltage quickly reduces current flow to a trickle.	'C' for a 1.2 AH battery, for example, is 0.3 amps. Full discharge continuing discharge the battery (to zero volts) on the battery is never happened as the supercapacitor acts as a high power density energy storage device to cater the power bursts. Battery voltage remains at about 2V/cell. At this point, only 20% of rated capacity has been discharged (0.25 C amps x 0.5 Hrs. = 0.125C Amp. Hrs.).

Figure 73 Energy flow for battery-only and SB-HESS

The diagrams in Figure 73 above shows two different cases. From the diagram, the C-rate is different for two cases shown above because the required battery capacity for both cases is different. This also implies that the battery DOD for both cases is different as more battery capacity is used up in Case 1 to deliver the peak power in short period. By considering a same load profile, batteries in battery-individual system are delivering the power peak and the battery is drained to release energy over a short period of time. As mentioned

previously, a high load current lowers the battery voltage, and the end-of-discharge voltage threshold should be set lower accordingly to cater the power peak. The battery discharges to a lower load current as the supercapacitor delivers power peak for the same high load current. It does not damage supercapacitor, as it is known as an ideal energy storage that undergoes frequent charge and discharge cycles at high current and short duration. This is due to the nature of supercapacitor that stores energy by means of a static charge as opposed to an electrochemical reaction.

This shortens battery life when the batteries are stressed and drained to supply the entire power bust of the load demand profile over a short period of time (for battery single energy storage system). For a higher discharge rate (1C-rate) (Case 1), it causes a hard and irreversible of sulphation. When the battery is not operated at a high discharge rate and the battery remains at a low state-of-charge (SOC) for a long period of time, the sulphate crystals grow in size and large sulphate crystals are created. Since these large crystals do not dissolve easily when the battery is charged, this eventually leads to hard or irreversible sulphation [32]. Evidently, it causes a loss of battery capacity because the sulphated part of the active material is no longer active and the large sulphate crystals grow into part of the insulated active material from the terminal electrode. Furthermore, the sulphate crystals have a larger volume than PbO_2 (and Pb), which causes a higher mechanical stress on the electrodes. This sulphate crystal causes inhomogeneous current distribution. The longer time at low SOC accelerates the hard and irreversible sulphation of battery.

Result in this section identifies the optimal parameter to design the EMS for this project. A comparison for the implemented system is presented in

Section 4.4. Table 102 shows the remaining state-of-charge (SOC) of a battery individual system and the supercapacitor-battery hybrid energy storage system after running on a same load profile for every 20 cycles. The remaining capacity of battery (indication of SOC) drops more in a battery single energy storage system compare with the SB-HES.

4.1.1 Summary

- The high load current for an instantaneous power delivery elevates the discharge rate and current of the battery. This damages battery more rapidly.

- Supercapacitor in SB-HESS delivers instantaneous power. It aids in prolonging battery lifespan by catering for the peak power.

- A higher end-of-discharge voltage for battery is guaranteed in SB-HESS. The calculated value is 12.07V and it is used in designing the EMS for this project.

4.2 Cost Structure of Renewable Energy System

Current cost structure for renewable energy system (RES) is simulated using HOMER and Genetic Algorithm (GA). The optimization results are presented in Section 4.2.1 and 4.2.2 respectively. Both methods are able to show the optimised cost of the PV-Wind-Battery and PV-Battery system. Simulation process models a particular system configuration; the optimization process determines the best possible system configuration. Due to the limitation of HOMER of adding supercapacitor as energy storage device, GA fitness functions were constructed to optimise the supercapacitor-battery hybrid energy storage system (SB-HESS). System cost of the supercapacitor-battery hybrid energy storage system in RES is lower than the battery alone RES. RES is also optimised subject to the desired loss of power supply probability (LPSP) and capacity shortage. The higher the capacity shortage, the lower the system cost. The result is shown in the section below.

Furthermore, the SB-HESS embraces the green technology by reducing the total number of batteries used throughout the lifespan of the system. Implemented energy control system using unsupervised learning machine, SVM for supercapacitor-battery hybrid energy storage system (SB-HESS) is also proven to further reduce the overall system cost and increase the power reliability of the system in Section 4.2.3.

4.2.1 Optimal Sizing of RES using HOMER

The optimum sizes of the system that meet the load profiles at the proposed site, given conditions of renewable energy resources and based on components data sheet were simulated using HOMER. HOMER provides the results in terms of optimization and sensitivity analysis. These results a component size (optimization and a sensitivity analysis) for three cases (Case 1: capacity shortage of 0%, Case 2: capacity shortage of 1% and Case 3: capacity shortage of 2%) are presented in section below. These three cases for this simulation is based on the fact that in the Tenth Malaysia Plan (2011-2015), Malaysia government emphasizes greatly on improving energy efficiency, sustainability achieved through energy efficiency [285]. Therefore, a zero downtime of power system (Case 1) is suggested in this study. This also means the 0% LPSP, one optimal set of configuration of a hybrid energy storage system can technically guaranteed the required reliability of power supply. As mentioned in [161], for a stand-alone system simulation, capacity shortage is often set up to a maximum of 2% as shown in [239] study for an allowable unmet load hour. Hence, for case 2 and 3 in this project are suggested because 1% and 2% shortage of power supply is considered low impact on the downtime (power reliability of system) as mentioned in [239]. This also implies that the capacity shortage percentage recommended in [239], blackouts is still possible but for a very small percentage of the time [225].

Case 1: PV-wind-battery with capacity shortage of 0%

This system is designed and constraint for a 0% capacity shortage. A capacity shortage is practically zero means there is no shortfall at any time between the required and the actual operating capacity.

1. Optimization Result

In HOMER, the best possible (optimal) system configuration is the one that satisfies the user-specified constraints at the lowest total net present cost. Finding the optimal system configuration involves deciding on the combination of components that the system should contain, the size or quantity of each component. In the optimization process, HOMER simulates many different system configurations, discards the infeasible ones (those that do not satisfy the user-specified constraints), ranks the feasible ones according to total net present cost, and presents the feasible one with the lowest total net present cost as the optimal system configuration.

Figure 74 shows the design of the battery alone system with PV panel and wind generator, which was simulated in HOMER. Primary Load 1 represents the load demand with 50% of discrepancy of the simulated load, Converter represents the DC/DC converter, PV represents the photovoltaic panels of the system, Generic 1kW represents the wind turbines and H200 represents the batteries used. A feasible system is defined as a hybrid system configuration that is capable of meeting the load.
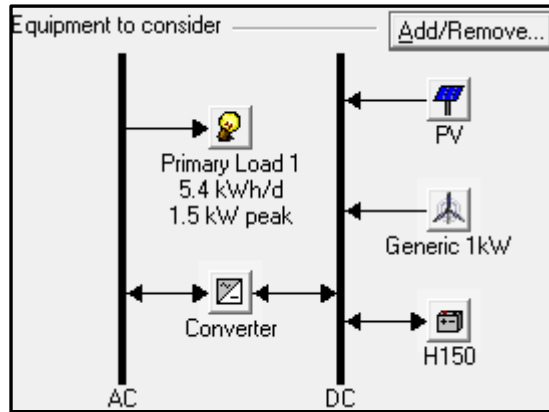
Figure 74 Block diagram of PV-wind-battery energy system
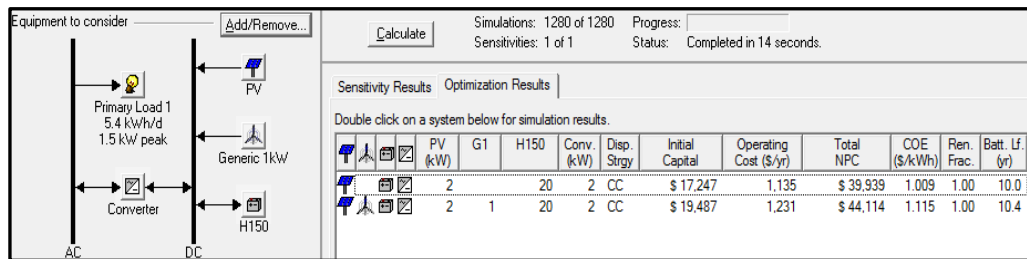
Figure 75 Optimization result for PV-wind-battery system (0% of capacity shortage)

The optimization result for the RES shown in Figure 74 is tabulated in Figure 75. From the optimization result shown above, the global solar radiation is 5.4kWh/m^2/day. This annual mean value is taken at the site shown in Section 3.2 – Semenyih, which is 4.12kW. Generally, optimization result shows feasible and optimised system. In Figure 75, it shows two RESs, one is PV-Wind-Battery system and one is PV-Battery system. The terms show in the figure above can be explained as follows:

Table 38 Indication for Optimization result in Figure 75

Column Shown in Figure 75	Indication
First column	Presence of PV panels
Second column	Presence of wind generators
Third Column	Presence of battery storage
Forth Column	Presence of converter

Fifth Column	Size of the PV array in kW
Sixth Column	Number of the wind generator
Seventh Column	Number of the batteries utilized
Eighth Column	Size of the converter in kW
Ninth Column	Dispatch Strategy
Tenth Column	Initial cost of the System
Eleventh Column	Operating Cost per year
Twelfth Column	Total net present cost
Fourteenth Column	Cost of Electricity ($/kW)
Fifteenth Column	Renewable Energy Fraction
Sixteenth Column	Battery lifespan in terms of years.

The project lifetime is 20 years, which follows the lifespan of the PV panel. Based on the optimization result, the PV-wind-battery power system comprised of 2kW PV array, 1 wind generator, total of 20 batteries used in addition to 2kW converter is found to be the most optimal and feasible system with a total minimum net of present cost (NPC) of $44,114 in the entire cycle life of the system. The optimization result is simulated according to the data input on the specification of the components, which is presented in Section 3.2.1. Renewable energy fraction (Ren. Frac.) shown in the fifteenth column in Figure above is renewable fraction of the system which is based on the amount of the renewable energy that supplies goes towards serving the primary load. The renewable fraction is 1.00, which means there is no diesel generator used in the system. This means there is no gas emission from the system, such as carbon dioxide, carbon monoxide, unburned hydrocarbon, sulphur dioxide and nitrogen oxide.

The dispatch strategy used is cycle-charging strategy. HOMER offers two dispatch strategies, which are called load-following and cycle-charging. Under the load-following strategy, a generator produces only enough power to serve the load, and does not charge the battery bank. Under the cycle-charging strategy, whenever a generator operates, it runs at its maximum rated capacity (or as close as possible without incurring excess electricity) and charges the battery bank with the excess. Barley and Winn [166] found that over a wide range of conditions, the better of these two simple strategies is virtually as cost-effective as the ideal predictive strategy that is how the idea is inspired by adding a supervisory machine learning system to control the energy flow in our renewable energy system). Because HOMER treats the dispatch strategy as a decision variable, the modeler can easily simulate both strategies to determine which is optimal in a given situation [14].

This means that under cycle-charging strategy used in this study, the system runs at full power and charge the battery with any excess. With the cycle charging strategy you can apply a setpoint state-of-charge, so that the energy sources or generators keep charging the battery and the battery is not allowed to discharge until it has reached the setpoint. This strategy is appropriate to use for this project because the implemented load predictive energy management system control the flow of energy from battery state-of-charge.

COE is the cost of the electricity. For the simulated PV-wind-battery system, the COE is $1.115/kWh. This is lower than systems with diesel generator, for example in [228], the COE is much higher ($25.41). This is because the use of diesel fuel is expensive and the price of fuel is increasing

over the years. In this site location, the solar irradiance is optimum for solar

energy system.
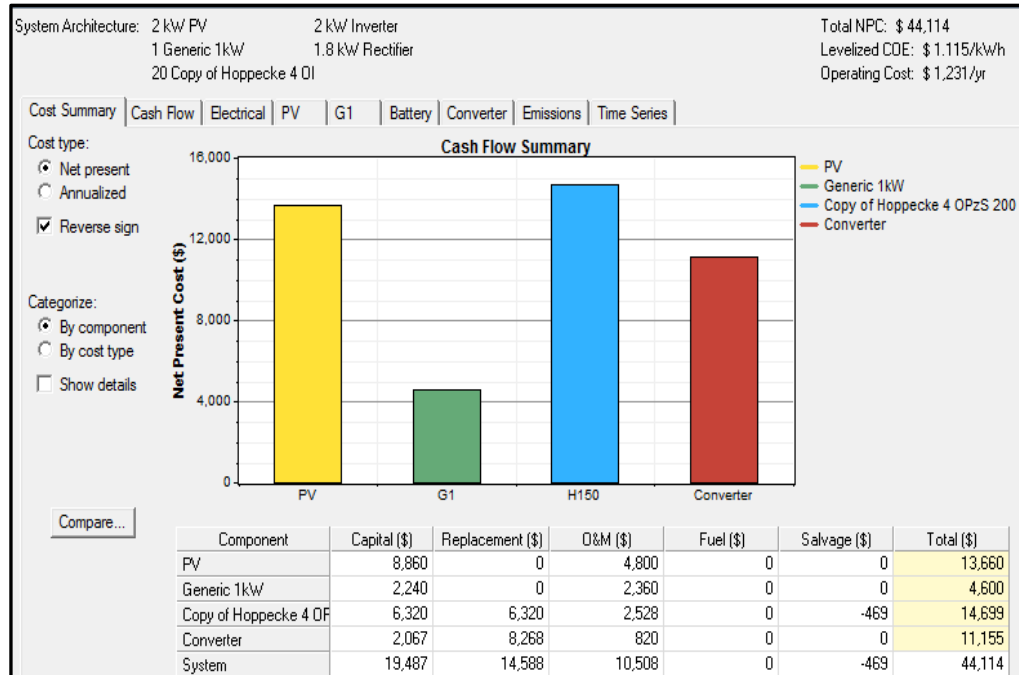
Figure 76 Cash Flow Summary of PV-Wind-Battery System

Figure 76 depicts the cash flow summary of the system. From the plot,

total cost of the battery (H150 in the plot) which combines initial capital

cost, replacement cost, operational and maintenance (O&M) cost gives the

highest impact in the overall cost of system.
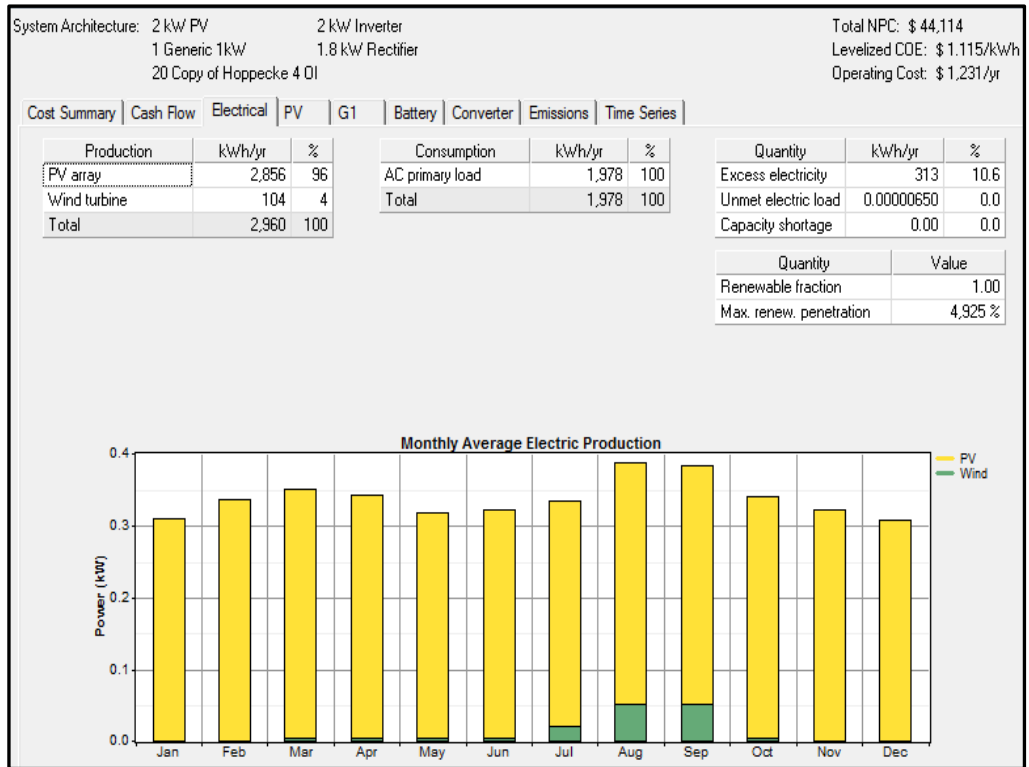
Figure 77 Electrical power for PV-wind-battery system (capacity shortage 0%)

Figure 77 depicts the excess electricity, unmet load, capacity shortage and renewable fraction for the most economically feasible system. It can be seen from Figure 77 that with the above system configuration, unmet load is 0 kWh and an excess energy of about 10.6% is generated. It should be mentioned here that this excess energy produced goes to waste due to lack of demand. This figure also summarizes that the monthly average PV generated power is much higher as compared to wind energy for this selected site as the velocity wind at this selected site is low. However, the solar irradiance is high to provide 96% of the renewable energy to the system.

2. Sensitivity Analysis

Sensitivity analysis helps assess the effects of uncertainty or changes in the variables over which the designer has no control, such as the average wind

speed or the future fuel price. In this case, fuel price is not considered. One of the primary uses of sensitivity analysis is in dealing with uncertainty and evaluates trade-off in capacity shortage, capital cost, maintenance cost, operational cost and replacement cost.
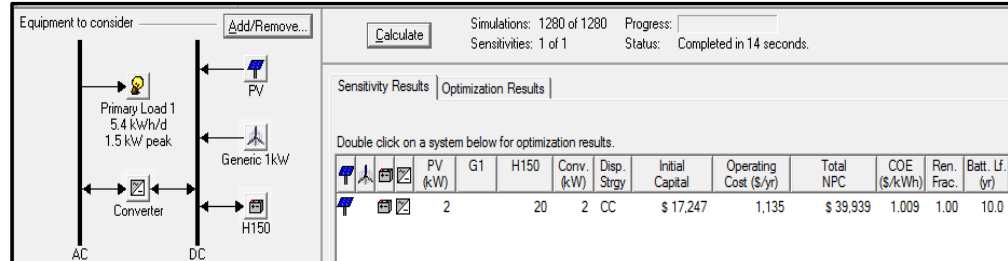
Figure 78 Sensitivity results for PV-wind-battery system (capacity shortage of 0%)

According to the simulation result, it tells us that the system without wind turbine is more favourable as the wind velocity is low in the selected site. It is not cost-effective in adding wind turbine to the system at this site. The COE is lower than the PV-wind-battery system, $1.009/kWh. The net present cost is $39939 as shown in the Figure 78. The figure below shows zero unmet electrical load and zero capacity shortage for this system.
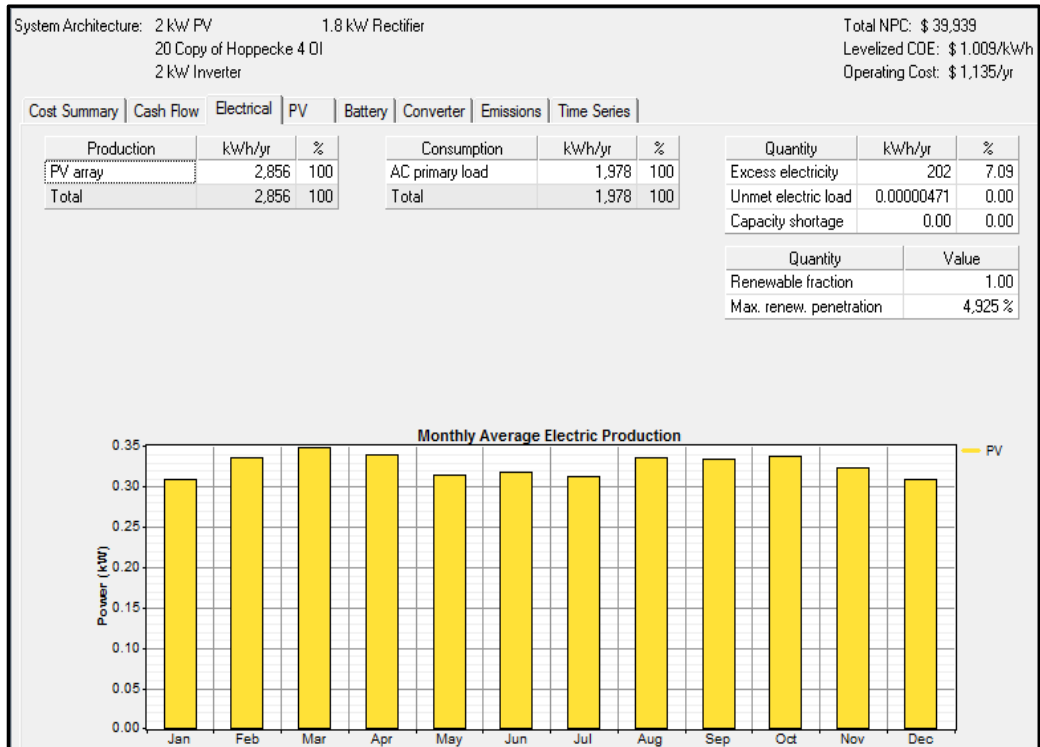
Figure 79 Electrical power for PV-battery system (capacity shortage of 0%)
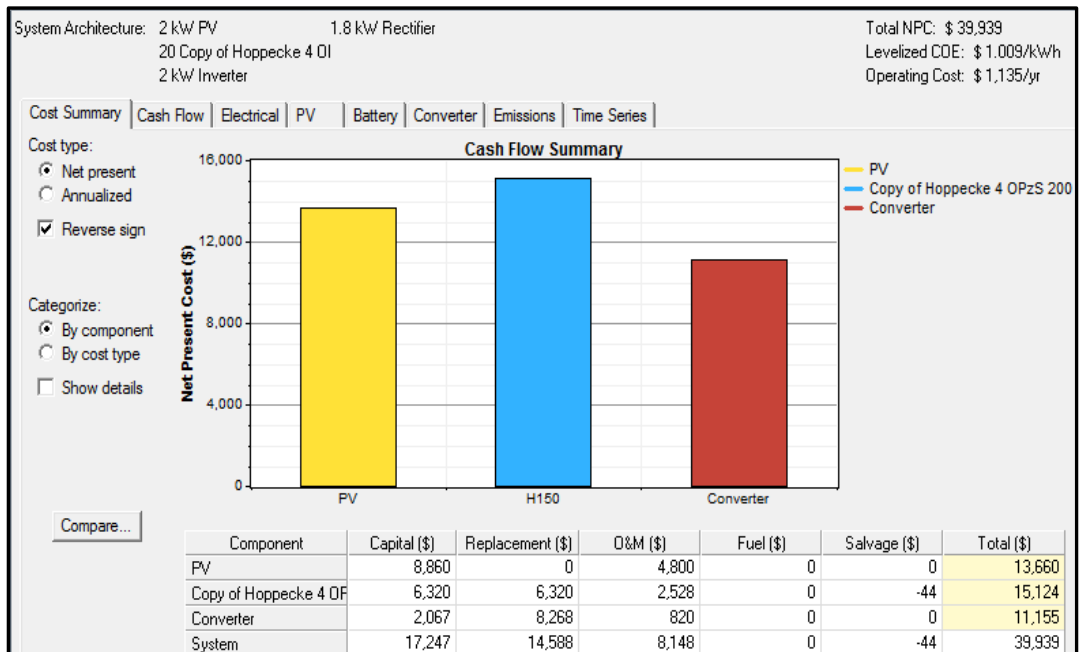
Figure 80 Cash flow summary for PV-battery system (capacity shortage of 0%)

From the figure above, overall cost of battery is still the highest among the other components even wind generator is not included in this system. This means that operating reserve (in this case is battery only) is large enough and always available for the system. Hence, there is no unmet load throughout the years.

Case 2: PV-wind-battery with capacity shortage of 1%

This system is designed and constraint for a 1% capacity shortage. The capacity shortage fraction (C.S.F) is the fraction of the total load plus operating reserve that system fails to supply. If a system is ever unable to supply the required amount of load plus operating reserve, HOMER records the shortfall as capacity shortage. Operating reserve is the surplus electrical generation capacity (above that required to meet the current electric load) that is operating and able to respond instantly to a sudden increase in the electric load or a sudden decrease in the renewable power output. For this case study, the C.S.F was taken equal to 1%.

1. **Optimization**
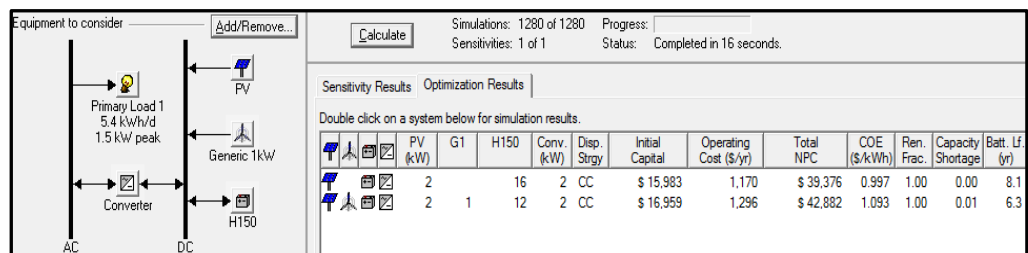
Figure 81 Optimization result for PV-wind-battery system (1% of capacity shortage)

Generally, the indication on the columns is same as those mentioned in Table 38. From the simulation result for this case, the NPC is $42882. The

total NPC is slightly lower as there is a shortfall that occurs between the required amount of operating capacity load plus required (operating reserve) and the actual operating capacity the system can provide. The number of batteries used is less compared to Case 1. Operating reserve is the amount of operating reserve that a power system provides is equal to the operating capacity minus the electrical load. Operating reserve is surplus electrical generating capacity that is operating and responds instantly to a sudden increase in the electric load or a sudden decrease in the renewable power output. This means operating reserve is the fraction of the primary load that hour, plus a fraction of the annual peak primary load, plus a fraction of the PV power output that hour, plus a fraction of the wind power output that hour. In this case, operating reserve is obviously lower than the previous case as the capacity shortage is 1%. A high operating reserve increases the unnecessary system cost with oversized system.

The battery lifespan is shorter in case 2 as compared to case 1. The expected battery lifetime is 10 years in case 1, whereas in case 2 (with capacity shortage of 1%), the expected battery lifetime is 6 years only. This causes higher battery replacement cost.
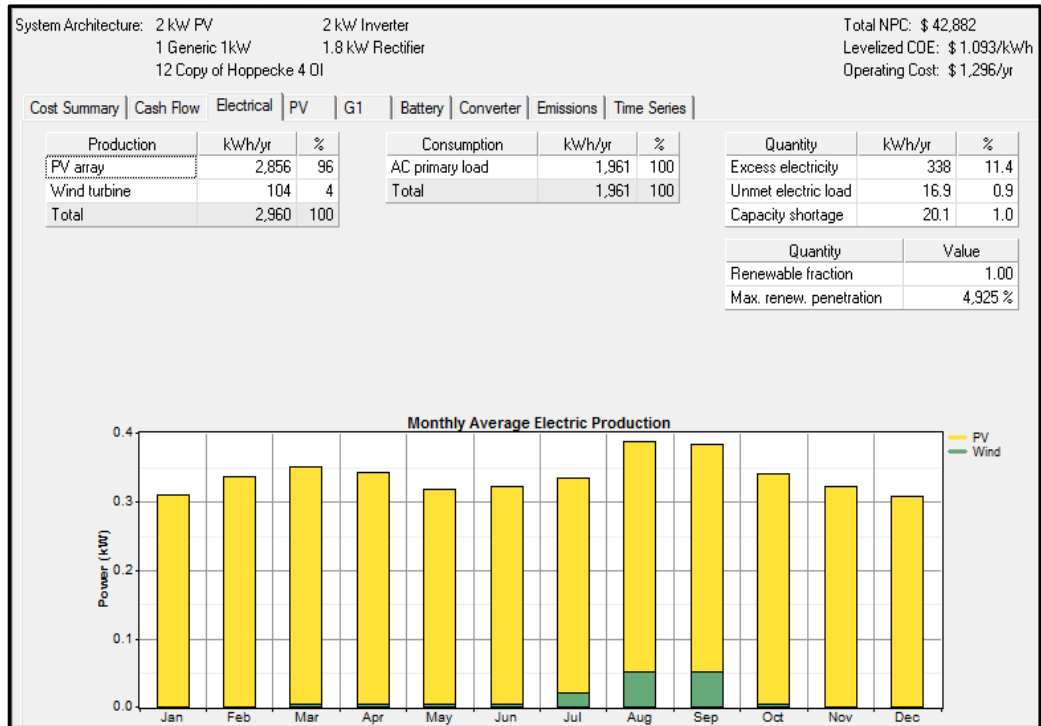
Figure 82 Electrical power for PV-wind-battery system (capacity shortage of 1%)

The unmet electric load is 1% as initially the capacity shortage was set to 1%. The difference between case 1 and case 2 is the COE and operating cost. The COE is lower in case 2. However, the operating cost in case 2 is high as mentioned earlier, the high number of replacement battery causes high replacement cost and O&M cost. This can be optimised using a load predictive energy control management system and adding high power density and less maintenance energy storage devices, such as supercapacitor.
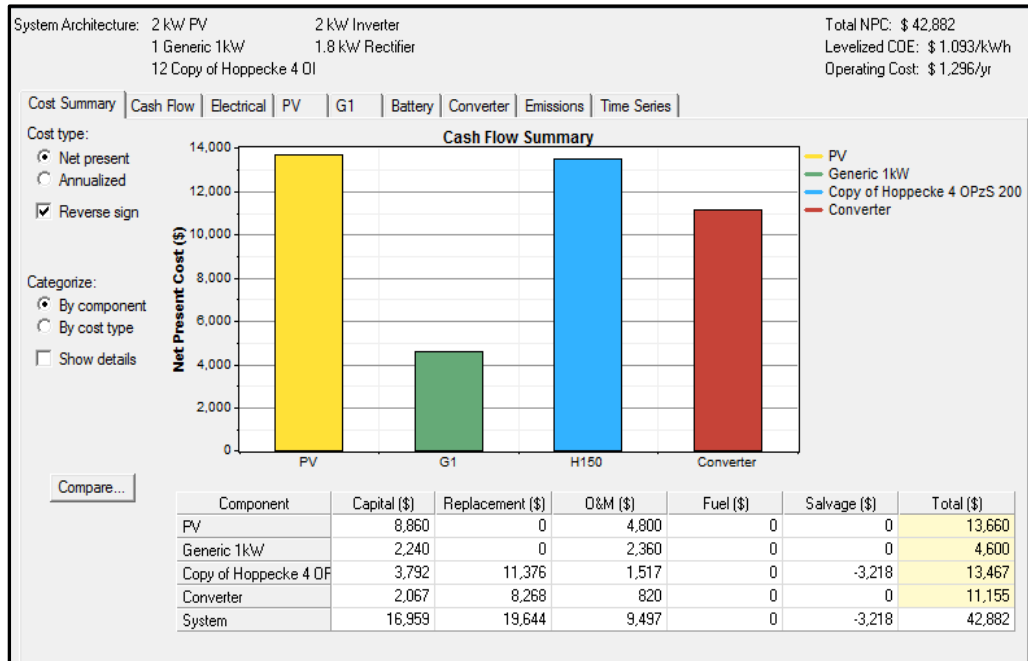
Figure 83 Cash flow summary of PV-wind-battery system with capacity shortage of 1%

The initial cost of the batteries is less compare to the system in case 1. This is because less number of batteries are considered in this case as the operating reserve is lower with the capacity of shortage is set to 1%. However, the battery lifespan is evidently short compare to the first case where the number of battery used is 20 for the initial instalment of the system. The initial set of the batteries are drained as low operating reserve is designed and set. This also leads to high replacement cost and O&M cost of the battery throughout the 20 years.

2. Sensitivity analysis
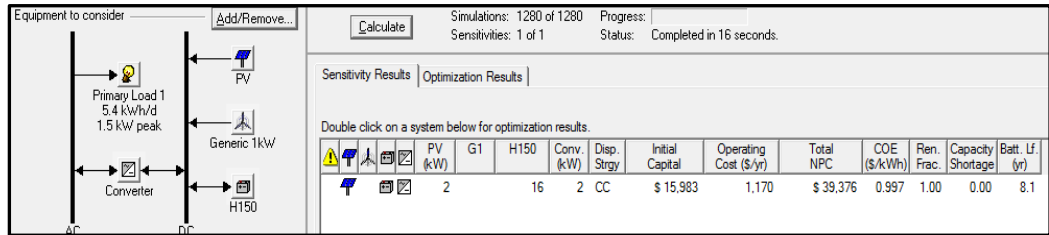
Figure 84 Sensitivity results for PV-wind-battery system (capacity shortage of 1%)

A system without wind turbine in the selected site is more feasible in terms of NPC. The NPC of RES with capacity shortage 1% is lower than the system in Case 1. The NPC is $39376 for this RES model. The unmet load shown in Figure 82 is lower than the PV-wind-battery system (capacity shortage of 1%) in Figure 79.
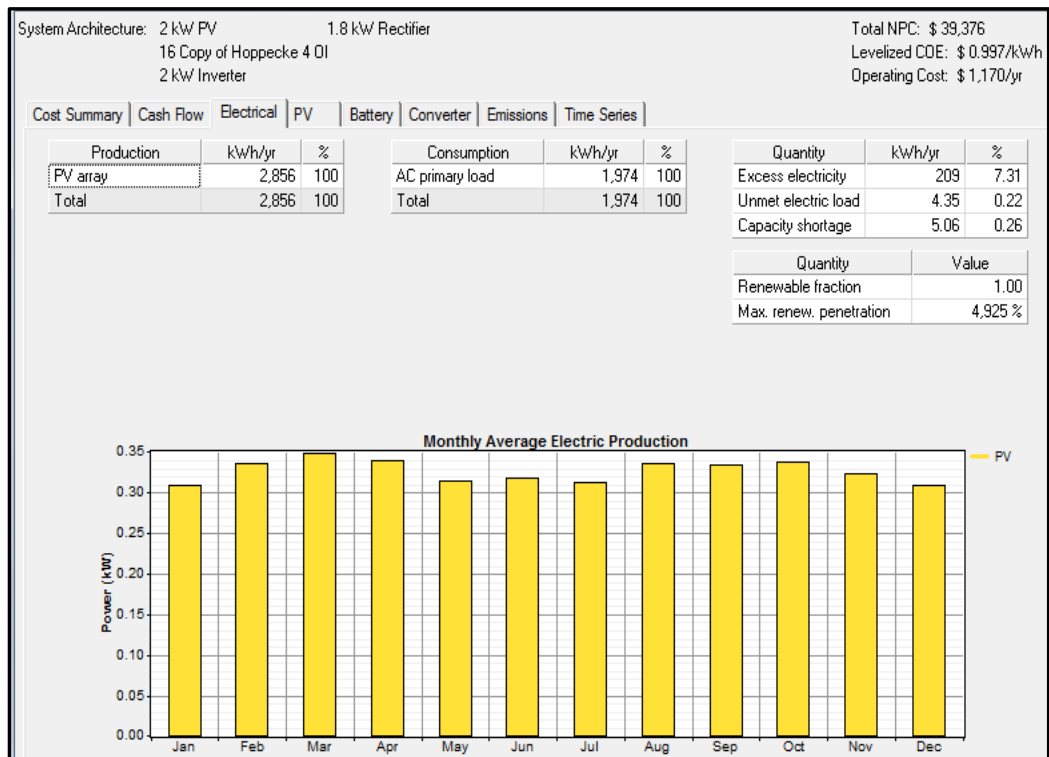
Figure 85 Electrical power for PV-battery system (capacity shortage of 1%)
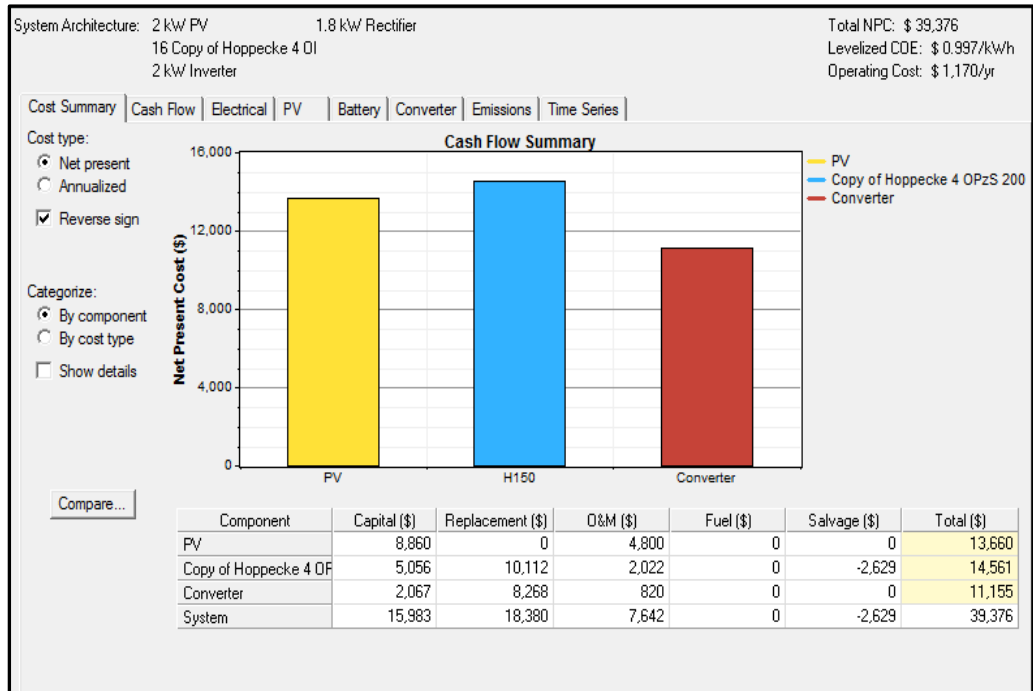
Figure 86 Cash flow summary for PV-battery system (capacity shortage of 1%)

Figure 86 shows the cash flow summary for the PV-battery system (capacity shortage of 1%). By observing Figure 80 and Figure 86, about 37% of the total system cost is caused by the initial, operational and maintenance cost of the batteries.

Case 3: PV-wind-battery with capacity shortage of 2%

Final design, simulation and optimization is done by changing the constraint in HOMER, which represents capacity shortage of 2%. It is clearly shown that PV-battery system has lower system cost (net present cost) compare to the previous cases. On the other hand, PV-wind-battery has the same total system cost as shown in case 2.

1. Optimization
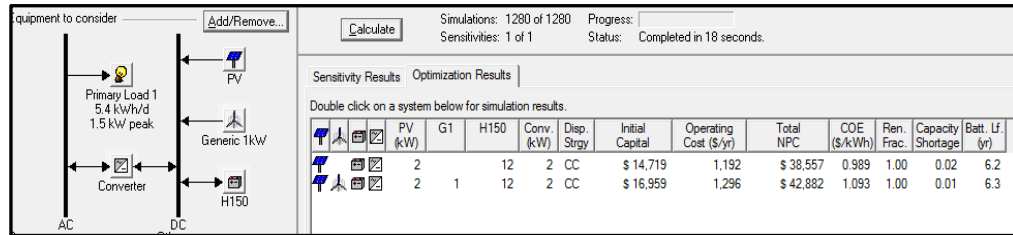
Figure 87 Optimization result for PV-wind-battery system (2% of capacity shortage)

Figure 87 shows the net present cost for PV-wind-battery with (capacity shortage of 2%) is the same as the in case 2 (PV-wind-battery with the capacity shortage of 1%) which is $42882. From the simulation results shown in Figure 88, it tells us that the insignificant unmet load (also known as capacity shortage) for this proposed power system has no impact on the system cost. This means that to allow a smaller, less expensive power system, the proposed system with capacity shortage of 2% is not feasible and cost-effective to increase the operating reserve(number of battery) to satisfy the unmet load.
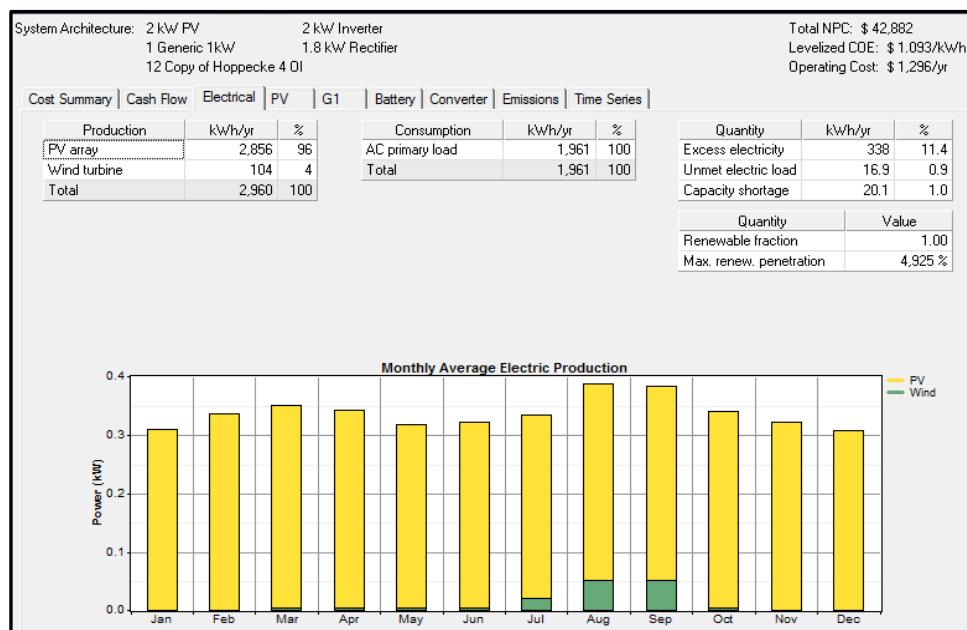
Figure 88 Electrical power for PV-wind-battery system (capacity shortage of 2%)

Based on the Figure 89 below, the initial cost of the battery is lower as compared to the initial cost for battery in case 1. However, the replacement cost of the battery is much higher in case 2 and case 3. This is due to the higher usable capacity of battery in case 2 and case 3. Hence, the expected lifetime of battery is shorter. This also means that the number of replacement batteries is higher in this case.
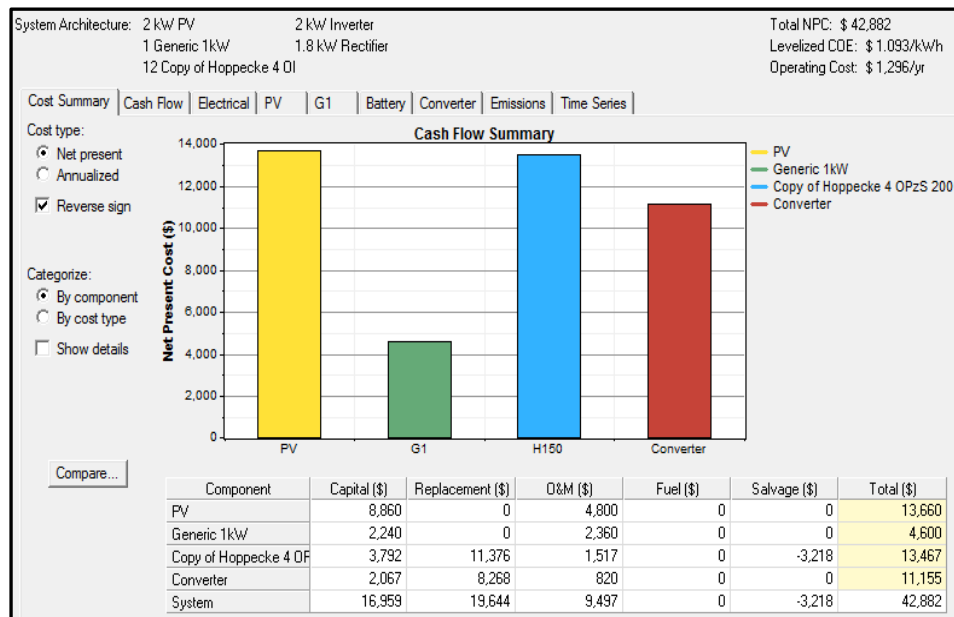
Figure 89 Cash flow summary for PV-wind-battery system (capacity shortage of 2%)

2. Sensitivity Analysis

Based on the three figures below, the NPC for this system is the lowest compare to the systems in case 1 and case 2. The NPC of this system is $38557. This always depends on the system specification which is designed by the user. It is a trade-off between the price that the user can afford and the power shortage and delivery.
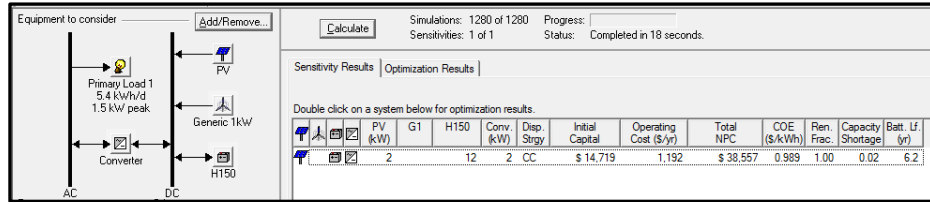
Figure 90 Sensitivity results for PV-battery system (capacity shortage of 2%)
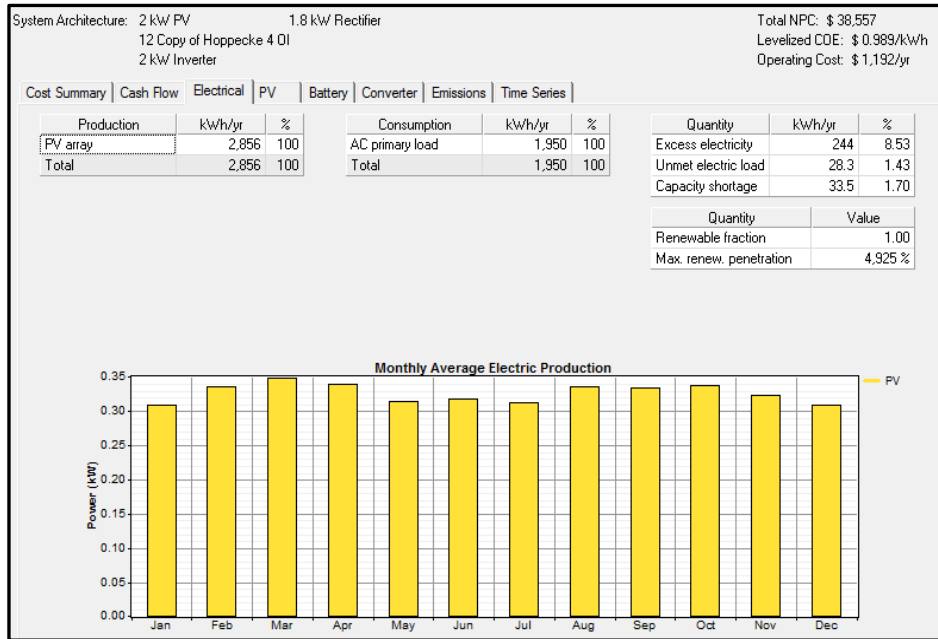
Figure 91 Electrical power for PV-battery system (capacity shortage of 2%)

From Figure 91, the unmet electrical load is approximately 2% which is the constraint input by the user earlier before the simulation.
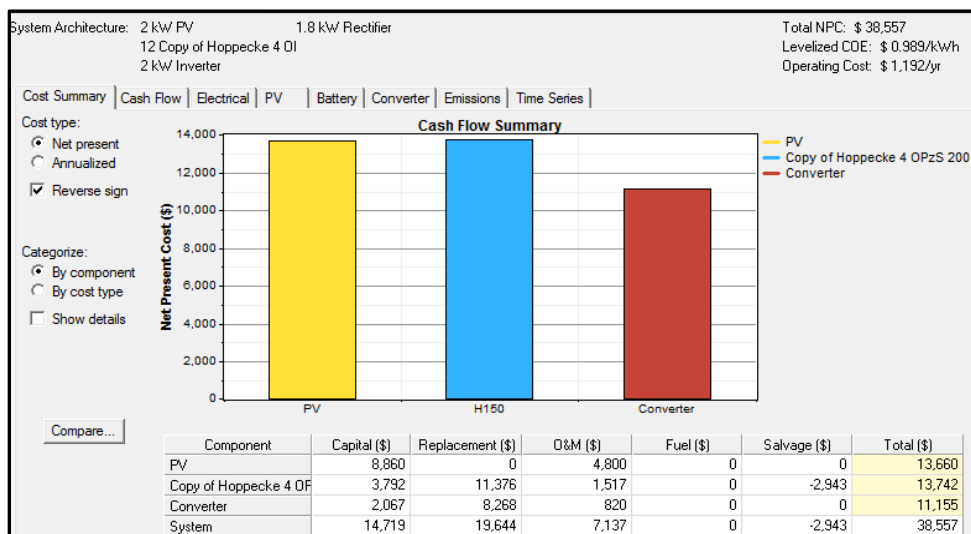
Figure 92 Cash flow summary for PV-battery system (capacity shortage of 2%)

This system is feasible even without wind generator as mentioned earlier; the wind power at this site does not contribute high generated power. Hence, systems is said to be more cost-effective and optimised according to the sensitivity results shown in. with only 1.70% of capacity shortage throughout a year.

4.2.1.1 Summary

- HOMER is a good tool to design, simulate, optimise and sensitively analyse different parameters for power systems. To limit input complexity, and to permit fast enough computation to make optimization and sensitivity analysis practical, HOMER's simulation logic is less detailed than that of several other time-series simulation models for micropower systems, such as Hybrid2, PV-DesignPro, and PV*SOL. On the other hand, HOMER is more detailed than statistical models such as RETScreen, which do not perform time-series simulations. Of all these models, HOMER is the most flexible in terms of the diversity of systems it can simulate.

- From the three cases simulated above, batteries always cause the highest impact in the overall cost for a long-term renewable energy system for this project (20 years is considered).

- The batteries cost mainly are from replacement cost, operational and maintenance cost. This can be optimised by adding a high power density and less maintenance energy storage device, such as supercapacitor. It is mentioned (in the next section). This could improve battery lifespan.

- Table 39 shows the net present cost for three cases mentioned in this section.

Table 39 Net Present Cost of different RES (found by HOMER)

No.	Renewable Energy System	Net Present Cost ($)	Battery Initial Cost ($)	Battery Replacement Cost ($)	Estimated Battery Lifespan (years)
1	PV-wind-battery with 0% capacity shortage	44114	6320	6320	10
2	PV-battery with 0% capacity shortage	39939	6320	6320	10
3	PV-wind-battery with 1% capacity shortage	42882	3792	11376	6.3
4	PV-battery with 1% capacity shortage	39376	5056	10112	8.1
5	PV-wind-battery with 2% capacity shortage	42882	3792	11376	6.3
6	PV-battery with 2% capacity shortage	38557	3792	11376	6.2

4.2.2 Optimal Sizing Renewable Energy System using a Genetic Algorithm (GA)

Homer does not allow the inclusion of supercapacitor within the optimization hence, to have this facility this project uses a GA for optimising the system. In this section, simulation result and discussion on the conventional PV-Wind-Battery and PV-Wind-Battery-Supercapacitor are presented. The optimised cost of the conventional renewable energy systems (RES) obtained using HOMER is compared with the optimised cost of the RES using Genetic Algorithm constraint optimization in this section. The cost of a RES with supercapacitor-battery hybrid energy storage system is lower than the conventional RES with battery only system. GA simulation result shows that supercapacitor aids in saving cost of the system by prolonging battery life i.e. reducing the cost of the initial number battery as well as the number of replacement battery throughout the project time. In this case, the project time follows the lifespan of a typical PV panel, which is 20 years. Two main simulation results are presented for the systems below:

1. Renewable energy system (RES) with battery,

2. RES with supercapacitor and battery.

4.2.2.1 Renewable energy system (RES) with battery

Constraint optimization using a Genetic Algorithm requires fitness function, which represents the domain in this case: RES (with battery), boundary and constraint which helps to place the objective function (fitness function) in the proper search space that is related to real life conditions in which we wish to optimise the system. In this section, PV-Wind-Battery and

269

PV-Battery for different capacity shortage, i.e. zero load rejection (loss of power probability, LPSP 0), 1% of capacity shortage (LPSP of 0.99) and 2% of capacity shortage (LPSP of 0.98). By applying the Equation 27 and 32, the fitness function, initial boundary and constraint for all the systems are presented as follows:

Table 40 Fitness Function (Equation 27)

Terms	Components	Cost		Lifetime
		Initial	O&M	
1.	$N_{PV} \cdot (C_{PV} + y_p \cdot M_{PV})$	$C_{PV} = \$335$	$M_{PV} = \$6.7$	y_p
2.	$N_{WG} \cdot (C_{WG} + y_p \cdot M_{WG} + h \cdot C_h + y_p \cdot h \cdot C_{hm})$	$C_{WG} = \$2240$ $C_h = \$74$	$M_{WG} = \$44.8$ $C_{hm} = \$1.48$	$y_p = 20$
3.	$N_{BAT} \cdot [C_{BAT} + R \cdot C_{BAT} + y_p - R -1) \cdot M_{BAT}]$	$C_{BAT} = \$316$	$M_{BAT} = \$6.32$	R and y_{batt} (Explained in Equation 28)
4.	$N_{CH} \cdot C_{CH} \cdot y_{CH} + 1) + N_{CH} \cdot M_{CH} \cdot y_p - y_C - 1)$	$C_{CH} = \$108$	$M_{CH} = \$2.16$	$y_{CH} = 4$
5.	$C_{INV} \cdot y_{INV} + 1) + M_{INV} \cdot y_p - y_{INV} - 1)$	$C_{INV} = \$2968$	$M_{INV} = \$41$	$y_{INV} = 4$

Replacement cost is defined as the cost of replacing a component at the end of its useful lifetime. In equation 27, it is clear that the replacement cost is caused by the batteries, charge controller and inverter as the renewable energy sources are optimised based on the project lifetime, y_p.

Boundary

The initial boundary is set to define the border of the search space of our domain. It ensures the optimization takes place in the correct search space. It also means that the optimised parameter obtained from the fitness function is feasible to implement in real life. For this case, boundaries for the parameters in Equation 27 are shown below:

Table 41 Boundary of the Algorithm

No.	Components/Parameters	Boundary
1	Number of PV panel, N_{PV}	$15 < N_{PV} < 30$
2	Number of wind generator, N_{WG}	$1 < N_{WG} < 3$
3	Height of the wind generator, h	$14 < h < 15$
4	Number of batteries, N_{BAT}	$4 < N_{BAT} < 36$
5.	Number of Charge controller, N_{ch}	$N_{ch} < 0$
6.	Number of Inverter, N_{INT}	$N_{INT} < 0$

The initial boundary for the components shown in Table 41 is computed based on the simulated load profile and the specification of the components. Lower bound and upper bound are assigned to each of the parameters. This boundary is important for the GA to search optimal parameters in a feasible search space. A maximum power point tracker (MPPT) is a solid-state device placed between the PV array and the rest of the dc components of the system that decouples the array voltage from that of the rest of the system, and ensures that the array voltage is always equal to the maximum power point. By ignoring the effect of the voltage to which the PV array is exposed, this algorithm effectively assumes that a maximum power point tracker is present in the

system. This means the PV array is outfitted with a maximum power point tracker (MPPT), in which case the output of the array is effectively linear with incident solar radiation, regardless of the DC bus voltage. This means the lower bound of the renewable energy sources are taking by considering the system power specification (for this case, is 2kW RES). The next decision variables is the installation height of the wind generator which highly affects both, the resulting energy production, installation and maintenance cost. The lower bound and upper bound of height of the wind generator is computed based on the data sheet from manufacturer Maglev.

However, battery is modelled by considering the DC bus voltage of the system. For our case, the DC bus voltage is 48V and the nominal voltage for the battery chosen is 12V. This is important to decide the minimum number of batteries the system can have. It is further explained in the next section.

Constraints

As mentioned in section 3.2.2, constraint optimization is important for a real-life situation and application. Constraints are made to locate the requirement on the search space, specifying regions for the space that are infeasible. This is important to solve the fitness function accurately and implement that solution in the feasible situation under consideration.

- **Renewable energy source,**

  By applying Equation 34, constraint of the output power, G, It is defined according to how much the renewable power it can supplies to the DC bus. It is 50% higher of the highest peak power in the simulated load profile. This system is a 2kW RES, hence, $\boldsymbol{G \leq 2kW.}$

272

- **Autonomy, A**

  This constraint is calculated using Equation 35. A decides the number of
  batteries used in system with different capacity shortage which depends
  on the energy control management of the designer. A depends on the
  LPSP value. For system with zero LPSP, $A \leq 24$ and systems with 0.99
  and 0.98 LPSP, , $A \leq 23.$ Depth-of-discharge is crucial in computing this
  constraint which also important to estimate the battery lifetime. The value
  of A for different condition of DOD is shown in Table 42, 45, and 47.

- **DC bus voltage, V_{DC} = 48V**

  DC bus voltage is determined based on the rated voltage of the battery.
  The battery can be sized for voltage and capacity by adding cells in series
  and parallel respectively.

  This is an autonomous system, which contains no diesel generator. It is
also called off-grid power system. An autonomous system must be controlled
carefully to match electrical supply and demand. Energy storage device battery
(in this case) is playing an important role in operating reserve, as diesel
generator is not considered in our case.

  These constraints allows the user to specify the number of hours of
autonomy for battery systems, and this can lead to a big cost impact on a small
system. Batteries are sized in terms of the number of batteries used causes the
day of autonomy for the system. For battery alone system, battery is often sized
to cater the highest peak. This means that the LPSP (capacity shortage) is set by
the designer.

It is difficult to predict battery lifetime. Real battery banks are subjected to all kinds of temperature and operational stresses that affect performance and lifetime in complex ways. Battery banks are complicated and difficult to model accurately. In this approach, battery lifetime is estimated based on the DOD set in the control strategy in the energy management system and the lifetime throughput of the battery life cycle of the battery before the battery fails to supply the amount of energy that cycled through the battery (before failure). This means the final voltage of the battery drops below the end-of-discharge voltage which is stated in the battery data sheet.

As mentioned earlier, the replacement cost of the battery show significant impact on the total cost of the system. R is the number of expected battery replacement throughout the project lifetime. y_{batt} represents the lifetime of the lead-acid battery. It is calculated based on the lifetime curve for a sealed lead acid battery data sheet of the battery. $Q_{lifetime}$, lifetime throughput is the amount of energy that cycled through the battery before failure. It can be calculated by finding the product of the number of cycles, the depth of discharge, the nominal voltage of the battery, and the aforementioned maximum capacity of the battery. Q_{annual} is the annual throughput. It represents the total amount of energy that cycles through the battery bank in one year. Assumption is made to calculate the battery lifetime. This implemented optimization models a single battery as a device capable of storing a certain amount of dc electricity at a fixed round-trip energy efficiency, with limits as to how quickly it can be charged or discharged, how deeply it can be discharged without causing damage, and how much energy can cycle through it before it needs replacement.

This optimization assumes that the properties of the batteries remain constant throughout its lifetime and are not affected by external factors such as temperature. Therefore, the key physical properties of the battery are its nominal voltage, capacity curve, lifetime curve, minimum state of charge, and round-trip efficiency. It estimates the life of the battery bank simply by calculating the amount of energy cycling through it. For the purpose of verifying the implemented GA and the fitness functions are working properly, GA also applied on the same renewable energy systems (including the PV-wind-battery system) which are simulated using HOMER.

Case 1: PV-wind-battery with LPSP = 0

For the case of LPSP = 0, the operating reserve battery (in this case) is always surplus for the load. The autonomy for this system is $A \leq 24 hours$. The operating reserve (battery) is sized according to the battery usable capacity and the highest power peak in the load demand curve. For this study, the power peak in the load profile is supplied by the battery only, P_A which can be found in Equation 35 is 1000W. Battery usable capacity varies slightly due to the different value of DOD.

Table 42 shows that with different DOD, the initial number of batteries used is different. The lower the DOD is used, the more the initial number of batteries is required to match the LPSP which is constraint by autonomy. DOD that is below 0.5 is not feasible in our case as the initial number of batteries to accommodate the autonomy is more than the total number of batteries N_{bat} used throughout the 20 years. The simulation result shows that only battery DOD of 1.0 and 0.9 are feasible as the battery lifetime is within the specification based

on [238]. Battery DOD of 0.9 is an optimal DOD for batteries in this system. The estimated battery lifespan is 10.27 years. The initial number of batteries is 20 and the number of replacement batteries is 20. The string size for battery is 4 batteries and the number of string in parallel is 5.

Table 42 Six cases with different Battery DOD, capital and replacement cost of the battery

	A (hour)	DOD	y_{batt} (year)	No. of battery	No. of replacement battery	Cost of battery ($)	Net Present Cost ($)	No. of cycles	Usable capacity (kWh)
1	28	1	8.03	20	40	21108	49886	350	28.32
2	25	0.9	10.27	20	20	14915	43692	500	25.48
3	27	0.8	12.13	24	24	17898	46675	550	27.19
4	27	0.7	13.50	28	28	20881	49658	600	27.75
5	27	0.6	15.34	32	32	23864	52641	700	27.19
6	25	0.5	20.55	36	36	15698	44476	1000	25.49

Table 42 shows the optimization result for different battery DOD set by the designer. The system with the lowest cost is chosen – system configuration 2. The optimised system architecture is 20 units PV panels with the rated power of 0.1kW, 1 unit of 1kW wind generator, 20 units of (12V, 118Ah) Batteries, 6 units of charge controllers and 1 2kW inverter.

Table below tabulates the cash flow summary of the PV-Wind-Battery (LPSP = 0, battery DOD = 0.9).

Table 43 Cash Flow Summary for the optimised system

Components	Capital Cost ($)	Replacement Cost ($)	O&M cost ($)	Total ($)
PV panels	6700	0	2680	9380
Wind Generator	2240	0	2346.40	4586.40
Batteries	6320	6320	2275.20	14915.20
Charge controller	720	2880	216	3816
Inverter	2067	8268	660	10995
System	18047	17468	8177.60	43692.60

It clearly shows that the cost of the batteries is the highest. In Section 4.2.2-2, initial cost, replacement, operational and maintenance cost of batteries are reduced with the inclusion of supercapacitor in the system. This system is subject to LPSP = 0, which also known as zero load demand rejection system. This also means that GA searches for the combination of components that can serve the electrical load and the required operating reserve (battery) at the lowest cost. Satisfying the load and operating reserve is important. For this capacity shortage of 0%, GA searches any cost to avoid capacity shortage and gives the combination of components at the lowest cost.

This system is oversized considering the number of batteries obtained from the GA simulation. Battery – the only operating reserve in this system is sized based on the highest peak power of the load profile (shown in Equation 35) and period without solar irradiance or wind velocity is low. The highest peak is not happening every hour. Hence, this system is oversized and not cost effective.
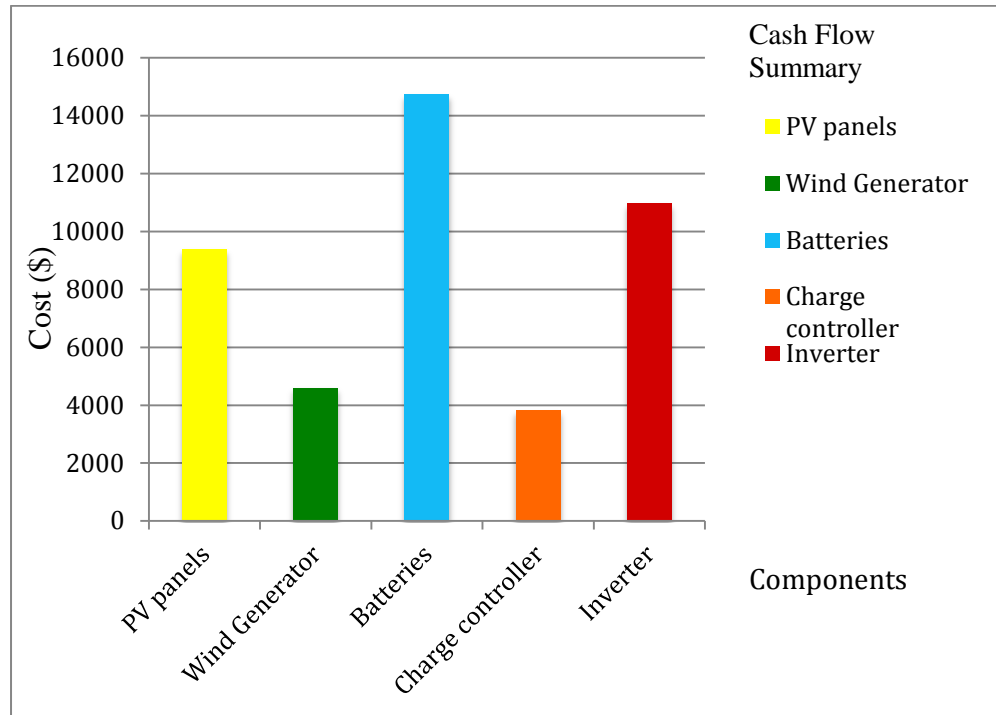
Figure 93 Cash Flow Summary for system with LPSP = 0

Table 44 Comparisons between HOMER and GA

Optimization method	Simulation Time seconds)	Net Present Cost (NPC)
HOMER	14	44114
GA	0.8554	43692

From the Table 44, GA uses less time to search for the optimal point in the search space. The net present cost (NPC) is more optimised as the freedom in GA to add different components and constraint. In HOMER, charge controller is not available in the HOMER library. To optimise a system with charge controller, user computes higher initial cost in PV panel column. However, GA fitness function provides the freedom to add components to the fitness function. This advantage of GA allows us to construct a fitness function for RES with Supercapacitor.

Case 2: PV-wind-battery with LPSP = 0.1 and 0.2

For the case of LPSP = 0.1 and 0.2, the simulation result shows the same optimised combination of components used in RES. This is due to the small changes percentage of capacity shortage. The result shows that two given LPSP values which are quite small difference in downtime, one set of configurations of a hybrid system can technically guarantee the required reliability of power supply.

The total power needed is 5.5kW per day from the load profile, however, the total power available generated from PV panel and wind generator and battery is only 5.39kW per day. This means that there is slight shortfall throughout the day. The simulation result obtained from GA is shown below:

Table 45 Optimization result for system with (LPSP = 0.1 and 0.2)

	A (hours)	DOD	y_{batt} (years)	No. of battery	No. of replacement battery	Cost of battery ($)	Net Present Cost ($)	No. of cycles	Usable capacity (kWh)
1	23	1	6.43	16	32	21841	50619	350	22.66
2	25	0.9	10.27	20	20	14915	43692	500	25.48
3	23	0.8	10.14	20	20	14915	43692	550	22.66
4	28	0.7	11.51	24	24	17898	46675	600	23.78
5	27	0.6	13.42	28	28	20881	49658	700	23.78
6	25	0.5	18.27	32	32	23864	52641	1000	22.66

The simulation result above shows the same trend with the result shown in Table 42. If the battery DOD is set 1 (100%), the usable capacity is high, however, for long run, the number of replacement battery is higher compare to the case where the battery DOD is 0.9, 0.8, 0.7 and 0.6. This also means that the lifetime for the battery is decreasing with the increase of DOD as the battery is

drained more to cater for the peak power. Based on the result in Table 45, the system configuration of option 2 and 3 (battery DOD is 0.9 and 0.8) possess the lowest cost. If the battery lifetime is more than 10 years above, the systems are not chosen because it is not feasible in real life based on the data sheet of the type of the battery used [238] .

Table 46 Cost Summary for the optimised LPSP = 1% and 2% system

Components	Capital Cost ($)	Replacement Cost ($)	O&M cost ($)	Total ($)
PV panels	6700	0	2680	9380
Wind Generator	2240	0	2346.40	4586.40
Batteries	6320	6320	2275.20	14915.50
Charge controller	720	2880	216	3816
Inverter	2067	8268	660	10955
System	18047	17468	8177.60	43692.60

It is clearly shown in Table 46 that optimal system configuration is same for both cases. This might be due to the small changes in the capacity shortage. Capacity shortage is a shortfall that occurs between the required amount of operating capacity (load plus required operating reserve) and the actual operating capacity the system can provide. Operating reserve (battery) plays an important role in the power reliability of the system. The optimal system architecture is 20 units PV panels with the rated power of 0.1kW, 1 unit of 1kW wind generator, 20 units of (12V, 118Ah) Batteries, 6 units of charge controllers and one unit of 2kW inverter. The initial number of batteries is 20 and the number of replacement batteries is 20. The string size for battery is 4 batteries and the number of string in parallel is 5.

The chart below shows the cost summary of the system. Initial, replacement, operational and maintenance cost for battery has significant

impact on the overall cost. It is the highest cost among the cost for other components.
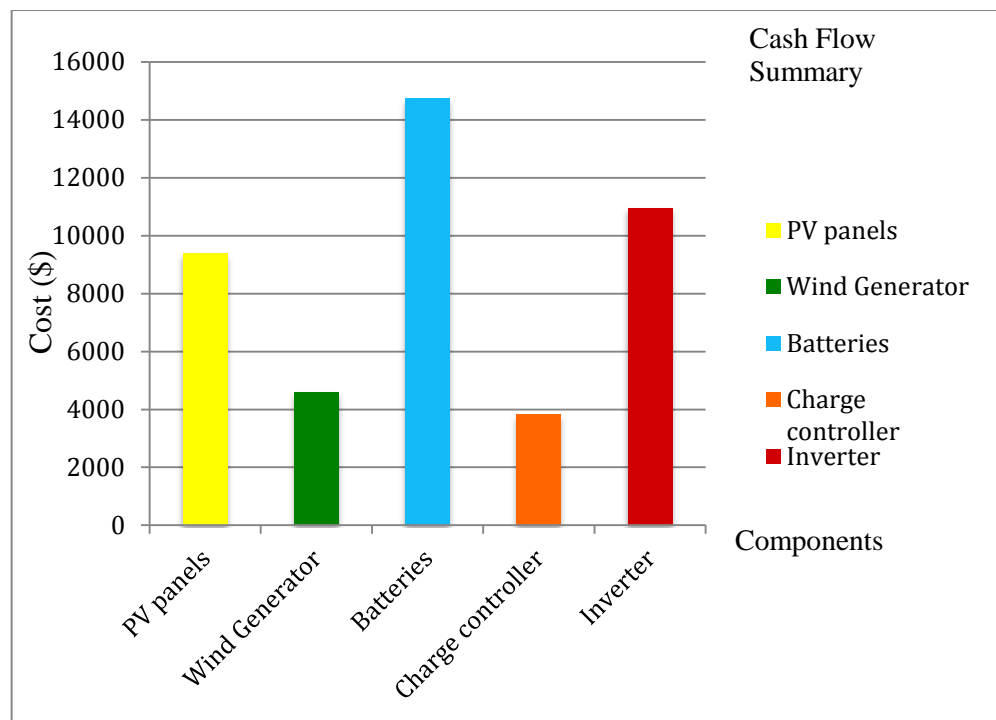
Figure 94 Cost Summary for system LPSP = 0.1 and 0.2

Case 3: PV-Battery System (LPSP = 0, 0.1 and 0.2)

Since the wind velocity at the site is low (about 2.89 ms^{-1}), it produces only approximately 0.04% of the power generated which is very small and not cost effective for this Semenyih site. The fitness function 1 is modified to search the net present cost of PV- Battery system. The wind generator term is eliminated. By applying the fitness function shown in Equation 32, result is obtained and shown below:

Table 47 Optimization result for PV-Battery system with LPSP = 0

	A (hour)	DOD	y_{batt} (year)	No. of battery	No. of replacement battery	Cost of battery ($)	Net Present Cost ($)	No. of cycles	Usable capacity (kWh)
1	28	1	8.03	20	40	21108	45299	350	28.32
2	25	0.9	10.27	20	20	14915	39106	500	25.48
3	27	0.8	12.13	24	24	17898	42089	550	27.19
4	27	0.7	13.50	28	28	20881	45072	600	27.75
5	27	0.6	15.34	32	32	23864	48055	700	27.19
6	25	0.5	20.55	36	36	15698	39889	1000	25.49

Table 48 Optimization result for PV-Battery system with LPSP = 0.1 and 0.2

	A (hour)	DOD	y_{batt} (year)	No. of battery	No. of replacement battery	Cost of battery ($)	Net Present Cost ($)	No. of cycles	Usable capacity (kWh)
1	23	1	6.43	16	32	21841	46032	350	22.66
2	25	0.9	10.27	20	20	14915	39106	500	25.48
3	23	0.8	10.14	20	20	14915	39106	550	22.66
4	28	0.7	11.51	24	24	17898	42089	600	23.78
5	27	0.6	13.42	28	28	20881	45072	700	23.78
6	25	0.5	18.27	32	32	23864	48055	1000	22.66

The cost is $39106 for RES without wind energy source. The cost of this system is lower than the RES with wind generator (shown in Table 45, $43465). As shown in the previous simulations, for the same location and load profile applied, it is clear that battery DOD of 0.9 is optimal for the optimal sizing of PV-battery system with LPSP = 0.

Table 49 Cost Summary for PV-Battery system

Components	Capital Cost ($)	Replacement Cost ($)	O&M cost ($)	Total ($)
PV panels	6700	0	2680	9380
Batteries	6320	6320	2275.20	14915.50
Charge controller	720	2880	216	3816
Inverter	2067	8268	660	10955
System	15807	17468	5771.20	39106.20
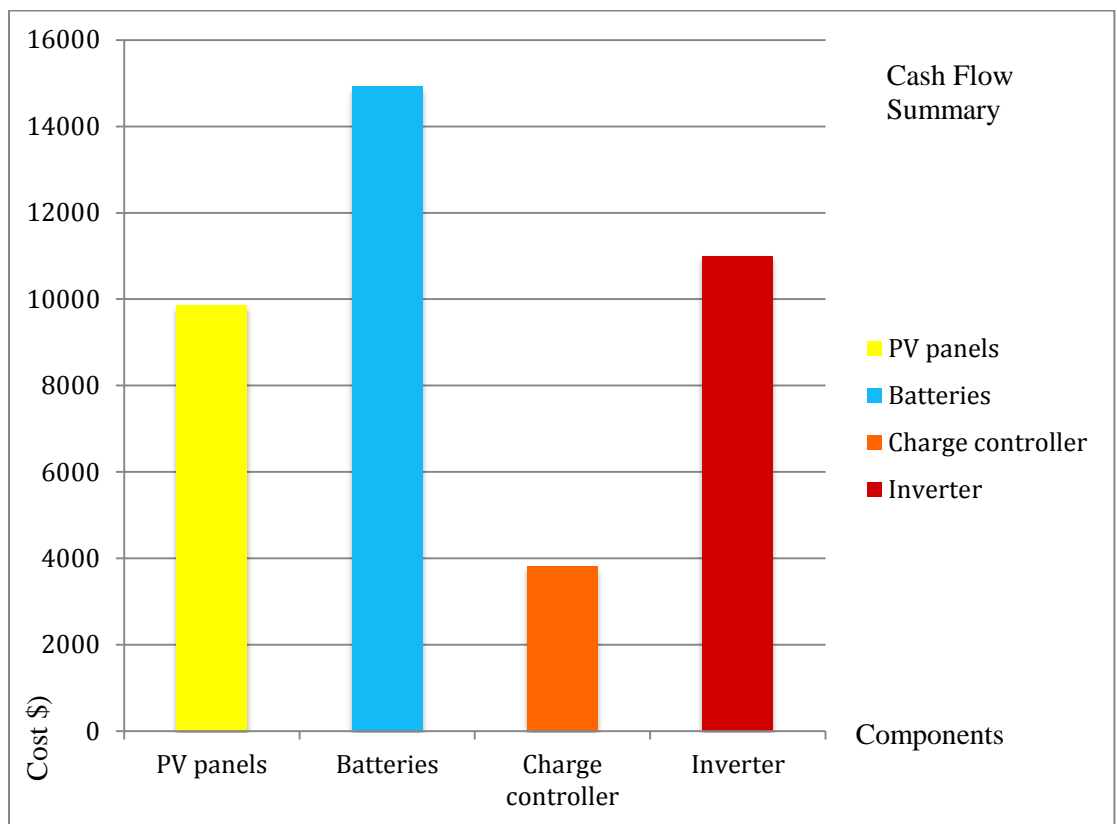
Figure 95 Cost Summary for PV-Battery system

The system architecture of this optimised PV-Battery system is 20 units of PV panels, 20 units of batteries, 6 units of charge controllers and 1 unit of inverter. There is more PV panels are used for this system due to the absence of wind generator.

283

Constraint in optimization problem plays an important role. From the optimization result obtained in this section, it is a trade-off between the power reliability and the net present cost of the system. Optimization result is practical if different constraint is set according to user specification.

4.2.2.2 Renewable energy system (RES) with Supercapacitor and Battery

As mentioned in the previous section, GA provides high degree of freedom to add components to the fitness function. It also has no restriction in adding constraint to the optimization algorithm. A new fitness function which include a new component - supercapacitor is constructed as shown in Equation 38 and Equation 39. The cost structure (value of constant and parameters) is summarised in Table 50.

Table 50 Fitness Function for RES with Supercapacitor and Battery

Terms	Components	Cost		Lifetime
		Initial	O&M	
1.	$N_{PV} \cdot (C_{PV} + y_p \cdot M_{PV})$	$C_{PV} = \$335$	$M_{PV} = \$6.7$	$y_p = 20$
3.	$N_{BAT} \cdot [C_{BAT} + R \cdot C_{BAT} + (y_p - R - 1) \cdot M_{BAT}]$	$C_{BAT} = \$316$	$M_{BAT} = \$6.32$	R (R is calculated using Equation 28.)
4.	$N_{CH} \cdot C_{CH} \cdot (y_{CH} + 1) + N_{CH} \cdot M_{CH} \cdot y_p - y_C - 1)$	$C_{CH} = \$108$	$M_{CH} = \$2.16$	$y_{CH} = 4$
5.	$C_{INV} \cdot (y_{INV} + 1) + M_{INV} \cdot (y_p - y_{INV} - 1)$	$C_{INV} = \$2968$	$M_{INV} = \$41$	$y_{INV} = 4$
6.	$N_{SCAP} \cdot C_{SCAP}$	$C_{SCAP} = \$1498.52$	NA	$y_{scap} = 20$

Equation 39 is also applied in the lab-scale SB-HESS. The cost for the components is different as the system is smaller size (i.e. lower power). Moreover, the simulated load profile is also in smaller scaled as shown in Figure 41.

The abbreviation and notation of the terms are the same as Equation 38. However, the initial cost for the prototype system is different as the components used are from different manufacturer and the specification of the components is different as well. This is because the implemented prototype is a lab scale system with smaller load profile, hence the components used for this system is different for optimisation. The cost structure for the components is shown in the table below:

Table 51 Fitness function for prototype with supercapacitor and battery

Terms	Components	Cost (RM)		Lifetime
		Initial	O&M	
1	$N_{PV} \cdot (C_{PV} + y_p \cdot M_{PV})$	$C_{PV} = 161$	$M_{PV} = 3.22$	$y_p = 20$
2	$N_{BAT} \cdot [C_{BAT} + y_p / R \cdot C_{BAT} + (y_p - y_p / R - 1) \cdot M_{BAT}]$	$C_{BAT} = 45$	$M_{BAT} = 0.9$	R
3	$N_{CH} \cdot C_{CH} \cdot (y_{CH} + 1) + N_{CH} \cdot M_{CH} \cdot (y_p - y_C - 1)$	$C_{CH} = 130.90$	$M_{CH} = 2.16$	$y_{CH} = 4$
4	$C_{INV} \cdot (y_{INV} + 1) + M_{INV} \cdot (y_p - y_{INV} - 1)$	$C_{INV} = 106.61$	$M_{INV} = 2.13$	$y_{INV} = 4$
5	$N_{SCAP} \cdot C_{SCAP}$	$C_{SCAP} = 25$	NA	$y_{scap} = 20$

Fitness function is constructed to optimise the cost for the RES without wind generator only. All the price of the components is taken from the manufacturer which is stated in Section 3.2.2. The same constraint and initial

boundary for PV panels, batteries, charge controller and inverter are the same as in Section 4.2.2-1 for the battery-only RES.

In this section, supercapacitor is coupled with the battery system which is known as supercapacitor-battery hybrid energy storage system. The constraint is the same as shown earlier and boundary for supercapacitor is shown in the following.

- By applying Equation 34, G, Output Power from renewable energy system. This system is a 2kW RES, hence, $G \leq 2kW$

- By applying Equation 35, **Autonomous, $A \leq 24$**

- By applying Equation 28, **Battery lifetime, $y_{batt} \leq 20$**

- The system specification is 48V. Hence, **DC bus voltage, V_{DC} = 48V.**

- By applying Equation 40 and 41, **constraint for supercapacitor, N_s,** the number of supercapacitor connected in series **and N_p,** the number of supercapacitor connected in parallel are $N_s \geq 1$ and $N_p \geq 2.$

Table 52 Boundary and Constraint for 2kW RES with SB-HESS

No.	Components/Parameters	Boundary
1	Number of PV panel, N_{PV}	$15 < N_{PV} < 30$
2	Number of batteries, N_{BAT}	$4 < N_{BAT} < 36$
3	Number of Supercapacitor, N_{SCAP}	$1 < N_{SCAP} < 3$
4	Number of Charge controller, N_{CH}	$N_{CH} < 0$
5	Number of Inverter, N_{INT}	$N_{INT} < 0$

Table 53 Optimization Result for RES with Supercapacitor and Battery

	A (hour)	DOD	y_{batt} (year)	No. of initial battery	No. of replacement battery	Cost of battery ($)	No. of Supercapacitor	Cost of super-capacitor	Net Present Cost ($)	No. of cycles	Usable capacity (kWh)
1	34	1	6.85	12	36	16381	2	2997	43569	600	16.94
2	31	0.9	9.86	12	24	12655	2	2997	39853	800	15.93
3	27	0.8	10.41	12	12	8949	2	2997	36137	950	13.59
4	24	0.7	9.59	12	24	12655	3	4495	41341	1000	11.89
5	27	0.6	13.15	16	16	11932	4	5994	42117	1200	27.19
6	28	0.5	20.55	36	36	15698	4	5994	45100	1400	25.49

GA only searches one combination of the optimal decision variables with the lowest cost which satisfies all the constraints mentioned above. The cost of the system is $36137. The cost of this system is lower than the RES with battery-only system. This is because the supercapacitor aids in prolonging the battery lifetime. It leads to cost reduction by reducing the number of battery replacement throughout the years as the battery DOD is lower compared to the battery-only RES. This is because battery DOD of 0.8 is required for the same load profile when battery is coupled with supercapacitor. This also means that lower usable capacity of the battery is required for this system as the battery is only required to cater the average power from the load profile (0.5kW) instead of 1kW (battery only system). This is constraint autonomy computed using the Equation 35. Besides that, supercapacitor also aids battery in delivering the sudden peak power. Therefore, the battery is sized based on the average power that is required to deliver, whereas, the number of battery in battery-only system is sized based on the highest peak power of the load profile.

Table 54 Cost Summary for RES with Supercapacitor and Battery

Components	Capital Cost ($)	Replacement Cost ($)	O&M cost ($)	Total ($)
PV panels	6700	0	2680	9380
Batteries	3792	3792	1365.12	8949.12
Supercapacitor	2997.04	0	0	2997.04
Charge controller	720	2880	216	3816
Inverter	2067	8268	660	10995
System	16276.04	14940	7267.52	36137.16

Figure 96 Cost Summary for PV-wind-supercapacitor-battery
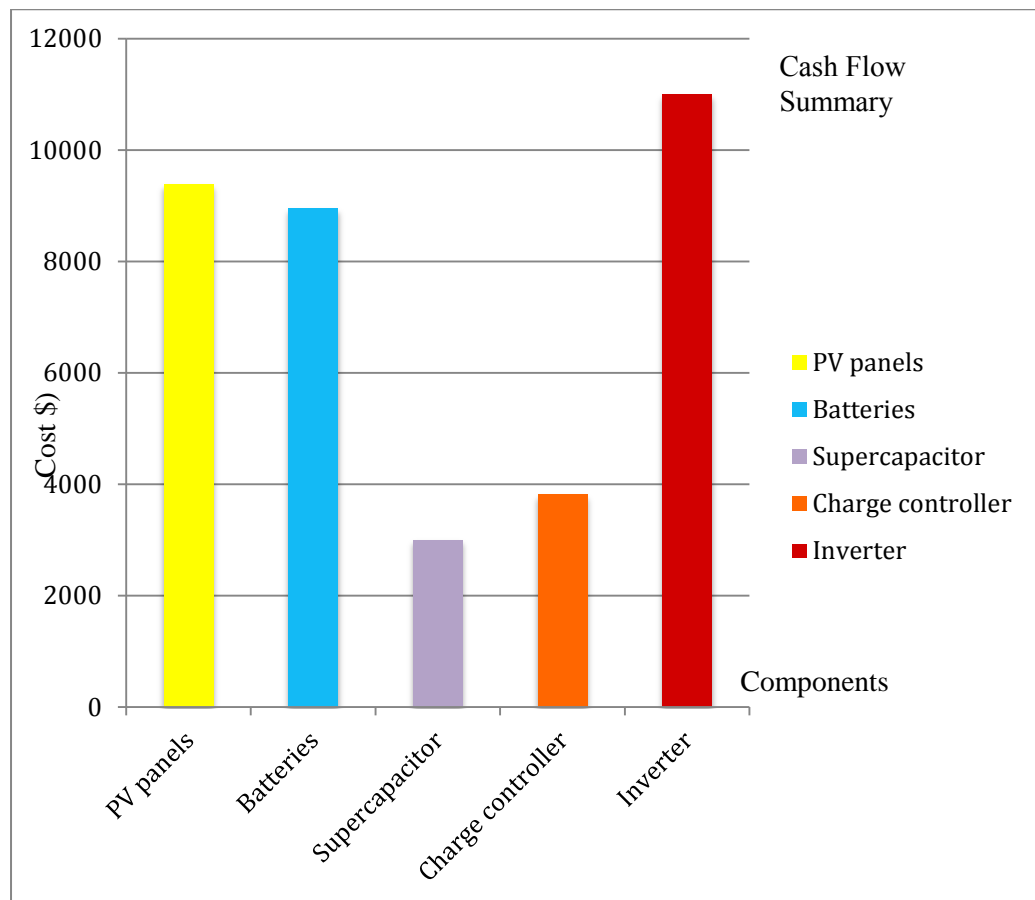
As seen in the Table 53, the system cost for RES with supercapacitor-battery is lower compare to the RES with battery-only system.

Lab-scaled prototype SB-HESS system

Constraint and boundary for a 72W RES with SB-HESS (Prototype)

- **Output power from renewable energy source $G \leq 72W$**

- **Autonomous, $A \leq 1$ hours,** where DOD = 0.5, $V_N \cdot C_N = 14.16Wh$, P_A= 11.085W (average power from load profile shown in Figure 41), battery turns off when the load current is above 0.95A. which means P_A= 11.085W.

- **Expected battery lifetime $R \leq 20$, where $Q_{lifetime} = 12744$,** $Q_{annual} = 1270$ this is an estimation as this value depends on inversion efficiency (round-trip efficiency) and also the solar output power.

- **Number of supercapacitor in series, $N_s \leq 6$** based on the specification of the chosen supercapacitor and the DC bus voltage.

- **Number of 6 supercapacitors in parallel, $N_p \leq 3$.**

Table 55 Boundary and Constraint for 72W prototype with SB-HESS

No.	Components/Parameters	Boundary
1	Number of PV panel, N_{PV}	$1 < N_{PV} < 3$
2	Number of batteries, N_{BAT}	$1 < N_{BAT} < 3$
3	Number of Supercapacitor, N_{SCAP}	$6 < N_{SCAP} < 24$
4	Number of Charge controller, N_{ch}	$N_{ch}^{PV} < 0$
5	Number of Inverter, N_{INT}	$N_{INT} < 0$

Table 56 Optimization Result for PV-Battery-Supercapacitor system

A (hour)	DOD	y_{batt} (year)	No. of battery	No. of replacement battery	Cost of battery (RM)	Net Present Cost (RM)	No. of cycles	Usable capacity (Wh)
1	0.5	10.1	2	2	285.3	2413	900	14.16

In the lab-scaled prototype SB-HESS, the specification of the components are limited to run different simulation for different parameters as it is not possible to set the different value of DOD and battery lifetime stated in the data

specification for our smaller scale load profile. Hence, the optimised value of battery DOD is 0.5.

Table 57 Cost Summary for PV-Battery-Supercapacitor system (Prototype)

Components	Capital Cost (RM)	Replacement Cost RM)	O&M cost (RM)	Total (RM)
PV panels	322	0	128.8	450.8
Batteries	270	270	15.3	555.3
Supercapacitor	150	0	0	150
Charge controller	130.9	523.6	37.4	696.9
Inverter	106.61	426.44	31.95	565
System	979.51	1220.04	213.45	2413
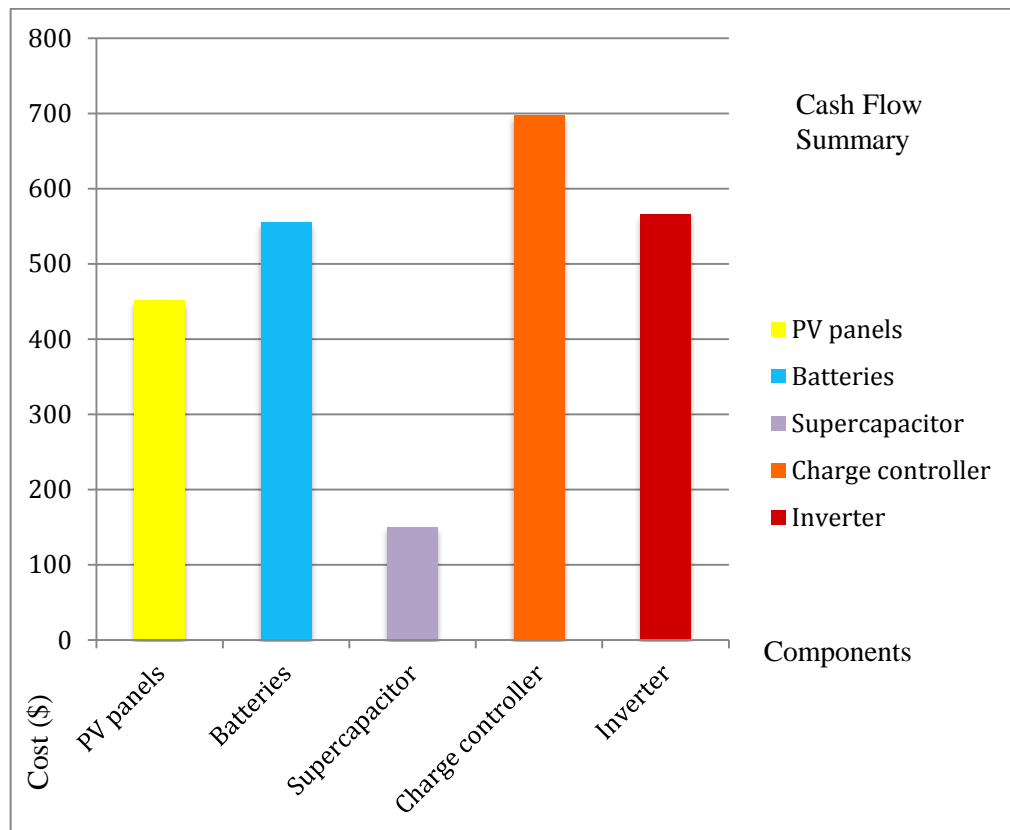
Figure 97 Cost Summary for PV-Supercapacitor-Battery System (Prototype)

The cost of this RES with Supercapacitor-Battery hybrid energy storage system (SB-HESS) is reduced as compared with the cost of the conventional PV-wind-battery system. This optimised RES with (SB-HESS) is possible because of the energy control strategies in between these two energy storage devices.

Generally, the overlapping of a battery's high energy density with a supercapacitor's high power density produces a straightforward benefit over either individual system by taking advantage of each characteristic. The resulting performance is the actual fact highly related to the interconnections and controls implemented in the system to exploit their strengths and avoid their weaknesses. The flow coordination and energy control management for improved energy efficiency is critical for any optimised system. There are two main energy control management, supercapacitor-battery direct coupling (passive control) and supercapacitor-battery indirect coupling (active control) [51]. The direct coupling of a supercapacitor and battery energy source is where the supercapacitor connects in parallel with batteries and load. The advantages contributed by this simple design relative to a battery-only system include a capability to elevate power, greater efficiency and extended battery life. However, this design might drain the battery more as the battery tends to charge the supercapacitors when the voltage of the supercapacitor drops (i.e. the energy stored drops). Limitation arising from this direct coupling approach:

1. The load and supercapacitor voltages both float based on the battery voltage that is affected by its SOC, and therefore limit exploitation of the power capability of the supercapacitor. In addition, the requirements of the supercapacitor module or cell voltage must match that of the

battery. As a result, control over the module bank size is restricted and is hard to be optimised.

2. The power provided by the hybrid energy storage system is largely governed by the equivalent series resistance of both coupled energy devices. The fixed partitioning of current supply shared by supercapacitor and battery can thus experience rippling during a pulse demand, particularly in the battery where a magnitude of peak power is endured at the end.

3. The terminal voltage of the HESS follows that of the battery rather than being properly regulated; thus the voltage difference between complete charge to discharge of a battery stack can have a significant effect on the power provided to the load.

The optimised size of the RES is built possible with the indirect coupling topologies active control). Indirect coupling of a supercapacitor and battery via the addition DC-DC power converter affords a means of stepping up or down as mentioned in Section 2.1.3.3. This approach leads HESS with higher degrees of freedom for operation and rectifies problems and constraint surrounding the passive direct coupling described above. Also, mentioned in Section 1.1, the power electronics is costly, for an optimised supercapacitor-battery HESS, our approach is to reduce the number of power electronics and in place with a battery management system which is able to do load forecasting using the SVM. These advantages are:

1. The supercapacitor and battery voltage can now differ from one another, providing optimization and design flexibility.

2. The weight of the power source to meet peak requirement is now readily reduced compared with passive direct coupling mentioned above.

3. A constant terminal voltage (only with small variation) can be maintained for HESS.

4. Regulated recharging of the battery can be achieved through a DC-DC converter without a need to introduce a charger.

5. This is also beneficial for controlling battery current supplied to the DC bus, but the bus voltage will fluctuate according to the SOC of the supercapacitor.

6. The safety limit of the battery is not exceeded as the microcontroller in the system avoid the overvoltage happens in battery. At high load currents, both the supercapacitor and battery work simultaneously. However, the microcontroller could take action switching on battery (or supercapacitor) base on the load forecast from SVM. It means that it maintains the steady discharge of the battery while the supercapacitor supplements the remaining high current.

Table 58 shows the number of batteries used in different systems. It shows that system with hybrid energy storage system has lower number of batteries. It is good for the environment and the cost reduction as initial cost and replacement cost of battery has the big impact on the overall cost. Result on optimal sizing of RES using the GA are summarised and presented in Table 59. For a clearer comparison, RES with battery DOD 0.8 are compared and the net present cost are presented in Table 61.
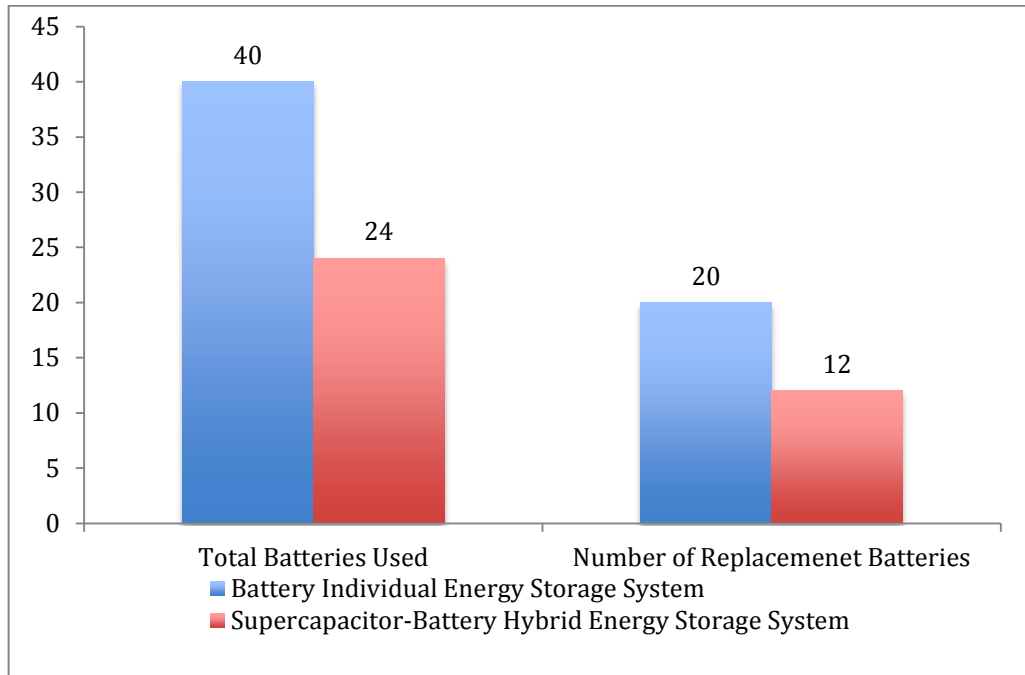
Figure 98 Comparison of number of batteries for Supercapacitor-battery hybrid energy storage system and battery individual storage energy storage system.

Table 58 Initial number of batteries and number of replacement battery

Renewable Energy System	Number of batteries	Number of replacement battery
PV-Wind-Battery	20	20
PV-Battery	20	20
PV-Wind-Battery-Supercapacitor	12	12
PV-Battery-Supercapacitor	12	12

Table 59 Optimised Net Present Cost (NPC) of RES found using the GA

Optimised NPC of Renewable Energy System	Cost ($)		Battery lifespan (Years)	
PV-Wind-Battery	LPSP = 0	LPSP = 0.1/0.2	LPSP = 0	LPSP = 0.1/0.2
	43692	43692	10.3	10.3
PV-Battery	39106	39106	10.27	10.27
PV-Wind-Battery-Supercapacitor	40723		10.4	
PV-Battery-Supercapacitor	36137		10.4	

Table 60 Net present cost of RES using battery DOD 0.5 found using the GA

Renewable Energy System using battery DOD 0.8	Cost ($)	Battery lifespan (Years)
PV-Wind-Battery	46675	12.13
PV-Battery	42089	12.13
PV-Wind-Battery-Supercapacitor	40723	10.4
PV-Battery-Supercapacitor	36137	10.4

4.2.2.3 Summary

- It is apparent that the net present cost is reduced for 7.5%

$$\frac{43692 - 36137}{36137} * 100\% = 7.5\%$$

by coupling the supercapacitor with battery. The main contribution of the cost reduction is the reduction of the number of replacement batteries throughout the 20-years of project time.

- The implemented control strategy allows for enhanced power capacity and reduction of battery loss are offset by the cost. It also includes operation of the battery and supercapacitor independent voltage, improved utilization of supercapacitor power capacity, and control of the battery current.

- Constraint plays an important role in optimization problem to be practical in real life domain. It changes with different user specification for that particular domain.

4.2.3 Energy Control Management System

One of the focuses of this project is the strategy of predicting the load beforehand for supercapacitor-battery hybrid energy storage system (SB-HEES). This system allows Ardrino microcontroller to control the MOSFET switch for turning on supercapacitor before the power burst. The supercapacitor is able to cater the entire power burst subject to zero load rejection. This allows the battery to discharge at lower current value at a desired C-rate (discharging rate). This aids to reduce the rate of damage mechanism of batteries by maintaining high end-discharge voltage of the battery. Hence, a high SOC of battery is maintained.

This section shows the reliability and the efficiency of the implemented EMS, which is called Support Vector Machine/Regression Energy Management System (SVMR_EMS) on the lab-scaled prototype of SB-HESS. There are three measures of metric to prove the supercapacitor-battery hybrid energy storage system is reliable and cost effective than conventional energy storage system:

Section 4.2.3.1

- Performance definition of the Support Vector Machine in load identification task,
- Performance definition of the Support Vector Regression in load prediction.

Section 4.2.3.2

- Performance comparison between standalone battery storage and hybrid energy storage.

Section 4.2.3.3

- Performance comparison between the software approach SVMR_EMS with the hardware approach DC/DC converter energy management system.

4.2.3.1 Performance definition of SVM and SVR

SVM in load Identification

The optimised load profile Classification model is trained using C-SVC type (SVM) which is highlighted in the following:

Table 61 Performance Definition of SVM

Kernel	Parameter value		Classification Accuracy (%)	No. of support Vector	Training Time (s)
	C	g			
Linear	2	0.25	100	24	0.005085
	4	0.5	100	21	0.006105
	8	0.1	100	17	0.005519
Polynomial	2	0.25	100	17	0.004866
	4	0.5	100	17	0.005640
	8	0.1	100	17	0.005643
Radial Basis Function	2	0.25	100	25	0.006726
	4	0.5	100	22	0.005222
	8	0.1	100	24	0.007163
Sigmoid	2	0.25	20	25	0.005024
	4	0.5	20	25	0.005881
	8	0.01	100	25	0.005059

From Table 61, it can be observed that the linear, polynomial and RBF kernels with optimised function yields excellent classification accuracy. Hence, the model with the least support vector and training time (highlighted) were selected for better faster classification as the SVM computational complexity is proportional to the number of support vector [286].

SVR in load prediction

As mentioned in Section 3.2.3. there are five simulated load profile. The optimised regression models for each load profile were shown as the following:

Table 62 Performance Definition of SVR

Load Profile	SVM type	Kernel	Parameter value			MAPE	Training
			C	g	p	%)	Time s)
1		polynomial	100	0.33	0.01	11.6882	0.294515
2		RBF	100	0.33	0.01	7.5650	0.018975
3	Epsilon -	RBF	10	0.33	0.01	5.7966	0.025643
4	SVR	RBF	0.1	0.33	0.02	9.5908	0.022941
5		RBF	10	0.33	0.01	4.9574	0.020495

Table 62 shows the accuracy percentage of (MAPE) and training time for the five simulated load profiles. A few runs of experiments were done to select the appropriate kernel for the different load profiles and obtain the optimised parameters value. These values and kernel type was used in the SVM_R energy management program as shown in Appendix A4.

The predicted and actual load profiles by using the optimised models were shown below:

Load Profile	Blue = Actual load profile Green = Predicted load profile
1	
2	
3	
4	

5
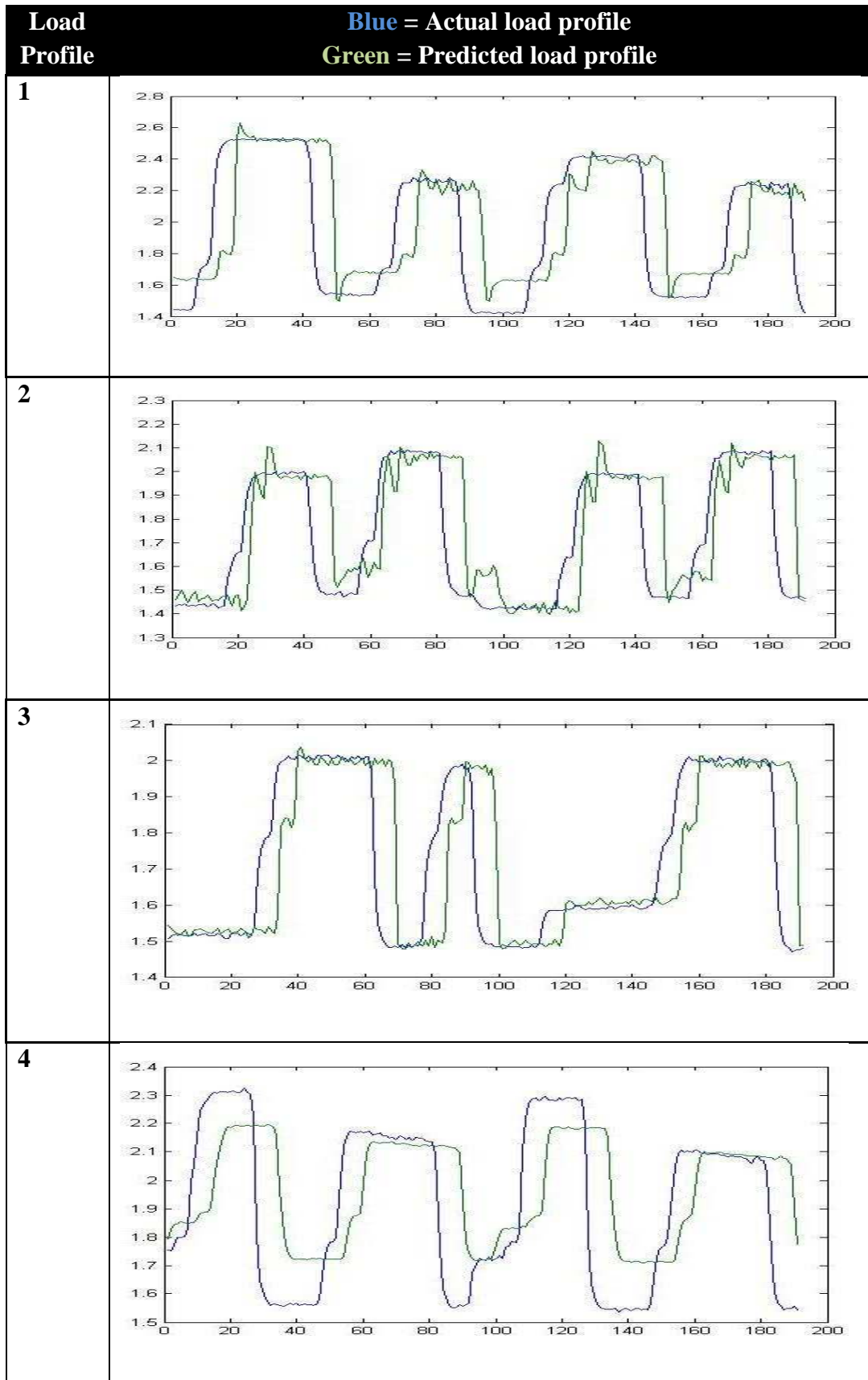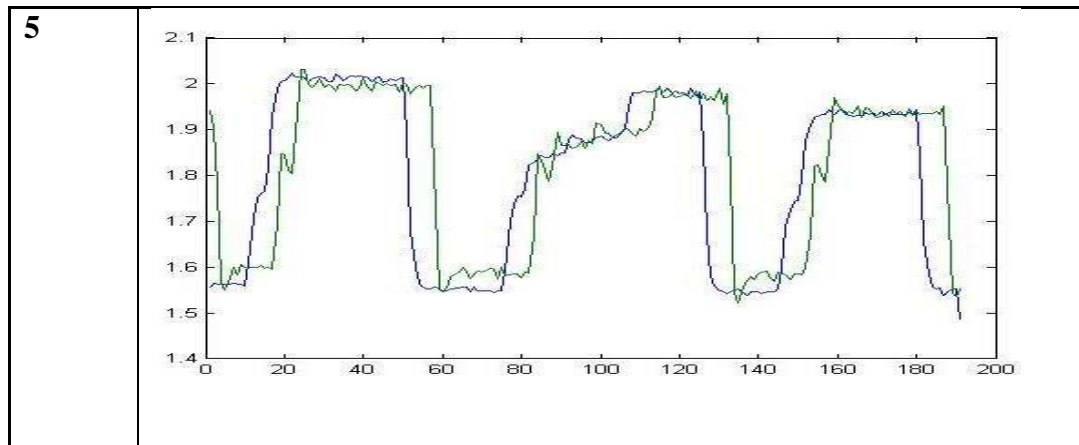
Figure 99 Predicted and Actual load for each load profiles

The regression model predicts the load before the actual load happens. It is shown in the Figure 99 above. It is a feature in the energy management system. It is important in delivering instantaneous peak power by turning on the supercapacitor without power electronic (to build bi-directional DC-DC converter).

4.2.3.2 State-of-Charge (SOC) comparison

The stress test was conducted on the lab scale battery-only system and the hybrid system to determine the remaining battery capacity. This result shows that the battery-only system possess the low SOC at the end of the stress test. The SOC over load cycle graphs for each system is plotted as follows:
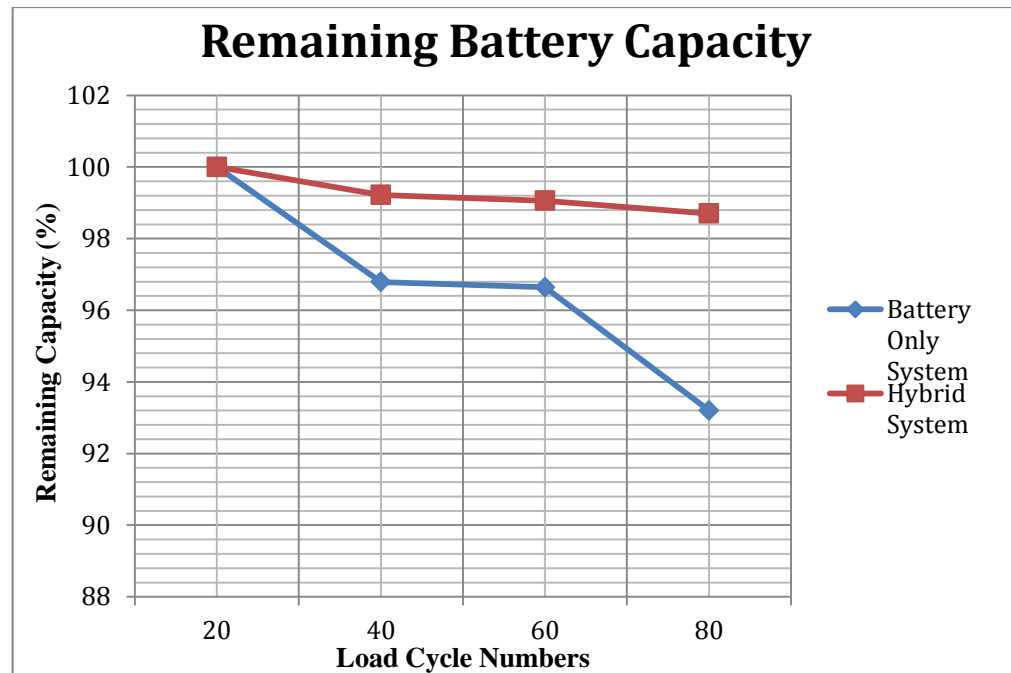
Figure 100 Graph of remaining battery capacity VS load cycle

As observed in Figure 100, the battery only system's remaining capacity has a steeper dropping gradient. On the other hand, the hybrid system's battery remaining capacity loss is smoother over the stress test load cycle. This has proven that with the use of supercapacitor in the hybrid system, the battery lifespan could be prolonged. The calculation is presented using Equation 26 and the results are plotted in Figure 101 - 103. The calculation for plotting the graph is shown in Appendix A5.
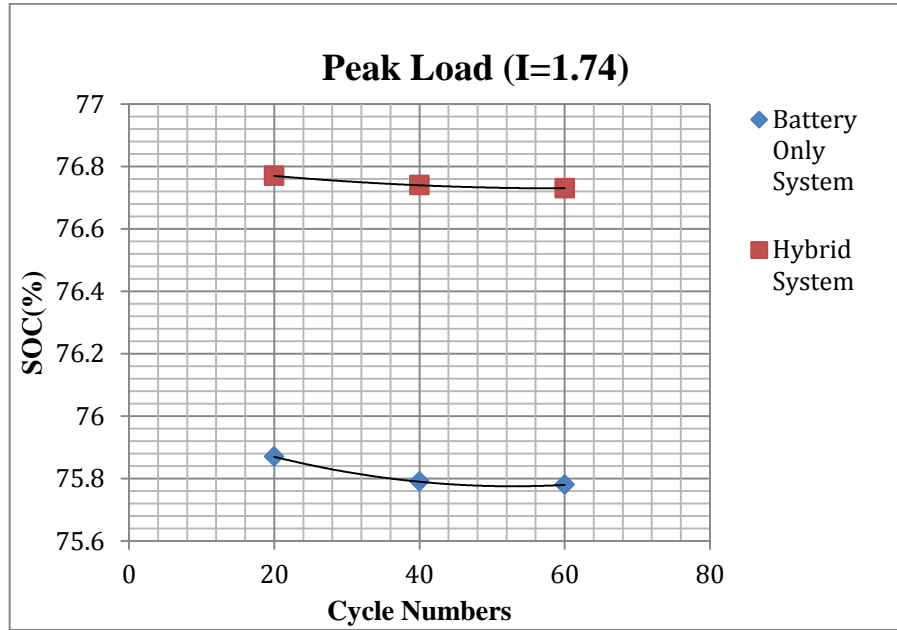
Figure 101 Graph of SOC in peak load VS load cycle
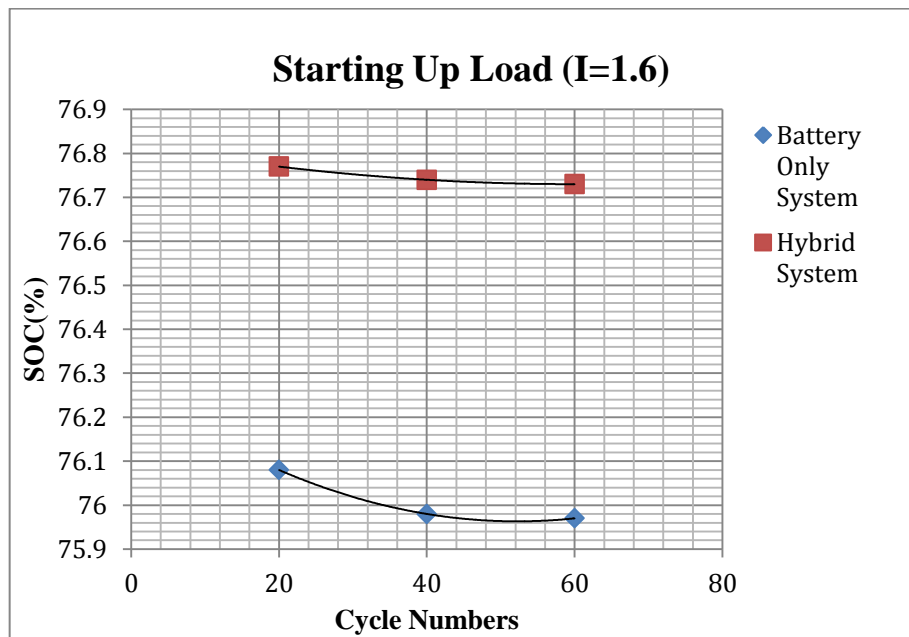
Figure 102 Graph of SOC in starting up load VS load cycle
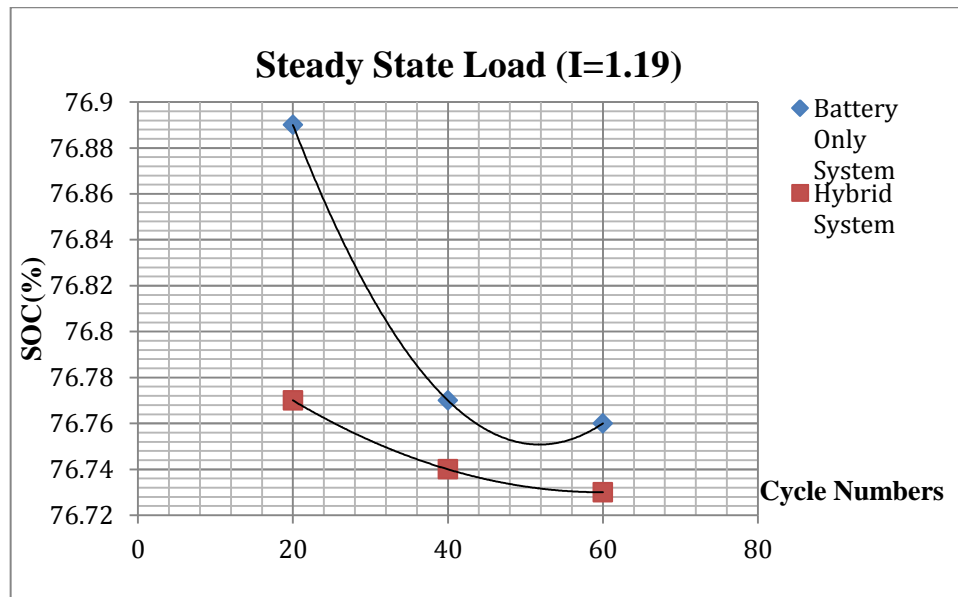
Figure 103 Graph of SOC in steady state load VS load cycle

In Figures 101, 102 and 103, the SOC of the battery in hybrid system is observed to have smoother drop compared to the battery-only system. The supercapacitor in the hybrid system will supply for the peak load and starting up load; hence, the battery in hybrid system does not suffer the high rate of discharge as much as the battery-only system. Besides, it's also noted that the SOC drop of the battery only system in the steady state load is higher; this is due to the higher DOD in the battery when the battery only system is used. In all, the supercapacitor helps to absorb the high discharge rate stress and maintains a higher SOC level for the battery which helps to prolong the battery lifespan.

4.2.3.3 Supercapacitor Time Response

As mentioned in Section 3.2.3, the load prediction without load profile classification lacks of automation and is prone to erroneous results. The following shows the supercapacitor response when the wrong load profile was used for the load prediction:

1. SVR Load Prediction without Load Profile Identification
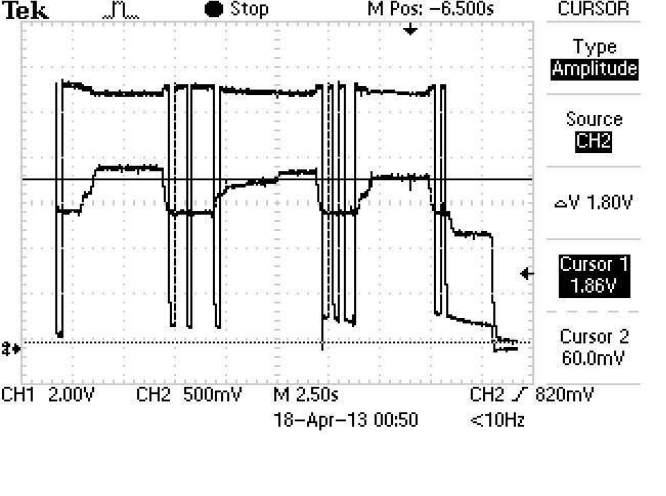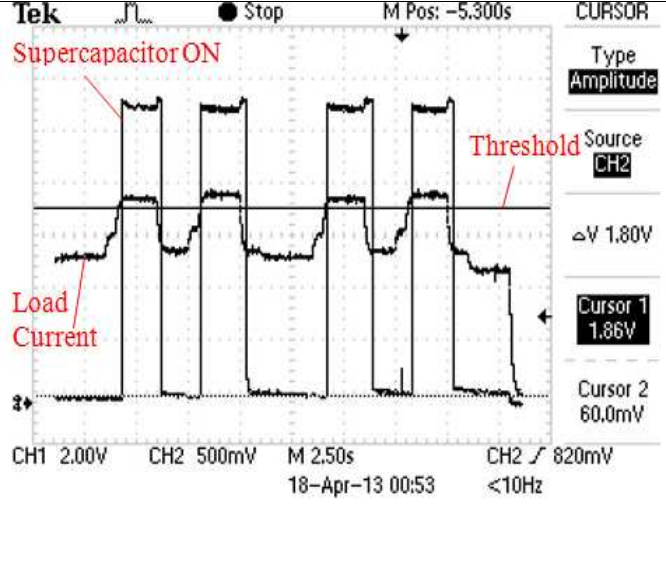
Actual Load Profile	Load Profile Model Used	Results
Load_5	Load_2	
Load_4	Load_5	

Figure 104 Time Response of SVMR-EMS without load profile identification

306
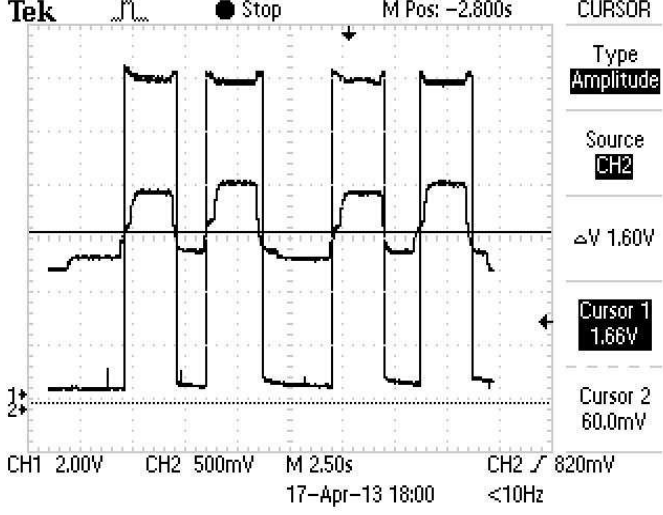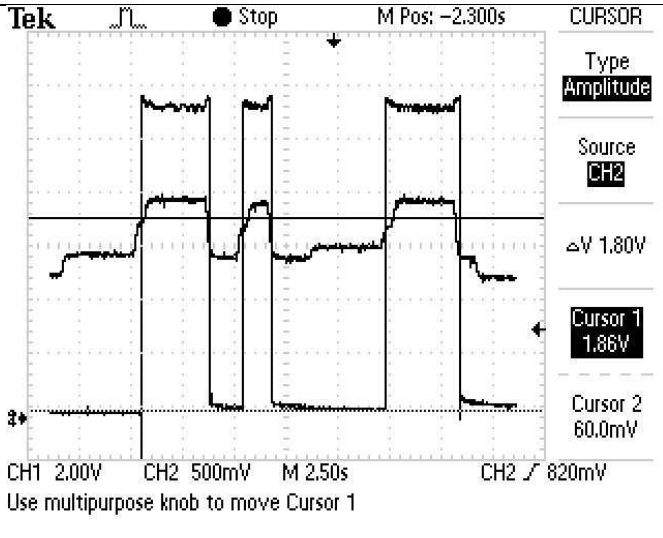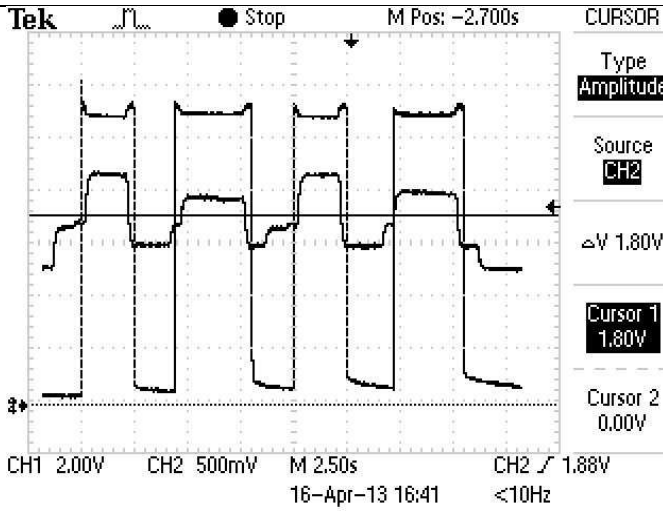
The square pulses in the diagram denote the time when supercapacitor turns on; while the varying graph is the load current. The horizontal line shows the peak current threshold where the supercapacitor should be turned ON when the load current exceeds the threshold.

As seen in Figure 104, when the wrong load profile model was used for the load prediction task, the supercapacitor was turned on either too early or too late corresponds to the peak current threshold.

2. SVR Load Prediction with Load Profile Identification

When the load profile was identified through SVM prior to the peak load prediction, the supercapacitor time response shows good results as shown in the following:

No.	Load Profile	Load profile identified	Results
1	Load_1	Load_1	

2			
	Load_2	Load_2	
3			
	Load_3	Load_3	
4			
	Load_4	Load_4	

| 5 | Load_5 | Load_5 | |

Figure 105 Time Response of SVMR-EMS with load profile identification

As shown in Figure 105, the supercapacitor was turned ON before the load current exceeds the peak current threshold. Hence, with the correct SVR load profile model used for the regression task, the SVMR_EMS shows a good time response as it is able to predict the peak load current and turn on the supercapacitor in advanced for all five load profiles. Below shows the closer looks of the load prediction results with and without load profile identification:

(a)

(b)
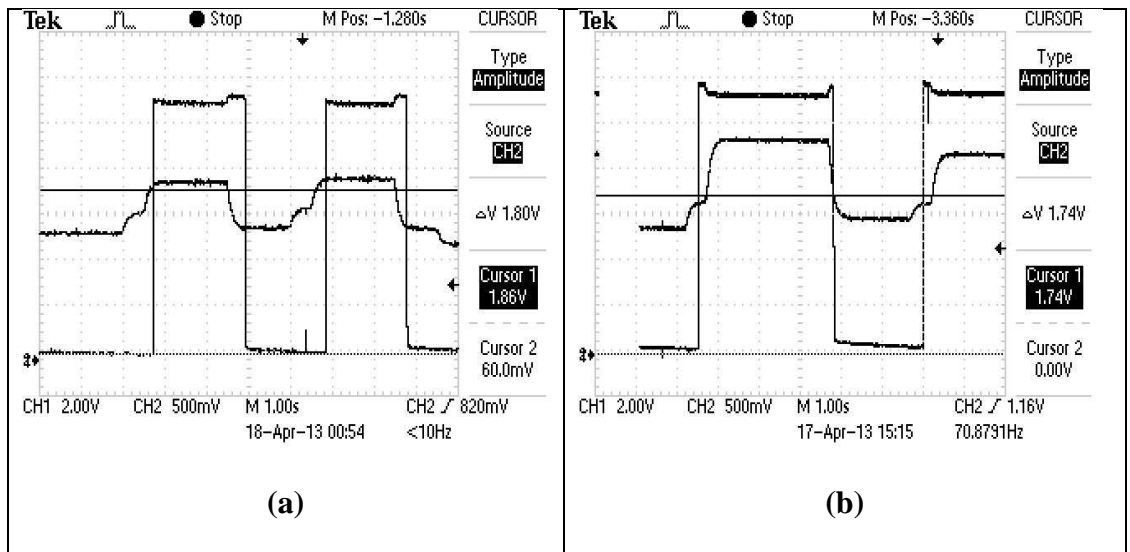
Figure 106 (a) Load prediction without load profile identification, (b) load prediction with load profile identification

As shown in Figure 106, when the wrong load profile was used for load prediction, the supercapacitor response lagged the peak load by 200-400ms. On the other hand, when the load profile was successfully identified through the SVM, the supercapacitor response leads the peak load current by 200ms as shown in Figure 106(b). This will allows the supercapacitor to absorb the high discharge rate stress and optimise the battery lifespan.

3. Time Response Comparison between SVMR_EMS and hardware approach
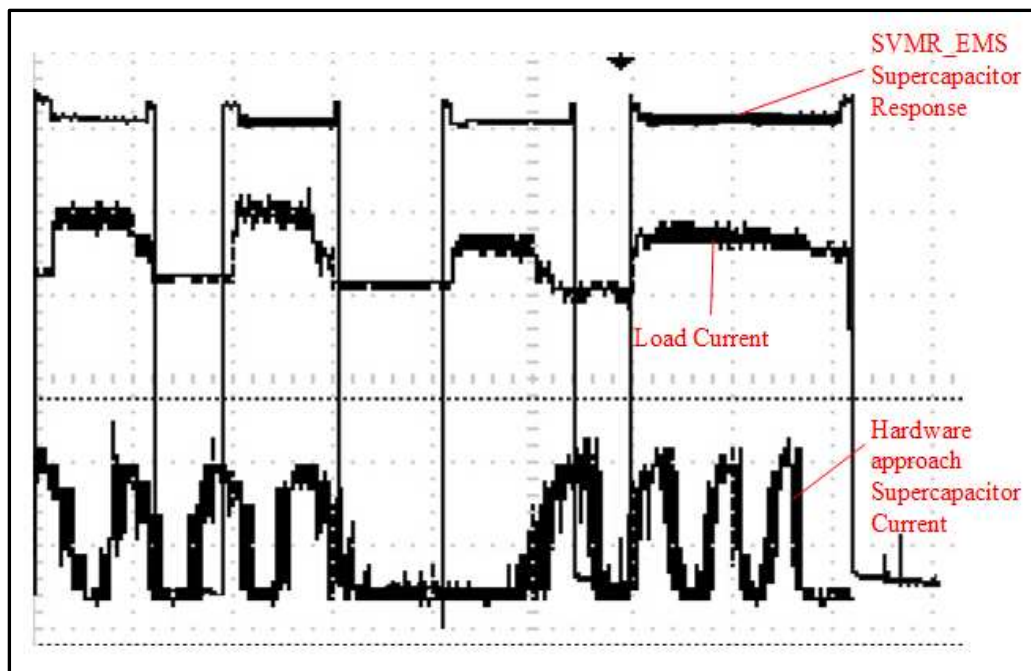
Figure 107 SVMR_EMS and Hardware approaches' Supercapacitor Response

As seen in Figure 107, the hardware approach supercapacitor supplies the load in pulsation manner. Hence, sometimes the supercapacitor response will randomly lead and lag the peak load current demand. On the other hand, the SVMR_EMS which predicts the peak load current in advanced will have the supercapacitor response leading the peak load demand.

4. Power Efficiency of the system

The efficiencies of software approach for various loads were calculated and plotted as follows:

Table 63 Software approach power efficiency with various loads

Load (Ω)	Power Efficiency (%)
22	$\eta = 100\% * (11.44\ V *I) / (13\ V*I) = 88\%$
44	$\eta = 100\% * (11.81\ V *I) / (13\ V*I) = 91\%$
100	$\eta = 100\% * (12.06\ V *I) / (13\ V*I) = 92\%$
144	$\eta = 100\% * (12.14\ V *I) / (13\ V*I) = 93\%$

The power efficiency versus load graph was plotted as shown in the following:
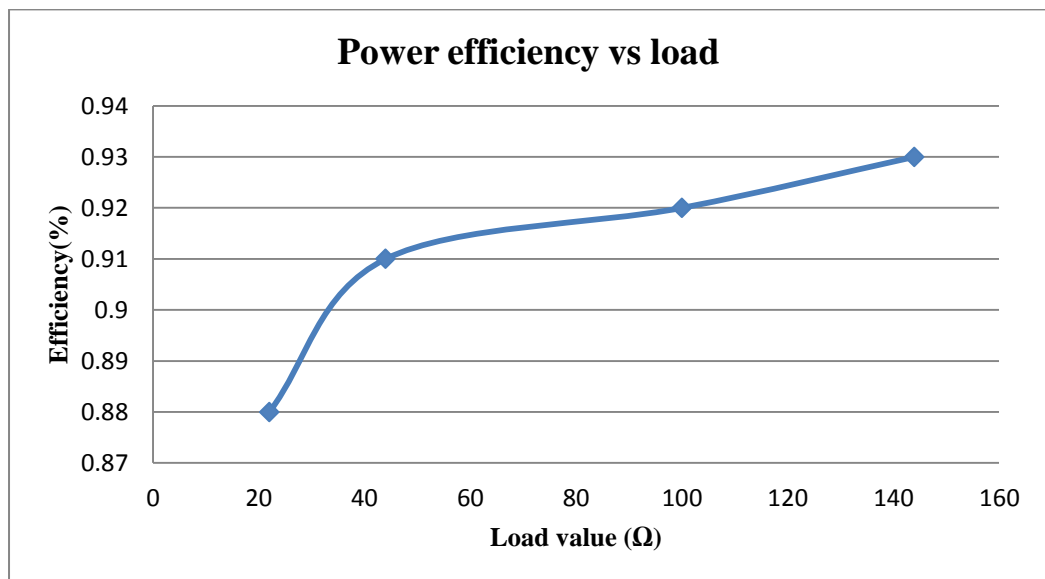
Figure 108 Software approach's power efficiency versus load

As shown in Figure 108, the software approach attains higher efficiency when a smaller load (higher resistance) is used. This is due to the 1 Ω current sensing resistor which formed a potential divider across the load terminal. Hence, by increasing the load's resistance, the voltage that supplies to the

311

terminal will increase and hence improves the power efficiency. On the other hand, the hardware approach's power efficiency has reported to be constant over the range of load tested [248]. The power efficiency comparison between the hardware approach and software approach was shown as follows:

Table 64 Comparison of power efficiency with various loads

Load Ω)	Hardware DC/DC converter Approach efficiency (%)	Software Approach efficiency (%)
22	93.48%	88%
44	93.48%	91%
100	93.48%	92%
144	93.48%	93%

From Table 64, it can be seen that the power efficiency of hardware approach stays constant at 93%, while the software approach's efficiency increases with the load's ohm and nearly matches the efficiency of hardware approach when 144 ohms load is used.

5. System Cost

One of the project's main aims is to reduce the use of expensive power electronic through the implementation of the Software approach Energy Management System. Hence, the itemized cost of the system were tabulated and compared with the hardware approach as followed:

Table 65 SVMR-EMS system cost

	Item	Quantity	Price (RM)	Cost (RM)
1. Software Control Board	Resistor	18	0.3~0.5	9
	FQP17P10 P-channel Power MOSFET	6	4.4	26.4
	2N3904 NPN switching Transistor	6	0.45	2.7
	Terminal connector	5	0.3	1.5
	Veroboard	1	3.8	3.8
	1N4007 diode	0.2	3	0.6
	P600K rectifier diode	3	7	21
	SB560 SCHOTTKY diode	1	0.71	0.71
	1 Ω 5W current sensing resistor	1	1	1
	3 A Fuse and holder	1	1	1
	Heat Sink	6	3.5	21
	Arduino Mega 2560 R3	1	178	178
			Total Cost	**266.71**
2. Hardware approach total cost				**297.11**

As seen in Table 65, the hardware approach energy management system is slightly more expensive than the software approach. The saving is significant using software approach. The cost is reduced by 10.23% . However, the hardware approach cost only covers for topology with discharging operation and management of one battery cell. On the other hand, the software approach system cost has covered the topology with full charging/ discharging operation

313

and management of multiple battery cells. Besides, unlike the hardware approach where the DC/DC components are designed specifically for the task requirement, the software approach offers modularity and flexibility as it could work with a larger range of voltages. Hence, the use of software approach has proven to be cost effective over the hardware approach.

In all, the SVMR_EMS with load prediction enables a good time response performance that is comparable with the hardware approach. Besides that, it could also match the power efficiency of hardware approach when smaller load is used. Lastly, the SVMR_EMS is much more cost effective over the hardware approach which is required the power electronics (to build the DC-DC converter).

4.2.3.4 Analysis and Summary

Throughout this section 4.2.3.4, there are few problem faced which could affect the reliability of the SVMR_EMS. They are listed as followed:

1. Load replicability

Since the programmable load operates by varying the opposing torque generated by the secondary motor. The secondary motor is required to have a constant supply of voltage and current drawn. Hence, an external DC power supply is required to ensure the replicability of the load. Besides, the lead acid battery voltage level varies from 12-13V as the capacity is used during the operation. This will affect the voltage level supplied to the primary motor and influence the load profile generated by the programmable load as seen in the following figure:

(a)   **b)**
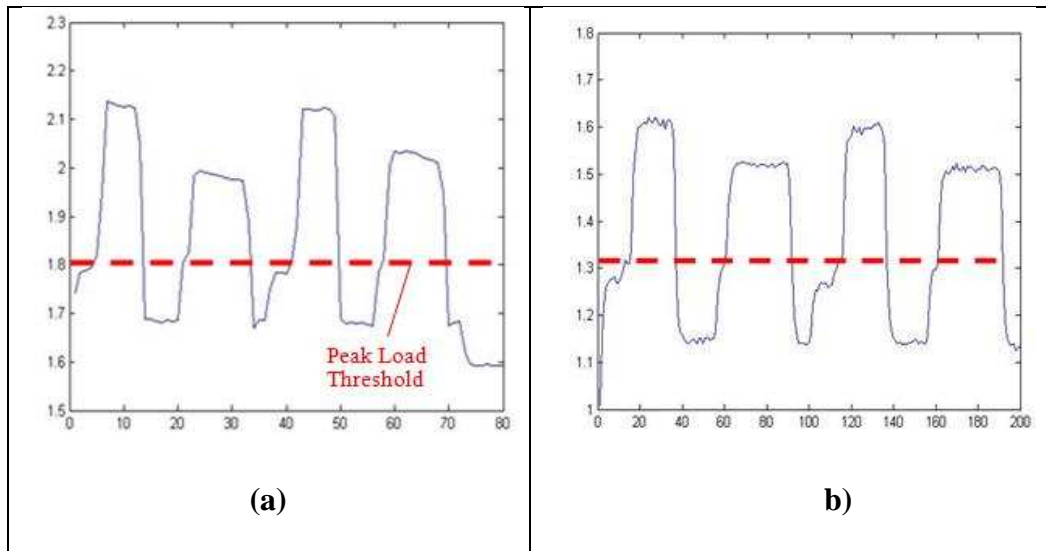
Figure 109 (a) Original load profile, (b) Load profile affected by Battery voltage level drop

As seen in Figure 109(a) and Figure 109(b), the battery voltage level drop has caused the load current profile to be lowered in magnitude. However, due to the good generalization of the SVR, it could still predict the load pattern when the overall load current magnitude has dropped to a certain extent. Yet, it is required that the peak load threshold to be adjusted for the prediction to for future work to gain 100% accuracy in all conditions.

2. Supercapacitor

Due to the lack of the voltage balancing circuit for supercapacitor, the charging of the six supercapacitors in series might cause the imbalance charging and discharging of the supercapacitor string. However, it added the overall system cost. As mentioned in Chapter 1, in some cases this leads to the use of balancing circuits, which reduce the efficacy of the supercapacitor bank. When balancing circuits are not used (sometimes to save operational costs), the systems runs the risk of draining the battery even more because the

315

supercapacitor will act as an additional load when its voltage is lower than the batteries nominal voltage.

As mentioned in Chapter 1, capacitance also varies with different DC bias voltages. Therefore, a manufactured supercapacitor, which has high reproducibility and reliability, is important in maximizing the power reliability of the supercapacitor after it is integrated in the power system to meet peak power demand.

An integrated of GA-Taguchi method was applied to optimise the process factor in supercapacitor fabrication process. Result and discussion on this methodology step is presented in the next section.

4.3 Optimization of Supercapacitor fabrication process

Methodology on supercapacitor fabrication process is shown in Chapter 3. Total of 42 supercapacitors were fabricated. In this section, performance profile of three supercapacitors is chosen and shown in the section 4.3.1. Result shows that the capacitance spread apart and the standard deviation is relatively large. In the next subsection (Section 4.3.2), result and discussion on the optimization process fabrication supercapacitor using genetic algorithm within Taguchi signal-to-noise ratio is presented. It shows an increase in standard deviation with the implemented Taguchi-Genetic Algorithm optimization technique on the supercapacitors compared with the conventional Taguchi method, which greatly involved engineering judgment.

4.3.1 Process fabrication of Supercapacitor

The test profile shown below is obtained using Autolab Potentiostat (PGSTAT302N) under cyclic voltammetry and galvanostatic charge-discharge tests. In chrono galvanostatic charge-discharge test, the current is set at 0.1A, 0.2A, 0.3A and 0.5A. For cyclic voltammetry, supercapacitors are tested in different scan rate of 2mV/s, 5mV/s, 10mV/s and 20mV/s. Test profile for three samples without any optimization technique is applied) is shown below.

Sample 1: Supercapacitor CS 16

1. **Chrono Galvanostatic Charge-discahrge Test**
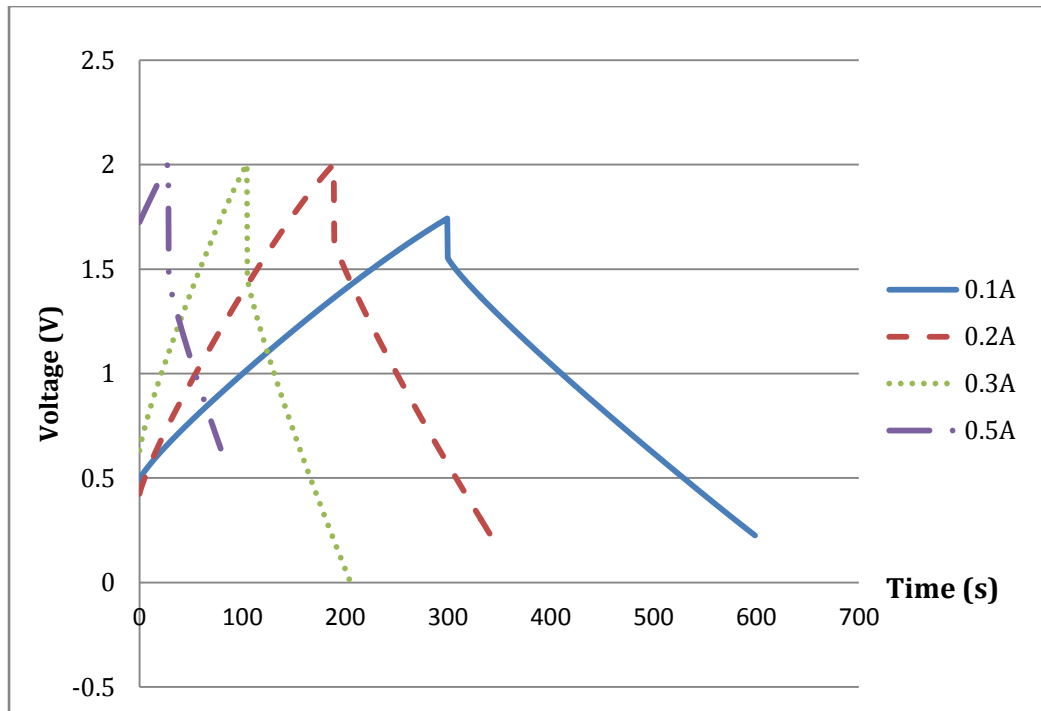
Figure 110 Voltage-Time plot from Galvanostatic charge-discharge test of Sample CS16 at different currents (0.1, 0.2, 0.3 and 0.5 A)
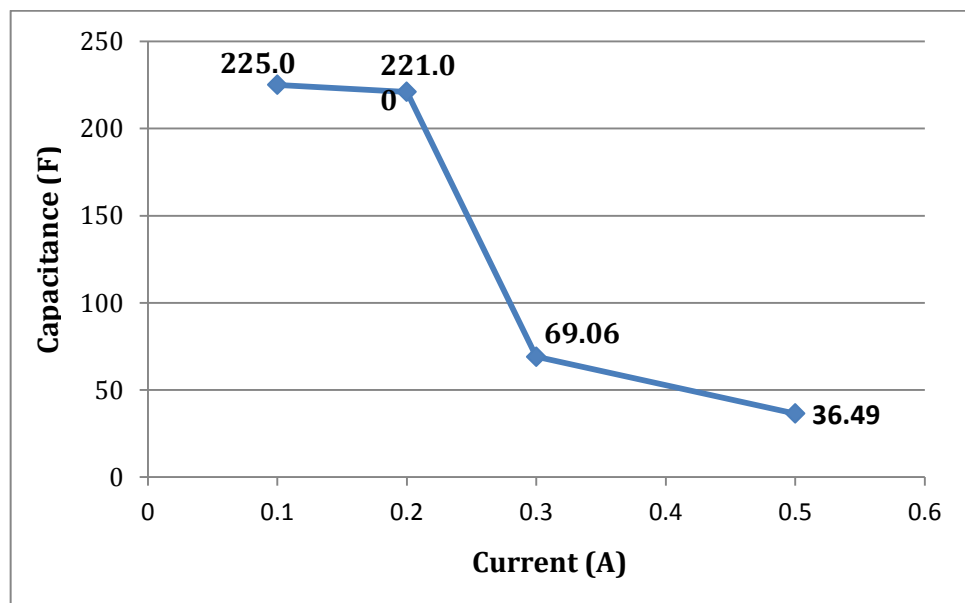
Figure 111 Capacitances of Sample CS16 at different currents (0.1, 0.2, 0.3 and 0.5 A)

318

2. Cyclic Voltammetry
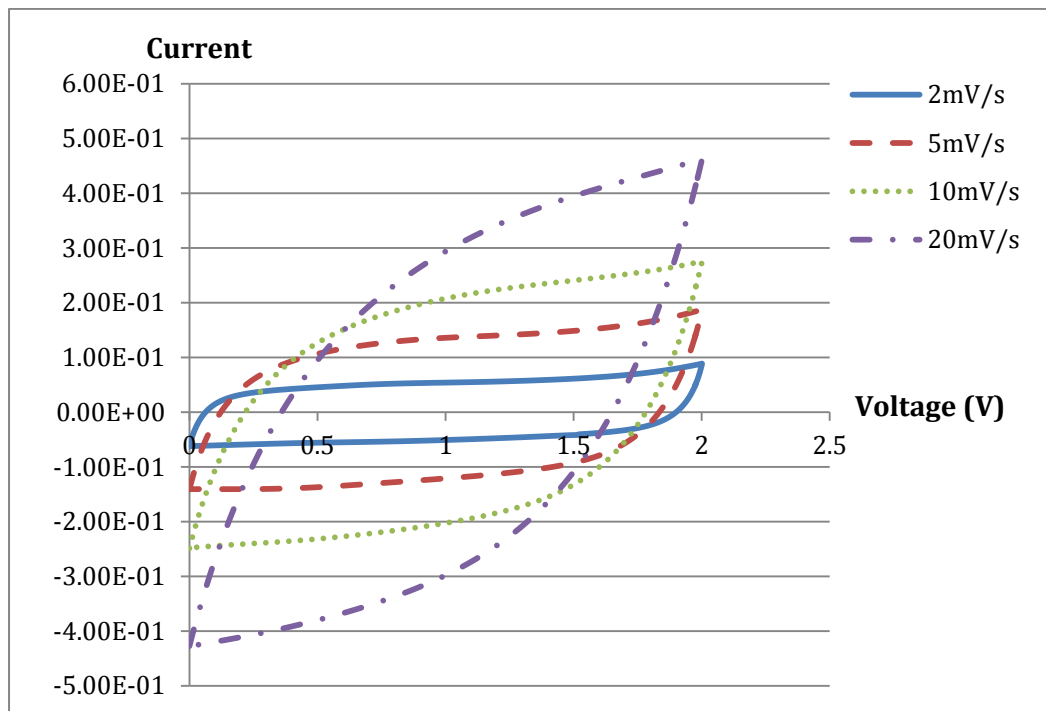
Figure 112 Cyclic Voltammograms at various scan rates (2, 5, 10, 20mV/s)
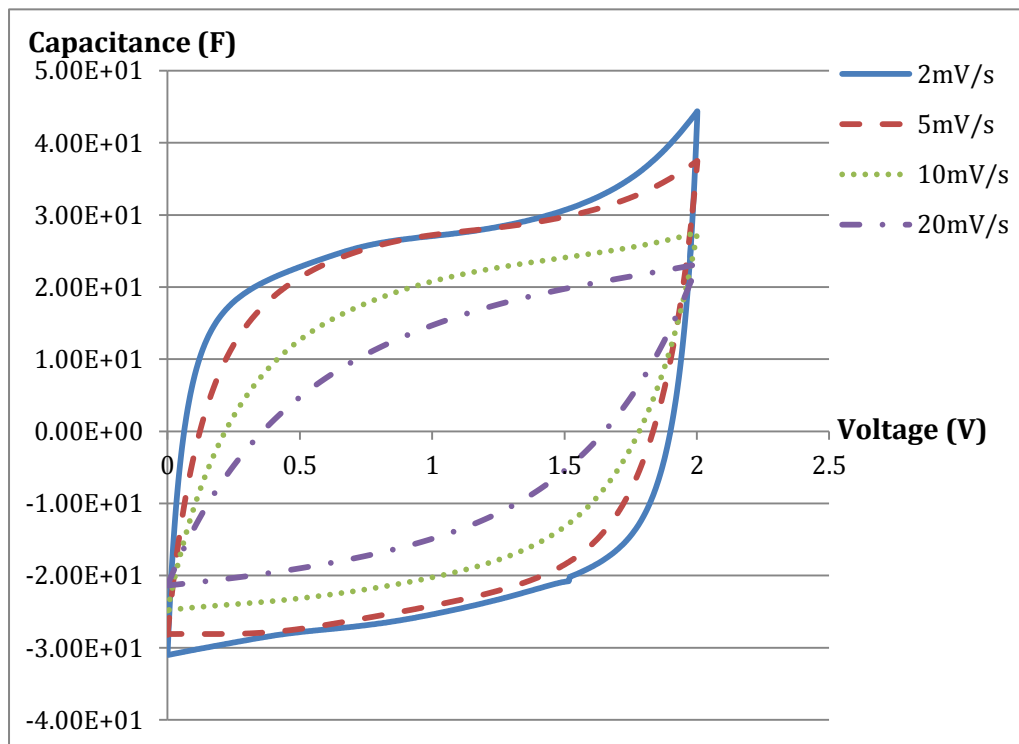
Figure 113 Capacitance plots of Sample CS16 at various scan rate (2, 5, 10, 20mV/s)

319
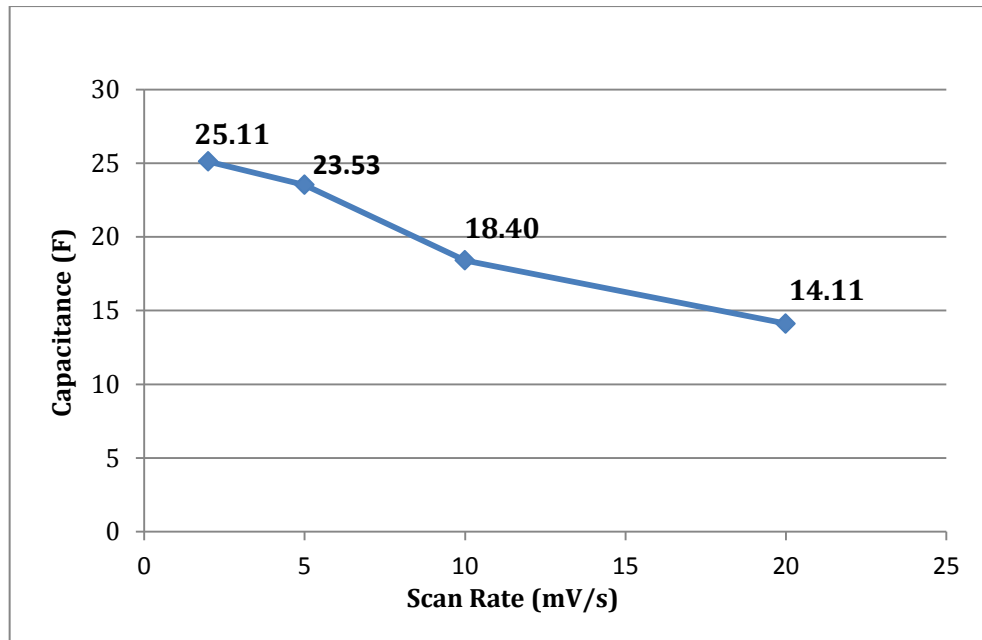
Figure 114 Overall capacitance of Sample CS16 at different scan rate (2, 5, 10, 20mV/s)

Sample 2:
Supercapacitor CS 33

1. **Chrono Galvanostatic Charge-discahrge Test**
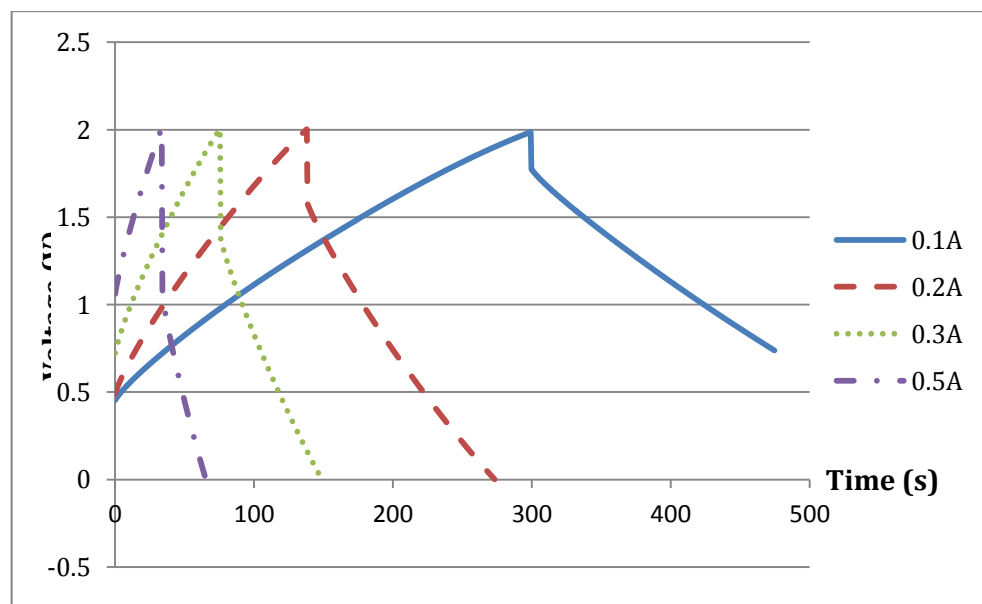
Figure 115 Voltage-time plot from galvanostatic charge-discharge test of Sample CS33 at different currents (0.1, 0.2, 0.3 and 0.5 A)
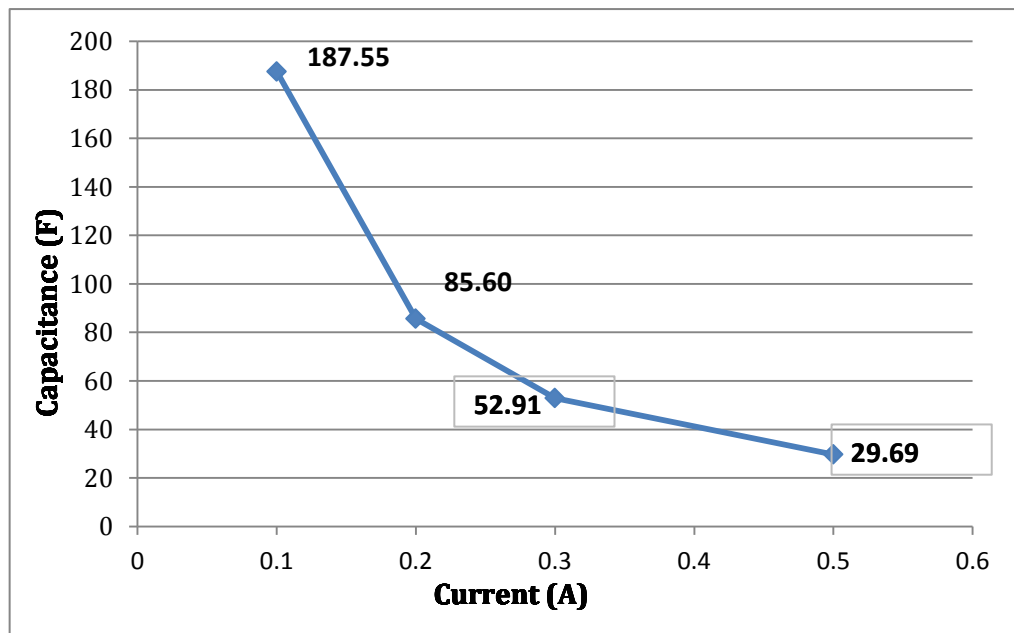
Figure 116 Capacitances of Sample CS33 at different currents (0.1, 0.2, 0.3 and 0.5 A)

2. Cyclic Voltammetry
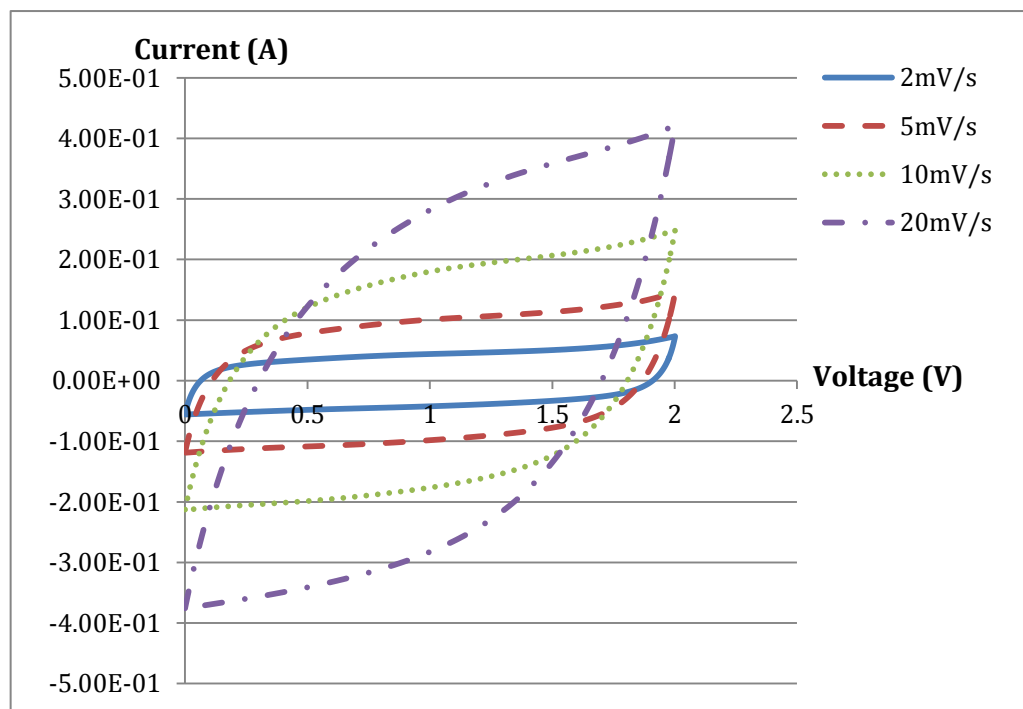
Figure 117 Cyclic Voltammograms at various scan rates (2, 5, 10, 20mV/s)
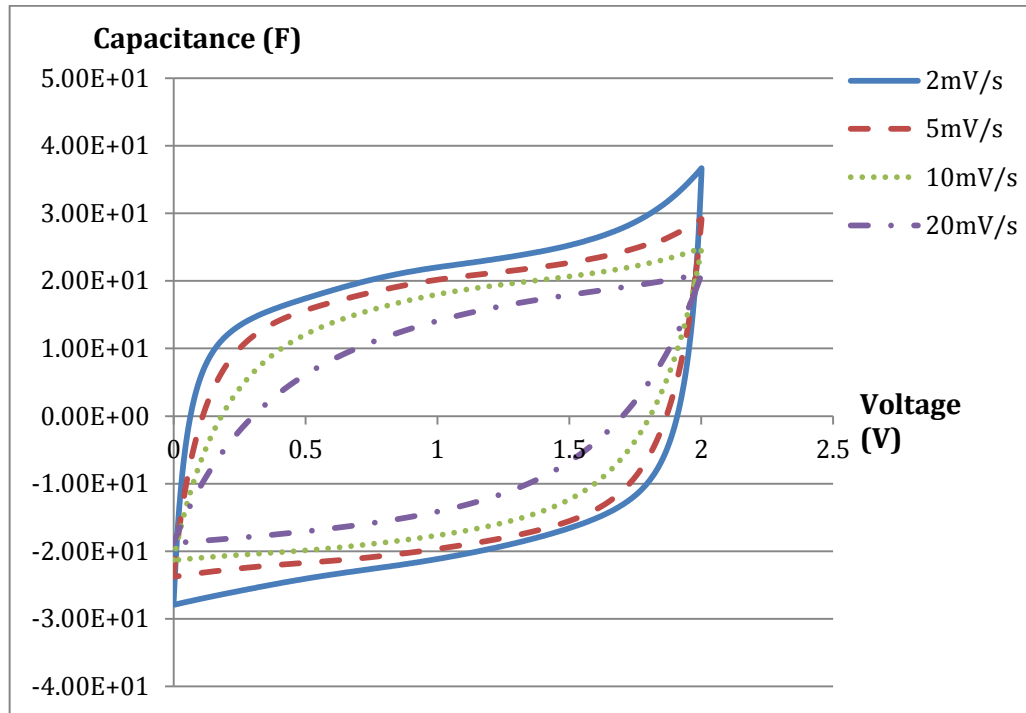
Figure 118 Capacitance plots of Sample CS33 at various scan rates (2, 5, 10, 20mV/s)
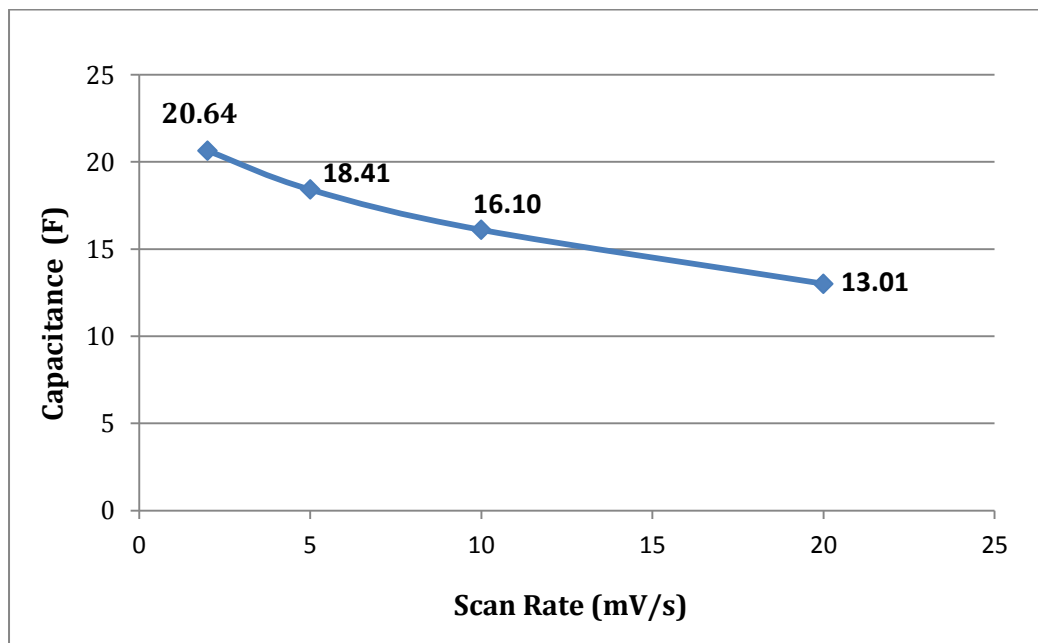
Figure 119 Overall capacitance of Sample CS33 at different scan rates (2, 5, 10, 20mV/s)

Sample 3:
Supercapacitor CS 34

    1. **Chrono Galvanostatic Charge-discahrge Test**
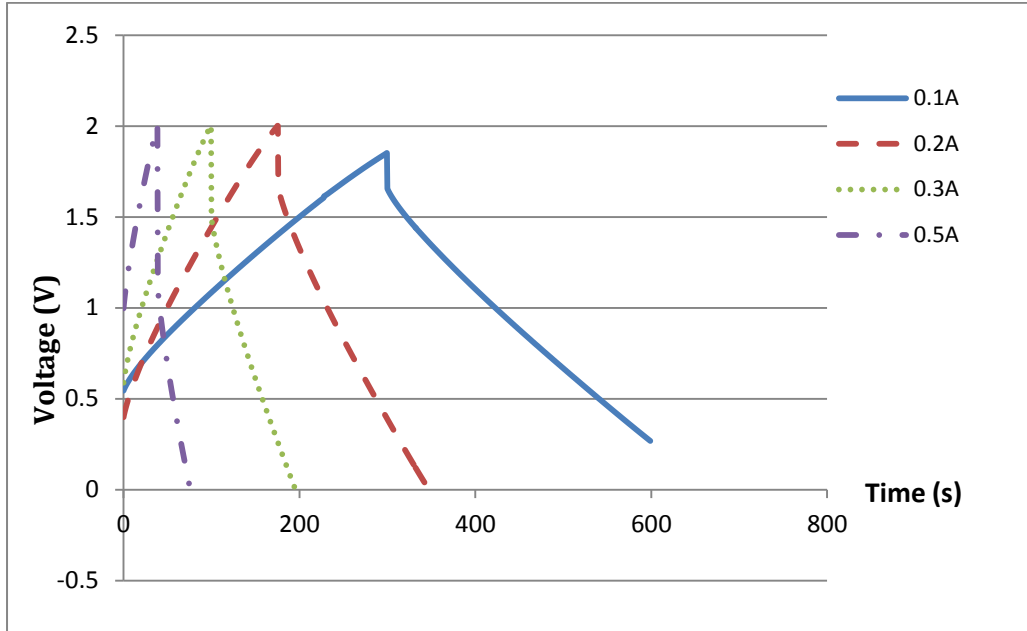
Figure 120 Voltage-time plot from galvanostatic charge-discharge test of Sample CS34 at different currents (0.1, 0.2, 0.3 and 0.5 A)
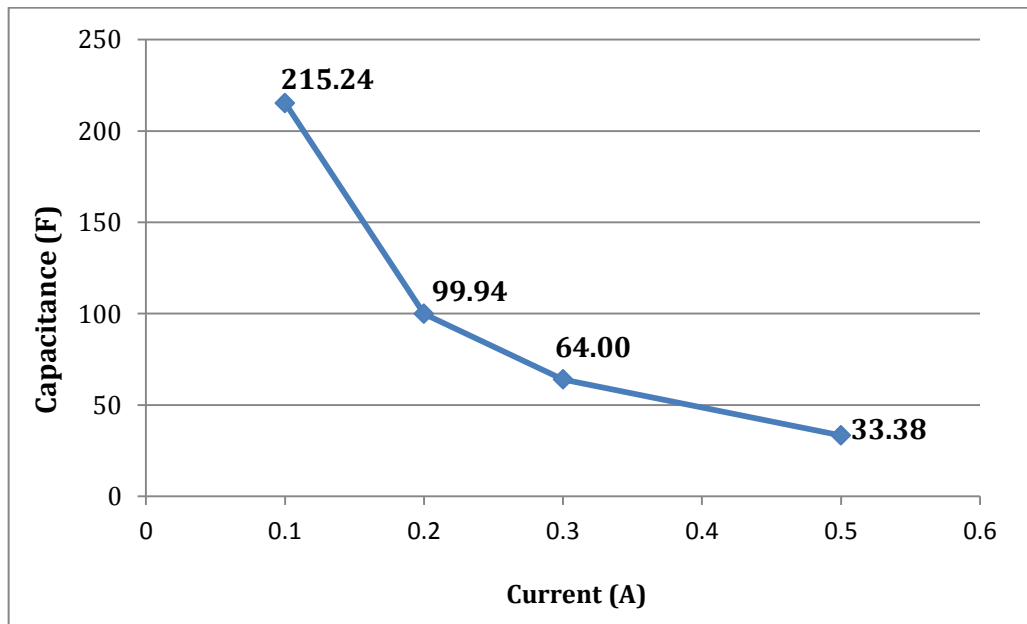
Figure 121 Capacitances of Sample CS34 at different currents (0.1, 0.2, 0.3 and 0.5 A)

2. **Cyclic Voltammetry**
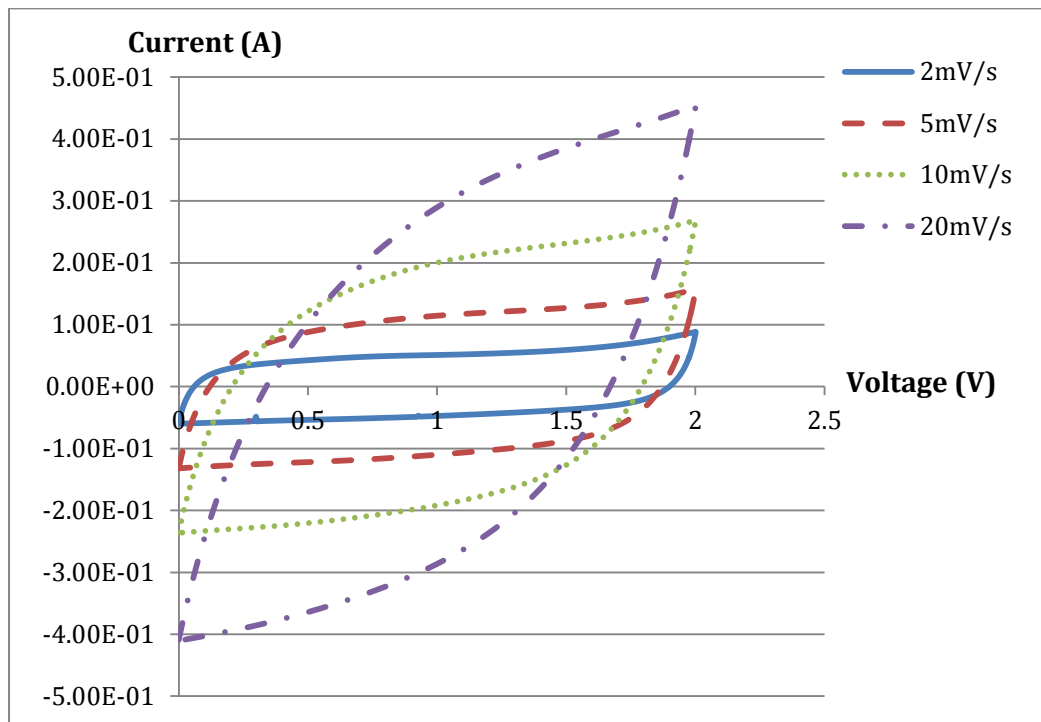
Figure 122 Cyclic Voltammograms at various scan rates (2, 5, 10, 20mV/s)
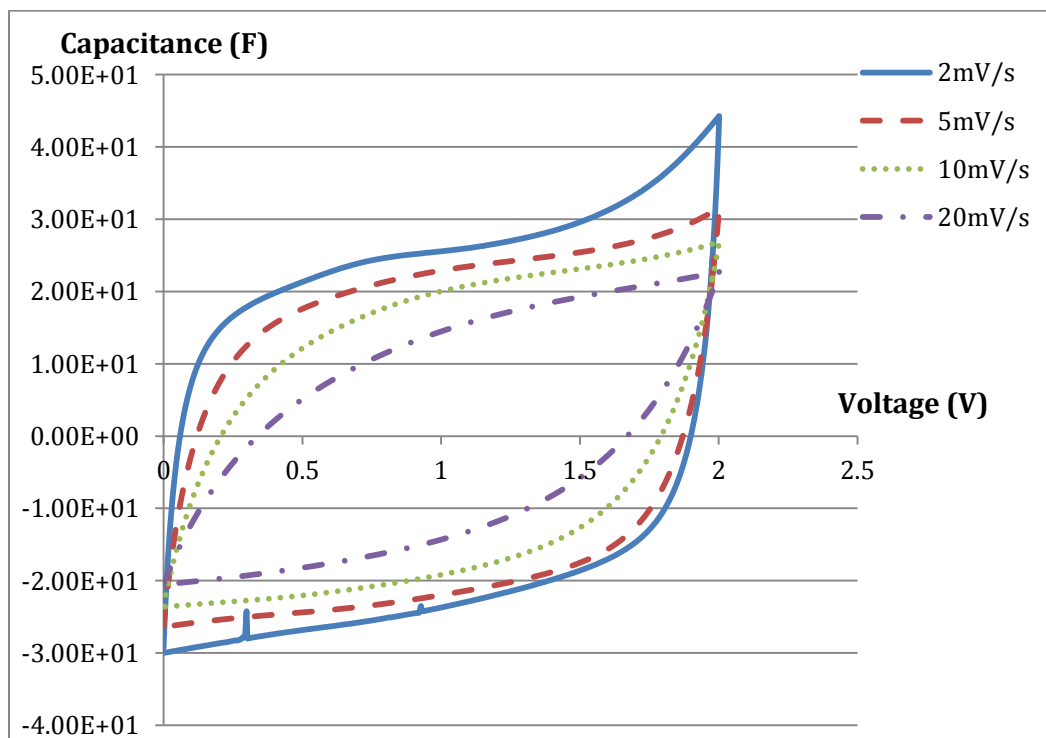
Figure 123 Capacitance plots of Sample CS34 at various scan rate (2, 5, 10, 20mV/s)
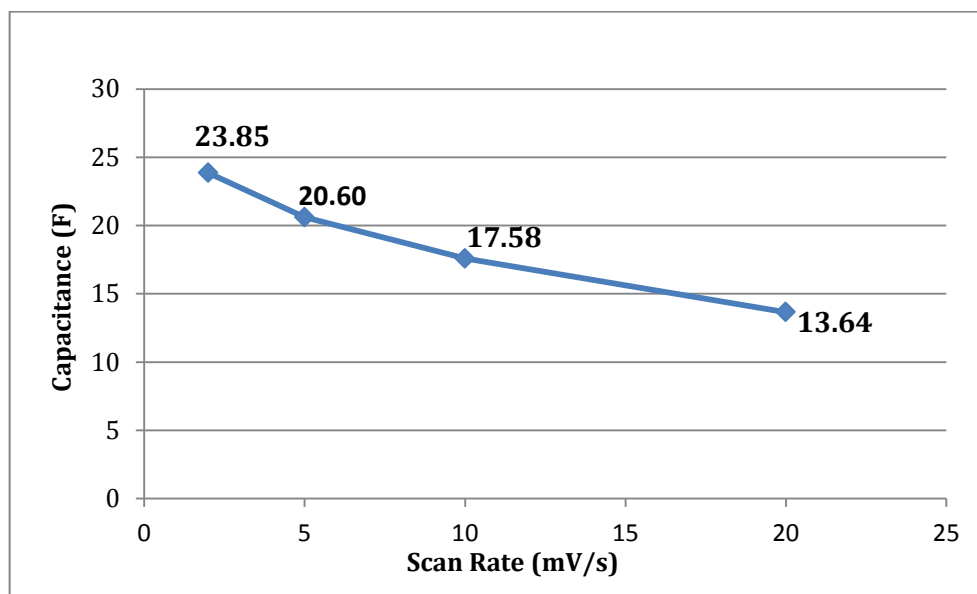
Figure 124 Overall capacitance of Sample CS34 at different scan rates (2, 5, 10, 20mV/s)

4.3.2 Summary and analysis

The graphs above are summarised and explained here. Value of capacitance for the three samples shown above is summarised in the figure and table below. The capacitance obtained from CV and charge-discharge test profiles shown previously is inconsistent. From observation, the curves in charge-discharge testing does not start from zero volts and consistently started from around 0.5V. This is due to the pre-treatment was not done correctly, for example, the supercapacitor was not discharge to zero completely before glavonastic charge-discharge test begins.
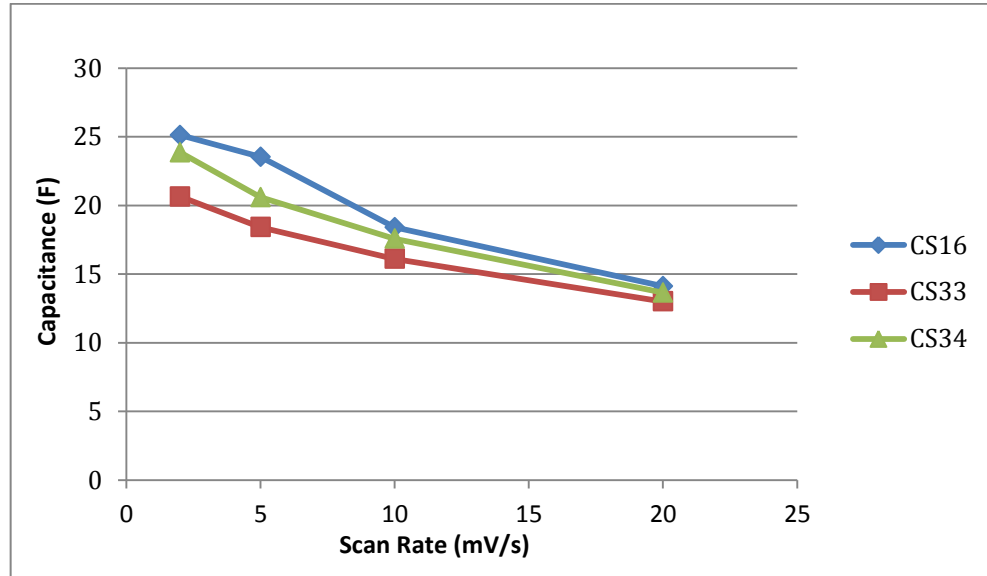
Figure 125 Capacitance for Supercapacitor Samples at different scan rates

Table 66 Capacitance for Supercapacitors at different scan rate

Supercapacitor	Capacitance at different scan rate			
	2mV/s	5mV/s	10mV/s	20mV/s
CS16	25.11	23.53	18.40	14.11
CS33	20.64	18.41	16.10	13.01
CS34	23.85	20.60	17.58	13.64

Table 67 Capacitance for Supercapacitors at different current

Supercapacitor	Capacitance at different current (F)			
	0.1A	0.2A	0.3A	0.5A
CS16	225.0	221.0	69.06	36.49
CS33	187.55	85.60	52.91	29.69
CS34	215.24	99.94	64.00	33.38

Table 67 above shows the capacitance of the supercapacitors at different

scan rate. From the equation shown in Section 3.3.1,

$$C = \frac{I}{s}$$ **Equation 44**

where is C the capacitance, I the applied electric current and

s is the scan rate.

Based on the Figure 125 and Table 66, it can be said that decreasing the sweep rate results in increasing the total capacitance of the supercapacitor. Lowering the sweep rates allows more amount of time for the ions to access the bulk of holes on the active material.

More importantly, from the profile shown above, the capacitance values going down the table is not consistent. By comparing readings for the same settings of the test procedure, the capacitance value spread over a wide range within the same scan rate shown in Table 66 and 67. We reckon that the supercapacitor fabrication process can be optimised to obtain smaller standard deviation for capacitance. To ensure a robust process, a novel optimization technique is introduced in the next section. The novelty consists of including a genetic algorithm within the Taguchi technique to optimise the normalised signal-to-noise ratio of the process for multiple output response. It proves that the capacitance and ESR are closer to the target value with the implemented strategy.

4.3.2 Optimization of process factors in Supercapacitor fabrication using the Genetic Algorithm within Taguchi Signal-to-Noise ratios

As mentioned in Section 3.3.2, L4 is used for DOE orthogonal array. All the trials were conducted and the results are shown in the Table 68. Three samples were produced for each run (experiment with the same setting of low and high level). The capacitance and ESR performance for the samples were tested using an Autolab Potentiostat (PGSTAT302N) under cyclic voltammetry and galvanostatic charge-discharge tests respectively. Table 69 summarizes the transformation values of raw data from the Table 68 into SNR and Z. Response 1 – capacitance (Farad, F) is calculated using Equation 66 while response 2 ESR (Ohm, Ω) is calculated using Equation 67 below. The calculation is based on the CV curve and Charge-discharge curve tested using Autolab. These testing profiles are shown in Appendix A6. Calculation is done using the Equation below. It is shown in Appendix A6.

$$Capacitance$$

$$= \frac{1}{2}$$

$$\cdot \left(\frac{|Charge\ at\ higher\ potential\ (Q^+| + |Charge\ at\ lower\ potential\ (Q^-)|}{Potential\ (V)} \right.$$

Equation 66
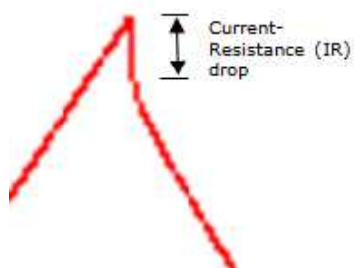
Figure 126 Charge and Discharge Curve

Table 68 Experimental output data

Process	Experiment, i	$(y_c)_n$ - Capacitance (F)			$(y_E)_n$ - ESR (Ω)		
		Sample 1	Sample 2	Sample 3	Sample 1	Sample 2	Sample 3
1	1	0.989	1.074	1.105	12.15	19.05	18.45
Mixing	2	1.942	2.070	2.074	12.80	4.70	14.15
	3	2.231	2.441	2.399	3.20	6.60	2.00
	4	1.624	1.675	1.820	9.05	17.45	11.20
2	1	2.035	2.039	2.132	2.30	3.50	3.15
Calendaring	2	2.583	2.440	2.654	2.35	2.05	3.20
	3	1.967	1.901	1.979	2.85	2.06	2.35
	4	2.140	2.173	2.406	2.25	3.00	2.95
3	1	2.295	2.462	2.409	2.85	2.50	2.55
Drying	2	2.558	2.317	2.680	2.30	2.90	2.75
	3	2.681	2.338	2.578	2.70	2.95	2.30
	4	2.448	2.581	2.459	2.45	2.50	2.70
4	1	1.757	1.901	1.653	3.35	2.85	3.00
Electrolyte	2	2.457	2.590	2.468	2.56	2.61	2.81
Treatment	3	1.622	1.598	1.605	5.10	6.45	4.25
	4	2.293	2.556	2.558	2.40	2.50	2.30

The equivalent series resistance, ESR value can be determined by using the following equation and the calculation and test profile are shown in Appendix A6.

$$\text{ESR } (\Omega) = \frac{difference\ between\ IR\ drop\ (V)}{current\ (I)} \qquad \textbf{Equation 67}$$

Table 69 shows the values for signal-to-noise ratio for capacitance and ESR output responses ($(SNR)_{ic}$ and $(SNR)_{iE}$). Response 1 – capacitance (Farad, F) is calculated using Equation 68 while response 2 ESR (Ohm, Ω) is calculated using Equation 69. For a clearer view, an example is shown below to illustrate how the values are obtained.

\

For experiment, i=1 in mixing process,

SNR for the capacitance response (larger-the-better)

$SN_{iC} = -10\,log_{10}(1/n)\sum_{i=1}^{n}\frac{1}{y_i^2}$ **Equation 68**

SN_{1C}

$$= -10log_{10}(\frac{1}{n}\left[\frac{1}{(y_{c1})^2 + (y_{c2})^2 + (y_{c3})^2}\right]$$

$$= -10log_{10}\left(\frac{1}{3}\left[\frac{1}{(0.989)^2 + (1.074)^2 + (1.105)^2}\right]\right)$$

$$= 10.03$$

SNR for the ESR response (smaller-the-better)

$SN_{iE} = -10\,log_{10}(1/n)\sum_{i=1}^{n}y_i^2$ **Equation 69**

SN_{1E}

$$= -10log_{10}(\frac{1}{n}[(y_{E1})^2 + (y_{E2})^2 + (y_{E3})^2]$$

$$= -10log_{10}\left(\frac{1}{3}[(12.15)^2 + (19.05)^2 + (18.45)^2]\right)$$

$$= -24.53$$

where y_i is the experimental data at the ith sample and n is the

number of samples.

In Table 69, the negative on the SNR for the ESR response indicates

that the smaller-the-better for this output response.

Table 69 Weighted SNR (WSNR) Values

Process	Experiment, i	$(SNR)_{ic}$	$(SNR)_{iE}$	Z_{ic}	Z_{iE}	$WSNR_i$
1 **Mixing**	1 2 3 4	10.03 *15.69* 16.99 14.19	-24.53 *-21.22* -12.85 -22.32	0.578 0.656 0.600 0.420	0.362 0.393 0.580 0.581	0.5778 *0.6557* 0.5998 0.4202
2 **Calendaring**	1 2 3 4	15.85 17.71 *15.34* 16.56	-9.62 -8.23 *-7.75* -8.80	0.3471 0.5561 0.6154 0.3747	0.4306 0.3333 0.5443 0.3556	0.3484 0.5526 *0.6143* 0.3744
3 **Drying**	1 2 3 4	17.11 17.58 *17.63* 17.45	-8.43 -8.50 *-8.51* -8.14	0.5609 0.5546 0.5666 0.3609	0.6190 0.4167 0.4615 0.6000	0.5612 0.5539 *0.5661* 0.3621
4 **Electrolyte** **Treatment**	1 2 3 4	14.52 *17.52* 13.67 16.34	-9.75 *-8.50* -14.55 -7.61	0.4731 0.3609 0.4306 0.6642	0.5667 0.6000 0.5379 0.5000	0.5649 *0.5953* 0.5358 0.5032

Output response for capacitance and ESR are also used to calculate

normalised SNR for the implemented GA fitness function to find the optimal

weights for each process. This is important to see which process factor has the

most influence to that particular process. Transformation SNR to normalised

SNR (Z_{ic} and Z_{iE}) is done using Equation 70 and Equation 71. For mixing

process and first experiment, the working is shown below:

Normalised SNR for the capacitance response (the-larger-the-

better) [13];

$$Z_{iC} = (Y_{avg.} - Y_{min})/Y_{max} - Y_{min})$$ **Equation 70**

$$Z_{1C} = (1.056 - 0.989)/1.105 - 0.989) = 0.578$$

Where Y_{avg} = is the average out of the n number of samples

produced, $Y_{avg} = \dfrac{y_{cn}}{n} = \dfrac{0.989+1.074+1.105}{3} = 1.056$

$Y_{min} = 0.989$ and $Y_{max} = 1.105$ are the least and highest data

value out of the n number of samples produced respectively.

Normalised SNR for the ESR response (the-smaller-the-better)

[13];

$$Z_{iE} = (Y_{max} - Y_{avg})/Y_{max} - Y_{min})$$ **Equation 71**

$$Z_{1E} = (19.05 - 16.55)/(19.05 - 12.15) = 0.362$$

where Y_{avg} is the average out of the n number of samples

produced, $Y_{avg} Y_{avg} = \dfrac{y_{En}}{n} = \dfrac{12.15+19.05+18.45}{3} = 16.55$

$Y_{min} = 12.15$ and $Y_{max} = 19.05$ are the least and highest data

value out of the n number of samples produced respectively.

These normalised SNR (Z_{ic} and Z_{iE}) values are used for GA fitness function

(Equation 72). By applying the implemented GA fitness function to the GA

programming, the optimal weight of w_c and w_E are found to determine the weighted normalised SNR, WSNR. Optimal weights for each response are obtained using the GA. From the GA simulation, weights for each process are maximized with the calculated SN ratio as shown in Table 69.

For example, in Process 1, w_c and w_E were found to be 0.9990 and 0.0001 respectively. From the GA simulation, the optimal weights are [0.9990, 0.0001].

$$F(x) = \sum_{j=1}^{k} \sum_{i=1}^{n} (W_j Z_{ij}) \qquad\qquad \textbf{Equation 72}$$

$$F(x) = w_c \cdot (0.578 + 0.656 + 0.600 + 0.420) + w_E \cdot (0.632 +$$

$$0.393 + 0.580 + 0.581)$$

The objective of this algorithm is to find the optimal weights so as to maximize the normalised SNR. Therefore, at the maximum point in the GA simulation, w_c and w_E were obtained and shown in Table 70.

Table 70 Optimal w_c and w_E

Process	w_C	w_E
1	0.9990	0.0001
2	0.9844	0.0156
3	0.9951	0.0049
4	0.0196	0.9804

To determine the value of $WSNR_i$ which is shown in Table 70:

For mixing process, experiment $i = 1$, optimal weights were obtained early is used to calculate the value $WSNR_i$.

$$WSNR_i = w_c\,Z_{iC} + w_E\,Z_{iE}$$

$$WSNR_1 = 0.999 Z_{1C} + 0.0001 Z_{1E}$$

$$WSNR_1 = 0.999 * (0.578) + 0.0001 * (0.362)$$

$$= 0.577$$

WSNR values for each trial and each process were computed (by substituting the w_C and w_E values into the WSNR formula as shown above), it was noticed that in Process 1 (mixing), experiment 2 (run 2) has the highest WSNR value. If we refer back to Table 35, it corresponds to A1, B2, C2 as the desired setting for the Process 1. However, this approach is less accurate as the interactions between factors and levels have not yet been taken into account. The same can be implied for the rest of the processes (Process 2, 3 and 4). A better approach is shown to evaluate the main effects on WSNR for each process factor using Equation 58, 59, 60, 61, 62 and 63 were performed to obtain the average WSNR. For example, for mixing process, for factor A1, L1 and L2 (which is shown in Table 71) are calculated using Equation 58 and Equation 59:

low level, L1 $= (WSNR_1 + WSNR_2) / 2$

$\qquad = (0.5778 + 0.6557) / 2$

$\qquad = 0.6167$ where $WSNR_1$ and $WSNR_2$ are taken from Table 69.

However,

for high level, L2 $= (WSNR_3 + WSNR_4) / 2$

$\qquad = (0.59998 + 0.4202) / 2$

$\qquad = 0.510$ where $WSNR_1$ and $WSNR_2$ are taken from Table 69.

This average WSNR values indicates the effect on the low and the high level for each factor. The higher the difference between the minimum (factor at low level) and maximum (factor at high level) is, the greater the effect it will have. Hence, in Table 71, ($WSNR_{max}$ -$WSNR_{min}$) provides the details of the main effects on WSNR. Figure 127 consists of four sets of the main effect plot for the respective process fabrication. This is a way to illustrate the information

obtained from Table 71. It provides the predicted optimal conditions for the process optimization. For Process 1, the optimal condition predicted is A_1, B_1, C_2 as for having higher WSNR values. Process 2 on the other hand is A_2, B_1, C_2 while Process 3 is A_1, B_1, C_2 and Process 4 is also A_1, B_1, C_2. An observation that can be seen is that Factor C (machine temperature) in Process 2 (calendaring) has the biggest margin with 0.2221 differences of its two levels. This tells us that such factor is quite sensitive if we change the level values thus it is a significant factor in producing a good quality of process or product. On the other hand, the very small margin of 0.0011 obtained in Process 4 (electrolyte treatment) and Factor B (molarity) indicates that such factor does not have much effect on the outcome if we change the level values. In a later section, a more appropriate way for determining significant and insignificant factors using ANOVA will be discussed.

Table 71 Main Effects on WSNR for every factor investigated of the respective process

Process	Factors	Low Level, L1	High Level, L2	$WSNR_{max}$ - $WSNR_{min}$
1 Mixing	A Mixing Speed	0.6167	0.5101	0.1066
	B Mixing Time	0.5889	0.5379	0.0509
	C Amount of AC	0.4990	0.6278	0.1288
2 Calendaring	A Calendaring time	0.4505	0.4943	0.0438
	B Thickness	0.4813	0.4635	0.0178
	C Machine temp.	0.3614	0.5835	0.2221
3 Drying	A Heating time	0.5575	0.4641	0.0934
	B Heating temp.	0.5636	0.4580	0.1057
	C Vacuum	0.4617	0.5600	0.0984
4 Electrolyte Treatment	A Electrolyte name	0.5801	0.5195	0.0606
	B Electrolyte molarity	0.5504	0.5493	0.0011
	C Electrolyte amount	0.5340	0.5656	0.0315

a.P1- (mixing)	b.P2-(calendaring)
c.P3-(drying)	d.P4-(electrolyte treatment)
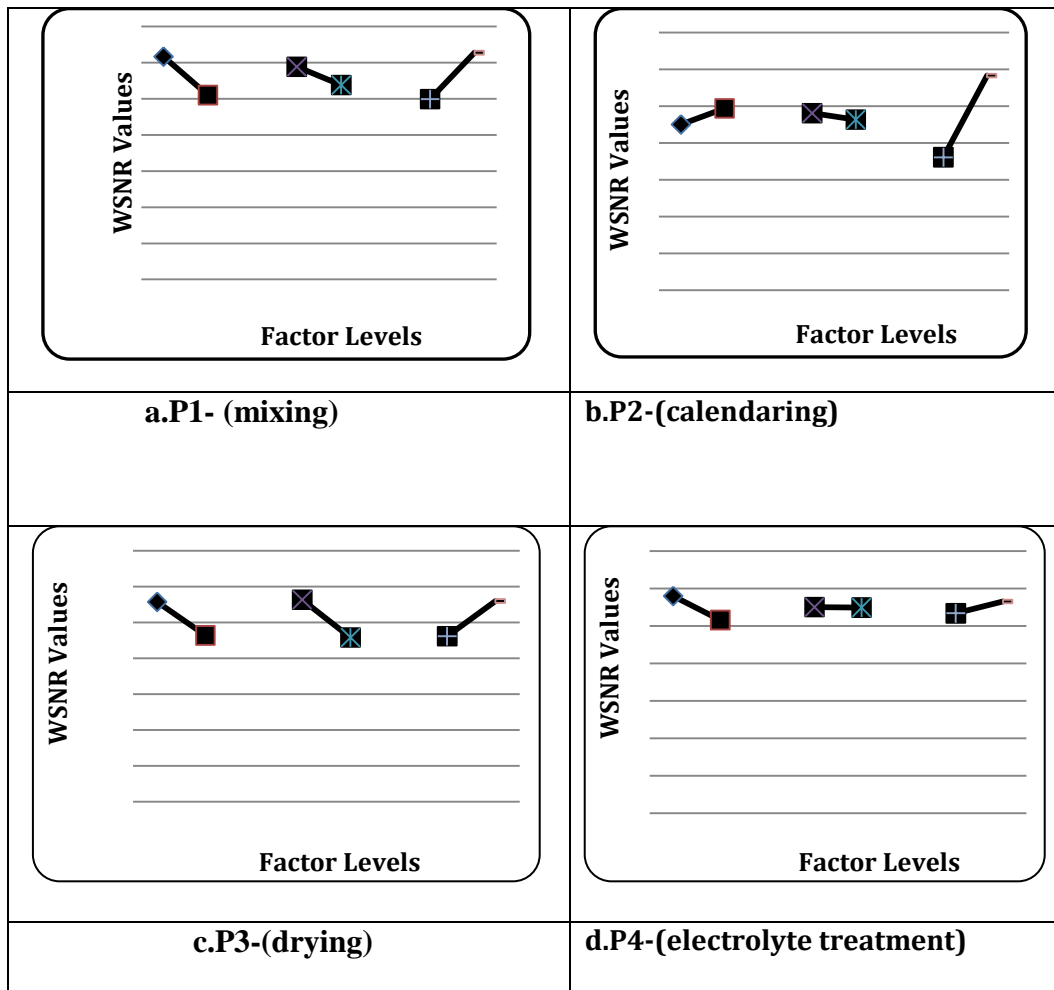
Figure 127 Factor effects on WSNR

Confirmation experiment

In confirmation of the predicted optimal settings obtained from the proposed Taguchi-GA approach, verification tests were conducted and another three samples were each produced and the results obtained are tabulated in Table 72. To evaluate the findings, a comparison of the standard deviation (SD) for all of the trials is conducted. The smaller value of SD implies the consistency of the samples and thus indicates that they are close to the target value. Consistency is related to process repeatability and robustness of product.

Table 72 Experimental output data for confirmation experiments

Process	Output Response		
	Sample 1	Sample 2	Sample 3
P1-Mixing (A_1, B_1, C_2)	2.425 F; 1.602 Ω	2.388 F; 3.691 Ω	2.403 F; 2.925 Ω
P2-Calendaring (A_2, B_1, C_2)	2.051 F; 1.811 Ω	2.026 F; 2.008 Ω	2.095 F; 1.760 Ω
P3-drying (A_1, B_1, C_2)	2.294 F; 2.571 Ω	2.310 F; 2.529 Ω	2.244 F; 2.708 Ω
P4-electrolyte treatment (A_1, B_1, C_2)	2.199 F; 1.98 Ω	2.222 F; 1.85 Ω	2.213 F; 2.00 Ω

The standard deviations (SD) were obtained using the following formula;

$$SD = \sqrt{\frac{N \sum (X^2) - \sum X)^2}{N\,N-1)}}$$

Equation 73

where N is the number of replication and X is the experimental data.

Table 73 SD for each experiment and under optimal conditions

Process	Experiment, i	SD (capacitance)	SD (ESR)
1	1	0.0601	3.8223
	2	0.0751	5.1110
	3	0.1766	2.3861
	4	0.1111	4.3636
	5 (A_1, B_1, C_2)	0.0186	1.0568
2	1	0.0549	0.6171
	2	0.1090	0.5965
	3	0.0420	0.3996
	4	0.1445	0.4193
	5 (A_2, B_1, C_2)	0.0349	0.1310
3	1	0.0853	0.1893
	2	0.1847	0.3122
	3	0.1760	0.3279
	4	0.0738	0.1323
	5 (A_1, B_1, C_2)	0.0650	0.0936
4	1	0.1245	0.2566
	2	0.0738	0.1323
	3	0.0123	0.1094
	4	0.1524	0.1000
	5 (A_1, B_1, C_2)	0.0116	0.0814

Table 73 shows that the predicted condition in every process yields a certain extent of improvement of capacitance and ESR standard deviation. Standard deviation for experiments 1 – 4 in Table 73 are the standard deviation before the process is optimised using Taguchi-GA method, whereas, experiment 5 is the standard deviation result after Taguchi-Ga method was applied. Overall, the standard deviation is improved. Such findings proved that the novel Taguchi-GA have successfully optimised the weighs and has thus maximized the values of SN ratio for both responses.

The SNRs for the initial condition are obtained by assigning 0.7 weighting for the capacitance response and 0.3 for the ESR response arbitrarily, based on the consensus that the capacitance performance should dominate the ESR response before conducting the GA approach. The GA method then searches for the optimal weightings that maximize the SNR for both responses to improve the performance of process factors. Refer to the outcome in thesis [287], experiments for few different value of OEC were carried out and different capacitance to ESR ratio (combinations total = 1) have also been tested - 0.6:0.4, 0.2:0.8 etc. It was found that after the capacitance ratio being altered gradually for example 0.2, 0.3, 0.4 etc, the outcome results in the same experimental run (e.g. Run 2) as the best run for the respective process. However, until at a certain ratio (e.g 0.8:0.2) the results turn up to give a different experimental run (e.g. Run 3) as the best run. This shows that the weight has certain impact on the optimal setting to be predicted. If that is so, there is a chance to fully optimise the SNR. This can be done without using engineering judgment.

For this case study, only one weight ratio of 0.7:0.3, was used for the OEC computation and comparison after considered that this OEC value has higher SNR value (shown in [287]). This is treated as the initial condition. It is compared with the WSNR obtained using the integrated Taguchi and GA method in the later part.

Table 74 OEC values to determine the optimal setting for the initial condition

Process	Experiment, i	Combination	OEC (0.7:0.3 weighting)
1	1	A_1, B_1, C_1	0.5125
	2	A_1, B_2, C_2	0.5756
	3	A_2, B_1, C_2	0.5940
	4	A_2, B_2, C_1	0.4669
2	1	A_1, B_1, C_1	0.3754
	2	A_1, B_2, C_2	0.5641
	3	A_2, B_1, C_2	0.5941
	4	A_2, B_2, C_1	0.3112
3	1	A_1, B_1, C_1	5.8250
	2	A_1, B_2, C_2	5.1260
	3	A_2, B_1, C_2	5.3430
	4	A_2, B_2, C_1	4.3260
4	1	A_1, B_1, C_1	0.5012
	2	A_1, B_2, C_2	0.2526
	3	A_2, B_1, C_2	0.4628
	4	A_2, B_2, C_1	0.6149

The overall improvement percentage is determined as the ratio between sums of the improvement values of all responses for the confirmation experiment (after optimised using Taguchi-GA method) and the sum of the SNRs of initial responses for all responses. Using the method shown in [256], this is called the addictive model. It is used to predict the anticipated improvements under the chosen optimum conditions (optimal level of the process factor); the SNRs for these two output responses are predicted and

shown in Table 75 (last column, improvement). For a clearer view, taking Process 1 (mixing) as an example,

$Improvement\ for\ capacitance$

$= SNR\ for\ confirmation\ (after\ optimisation)$

$- SNR\ for\ intial\ condition\ using\ OEC\ (before\ optimization)$

$= 17.166 - 16.99 = 0.176$

$Improvement\ for ESR$

$= SNR\ for\ confirmation\ (after\ optimisation)$

$- SNR\ for\ intial\ condition\ using\ OEC\ (before\ optimization)$

$= (|12.85| - |9.164|) = 3.686$

$Improvement\ in\ \%$

$$= \frac{sum\ of\ the\ improvement\ for\ two\ responses\ in\ db}{sum\ of\ the\ SNR\ for\ inital\ condition}$$

$$\times 100\% = \frac{(0.176 + 3.686)}{16.99 + |12.85|} \times 100\% = 12.9\%$$

Table 75 Initial, predicted and actual improvement of SN ratio

Process	Responses	Initial condition (dB)	Predicted condition (GA) (dB)	Confirmation (dB)	Improvement (dB)
1	SNR_c	16.99	15.69	17.166	0.176
	SNR_E	-12.85	-21.22	-9.164	3.686
	Optimal setting	A_2, B_1, C_2*	A_1, B_2, C_2**	A_1, B_1, C_2***	
	Overall improvement in (dB %)				**12.9 %**
2	SNR_c	15.34	15.34	15.340	0.000
	SNR_E	-7.75	-7.75	-5.798	1.952
	Optimal setting	A_2, B_1, C_2*	A_2, B_1, C_2**	A_2, B_1, C_2***	
	Overall improvement in (dB %)				**8.4 %**
3	SNR_c	17.11	17.63	17.18	0.07
	SNR_E	-8.43	-8.51	-8.31	0.12
	Optimal setting	A_1, B_1, C_1*	A_2, B_1, C_2**	A_1, B_1, C_2***	
	Overall improvement in (dB %)				**0.7 %**
4	SNR_c	16.34	17.52	16.44	0.10
	SNR_E	-7.61	-8.50	-5.78	1.83
	Optimal setting	A_2, B_2, C_1*	A_2, B_1, C_2**	A_1, B_1, C_2***	
	Overall improvement in (dB %)				**8.1 %**

* The setting combination for process level is obtained from OEC (overall evaluation criteria) computation (0.7:0.3) shown in Table 74, which the highest OEC is chosen for the optimum level for the process factor.

** The setting combination for process level is predicted using the highest WSNR given in Table 69. For example, in process 1 (mixing), the highest WSN value is at run 2 (experiment 2), hence, SNR for predicted setting combination for the process level is 15.69 for capacitance and -21.22 for ESR which are taken in Table 69 (the italic value).

***By using the output responses shown in Table 68 and apply the values to Equation 67 and Equation 68, the SNR values are calculated for the confirmation experiment (after optimised using Taguchi-GA method).

Table 75 presents how the combination of the initial condition is made by selecting the highest OEC values in every fabrication process. The SNRs of

those experimental runs that based on the processing parameters as in Table 75 are compared with the SNRs of the experiments which use WSNR values shown in Table 69. In Table 75, it is observed that 12.9%, 8.4% and 8.1% improvement in dB was obtained for the mixing, calendaring and electrolyte treatment process respectively by using the proposed Taguchi-GA approach. However, the drying process does not produce much improvement (0.7% only). One possible reason for this small improvement is that the optimization has reached its certain limit for given factors and levels assigned. Unless different factors are added in to be investigated, this could further improve the process.

The purpose of ANOVA in this study is to determine which of the process factors are significantly affect the performance characteristics [256] in the supercapacitor fabrication. To achieve this, the total variability of the multi-objective WSNR measured by the sum of squared deviations is separated from the total mean of WSNR, before converting into percentage contribution for every individual factor. This part was implemented by utilizing the Qualitek-4 software. Some of the factors are pooled to avoid calling something significant when it is not. This is to maximize the percentage contribution of the dominant and significant factors. Table 76 displays the ANOVA results.

Table 76 Results of ANOVA analysis on WSNR

Process	Factor	DOF	Sum of Squares	% Contribution
1	A	1	0.011	37.181
	B	1	0.002	8.360
	C	1	0.016	54.130
	Error	0		
	Total	3	0.030	100 %
2	A	1	0.001	3.16
	B	(1)	(0)	POOLED
	C	1	0.049	96.00
	Error	1	-0.01	0.84
	Total	3	0.051	100 %
3	A	1	0.008	29.230
	B	1	0.011	37.973
	C	1	0.009	32.458
	Error	0		
	Total	3	0.029	100 %
4	A	1	0.003	91.503
	B	(1)	(0)	POOLED
	C	1	0.001	24.803
	Error	1	-0.001	-16.306
	Total	3	0.004	100 %

Consequently, optimal conditions for every process can be set as A_1, B_1, C_2 for the mixing process, A_2, B_1, C_2 for the calendaring process, A_1, B_1, C_2 for the drying process, and A_1, B_1, C_2 for the electrolyte process. It is found that the most significant process factor for the respective process is in the sequence of machine temperature (96%) in the calendaring process, followed by the KCl electrolyte (91.503%) in the electrolyte treatment process, the amount of activated carbon (54.13%) in the mixing process, and finally the heating temperature (37.97%) in the drying process. Such process factors with a high percentage contribution obtained statistically are believed to have a huge impact towards the performance of the supercapacitor fabricated and outcome shown in Table 76 is good for future improvement where process factors that has low percentage contribution can be eliminated.

4.3.2.1 Summary

The supercapacitor fabrication process dealing with a multi response problem has been presented. From the experimental and analytical results, the conclusions are as follows:

- Taguchi method has successfully minimised the cost and time span of the experimental procedure consisting of three factors and two-level each. Only four trials are required when using the orthogonal array experiment.

- The proposed integrated approach has improved the SNR (dB) as shown in the Figure 128 below. Hence, optimal conditions have great influences on the design factors with less sensitivity to the noise factors.
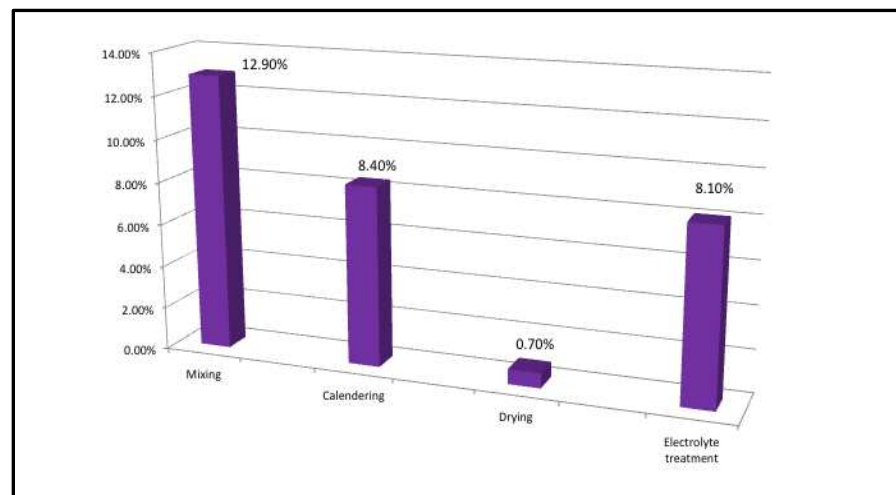
Figure 128 Percentage of SNR improvement after optimization as compared to using OEC method

- The proposed Taguchi-GA integrated strategy provides a robust design in the sense of reproducibility and reliability. This could not be achieved by the OEC approach alone as this approach is dependent on engineering judgment that has higher variation, a mean value that is far from the desired target value if those judgments were inaccurately made. The figure below shows that the standard deviation for both

output response (Capacitance and ESR) is improved as compared with

the conventional method (Taguchi and OED method).
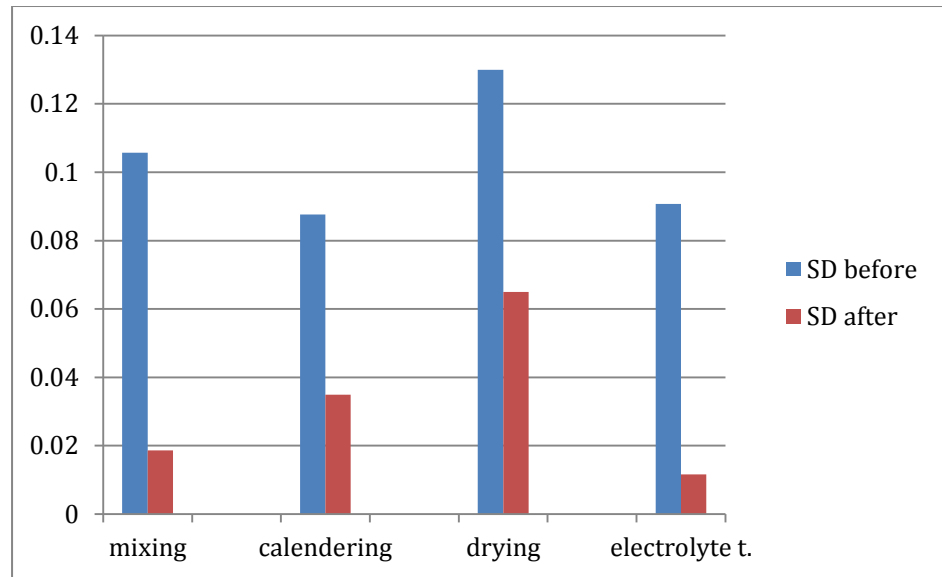
Figure 129 Standard deviation comparison before & after optimisation (Capacitance)
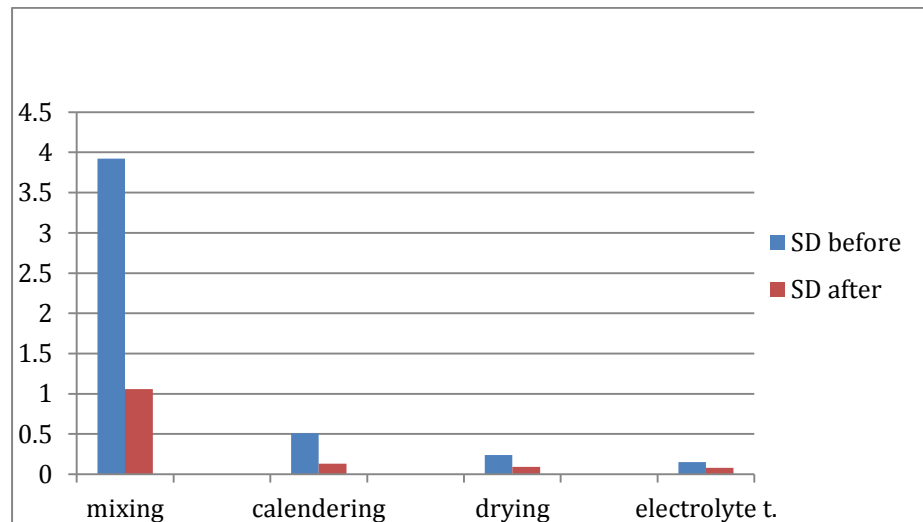
Figure 130 Standard deviation comparison before & after optimisation (ESR)

- The optimum process setting ensures optimum values for capacitance and ESR. By applying the optimum process setting (process condition), consistent capacitance and ESR values of supercapacitors are

345

guaranteed as shown in the lower standard deviation values as compared to the standard deviation for the samples which were not applied Taguchi-GA optimisation method. This is important for the optimised supercapacitor-battery hybrid energy storage system. This is to ensure power reliability of the system.

CHAPTER 5

CONCLUSION

This project dealt with the integration of supercapacitors into a battery energy storage system for solar applications in order to optimise overall cost by prolonging battery lifespan utilizing the Genetic Algorithm (GA) and Support Vector Machine (SVM) further reliability was optimised by using Genetic Algorithm within the Taguchi technique to reduce spread in tolerance of supercapacitors values which affect system performance.

The main achievement in this research is to minimise operational cost of a solar system by integrating supercapacitors into a hybrid lead acid battery energy management system. It has been accomplished as described in Table 77. This project sought to investigate and solve the research issues arising from combining supercapacitors with batteries in a hybrid energy system which is then made economically feasible thru process and operational optimization. This was done using a GA and a supervised learning machine – Support Vector Machine (SVM) to in place of costly power electronics (dc-dc converter). The general literature review on this subject and specifically in this context of optimising the supercapacitor-battery hybrid energy storage system in solar application is inconclusive on several vital research issues on pairing the supercapacitor and battery in an energy storage system. Simulation and optimization on model which involves supercapacitor could not be done in most of the commercial optimization software such as HOMER, HYBRID and etc. However, in this project, the implemented fitness function in GA has

successfully optimised the cost of the Supercapacitor-battery hybrid energy storage system by reducing the rate of battery damage mechanism.

It is also interesting to state that the overall cost of the implemented SB-HESS was further optimised by applying SVM and SVR (Support Vector Regression) within the energy management system which accurately predicts the load demand in advance. This was done by replacing part of the power electronics with intelligent software which allows the improvement of efficiency and lowers the cost of other components such as in eliminating the need for a bi-directional dc-dc converter used in balancing the voltage level between supercapacitor and battery. This is very crucial to make sure that the systems does not run the risk of draining the battery due to the supercapacitor acting as an additional load if its voltage is lower than the batteries nominal voltage as both energy storage devices are in direct parallel connection.

This implemented system is more cost effective as it is integrated with the wide availability and affordability of microcontrollers which allows these hybrid systems to be controlled using purely software methods such as by employing the Support Vector Machine (SVM) pattern classifier to decide when to switch energy sources depending on the load requirement. This supervised learning system was used to predict load demand before it occurs. It is proven that aids in reducing the delay in delivering power even when there are a few possibilities to be considered in connecting or disconnecting battery and supercapacitor to the load. This not only lowers the operational cost, but at the same time, allows the hybrid photovoltaic system to be flexible, which comes in handy in places with different seasons and unpredictable weather. The implementation using a microcontroller also allows the monitoring of multiple

parameters, which may affect the efficiency of the hybrid photovoltaic systems, optimising the operation of these systems by taking appropriate actions when needed.

The cost of the implemented system i.e the supercapacitor-battery hybrid energy storage system (SB-HESS) is reduced by approximately 7.51% compared to the conventional individual battery energy storage system. In SB-HESS, the number of batteries used was optimised to a lower number of batteries without jeopardizing the system power reliability. Some systems reviewed in literature use more batteries to bridge the mismatch between power supply and load demand. These batteries are assigned to primary and secondary energy storage and the secondary group of batteries acts as a backup and cater for sudden power bursts. This is not practical because the oversized energy storage system elevates the cost of the total renewable energy system. In contrast, in this project the pairing of supercapacitor and battery reduces system cost and is also advantageous to the environment because it cuts down the number of batteries. Supercapacitor can be completely refurbished after its cycle life of 16-20 years with much less chemical hazard.

Fuel cells with hydrogen tank is one of the alternatives in adding an energy buffer to the renewable energy system. However, the size of this energy storage device is huge and the catalyst used in fuel cells is expensive. Supercapacitor on the other hand is known as a high power density energy storage device which charges and discharges power fast to the load (in seconds). It was proven in this study the supercapacitor in SB-HESS is able to deliver the sudden power burst. The size of the supercapacitor is comparatively smaller but stores a larger amount of energy.

As shown in the simulation result in Section 4.2.2 , the overall cost for batteries which consists of the initial cost of battery, replacement cost of batteries, operational and maintenance of batteries have the significant impact in the overall system cost which makes the conventional renewable energy system less cost effective. The total number of batteries used throughout the project lifetime is 40 and 24 for battery-only system and SB-HESS respectively. Including supercapacitors within the system with proper methodology aids in prolonging battery life in the long run by maintaining high a state-of-charge (SOC) in the battery. In SB-HESS, the battery SOC is higher than the battery SOC in a battery only energy storage system by 6%.

One further aim in reducing overall costs is to be able to propose a method of consistently manufacturing robust supercapacitor cells which are able to conform to the standards previously mentioned Section 3.3. This aids in reducing the cost of producing a supercapacitor.

A supercapacitor, which has high reproducibility and reliability, was manufactured in this project where the process factors of the fabrication process are optimised using a genetic algorithm within the Taguchi signal-to-noise ratio method. It is important to ensure a robust process in the manufacture of the supercapacitor before it is integrated in the power system to meet peak power demand. This is because slight variation in supercapacitor values will affect the performance of the overall system. System is optimised and designed with the different value of LPSP (loss of power supply probability). An orthogonal array was used in designing the experiment instead of the full factorial of design-of-experiment (DOE) in order to save cost and time by reducing the size of the experiment. Capacitance and ESR are the output response which were

considered in the supercapacitor manufacturing process. In the conventional way of dealing with multi-response optimization, a method known as, overall evaluation criterion (OEC) is used to optimise the process factor. This method greatly involves engineering and expert judgement which is susceptible to human error and prejudiced experience. Whereas, the integration of genetic algorithm within the Taguchi signal-to-noise ratio has successfully improved the result obtained using the conventional technique – OEC. Standard deviation is improved using integrated GA-Taguchi method.

The objectives and deliverables were achieved as shown in the following:

Table 77 Project Objective and Achievements

No.	Objectives	Achievements/Deliverables
1.	To identify and optimise the significant parameters of the fabrication process simultaneously, by combining the Genetic Algorithm with Taguchi DOE methodology and improving the Taguchi Signal-to-noise Ratio which is a measure of product robustness.	• A more robust process fabrication supercapacitor is implemented as the standard deviation is improved. • Avoid SB-HESS running in the risk of draining the battery as the SB-HESS was designed and optimised based on the supercapacitor voltage and capacitance.
2.	To implement a fitness function which determines the optimal size and therefore reduce the cost) of a stand-alone hybrid supercapacitor-lead acid battery solar energy	• A simulation and optimization on SB-HESS is delivered using constraint optimization GA. • Initial cost, replacement cost, operational and maintenance of

	system using a Genetic Algorithm.	the batteries are reduced.
3.	To design a supercapacitor-lead acid battery hybrid energy storage system, which prolongs battery life and reduces the number of batteries used.	• SOC of battery in SB-HESS is higher than the battery individual energy storage system. It signifies that the battery life can be prolonged. • The cost of the system is optimised with the presence of supercapacitor.
4.	To employ Support Vector Machine in the hybrid energy storage control system in order to reduce the use expensive power electronic components.	• Further reduced the operational cost by placing some of the power electronics without jeopardizing the system power reliability. • A load predictive energy management system using SVM is implemented.

The study has offered a methodology on constraint optimization using GA to optimise the overall cost of implementing supercapacitor-battery hybrid energy storage system in solar applications. A main effort is the construction of prototype for the optimised supercapacitor-battery hybrid energy storage system with SVM energy management system to control the energy flow between supercapacitor and battery without any time delay in responding to the required power burst. As a direct outcome of this methodology, the study encountered a number of possible enhancements which need to be considered in the future for a high power specification for solar application.

5.1 Future Work

A prototype on supercapacitor-battery hybrid energy storage system (SB-HESS) is implemented. The benefits of this implemented system are feasible for outskirt rural area. However, for a bigger scale of SB-HESS in renewable energy system, a higher DC bus voltage and higher power for the system are needed for power outputs up to 12kW.

As mentioned, in the implemented system, balancing circuit is not included as to save the cost. However, this could cause imbalance individual voltages of any single cell exceeds its maximum recommended working voltage. As consequence, it could result in electrolyte decomposition, gas generation, ESR increase and ultimately reduce supercapacitor lifespan. For the implemented optimized supercapacitor-battery hybrid energy storage system, the cost was optimised based on the assumption that the supercapacitor has no maintenance cost throughout the project lifetime. A bipolar supercapacitor could introduce in this hybrid energy storage system for better power reliability in terms of charging and discharging phase (high level of cycling an active voltage). The nature of the bipolar supercapacitor mechanism allows the resistance of the bipolar design lower (no current collection voltage drops) and the packaging weight is less. High voltage bipolar supercapacitor stacks have been fabricated and that functioned well. It is believed that the manufacturing cost of the bipolar supercapacitor would be lower and helps in cost reduction of the hybrid energy storage system in the future.

In spite of the accuracy in the current supervised machine learning – SVM energy management system, data input for the training and testing phase

in SVM and SVR could be improved by collecting features of more dimensions of independent and dependant data input for classification and regression.

To improve performance, data involving weather forecast of the particular site can be included in the methodology for optimal sizing of the SB-HESS i.e. more constraints could be analysed to evaluate the fitness function. This will increase the practicability of the constraint optimization algorithm.

The capacitance and ESR of the resulting supercapacitors characterized by cyclic voltammetry (CV) and galvanostatic charge–discharge test in this research. However, prior knowledge of electrical circuit theory or electrochemistry is assumed for the output response obtained. However, the real world contains circuit elements that exhibit much more complex behaviour. These elements force us to abandon the simple concept of resistance, and in its place we use impedance, a more general circuit parameter. Like resistance, impedance is a measure of the ability of a circuit to resist the flow of electrical current, but unlike resistance, it is not limited by the simplifying properties in ohm's law. Electrochemical impedance can be measured using Electrochemical Impedance Spectroscopy (EIS). It is a well-established experimental technique that has applications in coatings, corrosion, sensors, electrochemical double layer capacitors, batteries among others. EIS partly has ability to access a very wide range of frequencies (typically from MHz to μHz). Having said that, parameters such as the internal resistance, electrode surface capacitance and leakage are accessible at different frequencies across the spectrum.

If the fund is permitted in the future, the packaging process in the supercapacitor manufacturing plant should also be considered to further optimised the standard deviation and make the process even more robust.

Moreover, adding more level shall be considered in the DOE (Design of Experiment) using Taguchi orthogonal array. This is believed to aid in the improvement of output responses (supercapacitor capacitance and ESR) instead of the standard deviation of the output response only.

REFERENCES

[1]   "British Standard BS-EN 62391-1:2006. Fixed Electric Double-Layer Capacitor for use in electronic equipment," June 2006.

[2]   D. E. Goldberg, Genetic Algorithms in Search, Optimization, and Machine Larning, Addison-Wesley, 1989.

[3]   L. Kang Seok and G. Zong Woo, "A new meta-heuristic algorithm for continuous engineering optimization: harmony search theory and practice," Computer Methods in Applied Mechanics and Engineering, vol. 194, no. 36-38, pp. 3902-3933, 2005.

[4]   G. Helton Cristiano , Francisco de Assis das Neves and Marcone Jamilson Freitas Souza, "Multi-objective metaheuristic algorithms for the resource-constrained project scheduling problem with precedence relations," Computers & Operations Research, vol. 44, pp. 92-104, 2014.

[5]   J. Holland, Adaptation in Natural and Artificial Systems, University of Michigan Press, Ann Arbor, MI (1975), 1975.

[6]   J. H. David E. Goldberg, "Genetic Algorithms and Machine Learning," Machine Learning, vol. 3, no. 2-3, pp. 95-99, October 1988.

[7]   M. Srinivas and Lalit M.Patnaik, "Genetic Algorithms: A Survey," IEEE Computer , vol. 27, no. 6, pp. 17-26, June 1994.

[8]   S.N. Sivanandam and S.N. Deepa, Introduction to Genetic Algorithm, Springer, 2008.

[9]   Andries P. Engelbrecht, Computational Intelligence (An Inroduction), John Wiley 7 Sons, Ltd., 2007.

[10]   K.F. Man, K.S. Tang and S. Kwong, "Genetic Algorithms: Concepts and Applications," IEEE Transaction on Indusctrial Electronics, vol. 43, no. 5, October 1996.

[11]   Franci Cus and Joze Balic, Robotics and Computer-Integrated Manufacturing, vol. 19, no. 1-2, pp. 113-121, 2003.

[12]   R. Jeyapaul, P. Shahabudeen and K. Krishnaiah, "Simultaneous optimization of multi-response problems in the Taguchi method using genetic algorithm," The International Journal of Advanced

Manufacturing Technology, vol. 30, no. 9-10, pp. 870-878, October 2006.

[13]   R. K. Roy, Design of experiments using the Taguchi approach : 16 steps to product and process improvement, New York: Wiley, 2001.

[14]   T. LAMBERT, PAUL GILMAN and PETER LILIENTHAL, "CHAPTER 15 MICROPOWER SYSTEM MODELING WITH HOMER," in Integration of Alternative Sources of Energy, John Wiley & Sons, Inc, 2006, pp. 379-418.

[15]   Glavin, M.E., Chan, P.K.W., Armstrong, S and Hurley, W.G, "A stand-alone photovoltaic supercapacitor battery hybrid energy storage system," in Power Electronics and Motion Control Conference, 2008. EPE-PEMC 2008. 13th, Poznan, September 2008.

[16]   Glavin, M.E and Hurley, W.G, "Ultracapacitor/ battery hybrid for solar energy storage," in Universities Power Engineering Conference, 2007. UPEC 2007. 42nd International, Brighton, September 2007.

[17]   Jin-uk Jeong, Hyeoun-dong Lee, Chul-soo Kim, Hang-Seok Choi and Bo-Hyung Cho , "A Development of an Energy Storage System for Hybrid Electric Vehicles Using Supercapacitor," 2002. [Online]. Available: http://pearlx.snu.ac.kr/Publication/IBHFESE02.pdf. [Accessed November 2013].

[18]   Zubieta, L. and Bonert, Richard, "Characterization of double-layer capacitors for power electronics applications," IEEE Transactions on Industry Applications, vol. 36, no. 1, pp. 199 - 205, Jan/Feb 2000.

[19]   W. Lajnef, J.-M. Vinassa, O. Briat, S. Azzopardi and E. Woirgard, "Characterization methods and modelling of ultracapacitors for use as peak power sources," Journal of Power Sources, vol. 168, no. 2, p. 553–560, 1 June 2007.

[20]   Nicolas Bertrand, Jocelyn Sabatier, Olivier Briat and Jean-Michel Vinassa, "Fractional non-linear modelling of ultracapacitors," Communications in Nonlinear Science and Numerical Simulation, vol. 15, no. 5, p. 1327–1337, May 2010.

[21]   G Vining, AI Khuri and RH Myers, "Response Surface Alternatives to the Taguchi Robust Parameter Design Approach," The American Statistician, vol. 46, no. 2, pp. 131-139, 1992.

[22]   E Del Castillo and D Montgomery, "A Nonlinear Programming Solution to the Dual Response Problem," Journal of Quality Technology, 1993.

[23]   Bindner, H., Cronin, T., Lundsager, P., Manwell, J.F., Abdulwahid, U. and Baring-Gould, I., "Lifetime modelling of lead acid batteries," Technical University of Denmark, 2005.

[24]   Ravinder Singh Batia, S. P. Jain, Dinesh Kumar Jain and Bhim Singh, "Battery Energy Storage System for Power Conditioning of Renewable Energy Sources," IEEE PEDS, 2005.

[25]   Garimella, N. and Nair, N.C., "Assessment of battery energy storage systems for small-scale renewable energy integration," in TENCON 2009 - 2009 IEEE Region 10 Conference, Singapore, January 2009.

[26]   Nirmal-Kumar C. Nair and Niraj Garimella, "Battery energy storage systems: Assessment for small-scale renewable energy integration," Energy and Buildings, vol. 42, no. 11, p. 2124–2130, November 2010.

[27]   James P. Dunlop and Brian N. Farhi, "Recommendations for Maximizing Battery Life in Photovoltaic Systems: A Review of Lessons Learned," in Solar Energy: The Power to Choose , Washington, DC, April 2001.

[28]   S. Armstrong, Glavin, M.E and Hurley, W.G., "Comparison of battery charging algorithms for stand alone photovoltaic systems," in Power Electronics Specialists Conference, 2008. PESC 2008. IEEE, Rhodes, June 2008.

[29]   V. Salas, E. Olías, A. Barrado and A. Lázaro, "Review of the maximum power point tracking algorithms for stand-alone photovoltaic systems," Solar Energy Materials and Solar Cells, vol. 90, no. 11, p. 1555–1578, July 2006.

[30]   Duryea, S., Islam, S and Lawrance, W., "A battery management system for stand alone photovoltaic energy systems," in Industry Applications Conference, 1999. Thirty-Fourth IAS Annual Meeting. Conference Record of the 1999 IEEE, Phoenix, AZ, 1999.

[31]   Xie Jun, Zhang Xing, Zhang chongwei and Wang Chengyue, "Research on Bi-Directional DC-DC Converter For a Stand-Alone Photovoltaic Hybrid Energy Storage System," in Power and Energy Engineering Conference (APPEEC), 2010 Asia-Pacific, Chengdu, March 2010.

[32]   R. Kaiser, "Optimized battery-management system to improve storage lifetime in renewable energy systems," Journal of Power Sources, vol. 168, no. 1, p. 58–65, May 2007.

[33]   D. U. Sauer and Heinz Wenzl, "Comparison of different approaches for lifetime prediction of electrochemical systems—Using lead-acid

batteries as example," Journal of Power Sources, vol. 176, no. 2, p. 534–546, February 2008.

[34]   P. D. Aurbach and Shmuel De-Leon , "USA Batteries & Fuel Cells Seminar," Plug-Volt LLC, San Diego, September2012.

[35]   S. Lukic, Wirasingha, S.G., Rodriguez, F., Cao, J. and Emadi, A., "Power Management of an Ultracapacitor/Battery Hybrid Energy Storage System in an HEV," in Vehicle Power and Propulsion Conference, 2006. VPPC '06. IEEE, Windsor, September 2006.

[36]   G. Baudo, Calasanzio, D. and Grossoni, M, "Operational Parameters of SLA Batteries in Standby Applications," in Telecommunications Energy Conference, 1987. INTELEC '87. The Ninth International, Stockholm, Sweden, June 1987.

[37]   J. O'Connor, "Choosing a Lead Acid Battery for Solar Charging," Voltaic, 25 October 2012. [Online]. Available: http://voltaicsystems.com/blog/choosing-a-lead-acid-battery-for-solar-charging/. [Accessed November 2012].

[38]   C. B.E, Electrochemical supercapacitors: scientific fundamentals and technological applications, Springer, 1999.

[39]   E. F. Francois Beguin, Supercapacitors: Materials, Systems and Applications, John Wiley & Sons, April 2013.

[40]   J. Cao and Emadi, A., "A New Battery/UltraCapacitor Hybrid Energy Storage System for Electric, Hybrid, and Plug-In Hybrid Electric Vehicles," Power Electronics, IEEE Transactions, vol. 27, no. 1, pp. 122 - 132, January 2012.

[41]   A. Khaligh and Zhihao Li, "Battery, Ultracapacitor, Fuel Cell, and Hybrid Energy Storage Systems for Electric, Hybrid Electric, Fuel Cell, and Plug-In Hybrid Electric Vehicles: State of the Art," Vehicular Technology, IEEE Transactions on , vol. 59, no. 6, pp. 2806 - 2814, July 2010.

[42]   R. Perez, "Lead-Acid Battery State of Charge vs. Voltage," 1993. [Online]. Available: http://www.scubaengineer.com/documents/lead_acid_battery_charging_graphs.pdf. [Accessed December 2012].

[43]   M. E. V. Team, "A Guide to Understanding Battery Specifications," December 2008. [Online]. Available: http://web.mit.edu/evt/summary_battery_specifications.pdf. [Accessed December 2012].

[44]   Heinz Wenzl, Ian Baring-Gould, Rudi Kaiser, Bor Yann Liaw, Per Lundsager, Jim Manwell, Alan Ruddell and Vojtech Svoboda, "Life prediction of batteries for selecting the technically most suitable and cost effective battery," Journal of Power Sources, vol. 144, no. 2, p. 373–384, 15 June 2005.

[45]   Henry A. Catherino, Fred F. Feres and Francisco Trinidad, "Sulfation in lead–acid batteries," Journal of Power Sources, vol. 129, no. 1, p. 113–120, 15 April 2004.

[46]   "Seal Lead-Acid BAtteries Technical Manual," Powr Sonic.

[47]   S. Drouilhet and B.L. Johnson, "A Battery Life Prediction Method for Hybrid Power Applications," National Renewable Energy Laboratory (NREL), Springfield, VA, January1997.

[48]   H. Yang, W. Zhou, L. Lu and Z. Fang, "Optimal sizing method for stand-alone hybrid solar–wind system with LPSP technology by using genetic algorithm," Solar Energy, vol. 82, no. 4, p. 354–367, April 2008.

[49]   M. E. V. Team, "A Guide to Understanding Battery Specifications," December 2008. [Online]. Available: http://web.mit.edu/evt/summary_battery_specifications.pdf. [Accessed December 2012].

[50]   Deepti, D.J. and Ramanarayanan, V., "State of charge of lead acid battery," in India International Conference on Power Electronics, 2006. IICPE 2006. , Chennai, 19-21 Dec. 2006.

[51]   A. Yu, Victor Chabot and Jiujun Zhang, Electrochemical Supercapacitors for Energy Storage and Delivery: Fundamentals and Applications (Electrochemical Energy Storage and Conversion), America: CRC Press, April 2013.

[52]   P. Sharma and T.S. Bhatti, "A review on electrochemical double-layer capacitors," Energy Conversion and Management, vol. 51, no. 12, p. 2901–2912, December 2010.

[53]   A. Burke, "Ultracapacitors: why, how, and where is the technology," Journal of Power Sources, vol. 91, no. 1, p. 37–50, November 2000.

[54]   "Battery Performance Characteristics," Electropaedia, 2005. [Online]. Available: http://www.mpoweruk.com/performance.htm. [Accessed 6 November 2012].

[55] Xin Zhao, Beatriz Mendoza Sánchez, Peter J. Dobson and Patrick S. Grant, "The role of nanomaterials in redox-based supercapacitors for next generation energy storage devices," The Royal Society of Chemistry 2011 Nanoscale, vol. 3, pp. 839-855, January 2011.

[56] "Review: The Supercapacitor Advantage," CAP-XX, 2008. [Online]. [Accessed 8 November 2012].

[57] T. B. Pawan Sharma, "A review on electrochemical double-layer capacitors," Energy Conversion and management, pp. 2901-2912, 2010.

[58] P. Barker, "Ultracapacitors for use in power quality and distributed resource applications," in Power Engineering Society Summer Meeting, 2002 IEEE , Chicago, IL, USA, July 2002.

[59] J. R. a. S. Miller, "Patrice Electrochemical Capacitors for Energy Management," Science Magazine (Open Archive Toulouse Archive Ouverte (OATAO)), vol. 321, pp. 651-652, 2008.

[60] R. A. Huggins, "Supercapacitors and electrochemical pulse sources," Solid State Ionics, vol. 134, no. 1-2, p. 179–195, October 2000.

[61] L. L. Zhang and X. S. Zhao, "Carbon-based materials as supercapacitor electrodes," The Royal Society of Chemistry 2009, vol. 38, pp. 2520-2531, June 2009.

[62] Martin Winter and Ralph J. Brodd, "What Are Batteries, Fuel Cells, and Supercapacitors?," Chemical Reviews: American Chemical Society, vol. 104, no. 10, pp. 4245-4269, September 2004.

[63] S. K. Martha, B. Hariprakash, S. A. Gaffoor, D. C. Trivedi and A. K. Shukla, "A low-cost lead-acid battery with high specific-energy," Journal of Chemical Sciences, vol. 118, no. 1, pp. 93-98, January 2006.

[64] R. Kötz and M. Carlen, "Principles and applications of electrochemical capacitors," Electrochimica Acta, vol. 45, no. 15-16, p. 2483–2498, 3 May 2000.

[65] Bryoe Gregory, "Ultracapacitor Sizing and Packaging for Cost Effective," IOXUS, Oneonta, New York, 2013.

[66] A. Govindaraj, King, M. and Lukic, S.M., "Performance characterization and optimization of various circuit topologies to combine batteries and ultra-capacitors," in IECON 2010 - 36th Annual Conference on IEEE Industrial Electronics Society, Glendale, AZ, November 2010.

[67]   Fangcheng Liu, Jinjun Liu and Linyuan Zhou, "A novel control strategy for hybrid energy storage system to relieve battery stress," in 2nd IEEE International Symposium on Power Electronics for Distributed Generation Systems (PEDG), 2010 , Hefei, China, 16-18 June 2010.

[68]   Stephen McCluer and Jean-Francois Christin, "Comparing Data Center Batteries, Flywheels and Ultracapacitors," Schneider Electric, 2011.

[69]   A. Shukla, Sampath, S and Vijayamohanan, K, "Electrochemical supercapacitors: Energy storage beyond batteries," Current Science, vol. 79, no. 12, pp. 1656-1661, September 2010.

[70]   L. Solero, Lidozzi, A and Pomilio, J.A., "Design of multiple-input power converter for hybrid vehicles," Power Electronics, IEEE Transactions, vol. 20, no. 5, pp. 1007 - 1016, September 2005.

[71]   G. Nielson and Emadi, A., "Hybrid energy storage systems for high-performance hybrid electric vehicles," in Vehicle Power and Propulsion Conference (VPPC), 2011 IEEE, Chicago, IL, September 2011.

[72]   A. Saplin, Meintz, A. and Ferdowsi, M., "Parametric study of alternative EV1 powertrains," in Vehicle Power and Propulsion Conference, 2008. VPPC '08. IEEE, Harbin, September 2008.

[73]   T. Kinjo, Senjyu, T., Urasaki, N. and Fujita, H., "Output levelling of renewable energy by electric double-layer capacitor applied for energy storage system," Energy Conversion, IEEE Transactions, vol. 21, no. 1, pp. 221 - 227, March 2006.

[74]   Tatsuto Kinjo, Tomonobu Senjyu, Katsumi Uezato and Hideki Fujita, "Output leveling of wind power generation system by EDLC energy storage system," Issue Electrical Engineering in Japan, vol. 154, no. 4, pp. 34-41, 20 JAN 2006.

[75]   K. Harada, Sakai, E., Anan, F. and Yamasaki, K., "Basic characteristics of electric double-layer capacitors controlled by switching converters," in Telecommunications Energy Conference, 1996. INTELEC '96., 18th International, Boston, MA, October 1996.

[76]   R. Dougal, Liu, Shengyi and White, R.E., "Power and life extension of battery-ultracapacitor hybrids," Components and Packaging Technologies, IEEE Transactions, vol. 25, no. 1, pp. 120 - 131, March 2002.

[77]   J. Lima, Corleta, J.M., Medeiros, A., Canalli, V.M. , Antunes, F., Libano, F.B. and Dos Reis, F.S., "A PIC controller for grid connected PV system using a FPGA based inverter," in Industrial Electronics,

2000. ISIE 2000. Proceedings of the 2000 IEEE International Symposium, Cholula, Puebla, 2000.

[78]   Y. Chen, Smedley, K. and Brouwer, J., "A Cost-effective Three-phase Grid-connected Inverter with Maximum Power Point Tracking," in Industry Applications Conference, 2006. 41st IAS Annual Meeting. Conference Record of the 2006 IEEE, Tampa, FL, October 2006.

[79]   L. Gao, Dougal, R.A and Liu, Shengyi, "Power enhancement of an actively controlled battery/ultracapacitor hybrid," Power Electronics, IEEE Transactions, vol. 20, no. 1, pp. 236 - 243, January 2005.

[80]   L. Ju-Jinn, "Intelligent Energy Management System for Battery Supercapacitor Hybrid Storage in PV Systems," The University of Nottingham, Malaysia Campus, Semenyih, 2011.

[81]   S. Dinesh, "Utilization of Support Vector Machines (SVM) to Forecast Load requirements in a Hybrid Battery -supercapacitor Energy Storage System," The University of Nottingham, Malaysia Campus, Semenyih, 2012.

[82]   J. Wang and Shuyi Sun, "Predictive Control Based on Support Vector Machine Model," in Intelligent Control and Automation, 2006. WCICA 2006. The Sixth World Congress on (Volume:1), Dalian, 2006.

[83]   C.-W. Hsu and Chih-Jen Lin, "A comparison of methods for multiclass support vector machines," Neural Networks, IEEE Transactions, vol. 13, no. 2, pp. 415 - 425, March 2002.

[84]   B.-J. Chen, Ming-Wei Chang and Chih-Jen Lin, "Load forecasting using support vector Machines: a study on EUNITE competition 2001," Power Systems, IEEE Transactions, vol. 19, no. 4, pp. 1821 - 1830, November 2004.

[85]   B.-J. C. a. C.-J. L. Ming-Wei Chang, "EUNITE Network Competition: Electricity Load Forecasting (2001)," Department of Computer Science and Information Engineering National Taiwan University, Taiwan, 2001.

[86]   N. Sapankevych and Sankar, Ravi, "Time Series Prediction Using Support Vector Machines: A Survey," Computational Intelligence Magazine, IEEE, vol. 4, no. 2, pp. 24 - 38, May 2009.

[87]   B.-L. Zhang and Zhao-Yang Dong, "An adaptive neural-wavelet model for short term load forecasting," Electric Power Systems Research, vol. 59, no. 2, p. 121–129, September 2001.

[88]   Martin Law, "A Simple Introduction to Support Vector Machines," 2010. [Online]. Available: http://www.cise.ufl.edu/class/cis4930sp11dtm/notes/intro_svm_new.pdf . [Accessed December 2012].

[89]   Vapnik, V.N. , "An overview of statistical learning theory," IEEE Transactions on Neural Networks, vol. 10, no. 5, pp. 988 - 999, Sep 1999.

[90]   Steve R. Gunn, "Support Vector Machines for Classification and Regression," May 1998. [Online]. Available: http://ce.sharif.ir/courses/85-86/2/ce725/resources/root/LECTURES/SVM.pdf. [Accessed Dec. 2012].

[91]   Isa, D., Lee, L.H., Kallimani, V. and RajKumar, R., "Text Document Preprocessing with the Bayes Formula for Classification Using the Support Vector Machine," IEEE Transactions on Knowledge and Data Engineering, vol. 20, no. 9, pp. 1264 - 1272, Sept. 2008.

[92]   Muhsin Hassan, Rajprasad Rajkumar, Dino Isa and Roselina Arelhi, "Pipeline Defect Classification by Using Non-Destructive Testing and Improved Support Vector Machine Classification," International Journal of Engineering and Innovative Technology (IJEIT), vol. 2, no. 7, pp. 85-93, January 2013.

[93]   K. -R. Müller, A. J. Smola, G. Rätsch, B. Schölkopf, J. Kohlmorgen and V. Vapnik, "Predicting time series with support vector machines," Artificial Neural Networks — ICANN'97 Lecture Notes in Computer Science, vol. 1327, pp. 999-1004, 1997.

[94]   Dino Isa and Rajprasad Rajkumar, "PIPELINE DEFECT PREDICTION USING SUPPORT VECTOR MACHINES," Applied Artificial Intelligence: An International Journal, vol. 23, no. 8, pp. 758-771, 05 Oct 2009.

[95]   Simon S. Haykin, Neural Networks: A Comprehensive Foundation, Prentice Hall International, 1999.

[96]   Nello Cristianini and John Shawe-Taylor, An Introduction to Support Vector Machines and Other Kernel-based Learning Methods, Cambridge University Press, 2000.

[97]   Zakria Hussain, "Malaysian Machine Learning Workshop," 2011.

[98]   [Online]. Available: http://www.imtech.res.in/raghava/rbpred/svm.jpg. [Accessed Dec 2012].

[99]   Ming Ge, R. Du, Guicai Zhang and Yangsheng Xu, "Fault diagnosis using support vector machine with an application in sheet metal stamping operations," Mechanical Systems and Signal Processing, vol. 18, no. 1, p. 143–159, January 2004.

[100]   "Support Vector Machine," 2010. [Online]. Available: http://scikit-learn.org/stable/modules/svm.html.. [Accessed December 2012].

[101]   Chih-Wei Hsu and Chih-Jen Lin, "A comparison of methods for multiclass support vector machines," IEEE Transactions on Neural Networks, vol. 13, no. 2, pp. 415 - 425, Mar 2002.

[102]   Chih-Wei Hsu, Chih-Chung Chang and Chih-Jen Lin, "A Practical Guide to Support Vector Classification," April 2010. [Online]. Available: https://www.cs.sfu.ca/people/Faculty/teaching/726/spring11/svmguide.pdf. [Accessed 2011].

[103]   Chih-Chung Chang and Chih-Jen Lin, "LIBSVM: A library for support vector machines," Journal ACM Transactions on Intelligent Systems and Technology (TIST), vol. 2, no. 3, April 2011 .

[104]   Qiong Li, Qinglin Meng, Jiejin Cai, Hiroshi Yoshino and Akashi Mochida, "Predicting hourly cooling load in the building: A comparison of support vector machine and different artificial neural networks," Energy Conversion and Management, vol. 50, no. 1, p. 90–96, January 2009.

[105]   Qiong Li, Qinglin Meng, Jiejin Cai, Hiroshi Yoshino and Akashi Mochida, "Applying support vector machine to predict hourly cooling load in the building," Applied Energy, vol. 86, no. 10, p. 2249–2256, October 2009.

[106]   Han Zhonghe, Zhu Xiaoxun and Yang Xiaojing, "Training Method of Support Vector Regression Based on Multi-dimensional Feature and Research on Forecast Model of Vibration Time Series," in 2010 International Conference on Intelligent Computation Technology and Automation (ICICTA), Changsha, 11-12 May 2010.

[107]   Qiong Li, Xiaoke Zhou and Yunlong Xu, "A Hybrid Support Vector Regression for Time Series Prediction," in Third International Conference on Knowledge Discovery and Data Mining, 2010. WKDD '10, Phuket, 9-10 Jan. 2010.

[108]   Ling Xiang, Yongli Zhu and Gui-ji Tang, "A Hybrid Support Vector Regression for Time Series Forecasting," in WRI World Congress on Software Engineering, 2009. WCSE '09, Xiamen, 19-21 May 2009.

[109]   Xiaoh Wang and Deh Wu, "Intelligent Prediction for Time Series Using Smooth Support Vector Regression," in IEEE International Symposium on Knowledge Acquisition and Modeling Workshop, 2008. KAM Workshop 2008, Wuhan, 21-22 Dec. 2008.

[110]   Setiawan, A., Koprinska, I. and Agelidis, V.G., "Very short-term electricity load demand forecasting using support vector regression," in International Joint Conference on Neural Networks, 2009. IJCNN 2009, Atlanta, GA, 14-19 June 2009.

[111]   Outhred, H., "The competitive market for electricity in Australia: why it works so well," in Proceedings of the 33rd Annual Hawaii International Conference on System Sciences, 2000., Hawaii, 4-7 Jan. 2000.

[112]   Iain MacGill, Hugh Outhred and Karel Nolles, "Some design lessons from market-based greenhouse gas regulation in the restructured Australian electricity industry," Energy Policy, vol. 34, no. 1, p. 11–25, January 2006.

[113]   Stojanović Miloš B., Božić Miloš M. and Stanković Milena M., "Mid-term load forecasting using recursive time series prediction strategy with support vector machines," Facta universitatis - series: Electronics and Energetics 2010, vol. 23, no. 3, pp. 287-298, 2010.

[114]   Reshma Khemchandani, Jayadeva and Suresh Chandra, "Regularized least squares fuzzy support vector regression for financial time series forecasting," Expert Systems with Applications, vol. 36, no. 1, p. 132–138, January 2009.

[115]   Jayadeva, Khemchandani, R. and Chandra, S., "Regularized Least Squares Fuzzy Support Vector Regression for Time Series Forecasting," in International Joint Conference on Neural Networks, 2006. IJCNN '06, Vancouver, BC, 2006.

[116]   Haibin Cheng, Pang-Ning Tan, Jing Gao and Jerry Scripps, "Multistep-Ahead Time Series Prediction," Advances in Knowledge Discovery and Data Mining Lecture Notes in Computer Science, vol. 3918, pp. 765-774, 2006.

[117]   Alex J. Smola and Bernhard Schölkopf, "A tutorial on support vector regression," Statistics and Computing, vol. 14, no. 3, pp. 199-222, August 2004.

[118]   N. E. Yik, "Implementation of the Support Vector Machine (SVM) for load prediction in a prototype hybrid supercapacitor-battery energy storage system for solar energy applications by using a simulated load profile for training and testing," The University of Nottingham ,

Malaysia, 2013.

[119] Mao XueMin and Yang Jie, "Time Series Prediction Using Nonlinear Support Vector Regression Based on Classification," in International Conference on Computational Intelligence for Modelling, Control and Automation, 2006 and International Conference on Intelligent Agents, Web Technologies and Internet Commerce, Sydney, NSW, Nov. 28 2006-Dec. 1 2006.

[120] Mori, H. and Kurata, E., "An efficient kernel machine technique for short-term load forecasting under smart grid environment," in Power and Energy Society General Meeting, 2012 IEEE, San Diego, CA, 22-26 July 2012.

[121] "Gaussian Processes," scikit learn, [Online]. Available: http://scikit-learn.org/dev/modules/gaussian_process.html. [Accessed 2012].

[122] Hassan, M., Rajkumar, R., Isa, D. and Arelhi, R., "Kalman Filter as a pre-processing technique to improve the support vector machine," in 2011 IEEE Conference on Sustainable Utilization and Development in Engineering and Technology (STUDENT), Semenyih, 20-21 Oct. 2011.

[123] Dunlop, E.D., Halton, D. and Ossenbrink, H.A., "20 years of life and more: where is the end of life of a PV module?," in Conference Record of the Thirty-first IEEE Photovoltaic Specialists Conference, 2005., 3-7 Jan. 2005.

[124] M.N.G.V.V.G. Kellogg W.D., "Generation unit sizing and cost analysis for stand-alone wind photovoltaic and hybrid wind/PV systems," IEEE Trans Energy Conversion, vol. 13, no. 1, p. 70–75, March 1998.

[125] John Schaeffer and Doug Pratt, Gaiam Real Goods solar living sourcebook : your complete guide to renewable energy technologies and sustainable living, Gaiam Real Goods, 2005.

[126] A. Ter-Gazarian and N. Kagan, "Design model for electrical distribution systems considering renewable, conventional and energy storage units," IEE Proceedings C (Generation, Transmission and Distribution), vol. 139, no. 6, p. 499 – 504, November 1992.

[127] N. Anglani and Muliere, G., "Analyzing the impact of renewable energy technologies by means of optimal energy planning," in 2010 9th International Conference on Environment and Electrical Engineering (EEEIC), Prague, Czech Republic, 16-19 May 2010.

[128] S. Mizani and Yazdani, A, "Design and operation of a remote microgrid," in Industrial Electronics, 2009. IECON '09. 35th Annual

Conference of IEEE, Porto, 3-5 Nov. 2009.

[129] O. Erdinc and M. Uzunoglu, "Optimum design of hybrid renewable energy systems: Overview of different approaches," Renewable and Sustainable Energy Reviews, vol. 16, no. 3, p. 1412–1425, April 2012.

[130] D. Connolly, H. Lund, B.V. Mathiesen and M. Leahy, "A review of computer tools for analysing the integration of renewable energy into various energy systems," Applied Energy, vol. 87, no. 4, p. 1059–1082, April 2010.

[131] W. Isherwood, J.Ray Smith, Salvador M Aceves, Gene Berry, Woodrow Clark, Ronald Johnson, Deben Das, Douglas Goering and Richard Seifert, "Remote power systems with advanced storage technologies for Alaskan villages," Energy, vol. 25, no. 10, p. 1005–1020, October 2000.

[132] K. A. H. D. A. Mousa, "Design of a hybrid solar-wind power plant using optimization," Engineering Systems Management and Its Applications (ICESMA), pp. 1-6, 2003.

[133] C. Darras, S. Sailler, C. Thibault, M. Muselli, P. Poggi, J.C. Hoguet, S. Melscoet, E. Pinton, S. Grehant, F. Gailly, C. Turpin, S. Astier and G. Fontès, "Sizing of photovoltaic system coupled with hydrogen/oxygen storage based on the ORIENTE model," International Journal of Hydrogen Energy, vol. 35, no. 8, p. 3322–3332, April 2010.

[134] E. Mazhari, Jiayun Zhao, Nurcin Celik, Seungho Lee, Young-Jun Son and Larry Head, "Hybrid simulation and optimization-based design and operation of integrated photovoltaic generation, storage units, and grid," Simulation Modelling Practice and Theory, vol. 19, no. 1, p. 463–481, January 2011.

[135] B. Y. Ekren and Orhan Ekren, "Simulation based size optimization of a PV/wind hybrid energy conversion system with battery storage under various load and auxiliary energy conditions," Applied Energy, vol. 86, no. 9, p. 1387–1394, September 2009.

[136] A. Akella, M.P. Sharma and R.P. Saini, "Optimum utilization of renewable energy sources in a remote area," Renewable and Sustainable Energy Reviews, vol. 11, no. 5, p. 894–908, June 2007.

[137] W. He, "Simulation module for wind-diesel systems with multiple units," in Proceedings of the Conference on Renewable Energy - Clean Power 2001, London, UK, 17-19 November 1993.

[138] R. Belfkira, Barakat, G, Nicolas, T and Nichita, C, "Design study and

optimization of a grid independent wind/PV/Diesel system," in EPE '09. 13th European Conference on Power Electronics and Applications, 2009., Barcelona, 8-10 September 2009.

[139] R. Belfkira, Nichita, C., Reghem, P. and Barakat, G., "Modeling and optimal sizing of hybrid renewable energy system," in EPE-PEMC 2008. 13th Power Electronics and Motion Control Conference, 2008. , Poznan, 1-3 Sept. 2008.

[140] P. Berberi, Thodhorjani, S. and Aleti, R., "Integration and optimization of alternative sources of energy in a remote region," in 8th International Symposium on Advanced Electromechanical Motion Systems & Electric Drives Joint Symposium, 2009. ELECTROMOTION 2009., Lille, 1-3 July 2009.

[141] W. Schmitt, "Modeling and simulation of photovoltaic hybrid energy systems-optimization of sizing and control," in Twenty-Ninth IEEE Photovoltaic Specialists Conference, 2002., New Orleans, LA, 19-24 May 2002.

[142] S. Malinchik, Roberts, A. and Fierro, S., "Geo-Spatial resource analysis and optimization of investment strategies for renewable energy," in 2010 IEEE Conference on Innovative Technologies for an Efficient and Reliable Electricity Supply (CITRES), Waltham, MA, 27-29 September 2010.

[143] S. Sukumar, Olama, M.M., Shankar, M. and Hadley, S. , "Modeling resource, infrastructure, and policy cost layers for optimizing renewable energy investment and deployment," in 2010 IEEE Conference on Innovative Technologies for an Efficient and Reliable Electricity Supply (CITRES), Waltham, MA, 27-29 September 2010.

[144] Rodolfo Dufo-López, José L. Bernal-Agustín and Franklin Mendoza, "Design and economical analysis of hybrid PV–wind systems connected to the grid for the intermittent production of hydrogen," Energy Policy, vol. 37, no. 8, p. 3082–3095, August 2009.

[145] G. Krajačić, Neven Duić and Maria da Graça Carvalho, "H2RES, Energy planning tool for island energy systems – The case of the Island of Mljet," International Journal of Hydrogen Energy, vol. 34, no. 16, p. 7015–7026, August 2009.

[146] Jose ́ L. Bernal-Agusti ́n and Rodolfo Dufo-López, "Simulation and optimization of stand-alone hybrid renewable energy systems," Renewable and Sustainable Energy, vol. 13, no. 8, p. 2111–2118, October 2009.

[147]   G. Seeling-Hochmuth, "A combined optimisation concet for the design and operation strategy of hybrid-PV energy systems," Solar Energy, vol. 61, no. 2, p. 77–87, August 1997.

[148]   N. Razali and Hashim, A.H., "Backward reduction application for minimizing wind power scenarios in stochastic programming," in 2010 4th International Power Engineering and Optimization Conference (PEOCO), Shah Alam, 23-24 June 2010.

[149]   "Optimizing Clean Power Everywhere," 9 November 2013. [Online]. Available: http://www.homerenergy.com/. [Accessed 30 November 2013].

[150]   E.I. Zoulias and N. Lymberopoulos, "Techno-economic analysis of the integration of hydrogen energy technologies in renewable energy-based stand-alone power systems," Renewable Energy, vol. 32, no. 4, p. 680–696, April 2007.

[151]   S. Rehman, I.M. El-Amin, F. Ahmad, S.M. Shaahid, A.M. Al-Shehri, J.M. Bakhashwain and A. Shash, "Feasibility study of hybrid retrofits to an isolated off-grid diesel power plant," Renewable and Sustainable Energy Reviews, vol. 11, no. 4, p. 635–653, May 2007.

[152]   C. C. Fung, W. Rattanongphisat and C. Nayar, "A simulation study on the economic aspects of hybrid energy systems for remote islands in Thailand," TENCON '02. Proceedings. 2002 IEEE Region 10 Conference on Computers, Communications, Control and Power Engineering, vol. 3, pp. 1966 - 1969 , 28-31 Oct. 2002.

[153]   D. Nelson, M. Nehrir and C. Wang, "Unit sizing and cost analysis of stand-alone hybrid wind/PV/fuel cell power generation systems," Renewable Energy, vol. 31, no. 10, p. 1641–1656.

[154]   Asmerom M. Gilau and Mitchell J. Small, "Designing cost-effective seawater reverse osmosis system under optimal energy options," Renewable Energy, p. 617–630, April 2008.

[155]   M.J. Khan and M.T. Iqbal, "Pre-feasibility study of stand-alone hybrid energy systems for applications in Newfoundland," Renewable Energy, p. 835–854, May 2005.

[156]   K. Karakoulidis, K. Mavridis, D.V. Bandekas, P. Adoniadis, C. Potolias and N. Vordos, "Techno-economic analysis of a stand-alone hybrid photovoltaic-diesel–battery-fuel cell power system," Renewable Energy, p. 2238–2244, August 2011.

[157]   Alam Hossain Mondal and Manfred Denich, "Hybrid systems for

decentralized power generation in Bangladesh," Energy for Sustainable Development, vol. 14, no. 1, p. 48–55, March 2010.

[158] Getachew Bekele and Björn Palm, "Feasibility study for a standalone solar–wind-based hybrid energy system for application in Ethiopia," Applied Energy, p. 487–495, February 2010.

[159] M. Iqbal, "A feasibility study of a zero energy home in Newfoundland," Renewable Energy, vol. 29, no. 2, p. 277–289, February 2004.

[160] S. D. G. Notton, M. Belhamel, M. Haddadi and A. Louche, "Design and techno-economical optimization for hybrid PV/wind system under various meteorological conditions," Applied Energy, p. 968–987, October 2008.

[161] G.J. Dalton, D.A. Lockington and T.E. Baldock, "Feasibility analysis of stand-alone renewable energy supply options for a large hotel," Renewable Energy, p. 1475–1490, July 2008.

[162] Y. Himri, A. Boudghene Stambouli, B. Draoui and S. Himri, "Techno-economical study of hybrid power system for a remote village in Algeria," Energy, p. 1128–1136, July 2008.

[163] MG Hoffman, A Sadovsky, MC Kintner-Meyer and JG DeSteese , "Analysis Tools for Sizing and Placement of Energy Storage in Grid Applications: A Literature Review," PACIFIC NORTHWEST NATIONAL LABORATORY, e United States of America, September 2010 .

[164] Ohsawa, Y., Emura, S. and Arai, K., "Optimal operation of photovoltaic/diesel power generation system by neural network," in Proceedings of the Second International Forum on Applications of Neural Networks to Power Systems, 1993. ANNPS '93., Yokohama, Japan, 1993.

[165] C. Dennis Barley and C. Byron Winn, "Optimal dispatch strategy in remote hybrid power systems," Solar Energy, vol. 58, no. 4-6, p. 165–179, October–December 1996.

[166] C.D. Barley, C.B. Winn, L. Flowers and H.J. Green , "Optimal control of remote hybrid power systems. Part 1: Simplified model," in National Renewable Energy Laboratory , United States, April 1995.

[167] B. Borowy and Z. Salameh, "Methodology for optimally sizing the combination of a battery bank and PV Array in a Wind/PV Hybrid system," IEEE Trans Energy Convers, vol. 11, no. 2, p. 367–375, 1995.

[168] Tomas Markvart, "Sizing of hybrid photovoltaic-wind energy systems," Solar Energy, p. 277–281, October 1996.

[169] Chedid, R and Saliba, Y., "Optimization and control of autonomous renewable energy systems," International Journal of Energy Research, vol. 20, no. 7, pp. 609-624, 1996.

[170] T.R. Morgan, R.H. Marshall and B.J. Brinkworth, "'ARES'—A refined simulation program for the sizing and optimisation of autonomous hybrid energy systems," Solar Energy, p. 205–215, 1997.

[171] S. H. El-Hefnawi, "Photovoltaic diesel-generator hybrid power system sizing," Renewable Energy, p. 33–40, 1998.

[172] B. B. R. M. C. Protogeropoulos, "Sizing and techno-economical optimization for hybrid solar photovoltaic/wind power systems with battery storage," Int J Energy Res, p. 465–479, 1998.

[173] M.a Elhadidy and S.M Shaahid, "Optimal sizing of battery storage for hybrid (wind+diesel) power systems," Renewable Energy, vol. 18, no. 1, p. 77–86, September 1999.

[174] Rodolfo Dufo-López and José L. Bernal-Agustín, "Design and control strategies of PV-Diesel systems using genetic algorithms," Solar Energy, vol. 79, no. 1, p. 33–46, July 2005.

[175] Rodolfo Dufo-López, José L. Bernal-Agustín and Javier Contreras, "Optimization of control strategies for stand-alone renewable energy systems with hydrogen storage," Renewable Energy, vol. 32, no. 7, p. 1102–1126, June 2007.

[176] Eftichios Koutroulis, Dionissia Kolokotsa, Antonis Potirakis and Kostas Kalaitzakis, "Methodology for optimal sizing of stand-alone photovoltaic/wind-generator systems using genetic algorithms," Solar Energy, vol. 80, no. 9, p. 1072–1088, September 2006.

[177] S.M. Shaahid and M.A. Elhadidy, "Technical and economic assessment of grid-independent hybrid photovoltaic–diesel–battery power systems for commercial loads in desert environments," Renewable and Sustainable Energy Reviews, vol. 11, no. 8, p. 1794–1810, October 2007.

[178] S. Ashok, "Optimised model for community-based hybrid energy system," Renewable Energy, vol. 32, no. 7, p. 1155–1164, June 2007.

[179] Hongxing Yang, Zhou Wei and Lou Chengzhi, "Optimal design and

techno-economic analysis of a hybrid solar–wind power generation system," Applied Energy, vol. 86, no. 2, p. 163–169, February 2009.

[180]   B. Ould Bilal, V. Sambou, P.A. Ndiaye, C.M.F. Kébé and M. Ndongo, "Optimal design of a hybrid solar–wind-battery system using the minimization of the annualized cost system and the minimization of the loss of power supply probability (LPSP)," Renewable Energy, vol. 35, no. 10, p. 2388–2390, October 2010.

[181]   Lagorse, J, Paire, D. and Miraoui, A., "Hybrid stand-alone power supply using PEMFC, PV and battery - Modelling and optimization," in International Conference on Clean Electrical Power, 2009 , Capri, 9-11 June 2009.

[182]   Rodolfo Dufo-López and José L. Bernal-Agustín, "Influence of mathematical models in design of PV-Diesel systems," Energy Conversion and Management, vol. 49, no. 4, p. 820–831, April 2008.

[183]   Shahirinia, A.H, Tafreshi, S.M.M, Gastaj, A.H. and Moghaddomjoo, A.R., "Optimal sizing of hybrid power system using genetic algorithm," in International Conference on Future Power Systems, 2005, Amsterdam, 18-18 November 2005.

[184]   Tomonobu Senjyu, Daisuke Hayashi, Atsushi Yona, Naomitsu Urasaki and Toshihisa Funabashi, "Optimal configuration of power generating systems in isolated island with renewable energy," Renewable Energy, vol. 32, no. 11, p. 1917–1933, September 2007.

[185]   Javier Serrano González, Angel G. Gonzalez Rodriguez, José Castro Mora, Jesús Riquelme Santos and Manuel Burgos Payan, "Optimization of wind farm turbines layout using an evolutive algorithm," Renewable Energy, vol. 35, no. 8, p. 1671–1681, August 2010.

[186]   Soteris A. Kalogirou, "Optimization of solar systems using artificial neural-networks and genetic algorithms," Applied Energy, vol. 77, no. 4, p. 383–405, April 2004.

[187]   BK Bala and Saiful Azam Siddique, "Optimal design of a PV-diesel hybrid system for electrification of an isolated island—Sandwip in Bangladesh using genetic algorithm," Energy for Sustainable Development, vol. 13, no. 3, p. 137–142, September 2009.

[188]   Y. Thiaux, J. Seigneurbieux, B. Multon and H. Ben Ahmed, "Load profile impact on the gross energy requirement of stand-alone photovoltaic systems," Renewable Energy, vol. 35, no. 3, p. 602–613, March 2010.

[189]   Katsigiannis, Y.A., Georgilakis, P.S. and Karapidakis, E.S., "Multiobjective genetic algorithm solution to the optimum economic and environmental performance problem of small autonomous hybrid power systems with renewables," Renewable Power Generation, IET, vol. 4, no. 5, pp. 404 - 419, September 2010.

[190]   Logenthiran, T., Srinivasan, D., Khambadkone, A.M. and Raj, T.S., "Optimal sizing of an islanded microgrid using Evolutionary Strategy," in IEEE 11th International Conference on Probabilistic Methods Applied to Power Systems (PMAPS), 2010, Singapore, 14-17 June 2010.

[191]   G. Tina, S. Gagliano and S. Raiti, "Hybrid solar/wind power system probabilistic modelling for long-term performance assessment," Solar Energy, vol. 80, no. 5, p. 578–588, May 2006.

[192]   Hongxing Yang, Lin Lu and Wei Zhou, "A novel optimization sizing model for hybrid solar-wind power generation system," Solar Energy, vol. 81, no. 1, p. 76–84, January 2007.

[193]   J.F. Gonçalves, J.J.M. Mendes and M.G.C. Resende, "A genetic algorithm for the resource constrained multi-project scheduling problem," European Journal of Operational Research, vol. 189, no. 3, p. 1171–1190, 16 September 2008.

[194]   Shyi-Ming Chen and Chung-Ming Huang, "A new approach to generate weighted fuzzy rules using genetic algorithms for estimating null values," Expert Systems with Applications, vol. 35, no. 3, p. 905–917, October 2008.

[195]   Raza, S.M.A., Kamran, F. and Akbar, M., "Dynamic and scenario based elicitation of genetic algorithms of agents for control of distributed power system networks and renewable energy resources," in The 17th International Conference on Microelectronics, 2005 (ICM 2005), 13-15 December 2005.

[196]   Adel Mellit and Soteris A. Kalogirou, "Artificial intelligence techniques for photovoltaic applications: A review," Progress in Energy and Combustion Science, vol. 34, no. 5, p. 574–632, October 2008.

[197]   David A. Shook, Paul N. Roschke, Pei-Yang Lin and Chin-Hsiung Loh, "GA-optimized fuzzy logic control of a large-scale building for seismic loads," Engineering Structures, vol. 30, no. 2, p. 436–449, February 2008.

[198]   Martín Safe, Jessica Carballido, Ignacio Ponzoni and Nélida Brignole, "On Stopping Criteria for Genetic Algorithms," Advances in Artificial Intelligence – SBIA 2004, vol. 3171, pp. 405-413, 2004.

[199] Fessi, B.A., Benabdallah, S., Hamdi, M. and Boudriga, N., "A new genetic algorithm approach for intrusion response system in computer networks," in IEEE Symposium on Computers and Communications, 2009. ISCC 2009, Sousse, 5-8 July 2009.

[200] Mitchell Melanie, An Introduction to Genetic Algorithms, London, England: Massachusetts Institute of Technology, 1999.

[201] Riccardo Poli, Nicholas Freitag McPhee and Jonathan E. Rowe, "Exact Schema Theory and Markov Chain Models for Genetic Programming and Variable-length Genetic Algorithms with Homologous Crossover," Journal Genetic Programming and Evolvable Machines, vol. 5, no. 1, pp. 31 - 70, March 2004.

[202] Mukbel M. Mustafa, "Enhanced Mutation and Crossover Operators for Genetic Algorithms," The University of Nottingham, Malaysia Campus, Malaysia, Decmber 2006.

[203] Charles Karr and L. Michael Freema, Industrial Applications of Genetic Algorithms, United Stateds of America: CRC Press LLC, 1999.

[204] Randy L. Haupt and Sue Ellen Haupt, Practical Genetic Algorithms Second Edition, United States od America: John Wiley & Sons Inc, 2004.

[205] Randy L. Haupt, "An Introduction to Genetic Algorithms for Electromagnetics," IEEE Antennas and Propagation Magazine, vol. 37, no. 2, pp. 7-15, April 1995.

[206] Zbigniew Michalewicz, Dipankar Dasgupta, Rodolphe G. Le Riche and Marc Schoenauer, "Evolutionary algorithms for constrained engineering problems," Computers & Industrial Engineering, vol. 30, no. 4, p. 851–870, September 1996.

[207] D. A. Coley, An Introduction to Genetic Algorithms for Scientists and Engineers, World Scientific Publishing Co. Pte. Ltd., 1999.

[208] W. M. Spears, "The Role of Mutation and Recombination in Evolutionary Algorithms," George Mason University Fairfax, Virginia, 1998.

[209] William M. Spears, "Crossover or Mutation?," 1991.

[210] Hidde de Jong, "Modeling and Simulation of Genetic Regulatory Systems: A Literature Review," Journal of Computational Biology, vol. 9, no. 1, pp. 67-107, July 2004.

[211] Thomas Baeck, D.B Fogel and Z Michalewicz, Evolutionary Computation 2: Advanced Algorithms and Operators, United Kingdom: IOP Publishing Ltd, 2000.

[212] Man, K.F., Tang, K.S. and Kwong, S., "Genetic algorithms: concepts and applications [in engineering design]," IEEE Transactions on Industrial Electronicsx, vol. 43, no. 5, pp. 519 - 534, Oct 1996.

[213] Man, K.F. and Tang, K.S., "Genetic algorithms for control and signal processing," in IECON 97. 23rd International Conference on Industrial Electronics, Control and Instrumentation, 1997. , New Orleans, LA, 9-14 Nov 1997.

[214] Lau Tung Leng, "Guided Genetic Algorithm," Department of Computer Science, University of Essex, United Kingdom.

[215] Horn, J., Nafpliotis, N. and Goldberg, D.E., "A niched Pareto genetic algorithm for multiobjective optimization," in Proceedings of the First IEEE Conference on Evolutionary Computation, 1994. IEEE World Congress on Computational Intelligence. , Orlando, FL, 27-29 Jun 1994.

[216] Niusha Shafiabady, Mohammad Teshnehlab and Mohammad Ali Nekoui, "SOME APPLICATIONS OF S.T. (SHAFIABADY-TESHNEHLAB) EVOLUTIONARY OPTIMIZATION ALGORITHM," International Journal of Innovative Computing, Information and Control, vol. 8, no. 2, pp. 1299-1305, February 2012.

[217] Kalyanmoy Deb, "An efficient constraint handling method for genetic algorithms," Computer Methods in Applied Mechanics and Engineering, vol. 186, no. 2-4, p. 311–338, 9 June 2000.

[218] Manoj Tiwari and Jenny A. Harding, Evolutionary Computing in Advanced Manufacturing, United Stated of America: John Wiley & Sonc Inc., 2011.

[219] Isidor Buchmann, "Supercapacitors coexist with batteries, not compete," Canadian Electronics, 22 November 2011. [Online]. Available: http://www.canadianelectronics.ca/blogs/supercapacitors-coexist-with-batteries-not-compete. [Accessed December 2012].

[220] David Linden and Thomas B. Reddy, Handbook Of Batteries 3rd Edition, United State: McGraw-Hill, 2002.

[221] Samuel C. Levy and Per Bro, Battery Hazards And Accident Prevention, New York: Plenum Press, 1994.

[222] "Complete Photovoltaic System: Sunlight to Electricity," Solar Direct, 2013. [Online]. Available: http://www.solardirect.com/pv/systems/systems.htm. [Accessed September 2013].

[223] Akiyama, K., Nozaki, Y., Kudo, M. and Yachi, T., "Ni-MH batteries and EDLCs hybrid stand-alone photovoltaic power system for digital access equipment," in Twenty-second International Telecommunications Energy Conference, 2000. INTELEC., Phoenix, AZ, 2000.

[224] Liu, S., Dougal, R.A. and Solodovnik, E.V., "Design of autonomous photovoltaic power plant for telecommunication relay station," IEE Proceedings-Generation, Transmission and Distribution, vol. 152, no. 6, pp. 745 - 754, 4 November 2005.

[225] G.J. Dalton, D.A. Lockington and T.E. Baldock, "Feasibility analysis of renewable energy supply options for a grid-connected large hotel," Renewable Energy, vol. 34, no. 4, p. 955–964, April 2009.

[226] Wies, R.W., Johnson, R.A., Agrawal, A.N. and Chubb, T.J., "Simulink model for economic analysis and environmental impacts of a PV with diesel-battery system for remote villages," IEEE Transactions on Power Systems, vol. 20, no. 2, pp. 692 - 700, May 2005.

[227] "The Nottingham University Malaysia Campus," [Online]. Available: https://maps.google.com.my/maps?safe=off&q=semenyih+nottingham+university&ie=UTF-8&ei=UmOxUsSmFcemrQfC2IGoBg&sqi=2&ved=0CAgQ_AUoAg.

[228] Alam Hossain Mondal and Manfred Denich, "Hybrid systems for decentralized power generation in Bangladesh," Energy for Sustainable Development, vol. 14, no. 1, p. 48–55, March 2010.

[229] A. Demiroren and U. Yilmaz, "Analysis of change in electric energy cost with using renewable energy sources in Gökceada, Turkey: An island example," Renewable and Sustainable Energy Reviews, vol. 14, no. 1, p. 323–333, January 2010.

[230] A. Shiroudi., R. Rashidi, G. B. Gharehpetian, S. A. Mousavifar and A. Akbari Foroud, "Case study: Simulation and optimization of photovoltaic-wind-battery hybrid energy system in Taleghan-Iran using homer software," Journal Renewable Sustainable Energy, vol. 4, pp. 0531111-11, 27 September 2012.

[231] H. D. S. b. K. Resolve, "10045-Clearness index in HOMER," HOMER Energy, [Online]. Available: http://support.homerenergy.com/index.php?/Knowledgebase/Article/Vie

w/203/0/10045---clearness-index-in-homer. [Accessed May 2013].

[232]   Mondal, M.A.H. and Islam, A.K.M.S., "Techno-economic feasibility of grid connected solar PV system in Bangladesh," in 1st International Conference on the Developments in Renewable Energy Technology (ICDRET), 2009, Dhaka, 17-19 Dec. 2009.

[233]   T. Khatib, "HOMER Software for Power Application in Renewable Energy," in Fakulti Kejuruteraan Dan Alam Bina, UKM, Kuala Lumpur, 2012.

[234]   O. Erdinc and M. Uzunoglu, "The importance of detailed data utilization on the performance evaluation of a grid-independent hybrid renewable energy system," International Journal of Hydrogen Energy, vol. 36, no. 20, p. 12664–12677, October 2011.

[235]   Abolfazl Shiroudi, Seyed Reza Hosseini Taklimi, Seyed Ahmad Mousavifar and Peyman Taghipour, "Stand-alone PV-hydrogen energy system in Taleghan-Iran using HOMER software: optimization and techno-economic analysis," Environment, Development and Sustainability, vol. 15, no. 5, pp. 1389-1402, October 2013.

[236]   G. Tzamalis, E.I. Zoulias, E. Stamatakis, E. Varkaraki, E. Lois and F. Zannikos, "Techno-economic analysis of an autonomous power system integrating hydrogen technology as energy storage medium," Renewable Energy, vol. 36, no. 1, p. 118–124, January 2011.

[237]   K. Resolve, "101650-Modeling a charge controller in HOMER," HOMER Energy , December 2010. [Online]. Available: http://support.homerenergy.com/index.php?/Knowledgebase/Article/Vie w/12/12/10165---modeling-a-charge-controller-in-homer. [Accessed June 2012].

[238]   "Power.bloc OPzV," HOPPECKE Power From Innovation, Germany.

[239]   T. Givler and P. Lilienthal , "Using HOMER® Software, NREL's Micropower Optimization Model, to Explore the Role of Gen-sets inSmall Solar Power Systems. Case Study: Sri Lanka," National Renewable Energy Laboratory, May 2005.

[240]   Chedid, R. and Rahman, S., "Unit sizing and control of hybrid wind-solar power systems," IEEE Transactions on Energy Conversion, vol. 12, no. 1, pp. 79 - 85, Mar 1997.

[241]   Holtz, J., Lotzkat, W. and Stadtfeld, S., "Controlled AC drives with ride-through capability at power interruption," IEEE Transactions on Industry Applications, vol. 30, no. 5, pp. 1275 - 1283, Sep/Oct 1994.

[242]   Abouzahr, I. and Ramakumar, R., "Loss of power supply probability of stand-alone wind electric conversion systems: a closed form solution approach," IEEE Transactions on Energy Conversion, vol. 5, no. 3, pp. 445 - 452, Sep 1990.

[243]   Abouzahr, I. and Ramakumar, R., "Loss of power supply probability of stand-alone photovoltaic systems: a closed form solution approach," IEEE Transactions on Energy Conversion, vol. 6, no. 1, pp. 1 - 11, Mar 1991.

[244]   Yang Qi, Zhang Jianhua, Liu Zifa and Xia Shu, "A new methodology for optimizing the size of hybrid PV/wind system," in IEEE International Conference on Sustainable Energy Technologies, 2008. ICSET 2008., Singapore, 24-27 Nov. 2008.

[245]   M. Technologies, "DATASHEET 48V MODULES," [Online]. Available: http://www.maxwell.com/products/ultracapacitors/docs/datasheet_48v_series_04302013.pdf. [Accessed September 2012].

[246]   P. P. Sonic, "Sealed Lead Acid Battery Technical Handbook Power Sonic," [Online]. Available: http://www.batteryweb.com/manuals/techman.pdf. [Accessed September 2012].

[247]   Panasonic, "Panasonic Electric Double Layer Capacitors (Gold Capacitor)/ HW," January 2008. [Online]. Available: http://www.panasonic.com/industrial/components/pdf/ABC0000CE8.pdf. [Accessed September 2012].

[248]   Hiu Kee Weng, "Implementation and integration to supervisory software of a buck-boost DC-DC convertor and programmable load for a prototype hybrid supercapacitor-battery energy storage system in solar energy application," The University of Nottingham, malaysia Campus, 2012.

[249]   Dinesh A/L Selvamurthy, "Utilization of Support Vector Machines (SVM) to Forecast Load Requirements in a Hybrid Battery-Supercapacitor Energy Storage System," The University of Nottingham, Malaysia Campus, 2011.

[250]   J.A.K. Suykens, J. De Brabanter, L. Lukas and J. Vandewalle, "Weighted least squares support vector machines: robustness and sparse approximation," Neurocomputing, vol. 48, no. 1-4, p. 85–105, October 2002.

[251]   Isabelle Guyon and André Elisseeff , "An introduction to variable and

feature selection," Journal The Journal of Machine Learning Research, vol. 3, pp. 1157-1182 , 2003 .

[252]   "ASAP 2050 XP Software Features and Reports," Micromeritics, [Online]. Available: http://www.micromeritics.com/Product-Showcase/ASAP-2050-Xtended-Pressure/ASAP-2050-XP-Software-Features-and-Reports.aspx. [Accessed 2011].

[253]   Wendy G Pell and Brian E Conway, "Analysis of power limitations at porous supercapacitor electrodes under cyclic voltammetry modulation and dc charge," Journal of Power Sources, vol. 96, no. 1, p. 57–67, June 2001.

[254]   Ng Kok Chiang, "Nanocomposites if Carbon Nanotubes and Transition Metal Oxides for Aqueous Asymmetric Supercapacitors," The University of Nottingham, 2009.

[255]   Frackowiak, E., Metenier, K., Bertagna, V. and Beguin, F., "Supercapacitor electrodes from multiwalled carbon nanotubes," Applied Physics Letters , vol. 77, no. 15, pp. 2421 - 2423, Oct 2000.

[256]   R. Jeyapaul, P. Shahabudeen and K. Krishnaiah, "Simultaneous optimization of multi-response problems in the Taguchi method using genetic algorithm," The International Journal of Advanced Manufacturing Technology, vol. 30, no. 9-10, pp. 870-878, October 2006.

[257]   R. Jeyapaul, P. Shahabudeen and K. Krishnaiah, "Quality management research by considering multi-response problems in the Taguchi method – a review," The International Journal of Advanced Manufacturing Technology, vol. 26, no. 11-12, pp. 1331-1337, November 2005.

[258]   Abbas Al-Refaie, Tai-Hsi Wu and Ming-Hsien Li , "Data development analysis approaches for solving the multiresponse problem in the Taguchi method," Artificial Intelligence for Engineering Design, Analysis and Manufacturing, vol. 23, pp. 159-173 , 2009.

[259]   Tung-Hsu Hou, Chi-Hung Su and Wang-Lin Liu, "Parameters optimization of a nano-particle wet milling process using the Taguchi method, response surface method and genetic algorithm," Powder Technology , vol. 173, pp. 153-162, 2007.

[260]   Hung-Chung Liao, "Multi-response optimization using weighted principal component," Int J Adv Manuf Technolgy, vol. 27, p. 720 – 725, 2006.

[261]   R. Ramakrishnan and L. Karunamoorthy, "Multi response optimization

of wire EDM operations using robust design of experiments," Int J Adv Manuf Technolgy, vol. 29, pp. 105 -112, 2006.

[262] Phadke, M. S. , Quality engineering using robust design, New Jersey, AT&T Bells Laboratory/Prentice-Hall., 1989.

[263] W.H. Yang and Y.S. Tarng, "Design optimization of cutting parameters for turning operations based on the Taguchi method," Journal of Materials Processing Technology , vol. 84, p. 122–129, 1998.

[264] Antony .J, "Simultaneous optimisation of multi quality characteristics in manufacturing processes using Taguchi's quality loss function," Int J Manuf Technolgy, vol. 17, p. 134, 2001.

[265] Jack Sifri, "Recent advancements in RFIC simulation technology for analyzing large RFICs," [Online]. Available: http://citeseerx.ist.psu.edu/viewdoc/download?doi=10.1.1.126.5763&rep=rep1&type=pdf. [Accessed 2011].

[266] Tatjana V. Sibalija and Vidosav D. Majstorovic, "Novel Approach to Multi-Response Optimisation for Correlated Responses," FME Transactions , vol. 38, pp. 39-48, 2010.

[267] Jami Kovach and Byung Rae Cho, "Constrained robust design experiments and optimization with the consideration of uncontrollable factors," The Int Journal of Adv Manuf Tech, vol. 38, no. 1-2, pp. 7-18.

[268] A. Kumar Dubey and V. Yadava, "Multi-objective optimization of laser beam cutting process," Optics & Laser Technology, vol. 40, pp. 562-570, 2008.

[269] Gabriella Dellino, Jack P.C. Kleijnen and Carlo Meloni, "Robust Simulation-Optimization using metamodels," in Proceedings of the 2009 Winter Simulation Conference, 2009.

[270] V. N. Gaitonde, S. R. Karnik and B. T. Achyutha, "Methodology of Taguchi for multi-drilling problem to minimize burr size," Int. J. Adv. Manuf. Technol., vol. 34, pp. 1-8, 2007.

[271] Chang-Yuan Tang, Yi-Leh Wu and Chien-Chin Peng, "Fundamental matrix estimation by multiobjective genetic algorithm with Taguchi's method," Applied Soft Computing , vol. 12, pp. 553-558, 2011.

[272] I. Mukherjee and P. K. Ray, "A review of optimization techniques in metal cutting process," Computer & Industrial Engineering, vol. 50, pp. 15-34, 2006.

[273] Morris H. DeGroot, "Reaching Consensus, Journal of The American Statistical Association," Journal of The American Statistical Association, vol. 69, no. 345, pp. 118-121.

[274] Pierre A. Balthazard, William R. Ferrell and Dorothy L. Aguilar, "Influence allocation methods in group decision support systems," Group Decision and Negotiation, vol. 7, no. 4, pp. 347-362.

[275] Ahmida Ajina and Dino Isa, "EDLC Capacitance Optimization Using the Taguchi Technique," International Journal of Engineering and Innovative Technology (IJEIT), vol. 2, no. 3, pp. 263-267, 2012.

[276] Tong l-I and Su C-T, "The optimization of multi response problems in Taguchi method," Int J Qual Reliab Manage, vol. 14, no. 4, pp. 367-380, 1997.

[277] Franci Cus and Joze Balic, "Optimization of cutting process by GA approach," Robotics and Computer Integrated Manufacturing, vol. 19, p. 113–121, 2003.

[278] David Eby, R.C. Averill, William F. Punch and Erik D. Goodman , "Optimal design of flywheels using an injection island genetic algorithm," AIEDAM, vol. 13, pp. 327-340, 1999.

[279] K. F. Man, K.S. Tang and S. Kwong, "Genetic Algorithm: Concepts and Applications," IEEE Transactions on industrial Electronics, vol. 43, no. 5, p. 519 – 534, 1996.

[280] Tung-Hsu (tony) Hou, Chi-Hung Su and Hung-Zhi Chang, "Using neural networks and immune algorithms to find the optimal parameters for an IC wire bonding process," Expert System with Applications, vol. 34, no. 1, pp. 427-436, January 2008.

[281] Chia Yen Yee, Ridhuan Ahmad Samsuri, Dino Isa, Ahmida Ajina and Khiew Pooi Sim , "Optimization of process factors in Supercapacitor fabrication using the Genetic Algorithm to optimize Taguchi Signal-to-Noise ratios," Internatinal Journal of Engineering Science and Innovative Technology, vol. 1, no. 2, 2012.

[282] Bindner, H, Cronin, T., Lundsager, P., Manwell, J.F., Abdulwahid, U. and Baring-Gould, I., "Lifetime modelling of lead acid batteries," 2005.

[283] "Datasheet Maxim," [Online]. Available: http://datasheets.maximintegrated.com/en/ds/DS2438EVKIT.pdf.. [Accessed 2012].

[284]   Hanington, G., Pin-Fan Chen, Asbeck, P.M. and Larson, L.E., "High-efficiency power amplifier using dynamic power-supply voltage for CDMA applications," IEEE Transactions on Microwave Theory and Techniques, vol. 47, no. 8, pp. 1471 - 1476, 2002.

[285]   S. Mekhilef, A. Safari, W. Mustaffa, R. Saidur, R. Omar and M. and Younis, "Solar energy in Malaysia: Current state and prospects," Renewable and Sustainable Energy Reviews, pp. 386-396, 2012.

[286]   "What is the relation between the number of Support Vectors and training data and classifiers performance?," Feb. 2012. [Online]. Available: http://stackoverflow.com/questions/9480605/what-is-the-relation-between-the-number-of-support-vectors-and-training-data-and. [Accessed Dec. 2012].

[287]   R. A. Samsuri, "The use of Taguchi technique to optimiseprocess parameters in the fabrication of coin supercapacitor of 1 volts, 2 Farads," The University of Nottingham Malaysia Campus, 2011.

[288]   A. P. V. E. Ioannies Hadjipaschalis, "Overview of current and future energy storage technologies for electric power applications," Renewable and Sustainable Energy Reviews, vol. 13, pp. 1513-1522, 2009.

[289]   D. E. G. a. J. H. H. L. B. Booker, "Classifier systems and genetic algorithms," Artificial Intelligence, vol. 40, no. 1-3, p. 235–282, Sep. 1989.

[290]   "HOMER Energy News -- July 2012- HOMER helps bring electricity to remote areas of Afghanistan," HOMER ENergy - NREL, July 2012. [Online]. Available: http://www.homerenergy.com/email/homer_news_July2012.html. [Accessed May 2014].

Appendix

A1. 2kWSolar Cabin
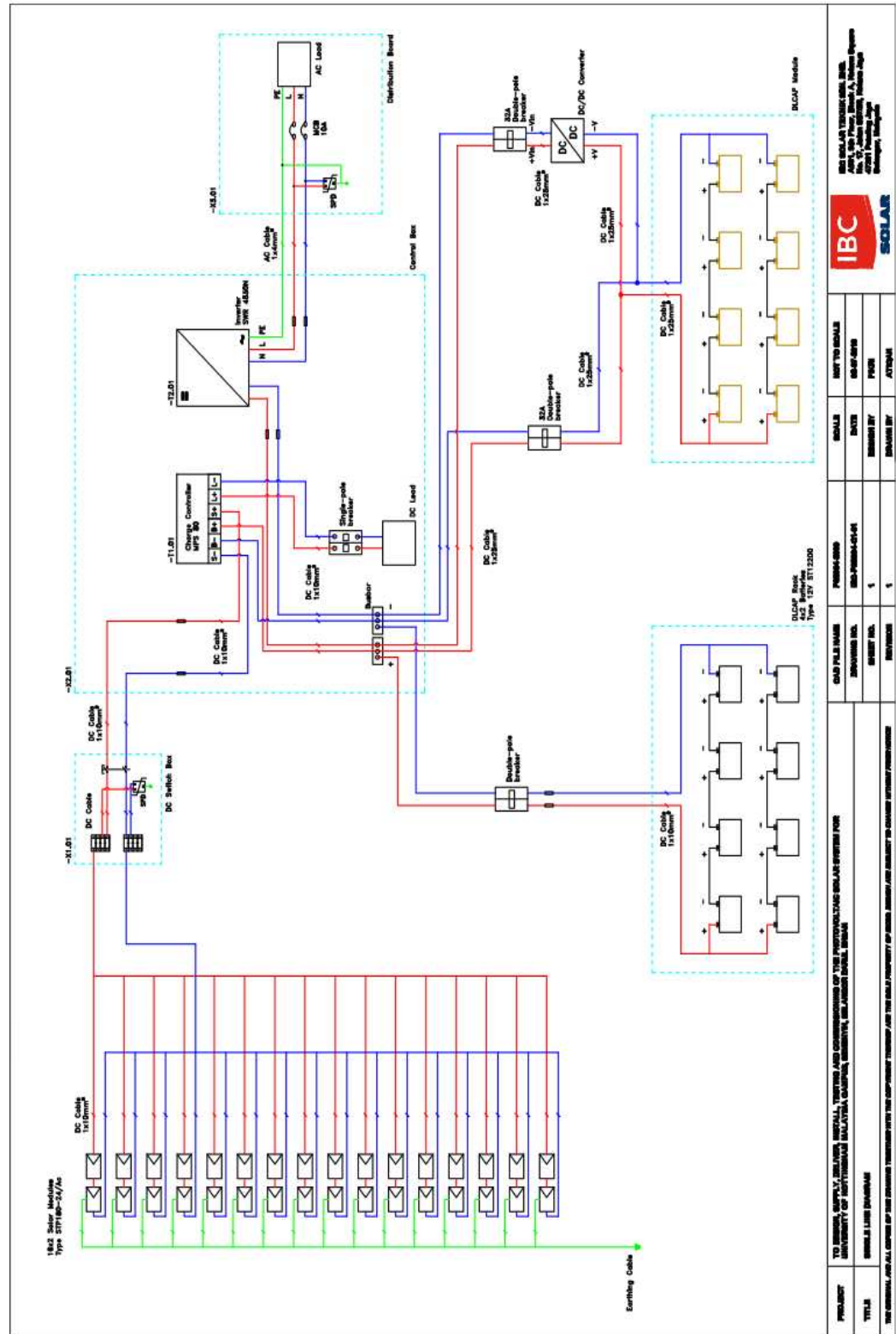
Figure 131Schematic Solar Cabin

Figure 132 Power Electronics used in Solar Cabin

Figure 133 Batteries used in Solar Cabin

Figure 134 Supercapacitor used in Solar Cabin

A2. GA code for optimal sizing RES

```
tic

close all
clear all
clc;
clear;

a = 20;
b = 25;
c = 1;
d = 5;
e = 4;
f = 32;
g = 14;
h = 15;
i = 4;
j = 7;


Population_Max=20;
Min_Value=100000000000;
Max_Generation = 500;
Population_Max=20;
Pc=0.3;
Pm = 0.1;
Var_x =[a,b;c,d;e,f;g,h;i,j;];
Min_Value=10000000000000000;
Max_Generation = 500;
Max_Gen=length(Var_x);


Beta=3;

Gbest=100000000000000000;
Max_Generation = 500;
Max_Gen=length(Var_x);


%%%%%%%%%%%%%%%%%%%%%%%%%%%%%%%%%%%%%%%%%%%%%%%%%%%%%%%%%%%%%%%%%%%%%%%%
%%%%%%%%%%%%%%%%%%%%

Delta_x=Var_x(2)-Var_x(1);

V =rand(Population_Max,Max_Gen)*Delta_x+Var_x(1);

%%%%%%%%%%%%%%%%%%%%%%%%%%%%%%%%%%%%%%%%%%%%%%%%%%%%%%%%%%%%%%%%%%%%%%%%
%%%%%%%%%%%%%%%%%%%%

for Generation=1:Max_Generation

    for Chromosome=1:round(Population_Max*Pc/2)

        Vector_v1=randint (1,1,[1,Population_Max]);
        Vector_v2=randint (1,1,[1,Population_Max]);
```

```matlab
        Parent_1=V(Vector_v1,:);
        Parent_2=V(Vector_v2,:);

        L1=rand;
        L2=1-L1;

        Child_1=L1*Parent_1+L2*Parent_2;
        Child_2=L1*Parent_2+L2*Parent_1;


        Cross_V(Chromosome*2-1,:)=Child_1;
        Cross_V(Chromosome*2,:)=Child_2;

    end

    for Chromosome=1:round(Population_Max*Max_Gen*Pm)

        M_Gen=randint(1,1,[1,Population_Max*Max_Gen]);

        Temp1=fix (M_Gen/Max_Gen);
        Temp2=M_Gen/Max_Gen;

        if (Temp1==Temp2)
            Vector_1=Temp1;
            M_Point=Max_Gen;
        else
            Vector_1=Temp1+1;
            M_Point=mod (M_Gen,Max_Gen);
        end

        Parent_1=V(Vector_1,:);
        Child_1=Parent_1;

        Mutation_Type=randint;

        if Mutation_Type==0;
            Y=Var_x(2)-Parent_1(M_Point);
            Delta=Y*rand*(1-Generation/Max_Generation)^2;
            Child_1(M_Point)=Parent_1(M_Point)+Delta;
        else
            Y=Parent_1(M_Point)-Var_x(1);
            Delta=Y*rand*(1-Generation/Max_Generation)^2;
            Child_1(M_Point)=Parent_1(M_Point)-Delta;
        end

        Mutated_V(Chromosome,:)=Child_1;
    end

    if round(Population_Max*Pc)==0 &&
round(Population_Max*Max_Gen*Pm)==0
        Merg_V=V;
    end
    if round(Population_Max*Pc)==0 &&
round(Population_Max*Max_Gen*Pm)~=0
        Merg_V=[V;Mutated_V];
    end
```

```matlab
    if round(Population_Max*Pc)~=0 &&
round(Population_Max*Max_Gen*Pm)==0
        Merg_V=[V;Cross_V];
    end
    if round(Population_Max*Pc)~=0 &&
round(Population_Max*Max_Gen*Pm)~=0
        Merg_V=[V;Cross_V;Mutated_V];
    end

    Total_V=length (Merg_V(:,1));

    for Chromosome=1:Total_V


        x1=Merg_V(Chromosome,1);
        x2=Merg_V(Chromosome,2);
        x3=Merg_V(Chromosome,3);
        x4=Merg_V(Chromosome,4);
        x5=Merg_V(Chromosome,5);

        %making sure the output is positive absolute number
        x(1)= abs(round(x1));
        x(2)= abs(round(x2));
        x(3)= abs(round(x3));
        x(4)= abs(round(x4));
        x(5)= abs(round(x5));


        if x(1)<a || x(1)>b
            x(1)=abs(round(a+(b-a)*rand));
        end


        if x(2)<c || x(2)>d
            x(2)=abs(round(c+(d-c)*rand));
        end

        if x(3)~=4 || x(3)~=8 || x(3)~=12 || x(3)~=16 ||
x(3)~=20 || x(3)~=24 || x(3)~=28 || x(3)~=32 || x(3)~=36
||x(3)~=40 || x(3)~=44 ||x(3)~=48 || x(3)~=52 || x(3)~=56

            uy=(round(14*rand));
             if uy==1
                 x(3)=4;
             else if uy==2
                     x(3)=8;
                 else if uy==3
                         x(3)=12;
                     else if uy==4
                             x(3)=16;
                         else if uy==5
                                 x(3)=20;
                             else if uy==6
                                     x(3)=24;
                                 else if uy==7
                                         x(3)=28;
                                     else if uy == 8
                                             x(3)=32;
```

388

```matlab
                                          else if uy == 9
                                              x(3)=36;
                                          else if uy == 10
                                              x(3)=40;
                                          else if uy == 11
                                              x(3)=44;
                                          else if uy
== 12

x(3)=48;
                                          else if
uy == 13

x(3) =52;


                                          else

x(3) =56;


                                          end
                                      end
                                  end
                              end
                          end
                      end
                  end
              end
          end
      end
    end
  end
end


 if x(4)<g || x(1)>h
     x(4)=abs(round(g+(h-g)*rand));
 end

 if x(5)<i || x(5)>j
     x(5)=abs(round(i+(j-i)*rand));
 end


%constraint_inequality
 G1= (0.96 * x(1)*0.100) + (0.04 * x(2)*1); %solar
irradiance and wind generator


%sizing battery at average power

%G2 = (x(3)*1.416*1)/0.226;    %for DOD=1
%G2 = (x(3)*1.416*0.5)/0.226;  %for DOD=0.5
%G2 = (x(3)*1.416*0.3)/0.226;  %for DOD=0.3
%G2 = (x(3)*1.416*0.1)/0.226;  %for DOD=0.1

%G2 =
((x(3)*1.416*0.8)+(x(5)*(0.5*83*10.2^2)/3600))/0.226    ;
```

389

```matlab
%for DOD=0.8 for case supercapacitor make up the difference
between the average power and the peak

        G2 =  (x(3)*1.416*0.8)/0.133 ;


        %G2 = (x(3)*1.416*0.4)/0.226;   %for DOD=0.4
        %G2 = (x(3)*1.416*0.6)/0.226;   %for DOD=0.6
        %G2 = (x(3)*1.416*0.7)/0.226;   %for DOD=0.7


        %battery lifetime

        %R= x(3)*(1*118*12*400)/1240000;      %for DOD 1
        %R= x(3)*(0.5*118*12*1000)/1240000;   %for DOD 0.5
        %R= x(3)*(0.4*118*12*1200)/1240000;   %for DOD 0.4
        %R= x(3)*(0.6*118*12*800)/1240000;    %for DOD 0.6
        %R= x(3)*(0.7*118*12*700)/1240000;    %for DOD 0.7
        %R= x(3)*(0.3*118*12*2200)/1240000;   %for DOD 0.3
        %R= x(3)*(0.1*118*12*3200)/1240000;   %for DOD 0.1
        R= x(3)*(0.8*118*12*1200)/1240000;     %for DOD 0.8


        C = x(5) *1/83; %sizing parallel supercapacitor



        if (G1<=2) && (G2>=100) && (R <= 20) && (C<=610)
           Penalty=0;
        else
Penalty=(16*Generation)^2.5*(abs(G1)^3+abs(G2)^3+abs(R)^3+abs(C)
^3);
        end



         %fitness function

        a_ch =(x(1)*100)/300;
        pv_b = x(1)*(335 + (20*6.7));
        wg_b = x(2)*(2240+ (20*44.8) + (x(4)*74) +
(20*x(4)*1.48));
        bat_b = x(3)*((20/R)*316)+ x(3)*(6.32*(round(20-(20/R))-
1));
        scap_b = x(5)*1498.52;
        ch_b = (a_ch*108*(4+1))+(a_ch*2.16*(20-4-1));
        inv_b = 2068*(4+1)+(41*(20-4-1));

        F=(pv_b+wg_b+bat_b+ch_b+inv_b+scap_b);

        Eval(Chromosome)=F+Penalty;

        if Eval(Chromosome)<Gbest
           Gbest=Eval(Chromosome);
           Gi=[G1,G2,R, C];

X_Gbest=[x(1),x(2),x(3),x(4),x(5),pv_b,wg_b,bat_b,scap_b,ch_b,in
v_b];
```

```
        end


    end

    Temp3=[Eval',Merg_V];
    Temp3=sortrows (Temp3,1);
    V=Temp3(1:Population_Max,2:5+1);

end


tee=toc


disp (' ');
disp ('Answer is:');
disp (' ');
disp ('    F(x)=');
disp (Gbest(1));
disp (' ');
disp ('    g1         g2           R        C');
disp (Gi);
disp (' ');
disp ('    x1        x2        x3        x4        x5
pv_b      wg_b      bat_b     scap_b    ch_b     inv_b');
disp (X_Gbest);
disp (' ');
```

A3. GA Coding for optimising process factor of supercapacitor fabrication process

Main:

```matlab
clc;clear all;

a = 0;   %domain
b = 1;

popSize = 30;    %rows
Slength = 20;    %columns

PC = 0.65;        %probability crossover
PM = 0.02;        %probability mutation

generation = 8000;
printGen = [generation,0];
aveFit = zeros(generation,1);

k = 1;
xValue = zeros(popSize,generation);
zValue = zeros(popSize,generation);
fValue = zeros(popSize,generation);

weakFValue = zeros(generation, 3);
bestFValue = zeros(generation, 3);
aveFitness = zeros(generation,5);


% initialize population
pop = initialise1(popSize, Slength, @func, a, b);


% for each generation
for (j = 1:generation)
    % initialize next generation to zeroes
    nextGen = zeros(popSize, Slength+3);


    % do selection
    [pop,aveFit(j,1)] = selection(pop);


    % do crossover
    selected = zeros(popSize,1);

    for i = 1:popSize/2
        % select parent1 for crossover
        parent1 = round(rand*(popSize-1))+1;
        while (selected(parent1))
```

```matlab
            parent1 = round(rand*(popSize-1))+1;
        end

        selected(parent1) = 1;

        % select parent2 for crossover
        parent2 = parent1;
        while (selected(parent2))
            parent2 = round(rand*(popSize-1))+1;
        end

        selected(parent2) = 1;

        [nextGen(i*2-1,:), nextGen(i*2,:)] =
crossover(pop(parent1,:), pop(parent2,:), PC, a, b);

    end

    % do mutation
    for i = 1:popSize
        nextGen(i,:) = mutation(nextGen(i,:), PM, a,
b);


    end


    % plot graph for next generation after
selection/crossover/mutation if being asked
    if (j == printGen(1,k))
        figure(k);
        k = k+1;

%       clf
%       colormap(white);

        x = -5:0.05:5;
        z = -5:0.05:5;
        xlabel('x');
        ylabel('z');
        zlabel('func');

        [X,Z]=meshgrid(x,z);
        surf(x,z,func(X,Z));

        hold on;
%        scatter(nextGen(:,Slength+1),
nextGen(:,Slength+3));
        groupName= sprintf('Fitness function of %d',
j);
```

```matlab
        title(groupName);


    end

    % make next generation the new population
    pop = nextGen;


    aveFitness(j,1) = aveFit(j,1);



    xValue(:,j) = pop(:,Slength+1);
    zValue(:,j) = pop(:,Slength+2);
    fValue(:,j) = pop(:,Slength+3);

    weakFValue(j,1) = min(pop(:,Slength+2));
    weakFValue(j,3) =
(weakFValue(j,1))./(weakFValue(j,2));

    bestFValue(j,1) = max(pop(:,Slength+3));
    bestFValue(j,3) =
bestFValue(j,1)./bestFValue(j,2);

    aveFitness(j,4) = bestFValue(j,1) -
aveFitness(j,1);
    aveFitness(j,5) = bestFValue(j,2) -
aveFitness(j,2);



end

% -------- plotting graph ---------


figure(k)
xlabel('generation');
ylabel('ave fitness level');
plot(1:generation, aveFit);
title('Generation, average fitness function without
FM');

figure, plot(1:generation,bestFValue(:,1));

xlabel('Generation');
ylabel('Fitness Level');
title('Best Fitness');
```

Fitness Function:

```
function [F] = func(x,z)


F = x*(0.3471+0.5561+0.6154+0.3747) +
z*(0.4306+0.3333+0.5443+0.3556);
```

Initialization:

```
%initialization

function [pop] =initialise1(popSize, Slength, func,
a, b)

pop = round(rand(popSize, Slength + 3));

base10_array = 2.^(size(pop(:,(1:Slength/2)),2)-1:-
1:0); % array of base 10 value depending on position
base10_matrix = repmat(base10_array, popSize, 1); %
duplicate to get 1 array for 1 individual

pop(:,Slength+1) =
sum(base10_matrix(:,1:Slength/2).*pop(:,1:Slength/2),
2)*(b-a)/(2.^(Slength/2)-1)+a;

pop(:,Slength+2) =
sum(base10_matrix(:,1:Slength/2).*pop(:,((Slength/2)+
1:Slength)), 2)*(b-a)/(2.^(Slength/2)-1)+a;

pop(:,Slength+3) = func(pop(:,Slength+1),
pop(:,Slength+2));

end
```

Crossover:

```
%Crossover

function[child1, child2] = crossover(parent1,
parent2, PC, a, b)
```

395

```matlab
if (rand<PC)

    Slength = size(parent1,2) - 3;          %total
column, then -2 to get the Slength
    cpoint=round(rand*(Slength-2))+1;
%cpoint will never start at 0, random number multiply
with the Slength -2 to cover the +1 and to cover the
cpoint when = 10

%cpoint=(Slength/2);

    child1=[parent1(:,1:cpoint)
parent2(:,cpoint+1:Slength)];
    child2=[parent2(:,1:cpoint)
parent1(:,cpoint+1:Slength)];


child1(:,Slength+1)=sum(2.^(size(child1(:,1:Slength/2
),2)-1:-1:0).*child1(:,1:Slength/2))*(b-
a)/(2.^(Slength/2)-1)+a;

child1(:,Slength+2)=sum(2.^(size(child1(:,1:Slength/2
),2)-1:-1:0).*child1(:,(Slength/2)+1:Slength))*(b-
a)/(2.^(Slength/2)-1)+a;


child2(:,Slength+1)=sum(2.^(size(child2(:,1:Slength/2
),2)-1:-1:0).*child2(:,1:Slength/2))*(b-
a)/(2.^(Slength/2)-1)+a;

child2(:,Slength+2)=sum(2.^(size(child2(:,1:Slength/2
),2)-1:-1:0).*child2(:,(Slength/2)+1:Slength))*(b-
a)/(2.^(Slength/2)-1)+a;

    child1(:,Slength+3)=func(child1(:,Slength+1),
child1(:,Slength+2));
    child2(:,Slength+3)=func(child2(:,Slength+1),
child2(:,Slength+2));


else
    child1=parent1;
    child2=parent2;

end
end
```

Mutation:

```matlab
%mutation

function [child]=mutation(parent,PM,a,b)

if (rand < PM)
    Slength = size(parent,2) - 3;
    mpoint = round(rand*((Slength)-1))+1;

    child = parent;
    child(mpoint) = abs(parent(mpoint)-1);


child(:,Slength+1)=sum(2.^(size(child(:,1:Slength/2),
2)-1:-1:0).*child(:,1:Slength/2))*(b-
a)/(2.^(Slength/2)-1)+a;

child(:,Slength+2)=sum(2.^(size(child(:,1:Slength/2),
2)-1:-1:0).*child(:,(Slength/2)+1:Slength))*(b-
a)/(2.^(Slength/2)-1)+a;


    if ( (child(:,Slength+1) + (child(:,Slength+2)) >
1))

        child(:,Slength+3) = (((child(:,Slength+1)) +
(child(:,Slength+2))) - 1)/2;

        child(:,Slength+1) = child(:,Slength+1) -
child(:,Slength+3);
        child(:,Slength+2) = child(:,Slength+2) -
child(:,Slength+3);

        child(:,Slength+3)=func(child(:,Slength+1),
child(:,Slength+2));

    elseif (((child(:,Slength+1)) +
(child(:,Slength+2))) < 1)

        child(:,Slength+3) = (1 -
((child(:,Slength+1)) + (child(:,Slength+2))))/2;
        child(:,Slength+1) = child(:,Slength+3) +
child(:,Slength+1);
        child(:,Slength+2) = child(:,Slength+3) +
child(:,Slength+2);
```

```matlab
        child(:,Slength+3)=func(child(:,Slength+1),
child(:,Slength+2));

    else

        child(:,Slength+3)=func(child(:,Slength+1),
child(:,Slength+2));

    end

else
    Slength = size(parent,2) - 3;
    child=parent;


child(:,Slength+1)=sum(2.^(size(child(:,1:Slength/2),
2)-1:-1:0).*child(:,1:Slength/2))*(b-
a)/(2.^(Slength/2)-1)+a;

child(:,Slength+2)=sum(2.^(size(child(:,1:Slength/2),
2)-1:-1:0).*child(:,(Slength/2)+1:Slength))*(b-
a)/(2.^(Slength/2)-1)+a;

    if ( (child(:,Slength+1) + (child(:,Slength+2))
> 1))

        child(:,Slength+3) = (((child(:,Slength+1)) +
(child(:,Slength+2))) - 1)/2;

        child(:,Slength+1) = child(:,Slength+1) -
child(:,Slength+3);
        child(:,Slength+2) = child(:,Slength+2) -
child(:,Slength+3);

        child(:,Slength+3)=func(child(:,Slength+1),
child(:,Slength+2));

    elseif (((child(:,Slength+1)) +
(child(:,Slength+2))) < 1)

        child(:,Slength+3) = (1 -
((child(:,Slength+1)) + (child(:,Slength+2))))/2;
        child(:,Slength+1) = child(:,Slength+3) +
child(:,Slength+1);
        child(:,Slength+2) = child(:,Slength+3) +
child(:,Slength+2);

        child(:,Slength+3)=func(child(:,Slength+1),
child(:,Slength+2));
```

```
    else

        child(:,Slength+3)=func(child(:,Slength+1),
child(:,Slength+2));
    end

end

end
```

A4. SVM_SVR EMS

```
for r=1:80,
    time1(r)=r;
end

[a,b]=libsvmread('SVC.txt');

[c,d]=libsvmread('load1.txt');
[e,f]=libsvmread('load2.txt');
[g,h]=libsvmread('load3.txt');
[i,j]=libsvmread('load4.txt');
[k,l]=libsvmread('load5.txt');

%classifcation model
model=svmtrain(a,b, '-t 0 -s 0 -c 100');

%regression models
model1=svmtrain(c,d, '-t 2 -s 3 -c 10 -p 0.01');
model2=svmtrain(e,f, '-t 1 -s 3 -c 10 -p 0.01');
model3=svmtrain(g,h, '-t 2 -s 3 -c 10 -p 0.01');
model4=svmtrain(i,j, '-t 2 -s 3 -c 10 -p 0.01');
model5=svmtrain(k,l, '-t 1 -s 3 -c 10 -p 0.01');

model_choice=1;

m.digitalWrite(49,1); %start battery

%Setup DAQ for clasifcation
g=[1];          %random label
g=sparse(g);
ai.SampleRate = 100;  %higher sampling rate, faster classification
ai.SamplesPerTrigger = 100;


%Scynchronize with programmable load
while m.digitalRead(41)==0
end

%Start DAQ
start(ai);
wait(ai,1.1); %prevent timeout duration
[data_R] = getdata(ai);
data_R=transpose(data_R);
s_data_R=sparse(data_R);

[predict_label_C, accuracy, prob_values] = svmpredict( g,s_data_R, model);

switch predict_label_C
```

```
    case 1
      model_choice=model1;
    case 2
       model_choice=model2;
    case 3
       model_choice=model3;
    case 4
       model_choice=model4;
    case 5
       model_choice=model5;
end

%Setup DAQ for Regression
hold=[1];          %random label
hold=sparse(hold);
ai.SampleRate = 10;
ai.SamplesPerTrigger = 3;


for j=1:80,              % load profile duration

start(ai);              %start DAQ
wait(ai,0.3);           %prevent timeout duration*1.1+0.5
[data_R] = getdata(ai);
data_R=transpose(data_R);      %prepare data format for libsvm
s_data_R=sparse(data_R);

[predict_label, accuracy, prob_values] = svmpredict(hold, s_data_R,
model_choice);
if predict_label> 1.1
   m.digitalWrite(49,0);
   m.digitalWrite(53,1);
else
   m.digitalWrite(53,0);
   m.digitalWrite(49,1);
end

if j==80
   m.digitalWrite(53,0);
   m.digitalWrite(49,0);
end

datahold(j)= predict_label;
end
plot(time1,datahold)
```

A5. (Calculation for SOC)

For battery-only system

At Steady State Load (I=1.19A)

For 20 cycles,

$$13.09 = 2.26 - (0.13071)\left(\frac{13.09 - 12.1}{13.09}\right) + (0.43609)\left(\frac{1.19}{0.01}\right)$$
$$+ (0.43609)(0.36488)\left(\frac{1.19}{0.01}\right)\left(\frac{SOC}{1.001 - SOC}\right)$$
$$\frac{SOC}{1.001 - SOC} = 3.3131$$
$$3.3164 - 3.3131SOC = SOC$$
$$3.3164 = 4.3131SOC$$
$$\boldsymbol{SOC = 0.7689}$$

For 40 cycles,

$$12.67 = 2.26 - (0.13071)\left(\frac{12.67 - 11.55}{12.67}\right) + (0.43609)\left(\frac{1.19}{0.01}\right)$$
$$+ (0.43609)(0.36488)\left(\frac{1.19}{0.01}\right)\left(\frac{SOC}{1.001 - SOC}\right)$$
$$\frac{SOC}{1.001 - SOC} = 3.291$$
$$3.2943 - 3.291SOC = SOC$$
$$3.2943 = 4.291SOC$$
$$\boldsymbol{SOC = 0.7677}$$

For 60 cycles,

$$12.65 = 2.26 - (0.13071)\left(\frac{12.65 - 11.5}{12.65}\right) + (0.43609)\left(\frac{1.19}{0.01}\right)$$
$$+ (0.43609)(0.36488)\left(\frac{1.19}{0.01}\right)\left(\frac{SOC}{1.001 - SOC}\right)$$
$$\frac{SOC}{1.001 - SOC} = 3.28996$$
$$3.2932 - 3.28996SOC = SOC$$
$$3.2932 = 4.28996SOC$$
$$\boldsymbol{SOC = 0.7676}$$

At Peak Load (I=1.74A)

For 20 cycles,

$$13.09 = 2.26 - (0.13071)\left(\frac{13.09 - 12.1}{13.09}\right) + (0.43609)\left(\frac{1.74}{0.01}\right)$$
$$+ (0.43609)(0.36488)\left(\frac{1.74}{0.01}\right)\left(\frac{SOC}{1.001 - SOC}\right)$$

$$\frac{SOC}{1.001 - SOC} = 3.132$$
$$3.1351 - 3.132SOC = SOC$$
$$3.1351 = 4.132SOC$$
$$\boldsymbol{SOC = 0.7587}$$

For 40 cycles,

$$12.67 = 2.26 - (0.13071)\left(\frac{12.67 - 11.55}{12.67}\right) + (0.43609)\left(\frac{1.74}{0.01}\right)$$
$$+ (0.43609)(0.36488)\left(\frac{1.74}{0.01}\right)\left(\frac{SOC}{1.001 - SOC}\right)$$
$$\frac{SOC}{1.001 - SOC} = 3.117$$
$$3.1201 - 3.117SOC = SOC$$
$$3.1201 = 4.117SOC$$
$$\boldsymbol{SOC = 0.7579}$$

For 60 cycles,

$$12.65 = 2.26 - (0.13071)\left(\frac{12.65 - 11.5}{12.65}\right) + (0.43609)\left(\frac{1.74}{0.01}\right)$$
$$+ (0.43609)(0.36488)\left(\frac{1.74}{0.01}\right)\left(\frac{SOC}{1.001 - SOC}\right)$$
$$\frac{SOC}{1.001 - SOC} = 3.116$$
$$3.119 - 3.116SOC = SOC$$
$$3.119 = 4.116SOC$$
$$\boldsymbol{SOC = 0.7578}$$

At Starting Up Load (I=1.6A)

For 20 cycles,

$$13.09 = 2.26 - (0.13071)\left(\frac{13.09 - 12.1}{13.09}\right) + (0.43609)\left(\frac{1.6}{0.01}\right)$$
$$+ (0.43609)(0.36488)\left(\frac{1.6}{0.01}\right)\left(\frac{SOC}{1.001 - SOC}\right)$$
$$\frac{SOC}{1.001 - SOC} = 3.1664$$
$$3.1696 - 3.1664SOC = SOC$$
$$3.1696 = 4.1664SOC$$
$$\boldsymbol{SOC = 0.7608}$$

For 40 cycles,

$$12.67 = 2.26 - (0.13071)\left(\frac{12.67 - 11.55}{12.67}\right) + (0.43609)\left(\frac{1.6}{0.01}\right)$$
$$+ (0.43609)(0.36488)\left(\frac{1.6}{0.01}\right)\left(\frac{SOC}{1.001 - SOC}\right)$$
$$\frac{SOC}{1.001 - SOC} = 3.14997$$
$$3.1531 - 3.14997 SOC = SOC$$
$$3.1531 = 4.14997 SOC$$
$$\boldsymbol{SOC = 0.7598}$$

For 60 cycles,

$$12.65 = 2.26 - (0.13071)\left(\frac{12.65 - 11.5}{12.65}\right) + (0.43609)\left(\frac{1.6}{0.01}\right)$$
$$+ (0.43609)(0.36488)\left(\frac{1.6}{0.01}\right)\left(\frac{SOC}{1.001 - SOC}\right)$$
$$\frac{SOC}{1.001 - SOC} = 3.1492$$
$$3.1523 - 3.1492 SOC = SOC$$
$$3.1523 = 4.1492 SOC$$
$$\boldsymbol{SOC = 0.7597}$$

For hybrid energy storage system:

The current of battery for Hybrid Battery-Supercapacitor System accounted for three conditions steady state load, peak load and starting up load) are the same because at 1.2A the battery is switched off from supplying power at the same time switching on supercapacitor.

For 20 cycles,

$$12.75 = 2.26 - (0.13071)\left(\frac{12.75 - 12.12}{12.75}\right) + (0.43609)\left(\frac{1.2}{0.01}\right)$$
$$+ (0.43609)(0.36488)\left(\frac{1.2}{0.01}\right)\left(\frac{SOC}{1.001 - SOC}\right)$$
$$\frac{SOC}{1.001 - SOC} = 3.2903$$
$$3.2936 - 3.2903 SOC = SOC$$
$$3.2936 = 4.2903 SOC$$
$$\boldsymbol{SOC = 0.7677}$$

For 40 cycles,

$$12.65 = 2.26 - (0.13071)\left(\frac{12.65 - 12.05}{12.65}\right) + (0.43609)\left(\frac{1.2}{0.01}\right)$$
$$+ (0.43609)(0.36488)\left(\frac{1.2}{0.01}\right)\frac{SOC}{1.001 - SOC})$$
$$\frac{SOC}{1.001 - SOC} = 3.2851$$
$$3.2884 - 3.2851SOC = DOD$$
$$3.2884 = 4.2851SOC$$
$$\boldsymbol{SOC = 0.7674}$$

For 60 cycles,

$$12.63 = 2.26 - (0.13071)\left(\frac{12.63 - 12.03}{12.63}\right) + (0.43609)\left(\frac{1.2}{0.01}\right)$$
$$+ (0.43609)(0.36488)\left(\frac{1.2}{0.01}\right)\frac{SOC}{1.001 - SOC})$$
$$\frac{SOC}{1.001 - SOC} = 3.284$$
$$3.2873 - 3.284SOC = SOC$$
$$3.2873 = 4.284SOC$$
$$\boldsymbol{SOC = 0.7673}$$

For 80 cycles,

$$12.59 = 2.26 - (0.13071)\left(\frac{12.59 - 12.02}{12.59}\right) + (0.43609)\left(\frac{1.2}{0.01}\right)$$
$$+ (0.43609)(0.36488)\left(\frac{1.2}{0.01}\right)\frac{SOC}{1.001 - SOC})$$
$$\frac{SOC}{1.001 - SOC} = 3.2819$$
$$3.2852 - 3.2819SOC = SOC$$
$$3.2852 = 4.2819SOC$$
$$\boldsymbol{SOC = 0.7672}$$

A6. Calculation on the CV and charge-discharge for the Output response (Capacitance and ESR) supercapacitor

(i) Data for Process 1 (mixing)

Table 78 Data obtained from Mixing Process.

Run 1		Run 2		Run 3		Run 4	
C (F)	ESR (Ω)	C (F)	ESR (Ω)	C (F)	ESR (Ω)	C (F)	ESR (Ω)
0.989	19.05	2.070	12.80	2.441	3.2	1.837	17.45
1.074	20.50	2.217	4.700	2.399	6.6	1.675	18.50
1.105	18.45	2.074	14.15	2.523	2.0	1.820	11.20
Average		Average		Average		Average	
1.0172	17.54	2.0758	11.55	2.3985	4.975	1.7390	12.55
Range (variation)							
0.204	8.350	0.275	9.85	0.292	6.1	0.213	9.45

(ii) Data for Process 2 (calendaring)

Table 79 Data obtained from Calendaring Process.

Run 1		Run 2		Run 3		Run 4	
C (F)	ESR (Ω)	C (F)	ESR (Ω)	C (F)	ESR (Ω)	C (F)	ESR (
2.035	2.30	2.583	2.35	1.967	2.85	2.140	2.25
2.039	3.50	2.440	2.05	1.901	2.06	2.173	3.00
2.132	3.15	2.654	3.20	1.979	2.35	2.406	2.95
Average		Average		Average		Average	
2.069	2.98	2.559	2.53	1.949	2.42	2.240	2.73
Range (variation)							
0.097	1.20	0.214	1.15	0.078	0.79	0.266	0.75

(iii) Data for Process 3 (drying)

Table 80 Data obtained from Drying Process.

Run 1		Run 2		Run 3		Run 4	
C (F)	ESR (Ω)	C (F)	ESR (Ω)	C (F)	ESR (Ω)	C (F)	ESR (
2.295	2.85	2.558	2.30	2.681	2.70	2.448	2.45
2.462	2.50	2.317	2.90	2.338	2.95	2.581	2.50
2.409	2.55	2.680	2.75	2.578	2.30	2.459	2.70
Average		Average		Average		Average	
2.389	2.63	2.518	2.65	2.532	2.65	2.496	2.55
Range (variation)							
0.167	0.35	0.363	0.60	0.343	0.65	0.133	0.25

(iv) Data for Process 4 (electrolyte treatment)

Table 81 Data obtained from Electrolyte Treatment Process.

Run 1		Run 2		Run 3		Run 4	
C (F)	ESR (Ω)	C (F)	ESR (Ω)	C (F)	ESR (Ω)	C (F)	ESR (
2.448	2.45	2.293	2.40	1.622	5.10	1.757	3.35
2.581	2.50	2.556	2.50	1.598	6.45	1.901	2.85
2.459	2.70	2.558	2.30	1.605	4.25	1.653	3.00
Average		Average		Average		Average	
2.496	2.55	2.469	2.40	1.608	5.27	1.770	3.07
Range (variation)							
0.133	0.25	0.265	0.20	0.024	2.20	0.144	0.50

(iv) Data for Process 5 (assembling and sealing)

Table 82 Data obtained from Assembling and Sealing Process.

Run 1		Run 2		Run 3		Run 4	
C (F)	ESR (Ω)	C (F)	ESR (Ω)	C (F)	ESR (Ω)	C (F)	ESR (Ω)
1.798	6.00	1.921	4.55	2.192	2.80	2.057	2.75
1.881	5.20	1.888	4.85	2.123	3.00	2.301	2.25
1.964	3.70	2.078	3.80	2.155	2.65	2.103	2.50
Average		Average		Average		Average	
1.881	4.97	1.962	4.40	2.157	2.82	2.154	2.50
Range (variation)							
0.166	2.30	0.190	1.05	0.069	0.35	0.244	0.50